GELATIN CHITOSAN AND BIOACTIVE NANOCERAMIC BASED COMPOSITE SCAFFOLD FOR ORTHOPAEDIC APPLICATION

Kanchan Maji

Department of Ceramic Engineering
National Institute of Technology Rourkela

Gelatin Chitosan and Bioactive Nanoceramic Based Composite Scaffold for Orthopaedic Application

Dissertation submitted in partial fulfillment of
the requirements of the degree of

Doctor of Philosophy

In

Ceramic Engineering

By

Kanchan Maji

(Roll Number. 512CR105)

Under the supervision of

Dr. Sudip Dasgupta
(NIT Rourkela)

and

Dr. Samit Nandi
(W.B.U.A.F.S)

Department of Ceramic Engineering
National Institute of Technology Rourkela
April 2017

Department of Ceramic engineering

National Institute of Technology Rourkela

April 11, 2017

Certificate of Examination

Roll Number: 512CR105

Name: Kanchan Maji

Title of Dissertation: Gelatin Chitosan and Bioactive Nanoceramic Based Composite Scaffold for Orthopaedic Application.

We the below signed, after checking the dissertation mentioned above and the official record book (s) of the student, hereby state our approval of the dissertation submitted in partial fulfillment of the requirements of the degree of *Doctor of Philosophy* in *Ceramic Engineering* at *National Institute of Technology Rourkela*. We are satisfied with the volume, quality, correctness, and originality of the work.

…….	…….
Sudip Dasgupta	*Samit Nandi*
Principal Supervisor	Co Supervisor
…….	…….
Swadesh Kumar pratihar	*Sumit Kumal Pal*
Member (DSC)	Member (DSC)
…….	…….
Amit Biswas	*Bikramjit Basu*
Member (DSC)	(Examiner)
.....	……....
Bibhuti Bhusan Nayak	*Debasish Sarkar*
(HOD)	Chairman (DSC)

Department of Ceramic Engineering
National Institute of Technology Rourkela

Dr. Sudip Dasgupta
Assistant Professor

11th April, 2017

Supervisor's Certificate

This to certify that the thesis entitled "**Gelatin Chitosan and Bioactive Nanoceramic based Composite Scaffold for Orthopaedic Application**" being submitted by Kanchan Maji for the award of the degree of Doctor of Philosophy in ceramic engineering of NIT Rourkela, is a record of bona-fide research work carried out by him under my supervision and guidance. Kanchan has worked for more than four years on the above topic. His research work at the Department of Ceramic Engineering from National Institute of Technology, Rourkela has reached the standard fulfilling the requirements and the regulations relating to the degree. The contents of this thesis, in full or part, have not been submitted to any other university or institution for the award of any degree.

.....
.Sudip Dasgupta

Ceramic Engineering Department
National Institute of Technology Rourkela

11th April, 2017

Supervisor's Certificate

This to certify that the thesis entitled "**Gelatin Chitosan and Bioactive Nanoceramic based Composite Scaffold for Orthopaedic Application**" being submitted by Kanchan Maji for the award of the degree of Doctor of Philosophy in ceramic engineering of NIT Rourkela, is a record of bona-fide research work carried out by him under our supervision and guidance. Kanchan has worked for more than four years on the above topic. His research work at the Department of Ceramic Engineering from National Institute of Technology, Rourkela has reached the standard fulfilling the requirements and the regulations relating to the degree. The contents of this thesis, in full or part, have not been submitted to any other university or institution for the award of any degree.

Dr.Samit Nandi
(Co Supervisor)
Associate Professor
Deapartment of Veterinary Surgery and Radiology
West Bengal University of Animal and Fishery Science
Kolkata, West Bengal

Dr.Sudip Dasgupta
(Principal Supervisor)
Assistant Professor
Department of Ceramic Engineering
NIT, Rourkela

Dedicated to

My Family and Friends

Declaration of Originality

I, Kanchan Maji, Roll Number 512CR105 hereby declare that this dissertation entitled "**Gelatin Chitosan and Bioactive Nanoceramic based Composite Scaffold for Orthopaedic Application**" represents my original work carried out as a doctoral student of NIT Rourkela and, to the best of my knowledge, it contains no material previously published or written by another person, nor any material presented for the award of any other degree or diploma of NIT Rourkela or any other institution. Any contribution made to this research by others with whom I have worked at NIT Rourkela or elsewhere, is explicitly acknowledged in the dissertation. Works of other authors cited in this dissertation have been duly acknowledged under the section "Bibliography". I have also submitted my original research records to the scrutiny committee for the evaluation of my dissertation.

I am fully aware that in case of any non-compliance detected in future, the Senate of NIT Rourkela may withdraw the degree awarded to me on the basis of the present Dissertation.

April, 2017 Kanchan Maji

NIT Rourkela

Acknowledgement

This manuscript would not have been possible without the help of my empathetic and supportive guide **Dr. Sudip Dasgupta**. I heartfelt thank him for his unconditional help, constant effort for improving my work, providing time to time feedback and never giving upon me. It has been an honor to be his first PhD student. You have been a tremendous mentor for me. I would like to thank you for encouraging my research and for allowing me to grow as a research scientist.

I would also like to express my gratitude to my co-supervisor **Prof. Samit Nandy** for his help and guidance. I am indebted to my Doctoral Scrutiny Committee (DSC) members **Prof. D. Sarkar, Prof. S.K. Pratihar, Dr. Sumit Pal of** Ceramic Engineering Department **and Prof. A.Biswas** of Biomedical Engineering Department**.**

Department of Biomedical Engineering, of our Institute for their kind co-operation and insightful comments throughout, which have been instrumental in the success of thesis.

I am highly obliged to **Prof. A. Biswas**, Director, National Institute of Technology (NIT), Rourkela and **Prof. B.B Nayak,** Head of the Department, of Ceramic Engineering, for the academic support and the facilities to carry out the research work efficiently at the institute.

I also express my thankfulness to the faculty and staff members of the Department of Ceramic Engineering for their continuous encouragement and suggestions. Special thanks to **Satyananda ,Jai Rao, Akhilesh, venus , Ashley, Bhisam Singh, Abhishek Badolia, Soumini** and all the research scholar for their kind cooperation in non-academic support during the research work.

11th April,2017
NIT Rourkel

Kanchan Maji
(Roll Number: 512CR105)

Abstract

Gelatin, chitosan and bioactive nanoceramic based composite scaffold with tailored architectures and properties has great potential for bone regeneration. Herein, we aimed to improve the physico chemical, mechanical and osteogenic properties of 3D porous scaffold by incorporation of bioactive ceramic phase into biopolymer matrix with variation in composition in the prepared scaffolds. Scaffolds were prepared from the slurry containing gelatin, chitosan and synthesized bioactive nanoceramic particulate using lyophilisation technique. Bioactive nanocermics such as hydroxyapatite, β-tricalcium phosphate and 58 S bioactive glass were synthesized and used in different concentration varying between 10-30 wt% to prepare GCH, GCB and GCT scaffolds. GCH scaffold having HA:Chi:Gel ratio of 28:42:30 with 78% average porosity showed a pore size distribution between 75–100 μm and exhibited a compressive strength of 3.45 MPa, which is within the range of that exhibited by cancellous bone. With increase in nanocaramic phase content from 10 wt% to 30 wt%, the compressive strength in the scaffold increased. GCH 30 showed the highest average compressive strength of 3.46 MPa whereas the lowest average compressive strength of 2.2 MPa was registered by GCB 30 scaffold. Higher cellular activity was observed in GCB 30 scaffold as compared to GCB 0 scaffold suggesting the fact that 58S bioactive glass nanoparticles addition into the scaffold promoted better cell adhesion, proliferation and differentiation. A Higher degree of lamellopodia and filopodia extensions and better spreading behaviour of MSC's were observed in FESEM micrographs of MSC cultured GCB 30 scaffold. Scaffolds prepared from 30 wt% 58S nano bioactive glass exhibited the highest bioactivity among all the scaffolds as evident from MTT assay, RUNX-2 and osteocalcin expression from mesenchymal stem cells cultured on the scaffold. Strongly positive osteocalcin signalling within 14 days of cell culture supported the fact that the prepared scaffolds stimulated new bone tissue regeneration. Moreover, by reverse-transcriptase (RT-PCR) analysis, it was observed the expression of osteogenic gene markers from cultured MSCs were relatively high in GCB 30 as compared to GCH 30 and GCT 30 composite scaffolds. In coherence with the in vitro appearance, histological analysis and fluorochrome study in a rabbit tibia model showed a significantly greater amount of new bone formation in GCB30 compared to other composite scaffold. The results demonstrated that the prepared GCB30 scaffold could be a good candidate as a synthetic substitute for bone tissue engineering.

Keywords*: Hydroxyapatite, β-TCP, 58s Bioglass, Chitosan, Gelatin, scaffold, compressive strength, bioactivity, *in vitro* ,*in vivo

Contents

LIST of FIGURE

List of Tables

Abbreviations

WORDS	ABBREVIATIONS
ALP	Alkaline Phosphatase.
ANOVA	Analysis of Variance.
β-TCP	Beta Tri Calcium Phosphate.
HAp	Hydroxyapatite.
HAp-Chi	Hydroxyapatite-Chitosan.
3D	Three Dimensional .
COL 1	Collagen 1.
CS	Chitosan.
GC	Gelatin-Chitosan.
GCH	Gelatin-Chitosan-HAp.
GCB	Gelatin-Chitosan-Bioactive glass.
GCT	Gelatin-Chitosan-β-TCP.
DMEM	Dulbecco's modified Eagle's medium.
ECM	Extracellular Matrix.
hMSCs	Human Mesenchymal Stem Cells.
FTIR	Fourier Transform Infra Red.
H&E	Hematoxylin & Eosin .
MTT	3-[4,5-dimethyltriazol-2-y1]-2,5-diphenyl tetrazolium .
OCN	Osteocalcin .
OPN	Osteopontin.
PBS	Phosphate Buffer Saline.
R&D	Research & Development.
RGD	Arginine-Glycine-Aspartic acid.
RT-PCR Reverse	Transcription Polymerase Chain Reaction.
TIPS	Thermally Induced Phase Separation.
UCB	Umbilical Cord Blood.

CHAPTER # 1

General Introduction

Review your goals twice every day in order to be focused on achieving them.

- Les Brown

1.1 General Introduction

Human beings across the globe are likely to face serious problems such as tissue damage and degeneration caused by diseases, accidents and aging during their lifetime. However, there was limited choice on biomaterial in past for solving these medical problems with removal of the damaged and diseased body parts or tissues being the most frequently applied solution. Today, advances in science and technology of medical materials significantly altered the choices of researchers for the solution of the implantation problems [1].

1.2 Background and Significance of the Study

To visualize and estimate the extent and prevalence of bone tissue related diseases and disorders, it is important to note that the World Health Organization, on January 13, 2000 finally launched a Bone and Joint decade for the period of 2000-2010 [14] More than 43 million people in United States of America suffer form of arthritis and it is estimated that this number will increase to 60 million by the end of 2020 [2].India is the second largest emerging economy and second most populated (1.2 billion people) country in the world with life expectancy is 67 years and is expected to increase to 71 years by 2025 and to 77 years by 2050. Indian Council for Medical Research (ICMR) carried out a large multicenter study, which confirmed data from smaller, single cantered studies, and showed that Indians have lower BMD than their North American counterparts [3]. Reasons ascribed for lower BMD in Indians include possible genetic differences, nutritional deficiency, and smaller skeletal size [4]. In private hospitals, the total cost of hip surgery is between Rs 150,000 to 250,000 (2,360-3,860 USD), and in public hospitals the cost is approximately Rs 50,000 (772 USD) However, each year approximately 170,000 fractures do not heal and are diagnosed as “non-unison” thus requiring some form of bone substitute to address this problem [5]. Hence, a great need for bone tissue substitute in the form of bone grafts and subsequent tissue engineering could be a viable option.

In this introductory chapter the chemical and biological composition of bone tissue engineering will briefly be discussed. Different materials, techniques and technologies that have been used for scaffold fabrication are outlined and explained. The ultimate theme of the thesis is to combine materials and technologies to create improvised functional scaffolds in terms of ability to provide physical and chemical cues to the *in vivo* neo bone tissue regeneration.

1.3 Tissue Engineering

Tissue engineering is an interdisciplinary field that applies the knowledge of principle of engineering and life science in order to construct biological substitutes to repair damaged/diseased tissues. In order to achieve successful tissue regeneration, three important key issues need to be considered; the isolation and cultivation of cells, the use of tissue-inductive biomolecules and the incorporation of cells in suitable scaffolds to support 3-D tissue regeneration as shown in Figure.1.1 [6]. In a traditional tissue engineering approach, cells are cultured and seeded on a scaffold and then implanted into the defect site to regenerate new tissue [7]. In this approach, the cells provide the main source for new tissue regeneration. The scaffolds act as three-dimensional matrices for cell growth and degrade away as the tissues are regenerated [8]. Despite the encouraging earlier research outcomes [9, 10], the limited number of donor cells and low quality of regenerated tissues remained two hurdles in tissue engineering approaches[11]. Scaffolds are required to provide various additional functions besides providing structural support and suitable degradation kinetics. Another approach is to implant a cellular scaffold in the defect site with the capability of delivering appropriate biomolecules in a controlled manner, thereby recruiting progenitor cells to the defect site and promoting cell proliferation and differentiation, inducing tissue regeneration [12].Cell supportive factor-releasing scaffolds are gaining popularity and have recently been used along with incorporated cells [13, 14]. These scaffolds are often called bioactive scaffolds [15, 16].

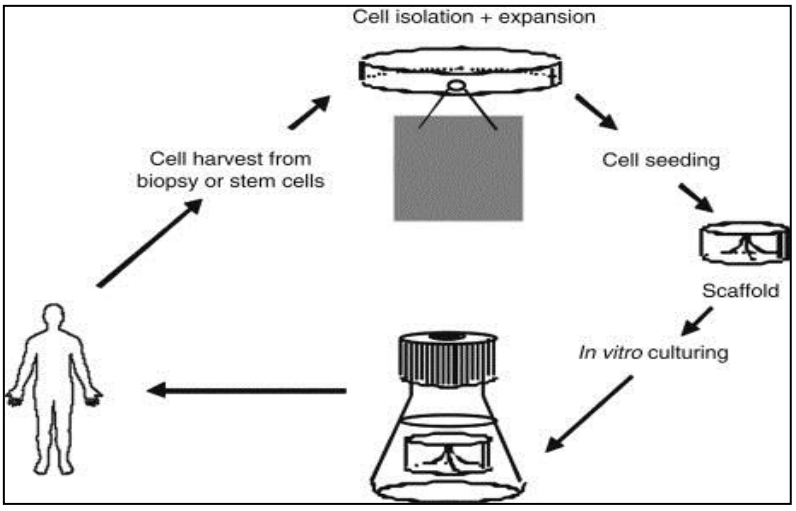

Figure.1.1.The basic principle of Tissue Engineering [17].

1.4 Bone

Bone is a highly vascularised mineralized tissue which ultimately provides a skeletal support to the body, including protection of various internal organs [18, 19]. Therefore, entire body functionality and thus lifestyle too are affected by major defects in its structure [20]. Bone tissue regeneration provides intricate factors one of which is to mimic the microenvironment of natural bone. Though bone tissue has intrinsic ability to regenerate to certain extent, but larger defects or disorders in bony sites make healing improper and thus may start damaging themselves in a long run [21].

1.4.1 Structure and Composition of Bone

Bone comprises three types of bone cells with specific functions with surrounding extracellular matrix (ECM). Collagen I being the major component of bone ECM, occupies almost 95% of bone's organic part of ECM. Proteoglycans and non-collagenous proteins contribute only 5% [22]. Glycosaminoglycan [GAG] is a kind of proteoglycans which is found in bone and cartilage. Calcium phosphate like minerals in the matrix provides rigidity and strength to bone [23]. All the properties of bone are directionally and regionally dependent. The composition of bone is given in Table 1.1.

Table.1.1. Composition of Bone

Component	Amount (wt.%)
Hydroxyapatite	69%
Organic matrix	22%
Water	9%

1.4.2 Types of bone

Bones are of two types namely cortical (hard) and cancellous/trabecular bone (spongy). The cortical bone typically occupies the outer layers of most of the bones and various long bones with 80-90% mineralization [24]. It is mainly responsible to provide mechanical strength to the entire skeleton. cancellous bone having 15-20% minerals generally occupies the interior parts of bones [25]. The cancellous bone is highly vasculaturized and hence metabolic actions are taken care by it. The mineral containing fibres form lamellar sheets which are arranged in concentric rings to form osteon [26] as shown in Figure 1.2.

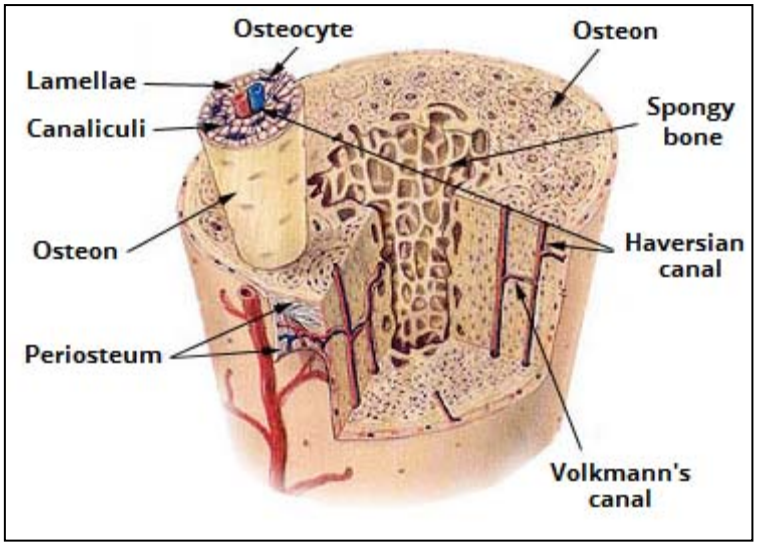

Figure.1.2. Structure of mature bone. Note the differing structure of compact and spongy bone types [27].

1.4.3 Types of Bone Cells

Three major types of bone cells that contribute to bone formation are the osteoblasts (bone-forming cells), osteoclasts (bone resorbing cell) and osteocytes (matured bone cells). The various types of bone cells and their functions are represented in Table 1.2 and Figure 1.3.

Table.1.2. Types of Bone cells and their function.

Cell Type	Morphology	Function	Reference
Osteoblast	Cuboidal in shape; located at the bone surface with their precursors	Synthesis and regulation of bone ECM deposition	[28]
Osteocytes	Stellated shaped	Calcification of osteoid matrix	[29]
Osteoclast	Multinucleated cells	Bone resorption	[30]

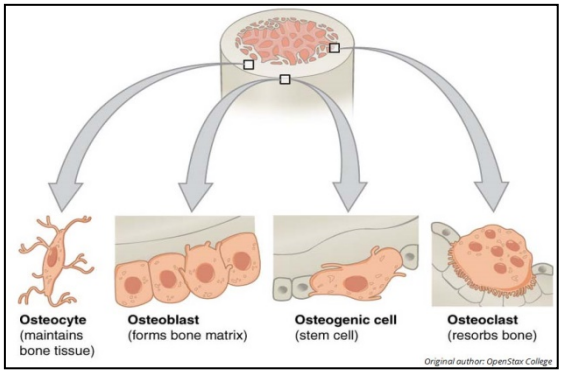

Figure.1.3. Different type of bone cells [31].

1.4.4 Mechanical Properties of Bone

Bone tissue is a highly dynamic form of connective tissue which undergoes required regular remodelling (the orchestrated removal of bone by osteoclasts followed by the formation of new bone by osteoblasts) to optimally adapt its structure to changing functional demands (mechanical loading, nutritional statusetc.). The mechanical properties mostly depend on the bone composition (porosity, mineralisation etc.) as well as the structural organisation (trabecular or cortical bone architecture, collagen fibre orientation, fatigue damage etc.) [32]. The resulting mechanical properties of the two types of bone tissue, namely the cortical bone and cancellous bone, are shown in Table 1.3.

Table.1.3. Mechanical properties of compact and spongy bone .

Type of Bone		Longitudinal Plane	Transverse Plane	Elastic Modulus	Reference
Compact Bone	Compression	131-224 MPa	106-133 MPa	13.7 GPa	[33]
	Tensile Shear	78.8-151 MPa	51-56 MPa		
		53.1-70MPa			
Spongy/Cancellous Bone	Compression	3-30 MPa	<5MPa	1.5 GPa	[34]
	Tensile	3-20 MPa	<5MPa		
	Shear	<5MPa	<5MPa		

1.4.5 Mechanism of Bone Healing

The architecture of damaged bone tissue is primarily restored by regeneration of normal cell and ECM rather by repair of injured area as it occurs in some other connective tissues [35]. The healing mechanism starts with immediate bleeding and blood clotting, which provides the basic platform for inflammation [36]. The neo bone tissue produced then replaces the blood clot with formation of soft callus (fibrous tissue and cartilage) and later on replaced by hard callus as shown in Figure 1.4. Finally the compact tissues grow and remodelling continues to occur.

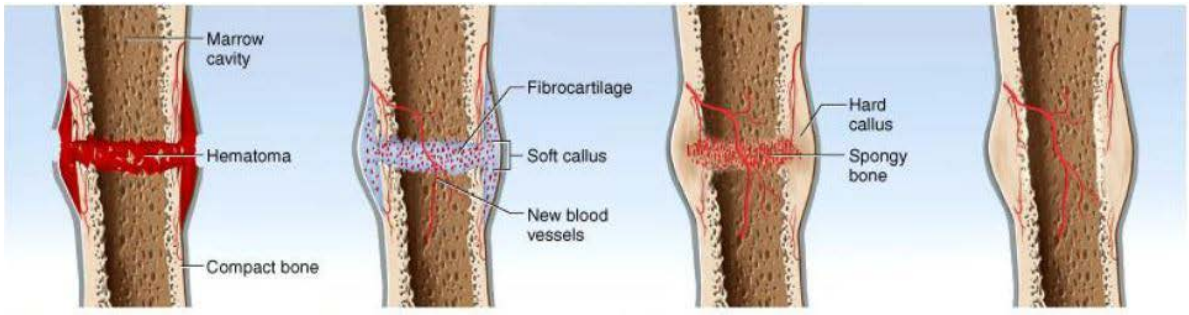

Figure.1.4.Preliminary bone healing mechanism [42].

1.5 Bone Grafts

1.5.1 Autograft

Autografts are considered as the gold standard for the bone replacement, mainly because they offer minimal immunological rejection, complete histocompatibility and provide the optimum osteoconductive, osteogenic and osteoinductive properties [37].The main advantages of autograft are their excellent success rate and low risk of disease transmission. Autogenous cancellous bone graft has been considered more osteogenic as compared to cortical bone graft because of their porous structure and allows the diffusion of nutrients and limited revascularization by microanastomosis of its circulating vessels. In an experimental study on Dog, it was observed that fresh autografts are incorporated rapidly and possess osteoinductive, osteoconductive and osteogenic properties.

1.5.2 Allograft

Allograft cortical bone grafts have little or no osteoinductive properties and are mostly osteoconductive, but the surviving osteoblast does provide some osteogenic properties as well as describe in Table 1.4 [38]. Vascularize cortical grafts heal rapidly at the host-graft-interface, and their remodelling is similar to that of normal bone[39]. However, disadvantages include potential morbidity at donor site, availability in limited quantities, risk of wound infection, increased blood loss and prolonged anaesthetic time [40].

Table.1.4. Bone graft and graft substitute [41].

Class	Description	Examples	Properties of action
Autograft based	Used alone		•Osteoconductive •Osteoinductive •Osteogenic
Allograft based	Allograft bone used alone or in combination with other materials	Allegro, Orthoblast, Grafton	•Osteoconductive •Osteoinductive

Cell based	Cells used to generate new tissue alone or seeded onto a support matrix	Mesenchymal stem cells	•Osteogenic, •Both osteogenic and osteoconductive with carrier materials
Ceramic based	Includes calcium phosphate, calcium sulfate, and bioactive glass used alone or in combination	Osteograf, ,Osteoset, NovaBone	•Osteoconductive •Limited osteoinductive when mixed with bone marrow
Polymer based	Includes degradable and nondegradable Polymers used alone or with other materials	Cortoss, OPLA, Immix	• Osteoconductive • Bioresorbable in degradable polymer

1.6 Biomaterials Classifications

1.6.1 Based on material-tissue interactions

Depending on the nature of scaffolding material, tissue reacts towards the implant in a variety of ways. The tissue response to the implant biomaterial surface ultimately governs activity and efficiency of implant material inside the body to regenerate damaged/diseased bone tissue. In general, biomaterials may be described in or classified into four categories such as bio-inert, bioactive, surface active and bio-resorbable depending on their interaction with tissues and cells as shown in Figure 1.5.

1.6.1.1 Bioinert

Materials when implanted inside the human body exert minimal biological interaction with its surrounding tissue. Generally, a fibrous capsule is formed around the Bioinert implants and hence bio-functionality of this kind of material depends on tissue integration. Examples of Bioinert biomaterials are stainless steel, titanium, alumina, partially stabilized zirconia, ultra high molecular weight polyethylene etc [42].

1.6.1.2 Bioactive

The material, when placed inside the human body interacts with the surrounding bone and soft tissues through the time dependent kinetic modification of the construct surface. A biologically active carbonate apatite (CHA) layer is formed and deposited on the bioactive implant surface by the ion exchange reaction between the bioactive implant and surrounding

body fluids. This biologically active carbonated apatite (CHA) layer is chemically and crystallographically equivalent to the mineral phase of natural bone tissue [43]. Prime examples of these bioactive materials are synthetic hydroxyapatite [$Ca_{10}(PO_4)_6(OH)_2$], glass ceramic A-W and bioglass.

1.6.1.3 Surface active

Surface active biomaterials form a bioactive layer on exposure to physiological environment and thus undergoes direct interactions with host bone through physicochemical and biological bonds without formation of fibrous capsule [43]. In biological environment, the surface layer of this kind of biomaterials consists of calcium and phosphorous that is crystallographically similar to inorganic part of natural ECM of bone[44]. The materials include bioactive glasses , bioactive glass ceramics , bioactive composites and bioactive coatings [45].

1.6.1.4 Bioresorbable

Materials are the one which is capable of being dissolved or resorbed and slowly replaced by advancing tissues, such as bone, when used as an implant material inside the body. Common examples of bio-resorbable materials are tri-calcium phosphate [$Ca_3(PO_4)_2$] and polylactic–polyglycolic acid copolymers [46].

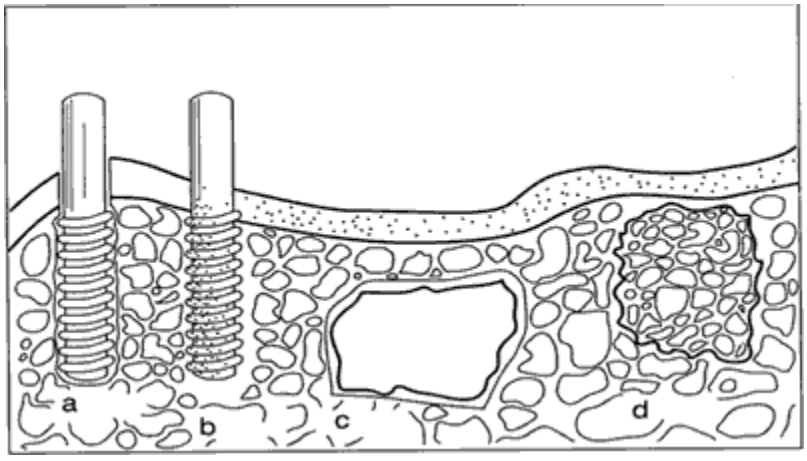

Figure.1.5 Classification of bioceramics according to their bioactivity; (a) bioinert, (alumina dental implant), (b) bioactive, hydroxyapatite ($Ca_{10}(PO_4)_6(OH)_2$) coating on a metallic dental implant, (c) surface active, bioglass or A-W glass, (d) bioresorbable tri-calcium phosphate implant [$Ca_3(PO_4)_2$][46].

1.6.2 Based on type of materials

Depending on the type of materials, biomaterials can primarily be divided into three categories- metals, ceramic and biopolymer. Sometimes a combination of these materials is used as composite structure to mimic ECM of natural bone tissue. Application of these

materials includes replacement of hips, knees, teeth, tendons and ligaments; repair of periodontal disease; maxillofacial reconstruction; spinal fusion, and bone repair.

1.6.2.1 Metal as biomaterial

Metallic biomaterials have been extensively used for load-bearing implants, such as hip and knee prostheses and fracture fixation wires, pins, screws, and plates [47]. Metals also find attractive application as parts of artificial heart valves, as vascular stents, and as pacemaker leads [48]. Metallic alloys with tailored materials properties, such as strength and corrosion resistance, are sometimes used as implant instead of pure metal. The main considerations in selecting metals and alloys for biomedical applications are biocompatibility, appropriate mechanical properties, corrosion resistance, and reasonable cost.

The mechanical properties of materials are of great importance when designing load-bearing orthopaedic and dental implants as alternative substitute. Mechanical properties of some of the most commonly used metallic implants are listed in Table 1.5.

Table.1.5. Select Properties of Metallic Biomaterials [49].

Materials	**Young Modulus E(GPa)**	**Yield Strength $\sigma_{y,}$(MPa)**	**Tensile Strength $\sigma_{UTS,}$ (MPa)**	**Fatigue Limit $\sigma_{end,}$(MPa)**
Stainless steel	190	221-1,213	586-1,351	241-820
Co-Cr alloys	210-253	448-1,606	655-1,896	207-950
Ti	110	485	760	300
Ti-6Al-4V	116	896-1,034	965-1,103	620
Cortical bone	15-30	30-70	70-150	

The elastic moduli of the metals listed in Table 1.5 are at least seven times greater than that of natural bone. This mismatch of mechanical properties of implants can cause stress-shielding associated with bone resorption (loss of bone) in the vicinity of implants [50]. Compared to the elastic moduli of either stainless or cobalt-chromium molybdenum alloys, Ti and Ti-6Al-4V have much lower moduli that are still almost an order of magnitude higher that of bone. Another advantage of Ti-based metals as bone implants is their favourable strength-to-density ratio [51].

1.6.2.2 Ceramic as Biomaterial

Bioceramics are employed as components of hip implants, dental implants and heart valves [52]. They are also designed and fabricated for repair and reconstruction of diseased, damaged or "worn out" parts of the body tissue. Some of the ceramics that have been used for biomedical applications are listed in Table 1.6.

Table.1.6. Ceramics Used in Biomedical Applications [53].

Ceramic	***Chemical Formula***	***Types of Attachment***	***Comment***
Alumina	Al_2O_3	Mechanical interlock (morphological fixation)	Bioinert
Zirconia	ZrO_2		
Bioglass	Na_2O $CaOP_2O_3$-SiO	Interfacial bonding with tissues (Bioactive fixation)	Bioactive
Highly dense pure Hydroxyapatite	$Ca_{10}(PO_4)_6$ $(OH)_2$		
Hydroxyapatite (sintered low temperature)	$Ca_{10}(PO_4)_6$ $(OH)_2$	Ingrowths of tissues in pores (Biological fixation)	Biodegradable
Tricalcium phosphate	$Ca_3(PO_4)_2$	Replacement with tissues	

Bioceramics are corrosion resistant, but may be susceptible to other forms of degradation when exposed to a physiological environment. The mechanism and rate of degradation vary depending on the type of bioceramics. Even alumina, a predominantly bioinert ceramic, suffers from time-dependent deterioration in strength when placed in physiological environment *in vitro* and *in vivo.* Calcium Phosphate (CaP) based bioactive ceramics are also degraded in the body by virtue of its dissolution in physiological fluid and osteoclasts mediated bioresorption. The rate of degradation of CaP ceramics will vary depending on their phase, chemical composition, and crystal structure. Table 1.8 shows different types of Calcium orthophosphate ceramics.

Table.1.7. Different types of calcium phosphates (CaP) [54].

Chemical Name	Abbreviation	Chemical formula	Phase	Ca/P	Solubility
Monocalcium Phosphate	MCP	$Ca(H_2PO_4)$, H_2O	--------	0.50	$1X\ 10^{-3}$
Dicalcium Phosphate Hydrate	DCPD	$CaHPO_4$, H_2O	Brushite	1.00	$1.87X\ 10^{-7}$
Dicalcium Phosphate Anhydrous	DPCA	$CaHPO_4$	Monetite	1.00	$1.26\ X\ 10^{-7}$
Octacalcium Phosphatepenta hydrate	OCP	$Ca_8H_2(PO_4).5\ H_2O$		1.33	$5.1\ X\ 10^{-15}$
Tricalcium Phosphate	α-TCP	$Ca_3\ (PO_4)_2$		1.50	
	β-TCP	$Ca_3\ (PO_4)_2$	Whitlockite	1.50	$2.83X10^{-30}$
Hydroxyl Apatite	HAp	$Ca_{10}\ (PO_4)_6(OH)_2$	Hydroxyapatite	1.67	$2.35\ X\ 10^{-59}$
Tetracalcium Phosphate monoxide	TTCP	$Ca_4O(PO_4)_2$	Hilgenstockite	2.00	

The solubility of different CaP minerals changes in the following order.

ACP > DCP >TTCP > α-TCP > β-TCP >> HAp .

The slowest rate of dissolution of HAp among all the CaP ceramics listed above is not surprising, because it is highly stable CaP compound at and above pH 4.2. The applications of CaP based bioresorbable ceramics include drug delivery vehicle, repairing damaged bone, repairing and fusion of spinal and lumbo-sacral vertebrae, repairing maxillofacial and dental defects.

Bioactive ceramics mostly include CaP based materials and bioactive glasses. A common characteristic of all bioactive implant is the formation of a hydroxyl carbonated apatite (HCA) layer on their surface when implanted. Depending on the nature of bioactive ceramics, the formation of HCA layer may take from days to weeks. The application of bioactive ceramics includes coating on prostheses, reconstruction of dental defects, bone plate and screws, replacements of middle ear ossicles and correcting periodontal defects.

Among the CaP ceramics discussed here, hydroxyapatite, and tricalcium phosphate are important as structural biomaterials because of their stability at high temperature, sinterability of the powders and comparatively higher mechanical properties of the dense bodies.

A. Hydroxyapatite

Figure.1.6 illustrates a schematic diagram of the structure of hydroxyapatite (HAp). The structure shown here is the stoichiometric composition of HAp whereby the unit cell is composed of $Ca_{10}(PO_4)_{12}(OH)_4$. The core framework of the HAp structure is constituted mainly of the PO_4^{3-} tetrahedron, with two types of channel structures that lie parallel to the c –axis. The OH ion and Ca^{2+} ion lie within each of these structures [55]. Eight of the 20 Ca^{2+} in the unit cell are located at the Ca^{2+} site (Ca I), with the remaining Ca^{2+} located on the second site (Ca II), which is also the peak of the equilateral triangle that is constructed from the OH^- ion channels. This Ca^{2+} is exposed on the crystal surface, thus playing a large role in the physical properties of HA, such as surface charge, and in interactions with organic compounds.

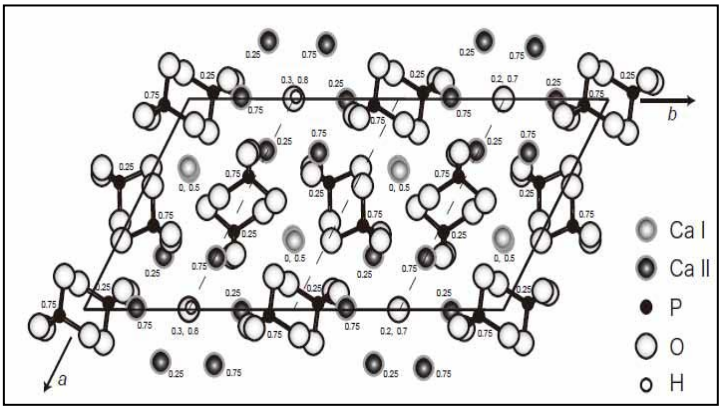

Figure.1.6. Crystal structure of Hydroxyapatite [56].

B. β–Tricalcium phosphate

Tricalcium phosphate $Ca_3(PO_4)_2$(TCP) is frequently used as bone graft substitutes in many surgical fields like the orthopaedic, dental, plastic surgeries [57]. It forms calcium deficient hydroxyapatite on exposure to physiological fluids that confers to its excellent biocompatibility and osteointegration properties. Moreover, its efficient resorbability in the human biological environment allows significant recolonisation of the operational site by advancing bone growth with the progressive degradation of this material. TCP can exist under two polymorphs, such as: β-TCP stable below 1120°C, α-TCP stable between 1120 and 1470 ◦C [58]. β-TCP is stable at room temperature and reconstructively transforms at 1125°C into α-TCP, which is metastably retained until room temperature during the cooling [59]. The ideal Ca/P ratio of β-TCP is 1.5. As reported by Dickens and al [60]. The β -TCP crystallizes in the rhombohedral space group R_3C with unit-cell parameters a = 10.4121(3); c = 37.3517(5) Å [61].

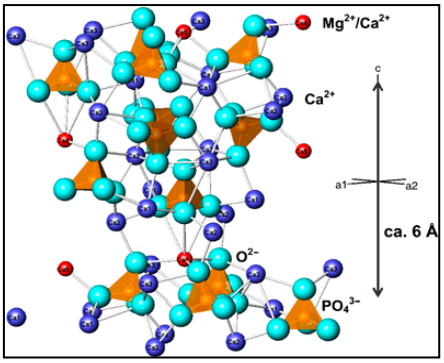

Figure.1.7. Crystal structure of Tri-calcium phosphate [62].

The major drawback of bioceramics based is that they fail catastrophically due to the presence of cracks or other defects [63]. Although some of the bioceramics exhibit outstanding strength when loaded in compression, they fail at low stress in tensile or bending environment [64]. The mechanical properties of CaPs and bioactive glasses make them unsuitable as load-bearing implants. Table 1.8 shows some of the mechanical properties of ceramic based biomaterials used for fabricating scaffold. Among the biomedical ceramics, alumina has the best mechanical properties, but its tensile properties are still below those of metallic biomaterials [63]. Additional advantageous properties of alumina are its low coefficients of friction and wear rate. Because of these properties, alumina has been used as a bearing surface in joint replacements.

Table.1.8. Mechanical properties of ceramic biomaterials [65].

Bioceramics	***Young's Modulus E (GPa)***	***Compressive Strength, (MPa)***	***Tensile Strength, (MPa)***
Alumina	380	4500	350
Bioglass-ceramics	22	500	56-83
Calcium Phosphate	40-117	510-896	69-193
Pyrolytic carbon	18-28	517	280-560

C. Bioactive glasses and glass-ceramics

Ceramics include various glasses and glass-ceramics. Gong et al. fabricated glass implants with 5% porosity and pores that ranged from 100–200 μm, and also glass-ceramic implants with macropores (100–200 μm) and micropores (0.5 μm). Glassy carbon pellets with 40% porosity induced bone growth in tibia defects in rabbits [66]. Bioglass (materials with different compositions of SiO_2,CaO, Na_2O, and P_2O_5 scaffolds have an inter-connected network, 10–500 μm and have been shown to support culture of human primary osteoblasts .

In other studies Bioglass implants with pores ranging from 100 to 600 micron induced ectopic bone formation in dogs [67]. Silica/calcium phosphate scaffolds with different porosities (51%, 47% and 43% generated by decreasing the silica content) and a broad distribution of pore sizes (10–300 μm) helped to regenerate bone in femoral defects in rabbits . Upon retrieval, the silica-rich scaffolds were almost filled with new bone and showed higher resorbability than scaffolds with lower silica content. This stronger osteogenic outcome was attributed to the chemical composition (high content of pyrophosphate) and not to differences in porosity. Properties of amorphous glass and glass-ceramic scaffolds are summarized in Table 1.9.

Table.1.9. Porosities and pore sizes of amorphous glass and glass-ceramic scaffolds for bone regeneration [68].

Material	Fabrication technique	Pore size (μm)	Porosity (%)	Application
Glasses	Sintering	100–200	5-40	Tibia defects in rabbits
Bioglass	Foaming	10–500		Primary human osteoblasts in vitro
	Sintering	100–600		Ectopic bone formation in dogs
Glass-ceramics	Sintering	100–200		
	Phase transformation	10–300	51, 47 and 43	Femoral defects in rabbits

1.6.2.3 Polymer as Biomaterial

Owing to their excellent biocompatibility, tunable chemical composition, good biological reorganization and adjustable biodegradation, biopolymers, including both natural and synthetic polymer composites, have been widely used as biomaterials for the fabrication of medical devices and tissue-engineering scaffolds [69].

1.6.2.3.1 Synthetic and natural polymer

The most often utilized biodegradable synthetic polymers for 3D scaffolds in tissue engineering are saturated poly-a-hydroxy esters, including poly(lactic acid) (PLA) and poly(glycolic acid) (PGA), as well as poly(lactic-coglycolide) (PLGA) copolymers [70]. Natural polymers used in bone tissue engineering include chitosan, collagen, fibrin, alginate, silk, hyaluronic acid, and gelatin [71]. Some of the synthetic polymers exhibit high mechanical properties suitable for application in bone implant, but their bioactivity is inferior to that of natural biopolymer. Again, most natural polymers are biocompatible, degradable, and readily solubilized in physiological fluid which can be used alone as a growth factor

delivery carrier or combined with other delivery materials such as synthetic polymers and inorganic materials. Despite higher biocompatibility, natural polymers are mechanically weak and undergo rapid degradation upon implantation. Therefore, optimization of degradation rate and molecular properties in natural polymer based bone implants are required to enhance their efficacy in application of bone tissue engineering. Research in this direction has been made by crosslinking collagen based implants with appropriate chemical reagents [72]. Here, we specially emphasize on the basic properties of two of the most important natural polymers such as chitosan and gelatin.

A. Chitosan

As the degree of deacetylation of chitin reaches about 50% (depending on the origin of the polymer), it becomes soluble in acidic aqueous media and is called chitosan. The solubilisation occurs by protonation of the $-NH_2$ functional group (Figure1.8) on the C-2 position of the D-glucosamine repeat unit, whereby the polysaccharide is converted to a polyelectrolyte in acidic media [73]. This polymer has been extensively investigated for industrial application based on film and fibre formation. Numerous derivatives of chitin have been developed to alter biological functions of chitosan, including enhancement of cellular interactions for tissue engineering approaches. Chitosan has been functionalized with sugar residues such as fructose or galactose for culture of hepatocytes and with proteins such as collagen, gelatin and albumin for neural tissue engineering [74].

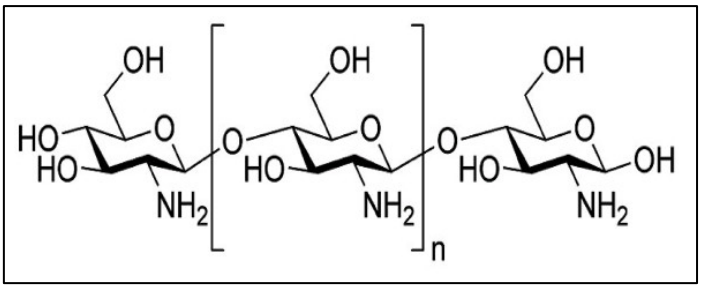

Figure.1.8. Chemical formulae of chitosan [74].

B. Gelatin

Gelatin comprises of heterogenous mixture of single or multi –stranded polypeptides, containing between 50-1000 amino acids [75]. Each peptide strand is conformed with extended left-handed proline helix. The triple helix of type I collagen, extracted from skin and bones, one of the sources of gelatin, is composed of two α1(I) and one α2(I) chains. Each helix is associated with molecular mass of of ~ 95 kD, width of ~1.5 nm and length of ~0.3

μm. The mixtures of these strands together with their oligomers and other breakdown polypeptides from the core of gelatin structure, as shown in Figure.1.9.

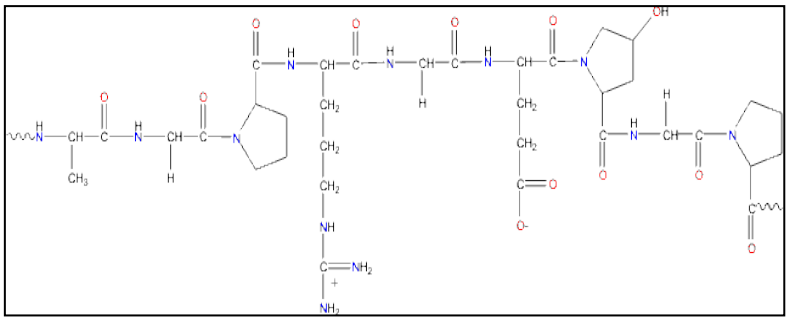

Figure.1.9. Chemical structure of Gelatin [75].

The mechanical properties of polymeric implants depend on several factors, including the composition and structure of the macromolecular chains and their molecular weight. Compared to ceramic and metals, polymers have much lower strength but they can be deformed to a greater extent before failure [76]. Table 1.10 shows some of the mechanical properties of selected polymeric biomaterials. Ultra high molecular weight polyethylene is used for bearing surface in hip and knee replacements.

Table.1.10. Mechanical properties of polymers [77].

Polymers	***Tensile strength (MPa)***	***Young's Modulus E (GPa)***	***% Elongation***
Polymethylmethacrylate	30	2.2	1.4
Nylon 6/6	76	2.8	90
Polylactic acid	28-50	1.2-3	2-6
Polypropylene	28-36	1.1-1.55	400-900
Polytetrafluoroethylene	17-28	0.5	120-350
Silicone rubber	2.8	Up to 10	160
Collagen	141.2-85.7	5-11.5	250-450
Chitin	0.0650	0.0001098	–
Alginate	71 ± 9	0.85 ± 0.08	–

Current applications of biomedical polymers include vascular grafts, heart valves, artificial hearts, contact lenses, intraocular lenses, sutures, adhesives. Table 1.11 shows some of the polymers and their uses.

Table.1.11. Examples of biomedical applications of polymers [78].

Applications	Polymers
Cardiovacular implants	Polyethylene, Polyvinyl chloride (PVC), polyester, silicone rubber, polytetrafluoroethylene
Orthopedic implants	Ultra-high-molecular-weight polyethylene (UHWMPE), polymethylmethacrylate
Drug release	Polylactide-co-glycolide
Tissue engineering	Polylactic acids, polyglycolic acid, Polylactide-co-glycolide

1.7 Summary

As it is evident from the above discussion, each material type has advantages and disadvantages and a combination of two or more materials would result in a final product with much improved characteristics in terms of bioactivity and desired mechanical properties. As bone chemically consists of an organic (predominantly collagen) and inorganic (biological apatite) phase, a combination of natural or synthetic polymer and a calcium phosphate ceramic in the form of composite or hybrid construct is a strategy that is currently used to create tissue engineering scaffolds for neo bone tissue regeneration.

CHAPTER # 2

Literature Review

The secret of getting ahead is getting started.
- Mark Twain

2.1 Introduction

Generation of neo bone and cartilage by transplantation of autogenous cell is considered as one of the most promising techniques in orthopedic surgery and biomedical engineering [79]. Treatment concepts based on these techniques would eliminate problems of donor site scarcity, immune rejection and pathogen transfer. Cells such as Osteoblasts, chondrocytes and mesenchymal stem cells derived from the patient's hard and soft tissues can be expanded by *in vitro* culture, and then seeded onto a scaffold that will slowly degrade and resorb as the tissue structures grow *in vitro* or *in vivo*. The scaffold or three-dimensional (3-D) construct provides the necessary support for cells to proliferate and maintain their differentiated function. The architecture of the scaffold defines the ultimate shape of the new bone and cartilage. Several scaffold materials have been developed and investigated for tissue engineering bone and cartilage including hydroxyapatite (HAp), bioactive glass,β-TCP and natural polymers such as collagen and chitosan. Several reviews have been published on the general properties and design features of biodegradable and bioresorbable polymers and scaffolds [80]. The aim of this review is to complete the information collected so far, with special emphasis on the evaluation of biomaterials and their properties which are of specific interest in tissue engineering based strategies of bone and cartilage tissues.

2.2 Stem Cells for Tissue Engineering

Stem cells are playing a major role in tissue regeneration and orchestrate tissue remodelling. Multilineage differentiation ability of mesenchymal stem cells (MSCs) makes them potential cell source for tissue regeneration applications [81]. The various sources to obtain MSCs include placenta, umbilical cord blood (UCB), blood, adipose tissue and bone marrow. Depending upon ease of handling and considering it as cheaper hospital waste product, UCB is considered as one of the promising sources for the isolation of MSCs [82]. Stem cells and their usage for curing tissue related defects/diseases are expected to continue as a foremost area of development for successful tissue engineering applications.

2.2.1 Embryonic stem cells

Embryonic stem cells (ESC) are derived from the inner cell mass of blastocyst from which the embryo derive and develop. The unique properties of the embryonic stem cells include their self-renewal potential and capacity to differentiate via precursor cells. ESC has the differentiation ability to adipocytes , chondrocytes , neuron , hepatocytes and osteocytes [83].

2.2.2 Adult stem cells

Apart from ESC, adult stem cells (ASC) are also considered as the most potential cell source for tissue engineering. These cells can be derived from bone marrow, periosteum, muscle, fat and skin. The prime role of ASC is to maintain and repair the tissue in which it is found [84].

2.2.3 Mesenchymal stem cells (MSCs)

Mesenchymal stem cells (MSCs) also known as somatic cells are undifferentiated and present in any tissue or organ. These cells are of mesodermal origin and develop into various connective tissue types like blood, muscle, bone, cartilage, tendon, and ligament [85]. These cells have the capacity of self-renewal and can differentiate into specialized cell types of different tissues. MSCs can be easily isolated, cultured and expanded under *in-vitro* conditions. MSCs, under culture conditions possess morphology similar to fibroblasts like spindle shape and exhibit good affinity to adhere over the tissue culture substrate. So, MSCs are good choice for tissue engineering applications including cell based therapies.

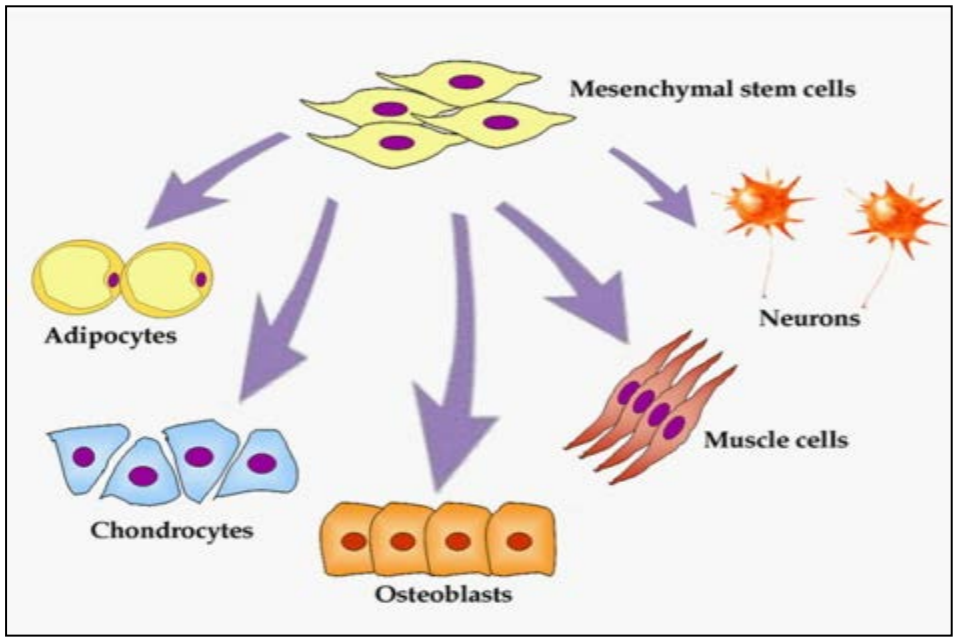

Figure.2.1. Mesenchymal stem cells differentiation in osteogenic, chondrogenic, adipogenic and neuronal lineages [86].

2.3 Scaffold

Scaffold is an artificial ECM which is vital to enable the cells to produce specific tissues of desired shape, size and functionality, therefore scaffold design and fabrication are the major areas of biomaterials research and important subjects to research related to tissue engineering and regenerative medicine [87]. The scaffold behaviour is heavily dependent on the several design variables such as microstructure, pore size and porosity, mechanical properties and

surface chemistry. Scaffold microstructure should mimic native tissue structure containing extracellular matrix for successful tissue regeneration. It should possess sufficient porosity and the pores should be well interconnected for transport of nutrient and waste [88]. While tissue regeneration is in progress, influx and efflux of nutrient and toxic by product through diffusion is limited to 100–200 μm and therefore, scaffold should have enough porosity so that cells in the scaffold can reside within 200 μm of capillary transports . Besides, scaffold should have a pore size depending on type of tissue engineering. For bone, muscle and skin, the required pore sizes are 100-300 μm, 100-200 μm and 20-120 μm respectively [89]. Another important aspect of scaffold designing is consideration of its mechanical properties. The scaffold must possess adequate mechanical properties to withstand stress and physiological load and mediate cues for new tissue regeneration. Generally, scaffold's mechanical properties should be similar to mechanical properties of corresponding tissues for which the scaffold is intended to. Surface chemistry of the scaffold is also important and should induce cell attachment, proliferation, migration and differentiation. Moreover, surface of the scaffold should possess specific functional groups for biomolecule attachment and mediate signalling cues for tissue regeneration. The topology of scaffold should be able to guide the orientation of cells for effective cell based construct formation. Scaffold materials should be endowed with some of the above properties and therefore, material selection is very important for intended tissue engineering using scaffolds.

2.4 Scaffold Fabrication Techniques

To engineer desired functional tissues and organs successfully, the scaffolds have to be designed to facilitate cell distribution and guide tissue regeneration in three dimensions. The potential for scaffolding techniques in spectrum of tissue engineering are still in their burgeoning stage and need to be established further to achieve excellence. Each method is unique in terms of its principle and working conditions. Depending upon the prerequisite requirement and application, fabrication techniques can differ. Various method currently in use for scaffold fabrication include electro spinning, phase separation, solvent casting, freeze drying, gas foaming, rapid prototyping [90] ,which are described below.

2.4.1 Particulate-leaching techniques

Particulate leaching is a technique that has been widely used to fabricate scaffolds for tissue engineering applications [91]. Briefly, porogen such as salt is first ground into small particles and those of the desired size are transferred into a mold. A polymer solution is then cast into the salt-filled mold and freezed. The freezed samples were then washed in a non-solvent but

solvent for porogen. After the evaporation of the solvent, the salt crystals are leached away using water to form the pores in the scaffold. The process is easy to carry out. The pore size and total porosity can be controlled by the size of salt crystals and salt/polymer ratio. However, certain critical variables such as pore shape and inter-pore openings can not be controlled. To overcome these shortcomings, new techniques are being developed.

2.4.2 Gas foaming

Gas foaming has been commonly employed to produce microcellular foams of thermoplastic polymers [92] such as polymethyl methacrylate and polystyrene, but only in 1994 Mooney *et al.* applied this method for the production of PLA50GA50 scaffolds for tissue engineering [93]. Since then gas foaming has become an appealing technique for fabricating microporous scaffolds.

2.4.3 Lyophilization

Lyophilization or freeze drying is one of the most promising techniques to fabricate microporous scaffold where scaffolding materials were dissolved and cast in mold followed by freezing and drying at lower temperature at low vacuum. Finally, polymer solution separates into two phases, a polymer-rich phase and a polymer-lean phase. After the removal of solvent, the polymer-rich phase solidifies and 3D porous scaffold is obtained. Phase-separation techniques have been used to fabricate porous membranes for filtration and separation by the following two methods [94].

2.4.3.1 Solid-liquid phase separation

Solid-liquid phase separation can be achieved at lower temperature to induce solvent crystallization from a polymer solution. And this process is defined as a solid-liquid phase separation (solid phase formation in a liquid phase). After the removal of the solvent crystals (sublimation or solvent exchange), the space taken by the solvent crystals becomes pores. This technique can be used to fabricate scaffolds from many types of polymers and polymeric composite materials [95].

2.4.3.2 Liquid-liquid phase separation

Liquid-liquid phase separation of a polymer solution occurs when temperature of the solution is reduced below upper critical solution temperature. When such a process leads to the formation of a bi-continuous structure (both the polymer-rich and polymer-lean phases are continuous), a scaffold with an open-pore structure is formed after the removal of the solvent.

For example, a mixture of di-oxane and water has been used for liquid-liquid phase separation to fabricate PLA and PLGA scaffolds [96].

2.4.4 Electro-spinning

Electro spinning was first introduced in the early 1930s and used to fabricate industrial or household nonwoven fabric textile products [97]. The technique has been further improved over the past decade to process biodegradable and/or biocompatible polymers in order to fabricate fibrous fabrics with an average fiber diameter at micrometer or nanometer scales for tissue engineering scaffolds. To form such fibers using electrospinning, a polymer solution is forced through a capillary, forming a drop of polymer solution at the tip. As the polymer jet travels through the air under applied high voltage, the solvent evaporates and a nonwoven polymer fabric is deposited on the target. However, there are challenges in using this technique to fabricate complex three-dimensional scaffold shapes and internal pore networks.

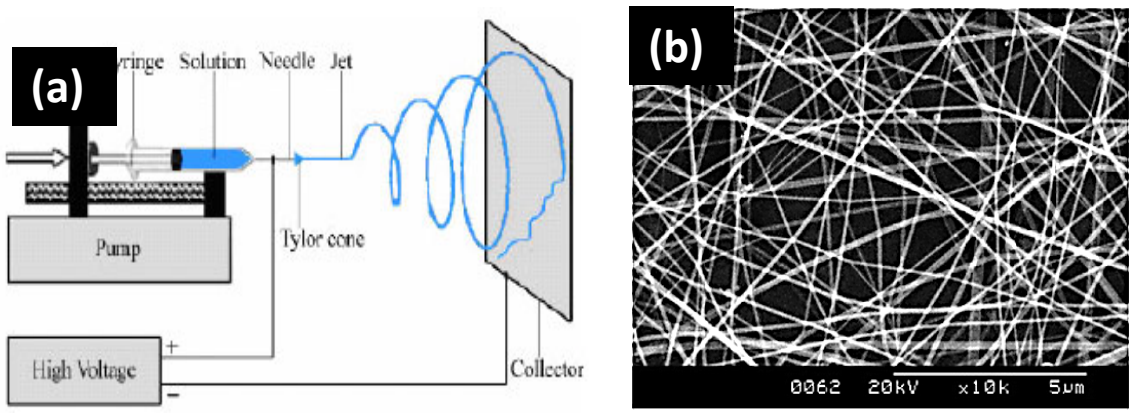

Figure.2.2. (a)Schematic diagram of polymer nanofiber formation using electro spinning method [32].(b)SEM image of electrospun nanofiber [54].

2.4.5 Solid freeform fabrication techniques (SFFT)

SFFT, such as fused deposition modeling or rapid prototyping, have been successfully employed to fabricate highly reproducible artificial ECM scaffolds with fully interconnected porous networks [98]. Using digital data produced by an imaging source such as computer tomography or magnetic resonance imaging accurate design of the scaffold structure can be executed. Solid free form (SFF) manufacturing coupled with conventional foam scaffold fabrication procedures (phase separation, emulsion-solvent diffusion or porogen leaching) might be used to create frameworks with controlled microscale and macroporous structures. Such biomimetic internal structures may demonstrate significant impact for multi tissue and structural tissue interface engineering [99].

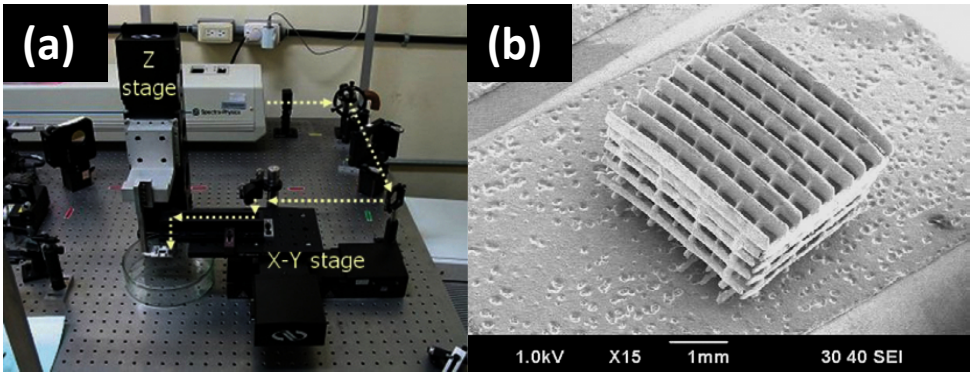

Figure.2.3. (a) Photograph of the newly developed scaffold fabrication system using the axiomatic approach. (b) SEM images of fabricated microstructure using the newly designed fabrication system [100].

Table.2.1.Fabrication routes for 3D composite scaffolds with high pore interconnectivity and their advantages and disadvantages.

Fabrication route	Advantages	Disadvantages
Thermally induced phase separation (TIPS) [101]]	High porosities (95%) Highly interconnected pore structures. Anisotropic and tubular pores possible. Control of structure and pore size by varying. preparation conditions.	Long time to sublime solvent (48 hours) Shrinkage issues. Small scale production. Use of organic solvents.
Solvent casting/particle leaching[102]	Controlled porosity Controlled interconnectivity (if particles are sintered)	Structures generally isotropic Use of organic solvents
Solid free-form [103]	Porous structure can be tailored to host tissue. Protein and cell encapsulation possible. Good interface with medical imaging.	Resolution needs to be improved to the micro-scale. Some methods use organic solvents.
Microsphere sintering [104]	Graded porosity structures possible Controlled porosity Can be fabricated into complex shapes	Interconnectivity is an issue Use of organic solvents
Scaffold coating [105]	Quick and easy	Clogging of pores, sometimes organic solvents used, coating adhesion to substrate can be too weak

2.5 Structural Design

It is very much accepted that a scaffold with a permeable structure favours tissue ingrowth, the mass-transportation of supplements and osteointegration with the host bone, and in addition long-term stable fixation of bone inserts [106]. To encourage recovery of damaged bone tissue desired bone tissue regeneration, the parameters for structural configuration of the scaffold such as porosity, pore size and shape, the orientation of the interconnected channel and a progressive control of structure are often considered.

2.5.1 Porosity

Porosity is characterized as the percentage of void space in a solid [31] and it is a morphological property independent of the material. Pores are fundamentals for bone tissue development since they permit relocation and proliferation of osteoblasts and mesenchymal cells . Moreover a permeable and porous surface enhances mechanical interlocking between the scaffold biomaterial and encompassing normal bone, giving noteworthy mechanical stability at this basic interface. The most widely recognized strategies used to make porosity in a biomaterial are salt leaching, gas foaming, phase separation, freeze-drying and sintering depending on the material used to fabricate the scaffold. In hydroxyapatite/chitosan-gelatin composites (with most pores between 300 and 500 μm) porosity can be increased by decreasing the chitosan gelatin concentration and increasing the chitosan gelatin/hydroxyapatite ratio [107]. These scaffolds supported the proliferation and mineralization of rat calvarial osteoblasts in vitro [58]. Higher porosity did not affect cell attachment, but resulted in increased cell proliferation, since pore space increased with porosity and facilitated transport of oxygen and nutrients [108].

2.5.2 Pore Size

The impact of various porosities and pores sizes on the degree of osteogenesis in vitro has been demonstrated both with osteoblasts and undifferentiated cells. In composites of apatite and collagen with pores ranging from 50 to 300 μm, higher apatite contents diminished the porosity, yet not significant contrast were observed in MC3T3-E1 osteoblast proliferation [109]. A extremely fascinating part of the impact of pore size on bone regeneration, is the effect of the progression toward osteogenesis. Regular honey-combed like hydroxyapatite scaffolds with small (90–120 μm) and large tunnel (350 μm) diameters were utilized for BMP-2 delivery and were implanted subcutaneously in rats [110]. In small diameter tunnels

scaffold chondrogenesis happened before osteogenesis; conversely, in tunnels with large diameter bone was formed directly.

2.6 Mechanical Properties

Although higher porosity and pore size encourage bone ingrowth, however the outcome is a reduction in mechanical strength, since this compromises the structural integrity of the 3D matrix. In tissue engineering applications, permeable scaffolds with higher porosity must have adequate mechanical quality to hold their underlying structures after implantation, especially in the reconstruction of hard, load-bearing tissues, for examples, bones and ligaments. The structure must not pack together under physiological pressure, which causes damage cells inside the scaffold.

Chitosan based sponges with a pore size of 100 μm were developed inside hydroxyapatite/β-tricalcium phosphate 3D scaffolds with macropores between 300 to 600 μm having both compressive modulus and yield stress increased about four times [111]. Porous foams like structure were fabricated after sintering poly(lactide- co-glycolide) microspheres and increase in in larger median pore size from 72 to 164 μm had no significant effect on total porosity (>30%) [112]. Similarly, higher porosity leads to the lower mechanical properties of porous poly (L-lactide-co-D,L-lactide) scaffolds, with compressive strength decreased from 11.0 to 2.7MPa and modulus from 168.3 to 43.5MPa [113].

The stability of various biomaterial based scaffold after implantation depends on factors such as strength, elasticity, absorption at the material interface and chemical degradation. Therefore, the investigation of mechanical properties such as compressive strength is of primary importance in determining the suitability of the designed scaffold. Firstly, it should be considered that at the end the scaffolds would be utilized in the physiological environment where the primary loading is compressive in case of bone or cartilage. Secondly, the presence of numerous tiny voids in the porous solid poses significant structural flaws to magnify the effect of crack propagation in stretching or bending. Therefore, the majority of research findings on tissue engineering scaffolds are focused on their compressive properties when reporting scaffold's mechanical properties.

The deformation behaviours of porous solids under compressive loads for honeycombs are shown in Figures 2.4 and 2.5. The mechanical properties of honeycombs are classified in two groups in-plane properties and out-of-plane properties. The in-plane properties are those relating to loads applied in the X1 and X2 plane. Responses to loads applied to the faces normal to X3 are referred to as out-of-plane properties.

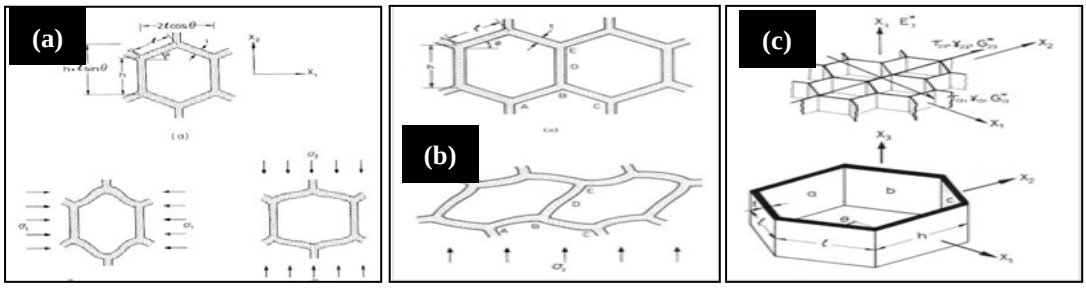

Figure.2.4 In-plane compression of honeycomb pores; (a) Initial elastic bending of pore walls, (b) Buckling of pore edges at higher stress levels and (c) Out-of plane compression of honeycomb pores.

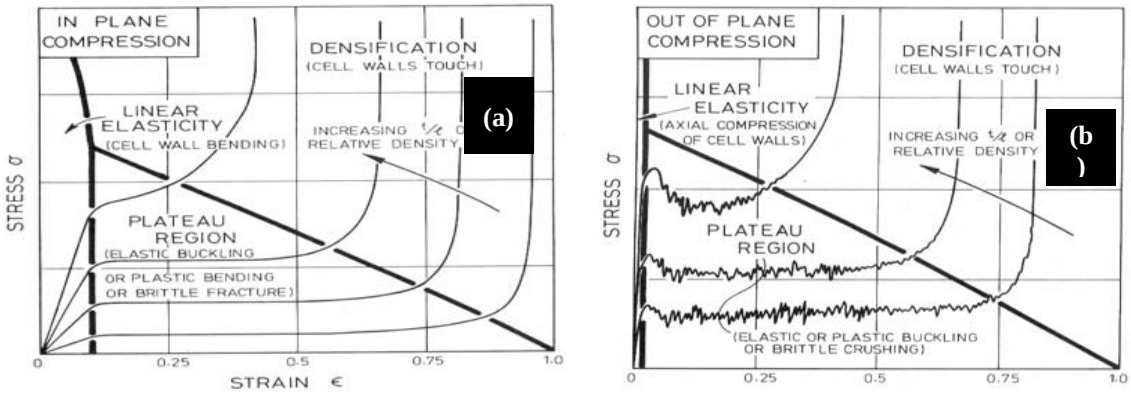

Figure.2.5. A schematic diagram for a honeycomb loaded in compression, showing linear elastic, collapse and densification regimes, and the way the stress-strain curves changes with t/l; (a) compressed in X1 – X2 plane, (b) compressed in axial (X3) direction [114].

When a honeycomb is compressed in-plane, the pore walls at first bend (Figure 2.4a), giving linear elastic deformation (shown on stress-strain curves in Figure 2.5a). Beyond a critical strain the pores collapse by elastic buckling, plastic yielding (Figure 2.4b), creep or brittle fracture, depending on the nature of the pore wall material. Pore collapse ends once the opposing pore walls begin to touch each other; as the pores close up, the structure is densified and its stiffness increases rapidly. On loading the honeycomb out-of-plane, the pore walls experience compression under both axial and bending stresses. The moduli and collapse stresses are much larger. Figure 2.5b shows the family of curves of honeycombs with different relative density, compressed out-of-plane.

2.7 Composite scaffold material

The term composite is normally considered for materials that contain two or more different constituent materials at larger scale. The physical and mechanical properties of these materials are modified fundamentally, and henceforth, these are more beneficial in comparison with homogeneous material.

Biocomposites can be fabricated using nontoxic material and possesses desirable scaffold properties able to simulate new bone regeneration. Thus, for biocomposites the biological compatibility appears to be more important than any other type of compatibility [115]. Thus, bioceramics based biocomposites and hybrid functional biomaterial appears to be new for efficient tissue regeneration ability. The most common properties from the bioorganic and inorganic domains are combined in biocomposites and have been summarized in Table 2.2.

Table.2.2. General respective properties from the bioorganic and inorganic domains, to be combined in various composites and hybrid materials [116].

Inorganic	Bioorganic
Hardness, brittleness	Elasticity, plasticity
High density	Low density
Thermal stability	permeability
hydrophilicity	hydrophobicity
High refractive index	Selective complexion
Mixed valance state	Chemical reactivity
strength	bioactivity

Various human tissues such as human hard tissues like bone, consist of inorganic-organic component [117]. In specifically, the property of a composite material relies upon the size and morphology of the heterogeneities, relative proportion of the components and nature of interfaces among the constituents. Among composite materials, bioceramics and biopolymer based composites have been found to possess significant biological characteristic and found to be suitable for tissue engineering applications as a biomaterial. The important properties and applications of some of the composites are summarized in Table 2.3.

Table.2.3. Important properties and applications of the nano composite.

S. No.	Name of the composite	Properties	Application	Reference
1.	Nano HAp/ collagen	HAp nanocrystals are regularly aligned along collagen fibrils	Synthetic bone materials in Medical applications[118]	Kikuchi *et al.* 2004
3.	HAp/SA nanocomposite beads	The well-swelling, drug loading and controlled release behaviour	Drug- controlled release[119]	Zhang *et al.* 2009
5.	Nano HAp/ Chitosan composite scaffold	Good biocompatibility and sufficient porosity	Bone tissue engineering[120]	Kong *et al.* 2005
6.	Chitosan/ nanocrystalline calcium phosphate	Increased proliferation of osteoblast cells and improved mechanical strength	Bone regeneration[121]	Chesnutt *et al.* 2009
7.	HAp/chitosan–gelatin (CG) composite	Enhanced protein and calcium ion adsorption and improved initial cell adhesion and long term growth	Development of human stem cell[122]	Zhao et al. 2006

2.7.1 Synthetic biopolymer/CaP composite scaffold

Synthetic polymer such as Poly(glycolic acid) (PGA), poly(lactic acid) (PLA), and their copolymers poly(lactic acid-co-glycolic acid) (PLGA) are commonly considered in tissue engineering to fabricate artificial ECM [123]. These polymers degrade through hydrolysis of the ester bonds that act as backbone of polymer structure [80].

Furthermore various linear aliphatic polyesters, such as poly(ε-caprolactone) (PCL) [124] and poly(hydroxy butyrate) (PHB), are also commonly considered in tissue engineering research. However, the degradation rate of PCL is significantly slower rate than PLA, PGA, and PLGA [125]. Thus slow degradation significantly affects utility of PCL for tissue engineering applications, however suitable for long-term implants and controlled release of functional molecules. Therefore, PCL-based copolymers are also synthesized to improve degradation properties.

Porous 3D scaffold of calcium phosphate ceramics with interconnected macropores (> 200 μm), micropores (~5 μm) and high porosities (~ 80%) have been produced by firing polyurethane (PU) foams coated with calcium phosphate bioceramic at 1200°C [126]. The micropores of the developed scaffold were infiltrated with poly (lactic-co-glycolic acid)

(PLGA) to achieve an interpenetrating bioactive ceramic/biodegradable polymer composite structure. Miao et al. [127] reported development of highly porous HA/TCP composite scaffolds having 87% porosity, infiltrated with PLGA to form bioceramic-polymer interpenetrating microstructures. However, in these composites PLGA provides significant improvement of the compressive strength. Furthermore, polycaprolactone (PCL) based scaffold also reported to be coated with HA and possess appropriate cell supportive property [128]. Chen et al. [129] demonstrated fabrication of Bioglass®-based scaffolds coated with PDLLA that provided appropriate osteogenic potential for healing of bone damage. Polyhydroxyalkanoate (P(3HB) has also been investigated for preparation of scaffolds for tissue engineering application [38]. Bretcanu et al. [130] reported the use of natural bacteria derived P(3HB) to infiltrate into 45S5 Bioglass® scaffolds. The mechanical properties of these novel scaffolds were investigated it was shown qualitatively that the work of fracture increased dramatically with the P(3HB) coating [131].

2.7.2 Natural Biopolymer/Bioactive ceramic Based Composite

Because of excellent biocompatibility and biological characteristics that are similar to human bone , natural biopolymer and CaP based composites were investigated extensively. Agarose, alginate, silk, hyaluronic acid, collagen, chitosan, gelatin are some of the well known natural biopolymers that have been used for tissue engineering application. Agarose**,** a polysaccharide, was used for making injectable scaffold that provided a three-dimensional environment to maintain the round shape of the chondrocyte. Furthermore, BCP (HA + β-TCP)/agarose macroporous scaffolds with high degree of interconnected open porosity and tailored pore size were prepared for application in bone tissue engineering [132]. Biocompatibility of this BCP/agarose system was studied using mouse L929 fibroblasts and human SAOS-2 osteoblasts during different colonization times [133]. In another study, porous HA/ alginate composites based on hydrogels were prepared both biomimetically [134] and using a freeze-drying technique [135]. The prepared HA-alginate scaffold exhibited high degree of.*in vitro* biocompatibility and controlled biodegradability. Osteoinductive properties of porous hybrid scaffolds prepared from β-TCP, alginate-gelatin was reported elsewhere [136].

A wide range of properties of silk fibroin such as their size, shape, crystallinity and mechanical properties[137]. A functionally graded HA/silk fibroin biocomposite was prepared by pulse electric current sintering [138, 139] that showed excellent mechanical strength and osteoconductivity. The 3D mesh of fibrin sealant was found to interpenetrate the macro- and microporous structure of calcium orthophosphate ceramics [140]. Le et al

proposed that the physical, chemical and biological properties of calcium orthophosphate bioceramics and the fibrin glue might cumulate in biocomposites suitable for preparation of advanced bone grafts [141]. Hyaluronic acid and derivatives have been used as therapeutic aids in the treatment of osteoarthritis as a means of improving lubrication of articulating surfaces and thus reducing joint pain [142]. Chitosan-gelatin-hyaluronic acid based scaffolds were found to be suitable for preparing a bilayer skin substitute[143].

Gea et al.[144] prepared HAp/chitin composite materials with HAp content varying between 25% to 75% wt% and studied in vivo bone regeneration ability in rat. Moreover, Lee et al[145] proposed in their research the use of chitosan/TCP sponges as tissue engineering scaffolds for bone regeneration. Bioglass-chitosan composite also exhibited the potential to support the growth of osteoprecursor cells in vitro and to favour differentiation of osteoblast after stimulating the synthesis of phenotypic markers such as alkaline phosphatase, Type I collagen, and osteocalcin [146]. Table 2.1 shows the properties of various CS based composite in various forms such as 3D porous scaffold, fibrous, films etc developed for tissue engineering applications.

Table 2.4. Chitosan-bioactive ceramic based composite scaffolds with enhanced properties.

Composite	Out come
CS/ALRGDN-peptide	Promoted biocompatibility[147]
CS/Gelatin/β-TCP	Increased osteoblast attachment and proliferation[148]
CS/Alginate/Carboxy methyl cellulose	Increased compressive modulus[149]
CS/RGD/ UV cross-linking	Increased proliferation [GAG and DNA][150]
CS/nHAp	Increased mechanical strength[151]
CS/PLGA	Increased stiffness of scaffold, Biocompatibility[152]
CS/gelatin/TCP/Glutraldehyde	Increased cell spreading[153]
CS/PLAGA/Fibrin	Increased mechanical strength, Osteoblast cell proliferation[154]
CS/Fibroin	Enhanced stiffness and biocompatibility[155]
CS/Ca_3P0_4	Increase in cell attachment, proliferation and phenotypic expression of osteoblastic markers[156]

HAp/collagen composite materials are promising candidates for bone replacement purposes because of their resemblance to bone in point of view of their bioactivity and biodegradability. Chang et al [157].reported a simple method to produce CaPs/collagen composites by adjusting the reaction conditions and the ratio of components. The mechanical

properties of these types of composites are still very poor and requires further improvement for its effective use in bone tissue engineering [158]. Collagen based implants are crosslinked to improve its mechanical properties and regulate cellular behavior when they are used in as processed form to prepare scaffolds [159]. Various crosslinking treatments including physical, [160], chemical [161],enzymatic [162] and combination treatments have been developed to tailor their mechanical and degradation properties. A composite scaffold formed by combining gelatin with bioceramics can yield tailored degradation rates, while also having improved biological and mechanical and physical properties. Yaylaoglu et al [163] developed a CaPs/gelatine composite implant that released drugs and growth hormone into the implant site to assist in bone healing.

Porous gelatin/collagen scaffolds especially gelatin sponges containing bioceramic particles were synthesized by the lyophilisation of a gelatin/calcium phosphate mixture [164]. Usually, gelatin/collagen scaffolds are highly cross-linked for better mechanical stability, but this can reduce the biocompatibility since crosslinking agents like glutaraldehyde leads to a cytotoxic reaction [165]. To prevent this limitation, a colloidal β-TCP/collagen composite was prepared for which further treatment was not required [166]. Further, collagen type I was also used as a matrix for CaP mineralization to obtain a collagen/CaP composite [167]. In another study, a 10% gelatin composite scaffold was formed by soaking a macroporous HAp to allow gelatin penetration to the bulk of the ceramic [168]. To maintain biocompatibility of the scaffold, cross-linker was used at a low concentration to prevent diffusion of gelatin out of the scaffold.

With the hopes of increased cytocompatibility and elucidation of desirable cellular response, a porous chitosan/gelatin network scaffold was developed for cartilage tissue engineering and artificial skin [169].Further, biomimetic 3D HA/chitosan–gelatin network composite scaffolds were prepared for bone tissue engineering [170]. The aim of this work was focused on improving the mechanical and biological properties of chitosan based scaffolds through incorporation of bioceramics such as hydroxyapatite (HA), β-tricalcium phosphate, calcium phosphate [171] and biopolymers like gelatin [172], alginate [173] or inorganic material such as wollastonite [174]. Incorporation of calcium phosphate into the chitosan matrix improved biocompatibility and hard tissue integration and assisted in tailoring degradation and resorption kinetics.

A biodegradable composite scaffold was developed using β-tricalcium phosphate (β-TCP) with chitosan (CS) and gelatin (Gel) in the form of a hybrid polymer network (HPN) via co-

crosslinking with glutaraldehyde. The macroporous composite scaffolds exhibited different pore structures with improved compressive modulus from 3.9-10.9 MPa.

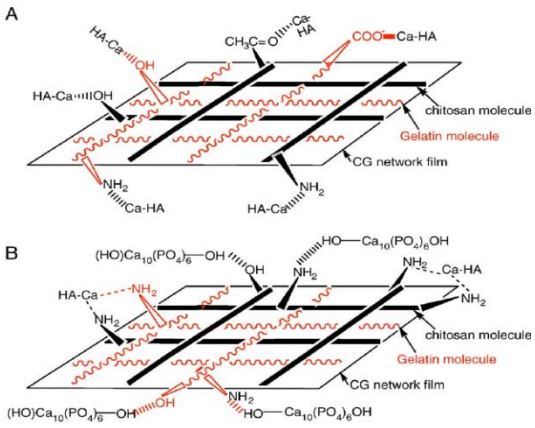

Figure.2.6. Possible interactions between a chitosan-gelatin (CG) network and HA crystals in HA/CG biocomposites: (A) In the case of a nano-dimensional HA (nHA); (B) In the case of a micro-dimensional HA (mHA) [175].

Another challenging aspect that needs to be focussed is the fabrication of scaffolds using a simple and cost effective method. Freeze-drying is one of the simplest scaffold development techniques that is time and energy saving [176].The amount of residual solvent and formation of surface skin is limited freeze-gelled scaffolds that helps in better growth of cells cultured on these [176]. Furthermore, scaffolds prepared using freeze drying technique usually possess interconnected porosity and better mechanical properties [177]. Earlier research suggests that freeze drying method is useful in developing 3D scaffolds from various biopolymers like collagen [178], carboxy methyl cellulose [179], poly (d,l-lactic-co-glycolic acid) [180], chitosan [181], pectin [182] and silk fibroin [137]. Chitosan can be easily modified in combination with other bio-materials to achieve required mechanical and surface properties of scaffold [183].

2.8 Challenges and Opportunities

2.8.1 Mechanical integrity of porous scaffolds

Till date manmade porous scaffolds suffer from insufficient mechanical integrity and various other properties relevant for bone tissue engineering. For comparison, data of elastic modulus and the compressive strength of dense bioactive ceramic, biodegradable polymers, cancellous and cortical bone and their porous monophasic scaffolds and composites were taken from Ref [184]. It can be found that some dense polymers match cancellous bone properties and

approach cortical bone properties. Moreover, mechanical properties of some of bioactive ceramics closely resemble the properties of cortical bone as well. Porous scaffolds however are at least one order of magnitude weaker than cancellous bone and orders of magnitude weaker than cortical bone.

2.8.2 In vitro degradation

Since tissue engineering aims at regeneration of new tissues, biomaterials are expected to be degradable and absorbable with a proper rate to match the speed of new tissue formation. The degradation behaviour has a crucial impact on the long-term performance of a tissue engineered cell/polymer construct. The degradation kinetics may affect arrange of process, such as cell growth, tissue regeneration, and host response. Gelatin containing chitosan scaffold has faster degradation rate due to the hydrophilicity of gelatin [185]. Bioglass and Calcium phosphates have been introduced to retard the degradation [186].

2.8.3 In vitro and in vivo characterization

Though a good number of *in vitro* and *in vivo* studies have already been carried out for biodegradable polymers and bioactive ceramics separately, in vitro studies for polymer/ceramic composites have just been started recently. Limited numbers of composite systems have been investigated in *in vivo* up to date. More research needs also to be directed at assessing the suitability of the reviewed bioactive composite scaffolds in hard-tissue engineering. Further investigations of the effect of dissolution products from the bioactive phase on vascularization and in vivo new tissue growth need to be carried out.

2.9. Discussion and Future Aspects

Bioactive ceramic based composite will be promising biomaterial for bone tissue engineering. The combination of bioactive ceramic such as HAp, bioactive glass and β-TCP with natural biopolymer like gelatin and chitosan is one of the best approaches to construct artificial bone. Combination of biopolymer with bioactive ceramic can result in the expected three dimensional scaffolds as bonegraft substitute with sufficient bone tissue construct properties such as mechanical strength, pore size and osteoconductivity. However, cell-material interaction, mechanical strength and biological response of bioactive ceramic based nanocomposites need to be analyzed in detail and further be investigated for their biomedical significance. In addition, clinical studies are needed to be performed on the bioactive ceramic based composite scaffold for further biophysichochemical implications.

CHAPTER # 3

Scope of the Work

We should not give up and we should not allow the problem to defeat us.

A. P. J. Abdul Kalam

3.1 Future Prospects of Tissue Engineering

Tissue engineering is an offset of regenerative medicine that can cater to the need of millions of patient's worldwide suffering from various tissue diseases. Though tissue engineering is promising as an exciting industry with a potential market, it is still facing numerous challenges like the establishment of a quality control program that can ensure the safety of the ultimate tissue engineered bone or other implant [17]. Recently, efforts to address these issues are on track and this technology is expected to have a major boom in cell based remedies. Thus, this promising wing of future medicine will enable us to enlighten lives of needful patients and prevail as an alternative to traditional bone and other grafting methodologies.

3.2 Current Status of Bone Tissue Diseases and Defects

Bone defects and diseases because of consequences of trauma, injury and infections are of major concerns in the field of health sector [187]. It is estimated that more than 50% of all osteoporotic hip fractures will occur in Asia alone by the year 2050 [188]. In India, the number of osteoporosis patients alone has been expected to increase to 46 million by 2023. Surgical reconstruction, transplantation (auto and allografts), drug therapy, artificial prostheses and medical devices are current clinical treatment options for various tissue related disorders including bone tissue [189]. These treatment options have disadvantages such as severe pain, risk of infections, hematoma, immune rejection, donor site morbidity, transmission of viral (HIV, hepatitis-B) and prion proteins [190]. In this context, in recent years bone tissue engineering has emerged as an appropriate strategy to repair and/or replace damaged and/or diseased bone tissue defects.

3.3 The main hypotheses of this thesis

Since natural bone matrix is a composite of natural apatite and collagen, a scaffold material that can closely mimic the natural extracellular matrix of bone can be a potential candidate for making artificial bone substitute material for bone replacement. Gelatin being a dehydrated derivative of collagen can ideally suit as a matrix for such scaffold material. Apart from gelatin, another natural polymer chitosan can closely resemble the structure of GAGs present in extracellular matrix of bone. Thus combination of gelatin and chitosan can play an useful role to form a bone scaffold where bone cell can find an appropriate environment for proliferation and differentiation. Moreover, incorporation of bioactive nanoceramic phase into gelatin-chitosan based matrix is important not only to serve as

reinforcing particulates of polymer based scaffold, but also for enhancement of mineralization of extracellular matrix, mesenchymal stem cell attachment and its differentiation into bone cell. The bioceramic phases such as hydroxyapatite, β- tricalcium phosphate and bioactive glass are supposed to aid to mineralization and subsequent differentiation of mesenchymal stem cell into matured osteoblast by releasing different ions in the surrounding environment that triggers enhanced activity of bone cells. Here we hypothesize, that by judicious variation in composition of gelatin, chitosan and bioactive nanoceramics, we can enhance mechanical, physicochemical and biological properties of the prepared scaffold with ideal porosity and pore size distribution suitable for osteoinduction, bone tissue in growth, and angiogenesis.

3.4 The specific objectives

i. Systematic investigation on the effects of compositional variation on the microstructure, mechanical strength of prepared scaffolds with varying composition.

ii. Study on physico-chemical, mechanical and in-vitro biological properties of the prepared composite scaffolds with variation in bioceramic phase content.

iii. Comparative *in vitro* and *in vivo* analysis on biocompatibility and osteogenic potentiality of the developed composite scaffolds prepared using nanophasic hydroxyapatite, β-tricalcium phosphate and 58S bioactive glass as reinforcing particulate in gelatin, chitosan matrix.

iv. Investigation on cryogenic treatment on the prepared gelatin based scaffolds in retention of mechanical strength and bioactivity under physiological environment.

v. To develop gelain-chitosan-hydroxyapatite/ β-TCP / 58S bioactive glass based composite scaffolds with improved biological and mechanical properties.

3.5 The scope of the research work is enumerated as follows

1. To optimize relative composition of gelatin, chitosan & bioceramic nanoparticles that will give better physico-chemical properties such as; porosity, pore size distribution, biodegradation and mechanical properties like compressive strength and young modulus of the composite scaffold.

2. Once the composition of the scaffold for better physico-chemical and mechanical strength is optimized, a comparative study on bio-activity, osteogenic potential and protein adsorption behaviour of the scaffold was performed using different bioceramic particles such as: hydroxyapatite (HAp), β-Tri calcium phosphate (β-TCP) and 58s bioactive glass as reinforcing phase in chitosan-gelatin biopolymer matrix.

3. Gelatin being sparsely soluble in water, the mechanical strength of gelatin based scaffold is to deteriorates on exposure to physiological environment due to constant uncontrolled bio-degradation. In this research work, measures have been taken to retard dissolution of gelatin and retain the mechanical strength of gelatin based scaffold within short period of exposure to physiological environment without compromising on its osteogenic potential.

3.6 Dissertation Overview

Chapter 2 provides a general literature review of the nanostructured biomaterials used in tissue regeneration. Emphasis is placed on two aspects: (1) Materials used in fabrication of porous 3D scaffold and fabrication using Freeze Drying and temperature induced phase separation, (2) evaluation of mechanical and biological properties in various 3-D porous scaffolds.

Chapter 4 begins the research part of this thesis with the fabrication of novel Gelatin-Chitosan-Hydroxyapatite (GCH) scaffolds. Here, *in-situ* hydroxyapatite-chitosan nanoparticles were incorporated into Gelatin matrix. The mechanical and biological characterization of the scaffolds were examined and both short term and long term *in-vitro* bioactivity study was reported. This work was published in *Journal of Biomaterial science ,Polymer edition* and *Transaction of Indian Ceramic Society* [17].

Chapter 5 details the development of Gelatin-Chitosan-Bioglass(GCB) scaffold and their mechanical and biological characterization. This work was published in *International journal of biomaterials* and *Transaction of Indian Ceramic Society*.

Chapter 6 deals with the preparation and characterization of Gelatin-chitosan-β-TCP (GCT) scaffold. The composite scaffolds were prepared using freeze drying technique. Physicochemical, mechanical and biological properties were evaluated for 3D porous scaffold. Osteoblast proliferation and differentiation were studied to characterize cellular response on addition of β-TCP nanoparticles. Biocompatibility of these GCT scaffolds was studied in a subcutaneous implantation model.

Chapter 7 presents a comparative study of the mechanical and biological properties of GCH, GCT and GCB composite scaffold. Bioactivities of three different type of scaffolds were compared both in vitro and in vivo using a defect site in rabbit tibia.

Chapter 8 represents the effect of cryogenic treatment on GCB scaffolds on its strength retention capacity in physiological environment.

Chapter 9 summarizes the thesis work with major conclusions and discusses some possible future directions of the research work carried out in this dissertation.

CHAPTER # 4

Development of Gelatin-Chitosan-HAp 3D porous scaffold

The most effective way to do it, is to do it.

Amelia Earhart

4.1 Abstract

Bone tissue engineering, using a porous scaffold material to induce formation of bone from the surrounding tissues has some distinct advantages over autografting and allografting, and it is a rapidly growing alternative approach to heal damaged bone tissue. The current study focuses on fabrication and characterization of hydroxyapatite and natural biopolymer composite scaffold for improving bone repair and regeneration at the sites of musculoskeletal disorder. The porous composite scaffold with varying weight per cent of hydroxyapatite (HAp), chitosan and gelatin was fabricated using freeze drying method. Glutaraldehyde was used as a cross linker between chitosan and gelatin matrix in the polymer based scaffolds. The prepared scaffolds exhibited 3D network of interconnected pores with total porosity varying between 70- 79% and an average pore size between 43- 165 μm. Microstructural analysis using field emission scanning electron microscopy (FESEM) showed an interconnected porous network in the scaffold where HAp-Chi composite nanoparticles were found to be randomly dispersed in the biopolymer matrix. Characteristic IR band for (–C=N–) group observed in IR spectra of the prepared scaffold, indicated crosslinking ability of glutaraldehyde with chitosan and gelatin. An optimum composition with HA: Chi: Gel ratio of 28:42:30 was obtained in GCH30 scaffold with an average pore size of 94 μm and the highest compressive strength. GCH30 scaffold having 78% porosity with pore size distribution between 75–100 μm exhibited a compressive strength of 3.46 MPa, which is within the range of that exhibited by cancellous bone. Thick bone like apatite layer deposition was observed on the surface of the scaffold on immersing it into simulated body fluid (SBF) at 37^{o}C for 7 days. The bioactivity of the scaffold was evaluated after investigating mesenchymal stem cell (MSC)–materials interaction and MTT (3-[4,5-dimethylthiazol-2-yl]-2,5-diphenyltetrazolium bro-mide) assay using cultured MSCs. The scaffold was found to be conducive to MSC's adhesion, proliferation, and differentiation up to 14 days of cell culture. These types of composite scaffolds find application as efficient biomaterial for natural bone tissue regeneration and bone tissue engineering.

4.2 Introduction

Research on biomaterials for bone replacement and bone healing has expanded considerably over the last four decades [191, 192]. In recent years, significant progress has been made in the area of bone replacement to treat the loss or failure of bone. Natural bone consists of organic and inorganic substances [193, 194]. Calcium deficient carbonated apatite is the major component in bone minerals [189, 195-198]. Hydroxyapatite (HAp), the most

commonly used calcium phosphate bioceramic, has excellent biocompatibility and is osteoconductive. It has been successfully used as bone fillers, coating of orthopaedic implant, filler of inorganic/polymer composites, cell culture carrier and so on but the application of pure HAp as structural bioceramic is being limited due to its brittle nature. Moreover, sintered HAp shows lower bioactivity as compared to its poorly crystalline particulate counterpart. In fact, natural bone is a biocomposite, composed of nano-hydroxyapatite (n-HAp) crystals dispersed in collagen matrix. Therefore, in the recent years, development of nano HAp-biopolymer composites has gained much more attention because of their analogy to bone matrix as well as good biological and mechanical performances to meet the specific clinical response. Natural biopolymers have received much more attention in the field of orthopaedic and other biomedical applications due to their excellent biocompatibility and biodegradability. Various kinds of polymer/ceramic composite system such as HAp/collagen [199, 200], HAp/chitosan [201], HAp / collagen / poly (lacticacid) [202], HAp / alginate / collagen [203], HAp / gelatin [198, 203-205] were employed for preparation of scaffolds for bone tissue engineering. A combination of Hap chitosan-gelatin seems to be a very interesting material for preparing bone scaffold as it can mimic natural bone matrix very closely. Chitosan (poly-1,4-D-glucosamine), a partially deacetylated form of chitin, is structurally similar to glycosamino glycan present in the extracellular bone matrix, and exhibits wound healing property [205]. Gelatin as a binding agent or matrix seems to be very attractive because it is derived from collagen and contains a lot of biological functional groups, such as amino acids within its backbone which can enhance cell growth and proliferation. Gelatin not only shows excellent biocompatibility and biodegradability, but also exhibits superior plasticity and adhesiveness, that is essential for developing mechanical strength in the scaffold. Moreover, its degradation rate and mechanical strength can be regulated after cross-linking with suitable cross linker such as glutaraldehyde. Again, uniform dispersion of the bioactive ceramic phase in the polymer matrix is often a critical challenge. Without proper interfacial adhesion between bioceramic and biopolymer, nonuniform phase distribution or segregation of phases and bioceramics agglomerates in different parts of the composite are common problems. To address this, in the present case, finely dispersed HAp–chitosan nanocomposite powder was synthesized which interacted with gelatin matrix through chitosan to develop intimate bonding between particle and polymer matrix and promoted uniform dispersion of HAp nanoparticles throughout the matrix. The aim of this study was to optimize the composition for the development of bioactive bone scaffold with controlled porosity and mechanical strength using gelatin, chitosan, and HAp. Porous HAp–

chitosan/gelatin (HAp:Chi:Gel) scaffold was prepared using lyophilization technique and post-cross-linking with glutaraldehyde that is the most common synthetic cross-linking reagent and can form intermolecular cross-links between protein molecules. These composite bone scaffolds with various compositions were compared in terms of their physical, mechanical properties. This study also assessed MSC's responses to the porous HAp:Chi:Gel bone scaffolds. The investigation represents a successful contribution toward the development of superior scaffolds for bone tissue engineering.

4.3 Materials and Methods

4.3.1 Materials

Chitosan (deacetylation: 85%, medium molecular weight) and gelatin (Type B) were purchased from Sigma Aldrich (USA). Di-ammonium hydrogen phosphate ($(NH_4)_2HPO_4$)and calcium nitrate tetra-hydrate ($Ca(NO_3)_2.4H_2O$) were purchased from Merk (Germany). Glacial acetic acid and ammonia solution (NH_4OH) were procured from LOBA chemical (India). Sodium Chloride (NaCl), Potassium Chloride (KCl), Calcium Chloride ($CaCl_2$), Magnesium Chloride ($MgCl_2$), Di-potassium Hydrogen Phosphate (K_2HPO_4), Sodium bi-Carbonate ($NaHCO_3$), Sodium Sulphate (Na_2SO_4) , glutaraldehyde ($C_5H_8O_2$), ethanol (C_2H_5OH) were procured from Sigma Aldrich (USA).

4.3.2 Preparation of HAp/Chitosan composite nanopowder

Figure 4.1 illustrates the whole experimental set up for fabrication of GCH scaffold. The HAp-Chi composite nanopowders were synthesized using co-precipitation method. A 2 wt% chitosan solution was prepared by dissolving 2 gm of medium molecular weight chitosan in a solution containing 2 mL of acetic acid and 96 mL of deionized water with continuous stirring for 5 h to get a perfectly transparent solution. After that 100 ml of $(NH_4)_2HPO_4$ (0.019 M) solution was added to 2 wt% 100 ml chitosan solution. The mixed chitosan $(NH)_2HPO_4$ solution was then dropped slowly into the solution of calcium nitrate (0.031 M) with vigorous stirring and the *p*H was adjusted to 10 using NH_4OH solution. The dropping speed of chitosan/$(NH)_2HPO_4$ solution was about 4 ml $min^{-1}$and the reaction was carried out in ambient condition at 25^oC. After titration, the stirring was continued for 24 h and the obtained slurry was aged for another24 h. Finally, the precipitate was washed through centrifugation at 15,000 rpm using deionized water and freeze dried at 253K and 77 torr pressure to obtain nearly 10 gm of HAp-Chi nanopowders. A typical flow diagram for the preparation of HAp-Chi composite nanopowders is described in Figure 4.2. Similarly, bulk

quantity nearly 50 gm of HAp-Chi nanopowders were prepared to carry forward its characterization and prepare 3D porous scaffolds for *in vitro* and *in vivo* studies.

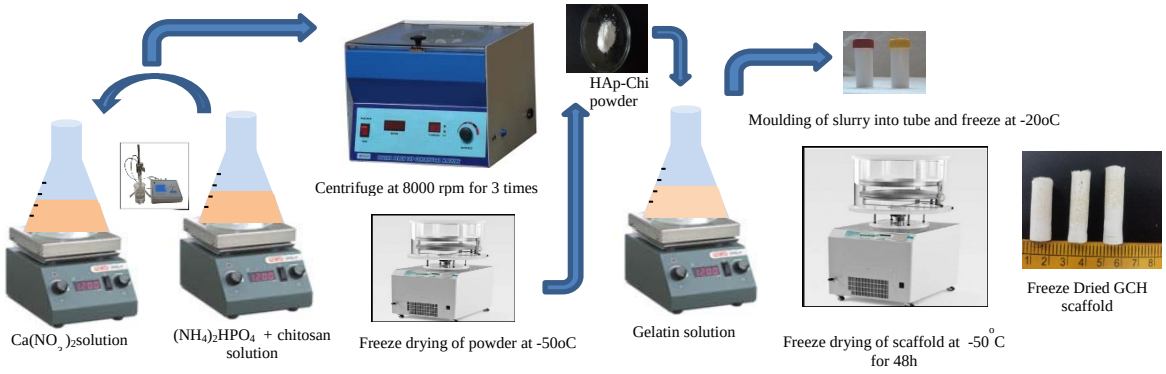

Figure.4.1. Schematic of experimental set up for the fabrication of GCH scaffold.

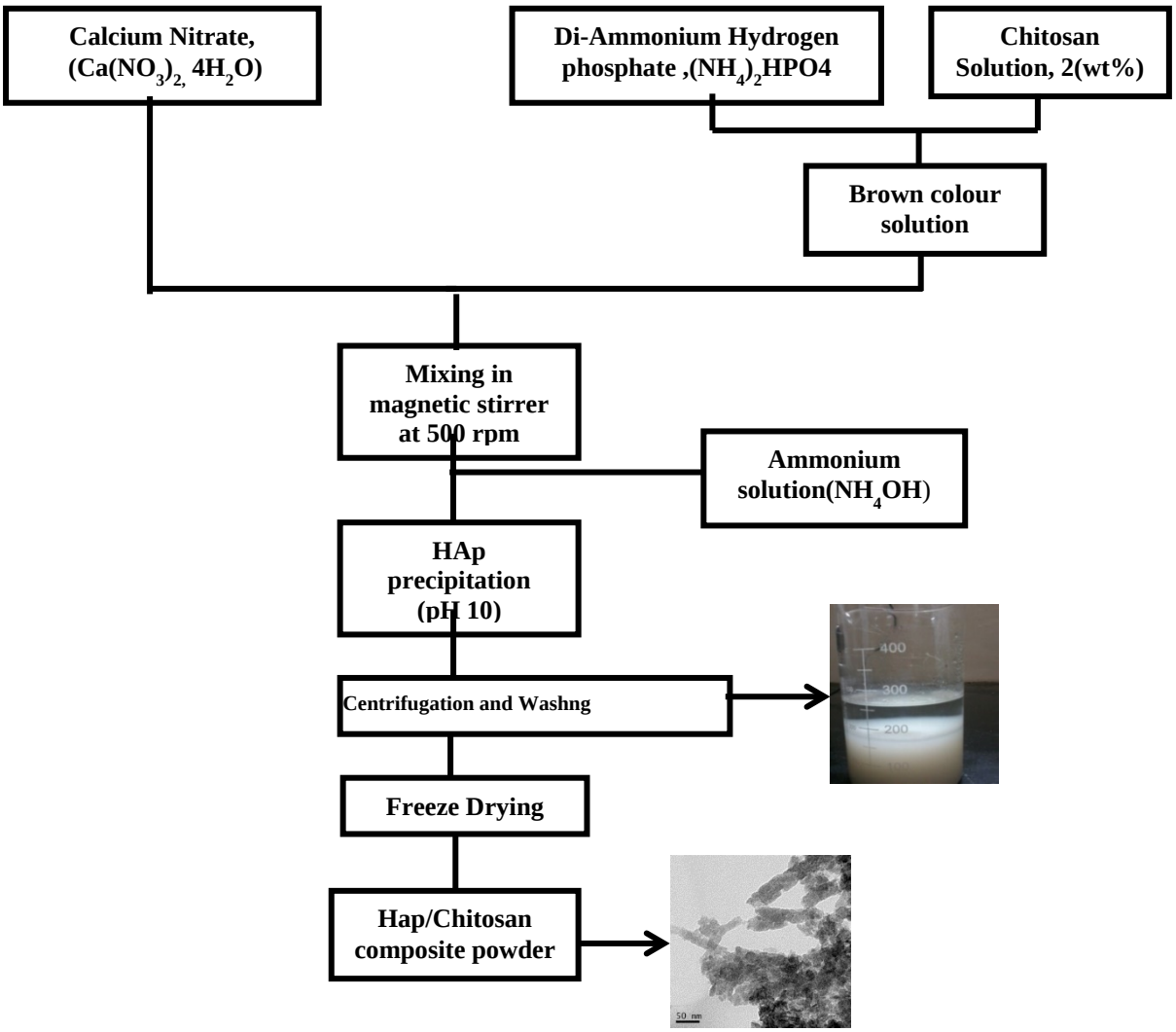

Figure.4.2. Flow diagram for synthesis of HAp-Chi nanopowders.

4.3.3 Preparation of porous HAp/Chitosan-Gelatin composite scaffold

Gelatin containing 1.4 gm in deionized water was heated up to 40^{o}C under continuous stirring for 4 hr. Two gram of HAp-chitosan composite nano powder was then added to gelatin solution with constant stirring for 40 min using an overhead mixer to disperse the HAp-chitosan nanoparticles. HAp-Chi powders were mixed together with gelatin solution based on the value of HAp to chitosan ratio as shown in Table 4.1. The mixed solution was then sonicated (IUltrasonic) for 30 min to remove any air bubble. A glutaraldehyde solution was prepared by dissolving 0.5 ml glutaraldehyde (50%) in 100 ml deionized water. Required amount aqueous solution of glutaraldehyde (0.25 vol%) was added to the slurry at 4^{o}C under manual agitation. The resulting slurry was put in 10 ml PTFE cylindrical mould and then rapidly pre-freezed at–20^{o}C (Labfreeze, FL1150) to solidify the water into ice and kept overnight. Next, the frozen samples were lyophilized using a freeze-dryer (Labconco, South Korea) at –50^{o}C for 48 h to form a composite 3D porous scaffold. Excess glutaraldehyde and residual acetic acid were removed from the lyophilized scaffold after washing it with 5% sodium borohydride and then with NaOH solution for three times for 2h. Finally, the freeze dried scaffolds were kept in the vacuum desiccator (size-150mm, Tarson) for further characterization. A typical flow diagram for the preparation of HAp-Chi composite nanopowders is described in Figure 4.3.

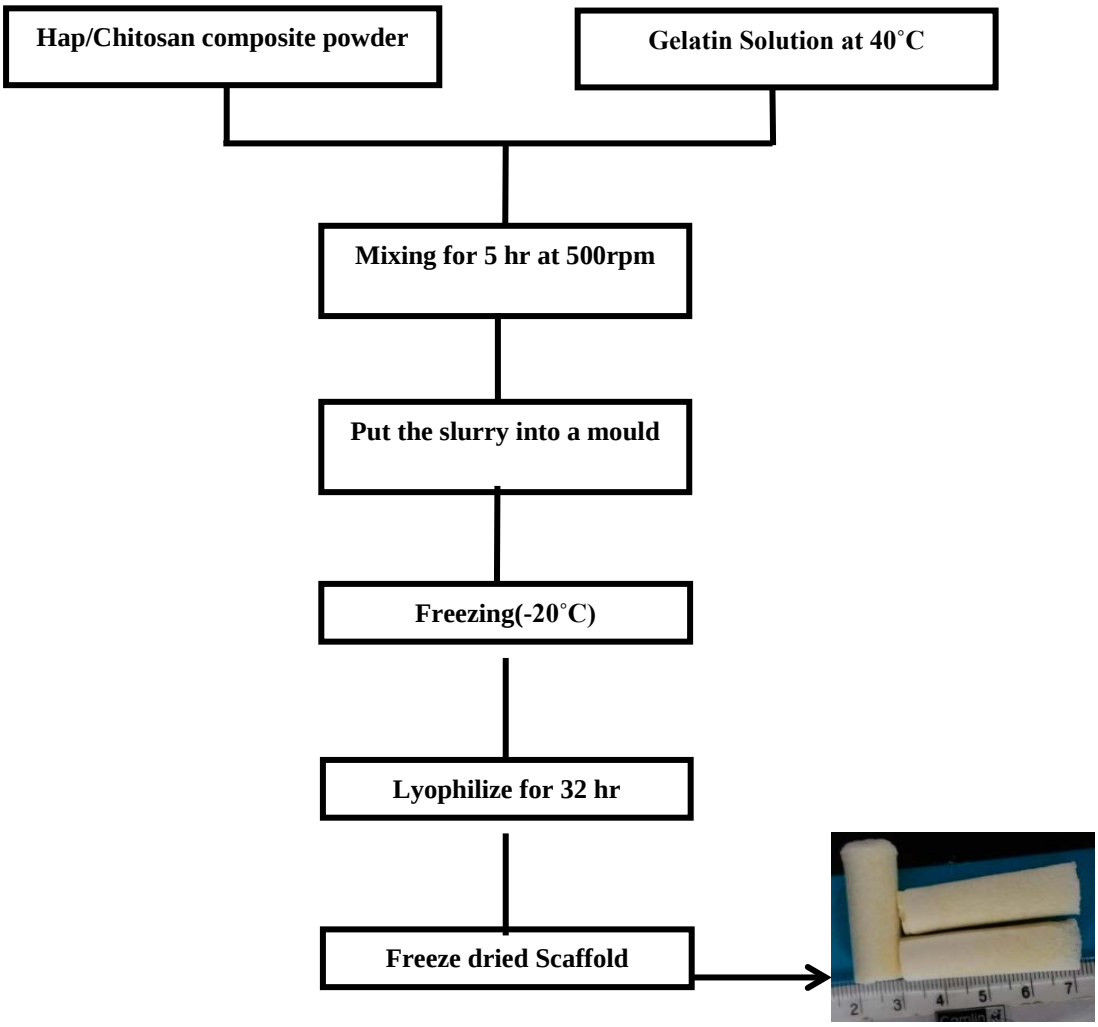

Figure.4.3. Flow diagram for the fabrication process of Gelatin/Chi-HAp scaffold.

Table.4.1. Composition of Gelatin/Chi-HAp composite scaffold.

HAp/Cht(%)		Gel/(HAp/Chi)	Gel/Cht/HAp	Gelatin (gm)	Chitosan(gm)	HAp(gm)
20/80	GCH18	10/90	10/72/18	0.22	1.6	0.4
	GCH16	20/80	20/64/16	0.5	1.6	0.4
	GCH14	30/70	30/56/14	0.85	1.6	0.4
30/70	GCH27	10/90	10/63/27	0.22	1.4	0.6
	GCH24	20/80	20/56/24	0.5	1.4	0.6
	GCH21	30/70	30/49/21	0.85	1.4	0.6
40/60	GCH36	10/90	10/54/36	0.22	1.2	0.8
	GCH32	20/80	20/48/32	0.5	1.2	0.8
	GCH28*	30/70	30/42/28	0.85	1.2	0.8
70/30	GCH63	10/90	10/27/63	0.22	0.60	1.40
	GCH56	20/80	20/24/56	0.5	0.60	1.40
	GCH49	30/70	30/21/49	0.85	0.60	1.40

***For the ease of experiment, we rename GCH28 scaffold as GCH30 and GCH21 as GCH20**

4.4 Characterization

4.4.1 XRD analysis HAp-Chi nanopowders

The phases of HAp-Chi composite nanopowders were analysed using X-ray diffraction (XRD) with fully automated X-ray diffractometer (Philips PAN analytical, USA) fitted with Ni-filter. The diffraction patterns were recorded with a XRD analyser using CuKα radiation (λ = 1.542 nm) at 35 kV and 10 mA. All samples were scanned from 10^o to 70^o in 2θ (where θ is the Bragg angle) in a continuous mode with a scanning speed of 0.02degree/sec. The peak position, phase purity, peaks for different atomic planes and their relative intensities in the powder diffraction pattern were identified in comparison with the reference powder diffraction data (JCPDS-09-0432). For phase evaluation of composite scaffold, the sample

was ground into powders, and the powder samples were characterized using XRD (Philips PAN analytical, USA).

4.4.2 FTIR analysis HAp-Chi nanopowders

The characteristic peaks of pure HAp and its composites were analysed using Fourier transform infrared (FTIR) (PerkinElmer, USA) spectroscopy. The pellet for the FTIR measurement was prepared by mixing 2 mg the sample with 200 mg of IR grade KBr at a pressure of 3 ton. The scaffolds were put in a vacuum oven at 50^{o}C for 48 h before they were ground to suitable size for IR analysis with spectrometer. The absorption spectra were measured using UV spectrometer in the wave number between 4000 to 400 cm^{-1} with a resolution of 1 cm^{-1}.

4.4.3 Particle size analysis of HAp-Chi nanopowders

The particle size and its distribution were estimated through zetasizer (Zetasizer nano zs, Malveron). The refractive index for both Hap-Chi nanopowders and water was considered as 1.65 and 1.33. The dispersed HAp-Chi nanoparticles were used for particle size analysis.

4.4.4 Transmission Electron Microscopy (TEM) of HAp-Chi nanoparticles

The particle size, morphology and crystallinity of as synthesized HAp-Chi powders were studied by TEM (FEI, Nederland), SAED (Selected Area Electron Diffraction) pattern. The TEM samples were prepared by dispersing a small amount of powder in acetone using 20 kHz and 500W ultrasonic energy for 30 minute. A well dispersed suspension was dropped on a carbon coated copper grid and dried to evaporate the solvent. The powder morphology was observed from TEM micrograph in bright field mode.

4.4.5 Thermo gravimetric analysis of HAp-Chi nanoparticle

Thermal analysis technique is an excellent approach to determine the decomposition behaviour which depends on the remaining mass content of the sample with respect to temperature. The thermo gravimetric (TG) analysis of the composite powders was studied on 50 mg of powder samples using a TG analyser (Netzsch, Germany) and measurements were recorded from 50^{o}-1000^{o}C at 10^{o}C.min^{-1} heating rate in air.

4.4.6 FESEM observation of scaffold

The microstructure of the scaffold was observed using field emission scanning electron microscopy (FESEM) Novanano 450, FEI, USA). The surface of the scaffolds was gold coated using sputter coater (FEI,USA), and then placed inside the FESEM chamber.

4.4.7 Apparent porosity of scaffold

The porosity of composite scaffold was measured using Archimedes principle [68] with xylene as liquid medium using the following equation.

$$\text{Porosity (\%)} = \frac{w_2 - w_1}{w_2 - w_3} \times 100 \quad \ldots\ldots\ldots\ldots \text{(i)}$$

Where W_1 is the weight of the sample in air, W_2 is the weight of the soaked sample with liquid in pores, and W_3 is the weight of the sample suspended in xylene. Dry weight of all freeze dried scaffolds was taken accurately using a digital balance. Scaffold with a defined shape kept inside a beaker filled with ethanol and placed this beaker inside a vacuum desiccator to remove entrapped air present inside the scaffold.

4.4.8 Mercury Intrusion Porosimetry

The characteristics of pore size and pore size distribution were evaluated using mercury (Hg) porosimetry (Porosimeter-33, Quanta chrome, USA). The freeze dried GCH scaffold samples were placed in a penetrometer and infused with mercury under increasing pressure. The pore morphology behaviour was measured on the approached theory by Washburn [68]. Mathematically Washburn equation is given as:

$$P = \frac{2\sigma \cos\theta}{r} \quad \ldots\ldots\ldots\ldots\ldots \text{(ii)}$$

P = Pressure of Hg
r = Radius of the pore
б = Surface tension of mercury
θ = Contact angle.

4.4.9 Mechanical testing of GCH scaffold

The mechanical properties of the composite scaffolds were determined using a Universal Testing Machine (Tinius Olsen, UK)[206]. For compressive testing, the samples were cylinders of approximately 5 mm in diameter and 12 mm in height using the load cell of 10 KN with a cross head speed of 1mm/min and determined by the following formula:

$$\text{Compressive strength} = \frac{P}{A} \quad \ldots\ldots\ldots\ldots \text{(iii)}$$

P = Load in KN
A = Cross sectional area of the cylindrical sample

4.4.10 Swelling behaviour of GCH scaffold

Water uptake of the scaffolds were measured using the method described by Thein and Misra [207]. A sample with 5 mm diameter and 12 mm height was immersed in distilled water for 30 h. Then the sample was gently removed and placed on a wire rack for 1 min. The weight of the sample was averaged from triplicate measurements for each group of samples. The water uptake of the scaffolds was calculated using the following equation [208].

$$\textbf{swelling}\ \% = \frac{W_s - Wd}{W_d} \times 100 \ldots\ldots\ldots\ldots\ldots\text{(iv)}$$

Where,

W_s = wet weight
W_d = Dry weight

4.4.11 Mineralization behaviour of Gelatin/HAp-Chi scaffold

The ability to form apatite when immersed into simulated body fluid (SBF) is an index of biocompatibility exhibited by the GCH 30 scaffold [209]. The SBF solution is known to be a metastable buffer solution and even a small, undesired variance in both of the preparation steps and the storage temperature may drastically affect the final nucleation of apatite phase. SBF solution was prepared in accordance with the chemical ion concentrations nearly equal to those of the inorganic constituents of human blood plasma and were used by A. Cuneyt Tas et al. [209]. Analytical grade pure NaCl (99.5%), $NaHCO_3$ (99.5%), KCl (99.0%), Na_2HPO_4 $2H_2O$ (99.5%), $MgCl_2$ $6H_2O$, (99.0%), Na_2SO_4, $(CH_2OH)_3CNH_2$ (99.5%), $CaCl_{2,}.H_2O$ (99.0%) and HCl (37 vol.%) were used in the preparation of SBF solution for this study. Fresh 1000 ml SBF solution was prepared by dissolving the required amount chemical reagents into a 2000 ml polystyrene (Tarson) beaker as mentioned in Table 4.2. In the beginning, reagents were added to 700 ml deionised water continuously one by one in sequence only after the previous reagent has completely dissolved. During the preparation of SBF solution, pH ~7 was maintained by addition of 1M HCl in each step and temperature 33 ^oC. Finally, volume of the solution was adjusted up to 1000 ml by deionised water to maintain solution pH~7.4 at 37 ^oC. The resulting solution was stored in air tight polystyrene (Tarson) container at 5^oC. Porous scaffold with 5 mm in diameter and 12 mm in height was placed in 50 ml of simulated body fluid (SBF) solution and kept in an incubator at 37^oC for 7 days. After every 3-day interval, old SBF solution was replaced by freshly prepared SBF

solution. After 7 days, the scaffold was removed from SBF, repeatedly washed with deionized water for three times and freeze dried at -20^{o}C for 24 h. The SBF treated dried scaffold was sputter coated with gold and examined using FESEM.

Table.4.2. Chemical composition of SBF.

Order	Reagent	Amount (gpl)
1	NaCl	6.547
2	$NaHCO_3$	2.268
3	KCl	0.373
4	$Na_2HPO_4, 2H_2O$	0.178
5	$MgCl_2 6H_2O$	0.305
6	$CaCl_2,2H_2O$	0.368
7	Na_2SO_4	0.071
8	$(CH_2OH)_3CNH_2$	6.057

4.4.12 Biodegradation of GCH scaffold

In vitro biodegradation was carried out in PBS buffer solution at 37 ^{o}C and pH ~ 7.4. GCH scaffolds were taken in a sealed polystyrene (Tarson) Petridis followed by soaked in PBS buffer solution for different time interval inside an incubator at 37 ^{o}C and pH ~ 7.4. Samples soaked in PBS were repeatedly washed with deionised water and dried at 100 ^{o}C. The final weight of the sample was taken through digital weighing balance. The weight loss was correlated with biodegradability of scaffold. The percentage of weight loss was estimated as:

$$weight\ loss\% = \frac{W_0 - W_1}{W_0} \times 100 \quad \text{.....(vi)}$$

Where,

W_0 = Initial weight
W_1 = Final weight

4.4.13 *In-vitro* cell culture study

4.4.13.1 Isolation and culture of MSCs

Human Umbilical cord (UCB) derived MSCs were used for *in vitro* cell culture. The UCB MSCs were collected from Ispat General Hospital, Rourkela, India with prior consent from patient and kindly provided by the Department of Biotechnology and Medical Engineering of

NIT Rourkela, India after getting required approval by institutional ethical board. The details of isolation and characterization can be obtained from the earlier research work in the Department of Biotechnology and Medical Engineering, NIT, Rourkela, India [210].

4.4.13.2 Cell seeding and culture

Scaffolds were sterilized prior to cell seeding by soaking in 70% ethanol and 10 U/ml penicillin solution for 2 hrs followed by sterile PBS wash. Cells from 4th passage were seeded on sterilized scaffolds with a seeding density of 5×10^6 cells/ml by static method [211]. The cell seeded GCH scaffolds were incubated in DMEM culture medium with a media change for every 3 days [212].

4.4.13.3 Cell morphology and cell attachment

Human mesenchymal stem cell (hMSCs) seeded composite GCH scaffolds were cross-linked with 4% paraformaldehyde in phosphate buffered saline (PBS). 2% (v/v) gluteraldehyde was used for fixing the cells and the samples were rinsed with wash buffer. Osmium tetroxide(OsO_4) (1%) was added to the samples and kept aside for 30 min. Then the samples were rinsed with phosphate buffer for five times and dehydrated with series of ethanol gradations (50, 70, 80, 95 and 100%) for 10 min each [213]. Finally, the samples were air dried at 37°C and sputter coated with gold, platinum for 30 sec prior to imaging. (Quorumtech, Q150RES, Czech Republic). Images were taken by SEM [JEOL-JSM 6480 LV], and Field Emission Scanning Electron Microscopy (FE-SEM) [Nova SEM-Nederland] in high vacuum at 30 kV.

4.4.13.4 Cytotoxicity assay

To estimate the number of viable cells onto GCH composite scaffolds a colorimetric assay i.e. MTT assay was used, which quantities the ability of mitochondrial dehydrogenases to metabolize 3-[4, 5-dimethylthiazol-2-yl]-2, 5-diphenyl-tetrazolium bromide to an insoluble formazan [28]. Fresh media was supplemented to the cells consisting of 100µl MTT solution (diluted in 1:10 PBS). Then the cells were incubated at 37°C for 4 hrs. 0.5 ml DMSO was added followed by centrifugation at 1000 rpm for 5 min. The optical density (O.D) of intense pink colored formazan derivative was measured using a spectrophotometric plate reader (2030 multi label reader Victor X3, Perklin Elmer, USA) at 595 nm.

4.4.13.5 Immunofluorescent imaging of Osteogenic cell marker: Osteocalcin and RUNX2

We also measured the expression of osteogenesis-related genes with the help of confocal microscopy. Expression of osteoblast markers, the transcription factor RUN-X2 and the bone-specific protein, osteocalcin coding gene (OCN) were observed in hMSC-seeded GCH scaffolds cultured in osteogenic medium. For immunostaining the scaffolds were cut into slice using sharpe blade and then placed in PBS solution. Then the immunostaining was carried out using standard protocols. On one side staining for osteocalcin was achieved using rabbit antimouse osteocalcin (1/100, Abcam) and Alexa 488 antimouse (1:400, Invitrogen) as a secondary antibody. On the other hand, staining of RUN-X2 was achieved using antirabbit RUN-X2 antibody (1:200, Abcam) and using Alexa 647 antirabbit (1:400, Invitrogen) as secondary antibody. Finally, the samples were mounted with Fluorsave Vectashield mounting medium with DAPI (Atom). All the specimens were examined using a confocal microscope [214].

4.5 Statistical Analysis of Experimental Data

Three samples were used for repeated experiments to get mean value on each time point. All data are expressed as mean ± standard deviation. The data were compared using Student's t-test and differences were considered significant when $*p < 0.05$. A p-value more than 0.05 ($p > 0.05$) was taken as indicating no significant difference.

4.6. Results and Discussion

4.6.1 XRD analysis HAp-Chi composite powder

Phase analysis of the HAp-Chi nanopowder was performed using XRD. The characteristic diffraction peaks for both chitosan and HAp were observed in the synthesized nanopowder. The sharp peaks of (002) and (112) plane in HAp (Figure. 4.4) confirmed that the synthesized powder was well crystallized. No other calcium phosphate phase was detected in XRD pattern in Figure 4.1 that indicated the presence of phase pure hydroxyapatite- chitosan in the synthesize nanopowders.

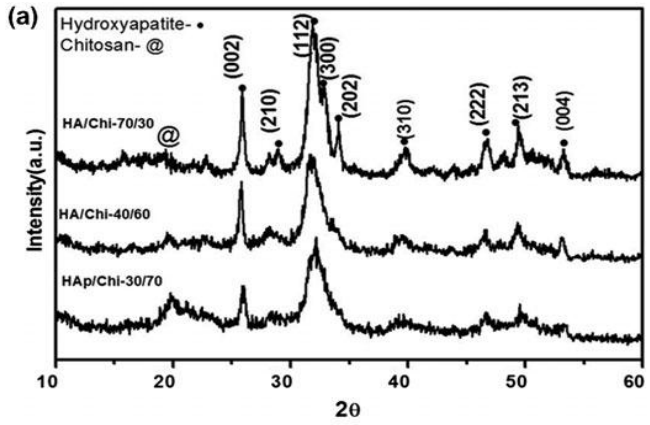

Figure.4.4. XRD pattern of chitosan/HAp composite nanopowders.

4.6.2 FTIR analysis HAp/Chitosan composite powder

Figure4.5 shows the FT-IR spectrum of pure chitosan and HAp-chitosan composite nanopowder. The characteristic bands for different functional groups present in the scaffold are shown in Table 4.3. Two bands were observed at 3570 and 622 cm^{-1} due to the stretching of hydrogen bond in OH ions present in HAp and liberation mode of hydrogen-bonded OH ions respectively. The band at 1024 cm^{-1} arises from v_3 PO_4, whereas the band at 603 and 555 cm^{-1} suggest the presence of v_4 PO_4. The absorptions bands observed at 2887, 1631, 1595, and 1543 cm^{-1} were

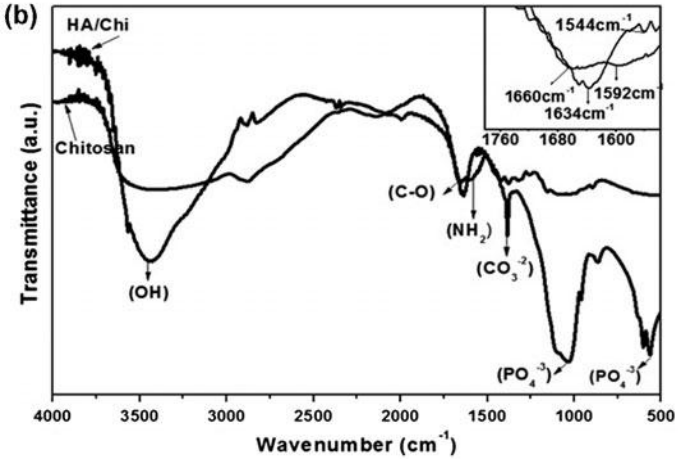

Figure.4.5. IR spectra of Chitosan and HAp-Chitosan composite powder.

assigned to methylene (-CH_2), amide I(C=O), amino (-NH_2), and amide II (-NH) groups in chitosan respectively. Carbonate bands at 1382, and 852 cm^{-1} appeared because of the carbonate incorporation in HAp from CO_2 in air. The FT-IR spectra also indicated the shifting of characteristic bands of amine (1655 cm^{-1}) and amide (1599 cm^{-1}) in chitosan to lower wavenumber in the HAp- chitosan composite nanopowder, as a result of interaction

between chitosan and HAp, through hydrogen bonds between $–NH_2$ and –OH as well as chelation between $–NH_2$ and Ca^{+2}.[215, 216]

Table.4.3.Peaks of infrared spectra assigned to synthesized HAp-chitosan nanopowders.

Compound	Assignment		Infrared frequency (cm^{-1})
HAp	$-PO_4$	bending	559
		stretching	1024
	$-CO_3^{2-}$		1480,876
	-OH		3390
Chitosan	$-CONH_2$ stretching		1650
	$-NH_2$		1595
	$-CH_2$	stretching	2876
Hap-Chi	($-CONH_2$) stretching		1660 → 1634
	amine (-NH)		1595 → 1544

4.6.3 TEM analysis of HAp/Chitosan composite powder

The synthesized HAp-chitosan composite powder showed a particle size distribution between 90 -100 nm (Figure 4.6) with aspect ratio of 1.7±0.18 and found to be well dispersed as in TEM micrographs in Figure 4.7(a). The electron diffraction pattern of HAp-chi crystals exhibited diffused ring pattern. The SAED pattern of pure HAp-Chi composite powder reveals the formation of spherical particles near to 50 nm diameter with a consistent strong concentric ring pattern for (120) of chitosan and (002), (211), (112) and (310) plane of polycrystalline HAp [217]. Elemental distribution data of both the samples confirmed the presence of HAp with a Ca/P ratio of nearly equal to 1.67.

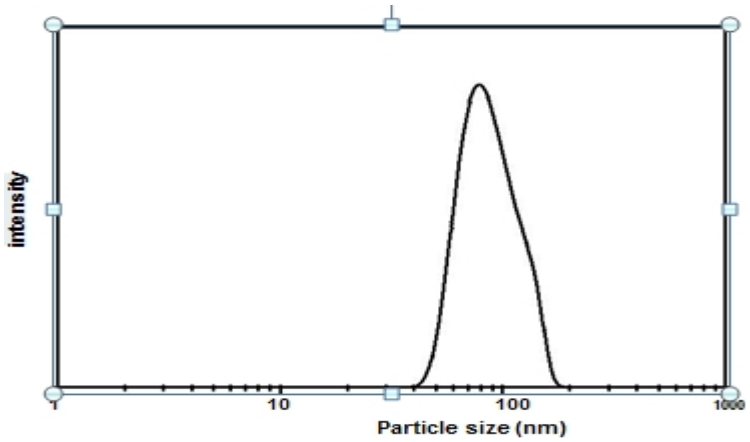

Figure.4.6. DLS measurement of particle size distribution of HA–Chi 40:60 nanopowder.

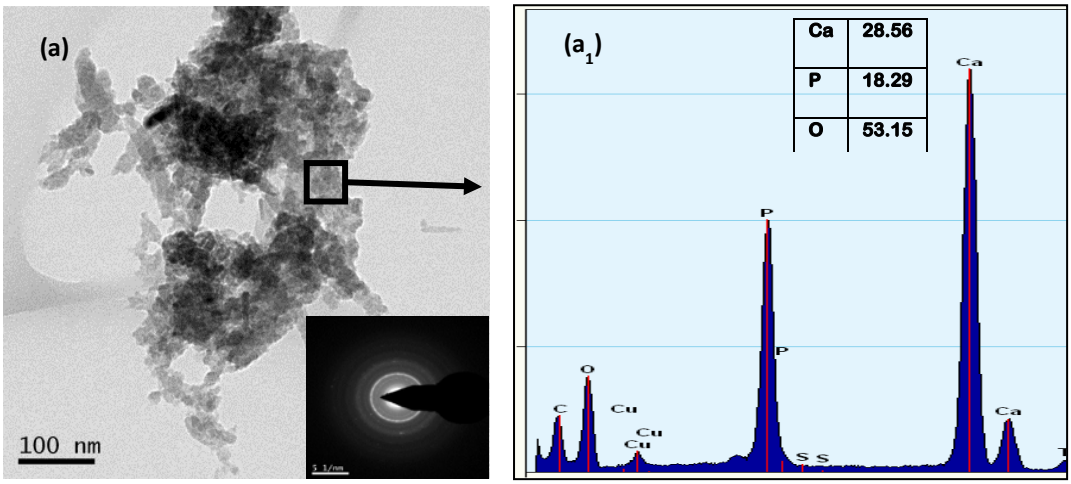

Figure.4.7. TEM micrograph of HAp-chitosan composite nanopowders.

4.6.4 Thermogravimetric analysis of HAp/Chitosan composite powder

Figure 4.8 shows the TG thermogram of the synthesized HA–chitosan nanopowders. The observed weight loss of 7 wt% between 70 and 150 °C was attributed to the loss of adsorbed water molecules in HAp and chitosan. Thermal decomposition of chitosan accounted for another 21–35 wt% weight loss between 310 and 600 °C. Almost all the organic macromolecules and carbonate were decomposed by 620 °C as negligible or no weight loss occurred after 620 °C. The calculated composition of HA–chitosan composite nanopowders from TG data closely resembled the theoretical composition of the powder as in Table 4 4.

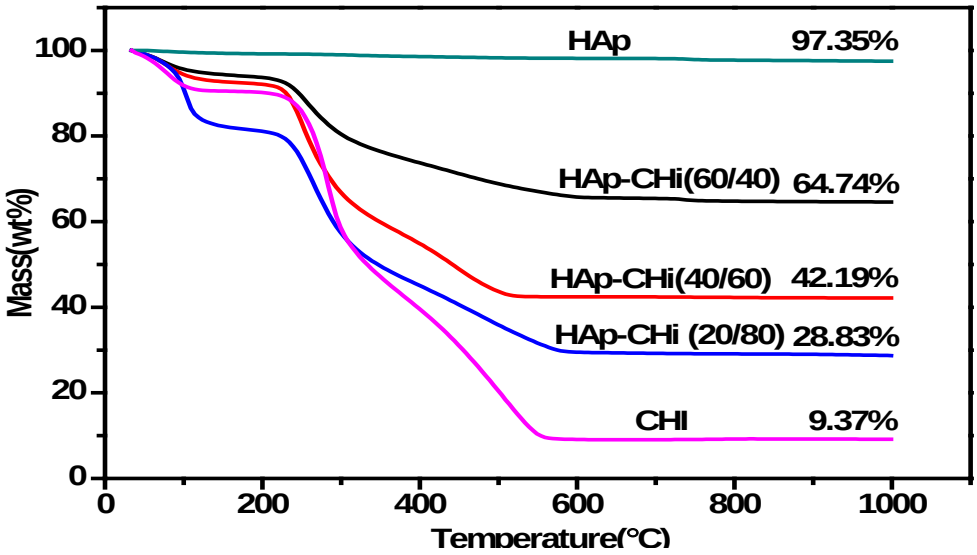

Figure.4.8. Thermo gravimetric analysis of pure HAp, pure chitosan and HAp- chi nanopowders.

Table 4.4. Theoretical and actual compositions of Chitosan/n-HAp nanopowder as determined by TG analysis at 1000˚C.

Sample	Theoretical chitosan/n-Hap composition		Actual Chitosan/n-Hap composition	
HAp-Chitosan	wt% Chitosan	Wt % -HAp	wt% Chitosan	wt% -HAp
	40	60	37.68	62.31
	60	40	62.19	37.81
	80	20	77.92	22.08

4.6.5 FTIR analysis of HAp-chitosan/gelatin composite scaffold

Figure 4.9 shows the FTIR spectrum of scaffold and different IR bands or peaks are shown in Table 4.5. Apart from PO_4^{3-} (1027, 562 cm^{-1}), CO_3^{2-} (875 cm^{-1}), OH^- (3406, 605 cm^{-1}) bands in HAp and amide I (1662 cm^{-1}), amide II (1232 cm^{-1}) and carboxylate (1446 cm^{-1}) bands in gelatin, a distinct band at 1552 cm^{-1} was detected, which signifies the formation of C=N- bond due to intergelatin and chitosan gelatin crosslinking to develop 3D interconnected network in the scaffold. The band at 1330 cm^{-1} is attributed to the interaction between carboxylate group in gelatin and Ca^{+2} ion in HAp to bind the particulate reinforced composite scaffold together, a fact that is well established in the earlier studies also [218, 219].

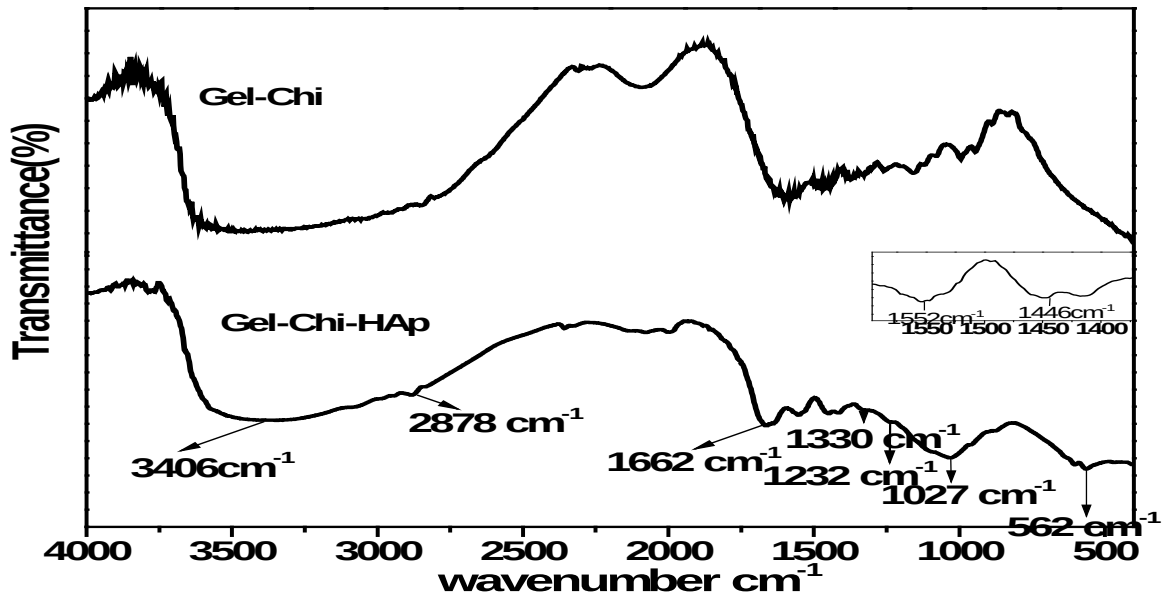

Figure.4.9. IR spectra of gel-chi and HAp / Chitosan-Gelatin composite scaffold.

Table.4.5. Peaks of infrared spectra assigned to fabricated GCH30 scaffold.

Compound	Assignment		Infrared frequency (cm^{-1})	Ref
HAp	$-PO_4$	bending	602 (weak)	16
		stretching	1027(weak)	
	$-CO_3^{2-}$		1480,876	
Gel-Chi	C=N		1552	17
	Amide I		1539 to 1662	
	COO^-		1446	
Gel-Chi-HAp	Ca^{+2}-----COO^-		1330	53
	Amide A, N-H stretching		3140 ,2878	

4.6.6 Analysis of microstructure, porosity and mechanical strength of prepared scaffolds with variation in HAp and gelatin content

The total porosity of the Gel:Chi:HAp -based scaffold was measured using Archimedes' principle as described earlier while pore size distribution in the scaffold was determined from Hg porosimetry data using Hg intrusion in the porous scaffold. Table 4.6 indicates the total porosity values and compressive strength exhibited by all the prepared scaffolds with varying composition. One interesting fact is that the mean porosity in the prepared scaffolds varied between 70 to 79% reflecting that compositional variation did not affect total porosity in the scaffold in a significant manner (all p values > 0.05). The scaffold having 30 wt% gelatin and prepared from HAp-Chi nanoparticle with 40:60 composition showed the highest average porosity of 78% and compressive strength of 3.46 MPa. The variation in compressive strength of all the prepared scaffolds with variation in gelatin content from 10 to 50 wt% is shown in Figure.4.11 (a). Irrespective of HAp and chitosan content, all the prepared scaffolds showed higher compressive strength value at 30 wt% gelatin content. With variation in gelatin content from 10 to 30 wt% the compressive strength in the scaffolds gradually increased and beyond 30 wt% gelatin content it decreased. The increase in compressive strength with increasing gelatin content can be explained by enhanced HAp-gelatin interaction in the pore wall of scaffold with higher degree of interconnected covalent networks.

The excess amount of gelatin beyond 30 wt% might present some uncrosslinked separated phase instead of forming crosslinked interconnected network which served as the weakest link in the matrix to lower down compressive strength value in the scaffold. Further the compressive strength value exhibited by the scaffold was gradually increased as HAp content in the prepared scaffold increased from 14 wt% to 28 wt%. Figure 4.10(b) represents the variation in average pore diameter with varying amount of HAp content in polymer matrix. With increasing HAp content beyond 30 wt% in the scaffold, the most frequent pore size in the scaffold was decreased as evident from Figure 4.10(b). This was due to clogging of pores in the scaffolds by excess HAp agglomerates instead of going into the pore wall formed by gelatin and chitosan matrix. With an increase in net amount of HAp beyond 28 wt% in the scaffold, the excess amount of HAp-Chi system formed a separate phase of HA agglomerate in the scaffold that initiated the weakest link in the scaffold and caused failure at lower compressive strength. Both from FESEM micrographs and pore size distribution data in Figure.4.10(b), it is clear that maximum amount of pores possessed a pore size below 35 μm with very narrow pore size distribution in GCH36 scaffold containing HAp 36 wt%. On this account, our subsequent study was focused on measuring properties of the scaffold containing ≤30 wt% HAp with gelatin content fixed at 30 wt%.

Table.4.6. Physiological characterization of prepared GCH scaffold.

HAP/Cht(%)	Sample id	Gel/Cht/HAp	Most frequent pore dia (μm)	Porosity	Compressive mechanical property (MPa)
20/80	GCH18	10/72/18	165±6.4	73.76±2.1	0.5
	GCH16	20/64/16	133±5.2	75.23±3.2	1
	GCH14	**30/56/14**	**120±5.3**	**76.14±3.2**	**1.2**
30/70	GCH27	10/63/27	135±9.6	72.15±5.2	1.45
	GCH24	20/56/24	121±7.3	69.87±4.6	1.8
	GCH21	**30/49/21**	**110±11.8**	**73.89±5.4**	**3.2**
40/60	GCH36	10/54/36	111±5.8	70.12±4.4	2.1
	GCH32	20/48/32	105±7.3	75.33±3.6	2.3
	GCH28	**30/42/28**	**94±6.9**	**78.12±3.2**	**3.46**
70/30	GCH63	10/27/63	59±9.5	78.13±3.1	0.5
	GCH56	20/24/56	51±7.1	76.32±3.2	1.16
	GCH49	**30/21/49**	**43±6.8**	**75.13±4.7**	**1.25**

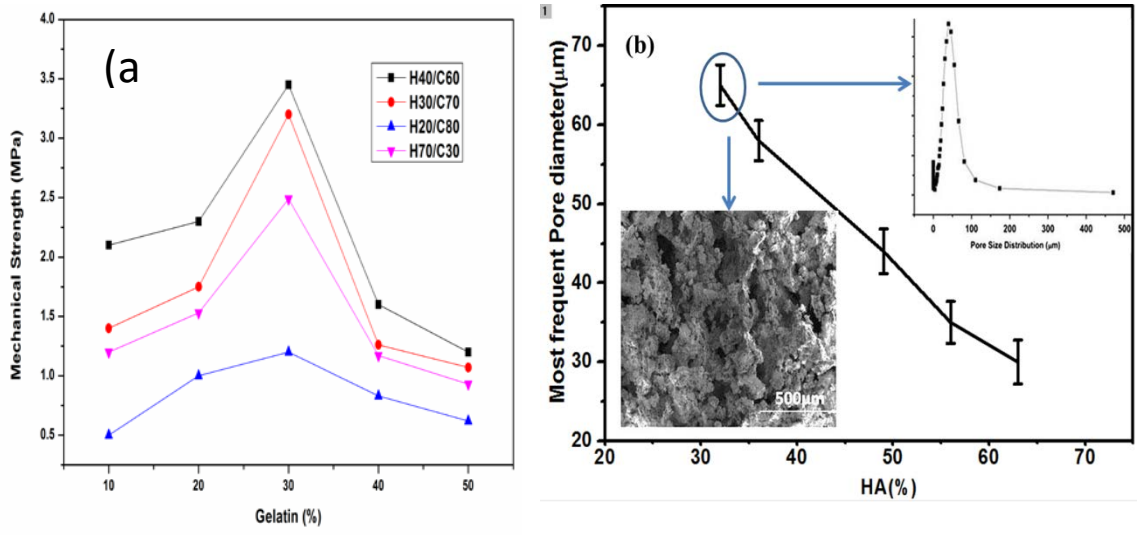

Figure.4.10. (a) Variation of mechanical strength with varying amount gelatin.(b)Variation of most frequent pore diameter with increasing amount of HAp in the GCH scaffold.

4.6.7 FESEM microstructure of fabricated GCH scaffold

Figure 4.11(a), (b), (c) show FESEM micrographs of the cross section of the scaffolds prepared after varying HAp content from 10 to 30 wt% keeping gelatin fixed at 30 wt% in GCH14, GCH20 and GCH30 scaffold. The reason for optimization of scaffold composition with ≤ 28 wt% of HAp content and 30 wt% gelatin in the prepared scaffold was discussed earlier in section 4.6.6 on the basis of physicochemical and mechanical properties of the corresponding GCH scaffold. All the FESEM micrographs in Figure.4.11, show an interconnected porous network of the prepared GCH14, GCH20 and GCH30 scaffolds, which is ideal for tissue ingrowth and osteoinduction. As it is evident from Figure 4.12(a) the pores were interconnected with irregular shapes with average pore size of 120 μm for GCH14 scaffold (Figure 4.11 (a)), where HAp-Chi particle distribution in pore wall of the scaffold is shown in Figure 4.11(d). Similarly, from figure 4.11(b), the microstructure of GCH20 scaffold exhibited open macroporous morphology with average pore diameter 110 μm and corresponding distribution of HAp-Chi particles in pore wall of the scaffold is shown in Figure 4.11(e). Nearly round shaped interconnected pores with average pore diameter of 94 μm was found in GCH28 scaffold as shown in Figure 4.11(c) and corresponding HAp-Chi particle distribution inside pore wall of GCH28 scaffold is presented in Figure 4.11(f). HAp-Chi nanoparticles were found to be randomly dispersed in gelatin matrix which suggests gelatin's role as a good binder for anchoring HAp- chitosan particulate together.

The average pore size of the prepared GCH scaffold was decreased with increasing HAp content from 14 to 28 wt% due to the presence of higher amount of hydrophilic HAp particles

in the slurry of prepared scaffold that hindered the growth of ice crystals during freezing. GCH30 exhibited smaller average pore diameter of 94 µm than that exhibited by GCH10 and GCH20 as shown in Table 4.7, but that is sufficient for attachment and ingrowth of osteoblast cell and exhibiting osteoinduction.

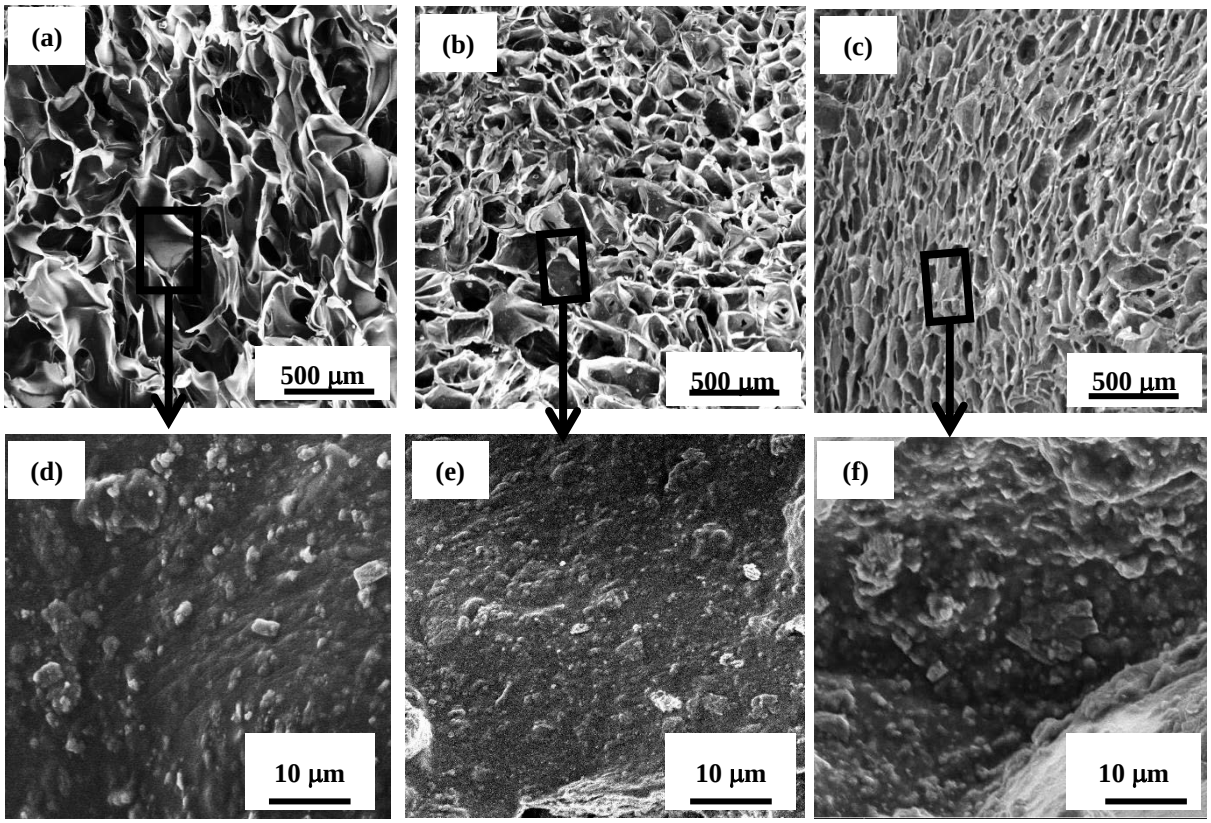

Figure.4.11. Microstructural observation HAp-chitosan/gelatin composite Scaffold fabricated from different amount of HAp content (a) GCH14, (b) GCH20, (c) GCH30 and their particle distribution in pore wall is (d), (e) and (f) respectively.

Table.4.7 Average pore diameter of GCH composite scaffold (FESEM data)

Sample name	Average Pore Diameter(µm)	Porosity
GCH 14	120 ± 5.3	76 ± 4.0
GCH 20	110±11.8	73.89±5.4
GCH 30	94 ±6.9	78.12±3.2

It can be inferred from this study that the pore size and its distribution in the prepared scaffold can be controlled by modifying the freezing rate, solids loading and composition of the slurry [220].

4.6.8 Mercury pore size distribution of GCH scaffold

In all the fabricated scaffolds some micropores were observed in the range of 0.5-5 μm. The pore size distribution data measured through mercury intrusion porosimetry, as shown in Figure 4.12 also revealed the fact that most frequent pore diameter was decreased from 150 μm to 80 μm on going from 10 to 30 wt% gelatin content in the scaffold. Also, scaffold containing 30 wt% gelatin showed the narrowest interconnected pore size distribution as evident from Figure 4.11 (c), which is ideal for bone tissue ingrowth and also exhibiting osteoinduction and osteointegration by the scaffold.

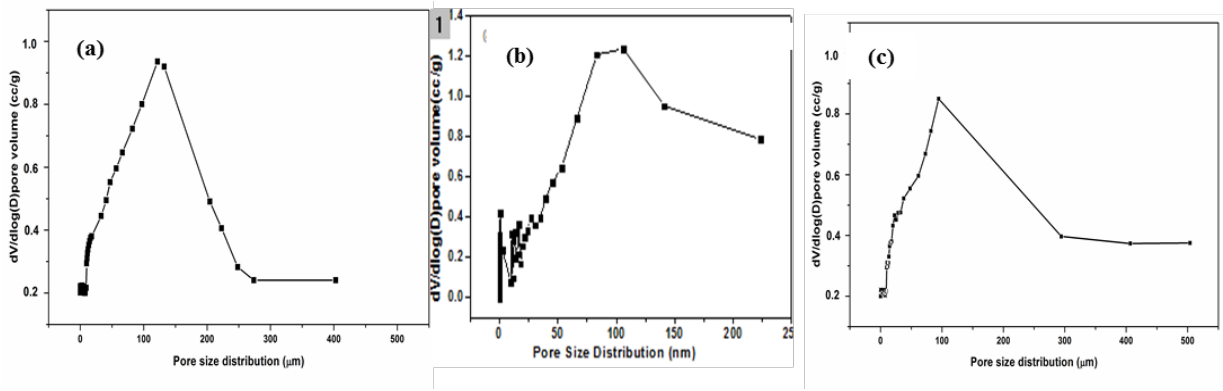

Figure.4.12. Mercury pore size distribution of freeze dried scaffold (a) GCH10,(b)GCH20, (c)GCH30.

4.6.9 Mechanical behaviours of GCH scaffold

The stress-strain behaviours of GCH scaffolds having HAp content varying between 14-49 wt% are presented in Figure 4.13. In all cases, the stress strain plot exhibits three regimes of

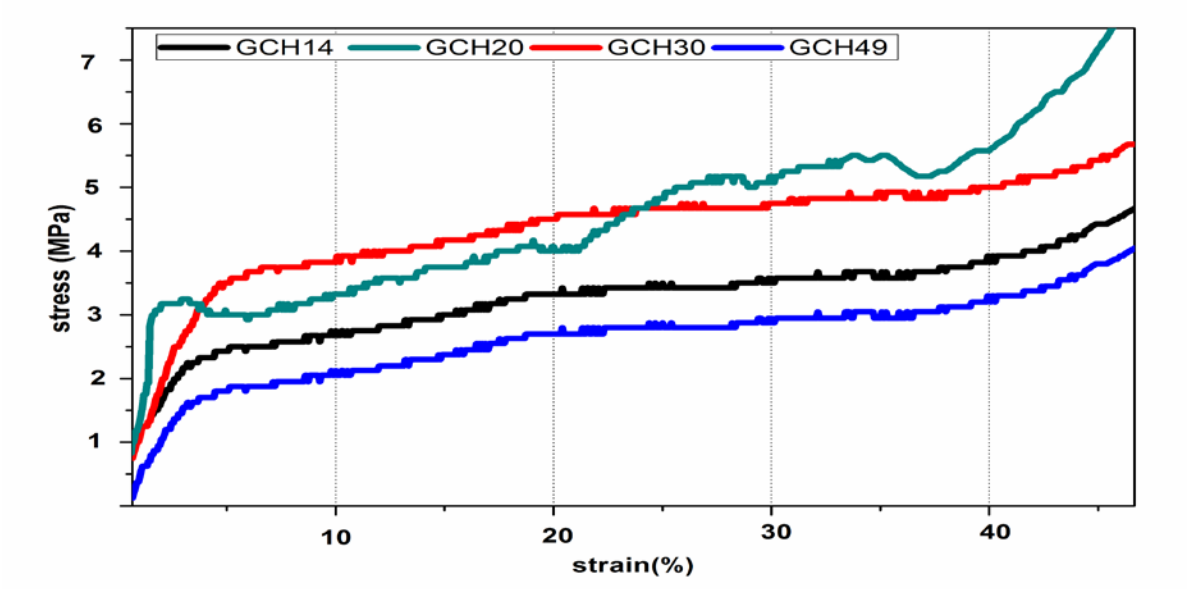

Figure.4.13. Stress strain plot of prepared GCH composite scaffold.

behaviour, namely linear elastic, a plastic collapse-plateau and densification regime. GCH30 scaffold exhibited the highest compressive strength of 3.46 MPa, which is close to the lower limit of compressive strength in human spongy bone [221]. The dispersed HAp-Chi particles in gelatin matrix inhibited the propagation of crack during compression and enhanced the resistance of the scaffold under compressive load. This explains why with the increase in HAp content in the prepared scaffold from 14 wt% to 28 wt%, the compressive strength of the scaffold gradually increased. The decrease in compressive strength in GCH 49 scaffold as compared to that exhibited by GCH 30 (Table 4.8) was due to the presence of HAp agglomerates in the former leading to the weakest link in the scaffold as discussed earlier. A further study on the interfacial bonding between organic and inorganic phase can highlight the origin of mechanical behaviour exhibited by the composite scaffold.

Table 4.8 Chemical composition and mechanical property of prepared GCB scaffold.

Sample Id	Gel:Chi:HAp(wt ratio)	Mechanical property (MPa)
GCH 14	30:56:14	1.2
GCH 20	30:49: 21	3.2
GCH 30	30:42: 28	3.45
GCH 49	30:21: 49	1.25

Here, we choose GCH30 scaffold having 30% gelatin and 28% HAp with an average pore diameter of 94 μm and compressive strength of 3.46 MPa for further biological characterization.

4.6.10 In vitro study

4.6.10.1 Mineralization ability of HAp-Chitosan-Gelatin composite scaffold

Mineralization ability of scaffold in SBF has been regarded as one of the key evidences of bioactivity for bone scaffold. It has been reported scaffold which supports osteoblast cell growth, proliferation and differentiation in vitro and in vivo, exhibits good mineralization behaviour in physiological environment [222, 223] . Highly dense bone-like carbonated apatite layer formation on SBF treated GCH30 scaffold (Figure. 4.14) indicates that the prepared scaffolds are not only biocompatible, but also bioactive.

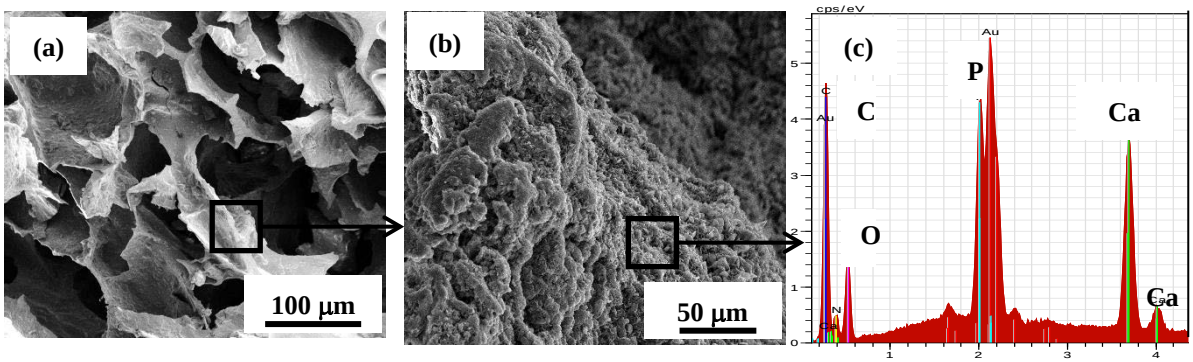

Figure.4.14. SEM micrographs of carbonated apatite layer formed on the surface of GCH30 scaffold immersed in SBF for 7 days.

4.6.10.2 In vitro biodegradability of GCH scaffold

Figure 4.15 illustrates the biodegradation of GCH scaffold in PBS buffer solution at 37^{o}C and pH~ 7.4, where a weight loss to the extent of 26 wt% in GCH14, 18 wt% in GCH 20 and 14 wt% in GCH30 was recorded after 18 days of incubation. Figure 4.15 follows an initial increase in degradation upto 12 days and steady state behaviour afterwards. It is reasonable to think that the strong interaction between gelatin macromolecular chains and HAp consumed some hydrophilic groups and depressed the solvent uptake, which protected the macromolecules from hydrolysing. Zheng et al [224] revealed a weight loss of 40 wt% of gel-chi-montmorillonite based scaffold for an incubation time of 6 days in tris-buffer solution of pH~ 7.4. The results showed that degradation of GCH scaffold can be modified by changing the concentration of HAp.

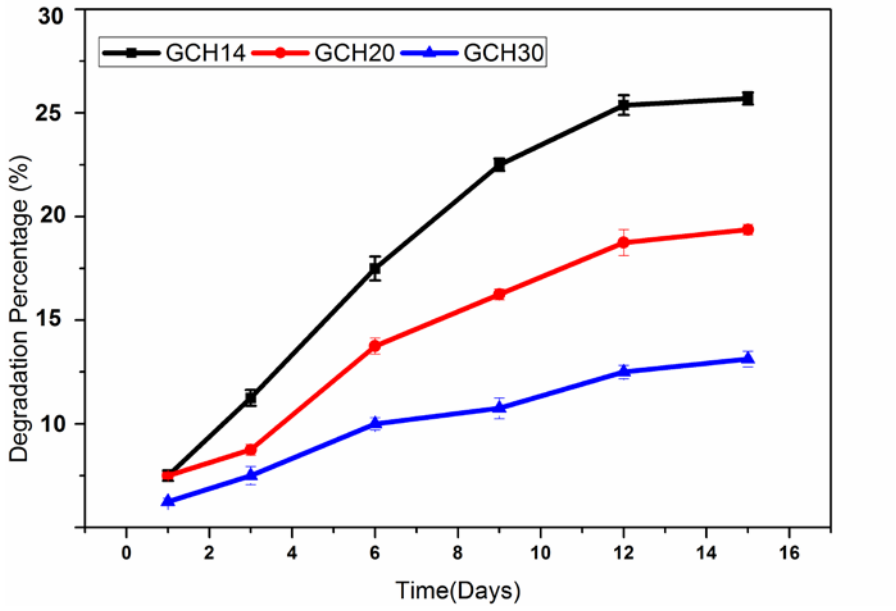

Figure.4.15 *In vitro* degradation behaviour of GCH scaffolds with varying HAp content.

4.6.10.3 Swelling studies of the GCH scaffold

Swelling study is an important index to the scaffold in relations to its pore size, interconnected porosity, to facilitate nutrients for cell adhesion and attachment. Figure 4.16

illustrates the result of swelling ratio exhibited by GCH14, GCH20 and GCH 30 scaffold. The HAp content influenced the swelling ratio of the prepared GCH scaffolds. The swelling ratio decreased as the HAp content increased from 14-30 % in the GCH scaffold. Since some of the NH_2^+ and Ca^{+2} bound together in gelatin matrix, the –OH group could not form hydrogen bond, hence decrease in swelling ration was observed [225].

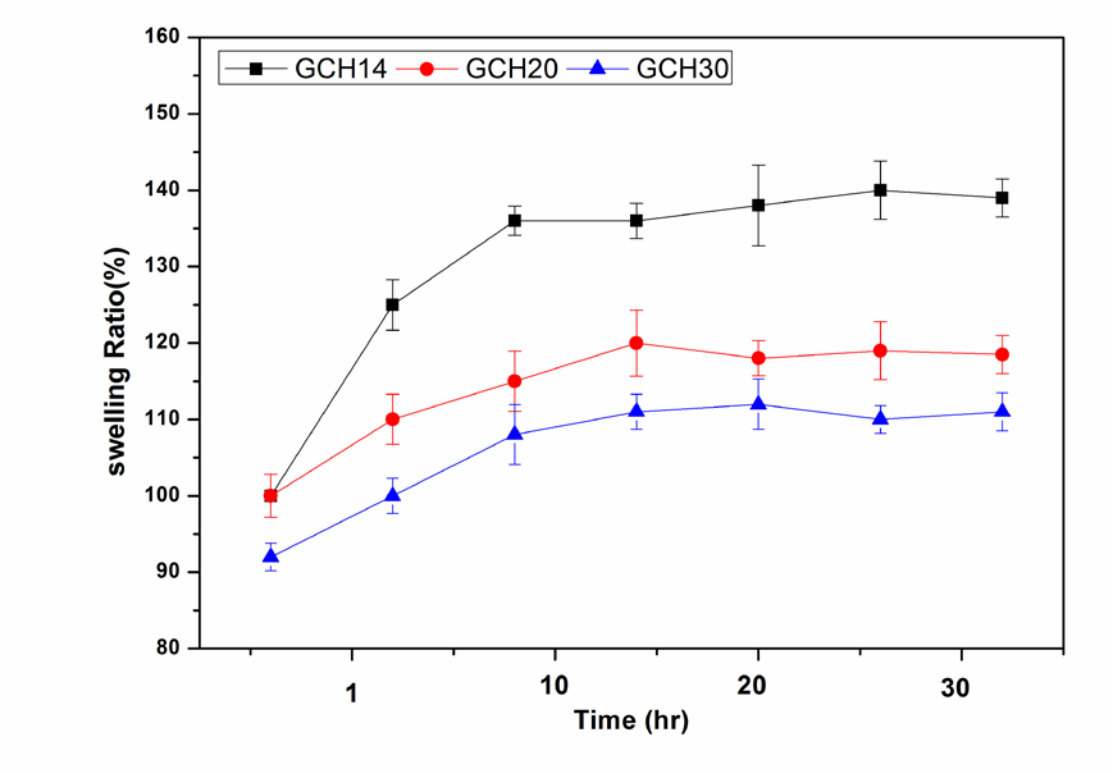

Figure.4.16. Swelling behaviour of GCH scaffolds with varying HAp content in PBS at 37°C.

4.6.11 In-vitro cell culture study

4.6.11.1 Cell attachment onto scaffolds

The scaffold having composition of GCH30 was chosen on the basis of its pore size and mechanical strength as an ideal scaffold to study the MSC–scaffold interaction in this work. The MSC and scaffold interactions after different days of cell culture are shown in the FESEM micrographs in Figure 4.17 that clearly exhibit that MSCs were attached, spread, and then proliferated with increasing cell culture time in the scaffold. The increasing numbers of lamellipodia and filopodia extensions from the cytoskeleton of MSCs were evident with progress in cell culture time as in Figure 4.17.(b) and (c). A separate image of a healthy MSC after 14 days culture on the scaffold is shown in inset of Figure 4.17(c). The attached cell exhibited numerous lamellipodia and filopodia from its cytoskeleton and spreading behaviour on to the scaffold. The fluorescent images in Figure 4.17 (d-f) also showed the increasing intensity of living cell on the scaffold with progress in cell culture time.

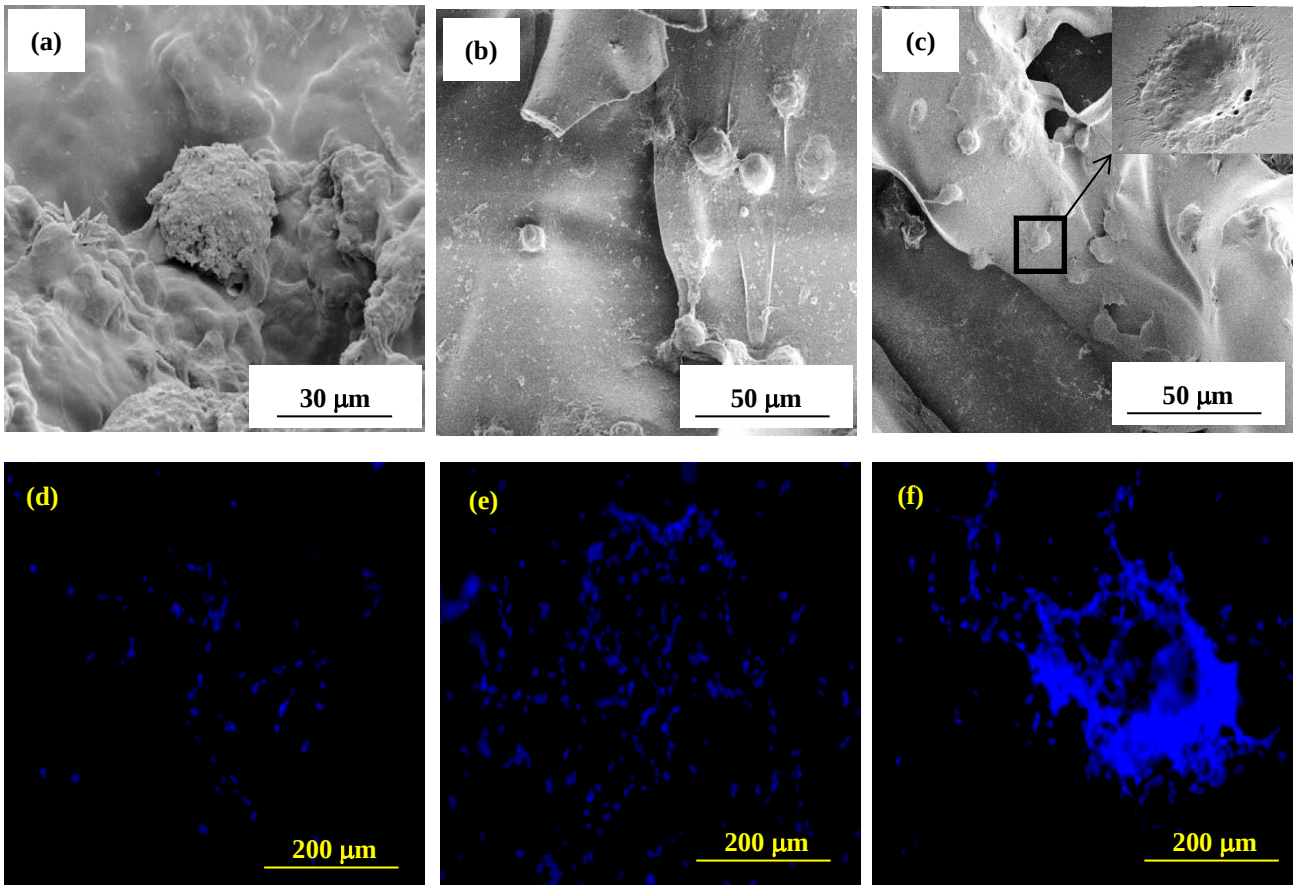

Figure.4.17. FESEM image showing MSCs attached on the HA:Chi:Gel (28:42:30) composite scaffold after (a) 3 days, (b) 7 days, (c) 14 days of cell culture. Dapi staining showing the distribution of cells on GCH28 scaffold (d) 3days, (e) 7 days (f) 14 days.

4.6.11.2 Metabolic activity of cells

After culturing it on the scaffold upto 7 days, MSC's viability in scaffold was studied using MTT assay, with MSCs cultured on tissue culture plate without Triton X100 and with Triton X100 in cell culture media were treated as positive control and negative control, respectively. Keeping up with the same trend as exhibited by the positive control, the scaffold material showed higher and higher number of a viable cell with progress in cell culture time as shown in Figure 4.18. The cell density on 5 days was significantly higher (p value < 0.001) from that on 3 days, and subsequently, viable cell density after 7 days of culture was significantly higher (p value $= 0.015$) as compared to that on day 5. This showed that the selected scaffold was conducive to cell attachment and proliferation [226].

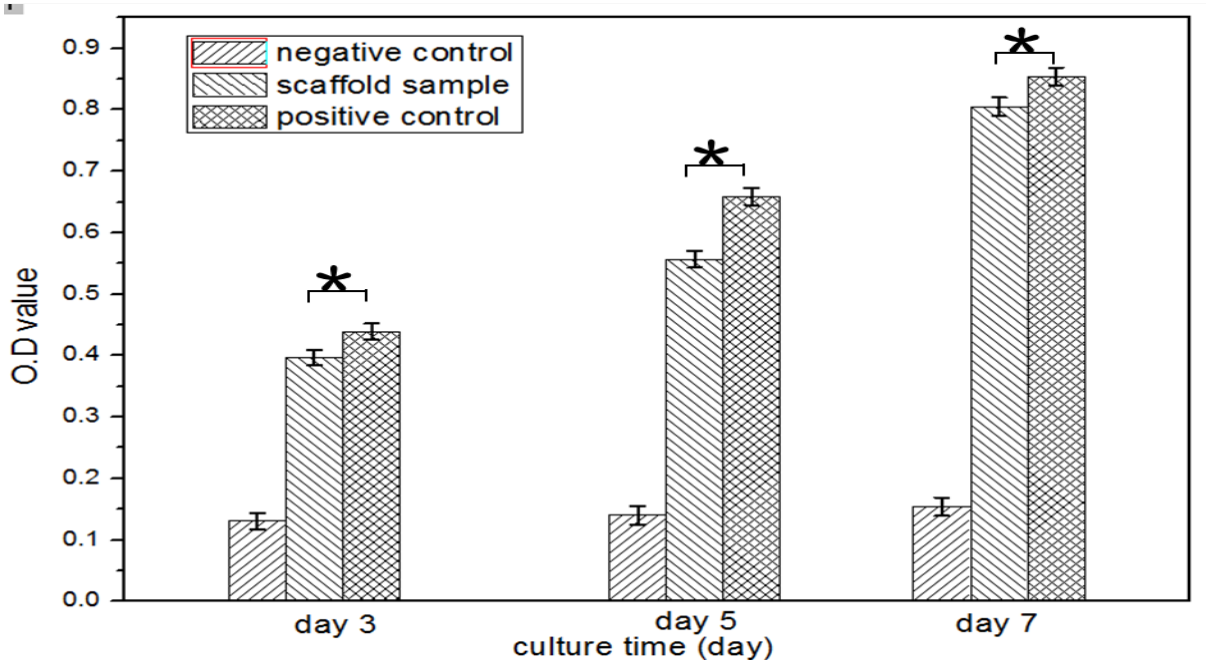

Figure.4.18. MTT assay for cell proliferation study in positive control, negative control GCT 30 scaffold using human Mesenchymal stem cell on days 3, 5, and 7. * indicates significant difference at $p \leq 0.05$.

4.6.11.3 Study of MSC's differentiation into osteoblast

Figure 4.19 shows the confocal images of RUNX2 and osteocalcin expressions after culturing MSCs for 7 and 14 days on control and sample group, respectively. RUNX2 expression appeared significantly higher in the Gel: Chi: HAp (30:42: 28) scaffold compared to pure gelatin-chitosan scaffold after 7 days (Figure 4.20(a, b) and 14 days (Figure 4.19 (c,d)) of cell culture study, supporting the differentiation of MSCs into osteoblast. The expression of the RUNX2 was only enhanced during early differentiation of osteogenic lineage and maintained at steady levels after initial commitment [227] as evident from Figure 4.19(a) and (b). Osteocalcin is a primary non-collagenous protein produced by osteoblasts, which signals the termination of osteogenic differentiation and is commonly used to measure new bone formation [228]. Osteocalcin expression for osteogenesis was much more pronounced in composite scaffold as compared to very negligible or no osteocalcin expression observed in control (pure gelatin-chitosan scaffold) (Figure 4.19 (c, d)) that suggests bone lineage and bonding osteogenesis on the scaffold within 14 days of cell culture. This study showed that scaffold prepared from 30 wt% gelatin, 42 wt% chitosan, and 28 wt % HAp promoted MSCs differentiation into osteoblast cell and then to osteogenic lineage.

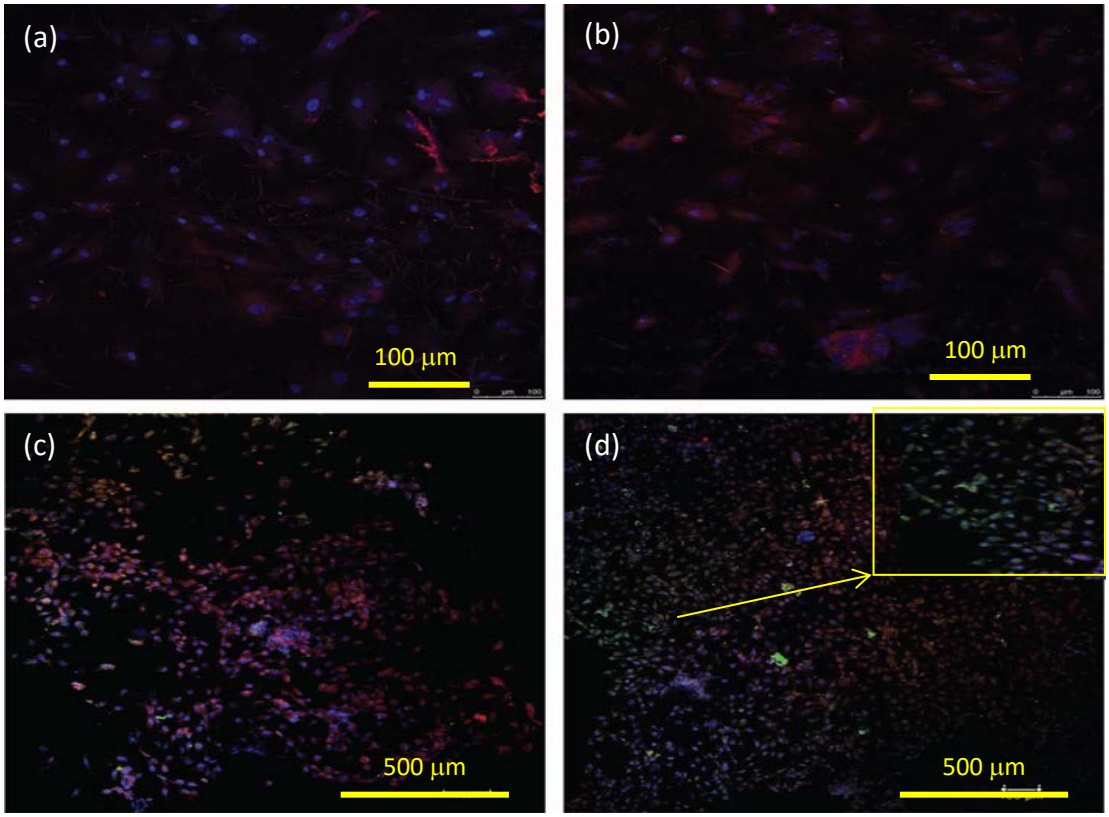

Figure.4.19. Confocal images of RUNX2 and osteocalcin (a, b) control (gelatin-chitosan) after culturing MSCs for 7- and 14-days culture and (c, d) HA–Chi/Gel (28:49:30) after culturing MSCs for 7- and 14-days culture.

4.7 Conclusions

In this study composite scaffold of nano HAp-chi and gelatin was prepared and characterized. HAp-chi composite nanopowders in the size range between 40-70 nm were synthesized using in situ co-precipitation method. The porous composite scaffold with varying weight per cent of hydroxyapatite (HAp), chitosan and gelatin was fabricated using freeze drying method. The FTIR spectrum indicated the ability of glutardaldehyde to form effective crosslinked network in the polymer matrix of the scaffold. The GCH30 scaffold exhibited the highest compressive strength and a pore size distribution ideal for bone tissue ingrowth and eliciting osteoinductive property. With increase HAp content upto 30 wt%, the compressive strength in the prepared GCH scaffold increased. Nanosize HAp-chi particles were found to be uniformly dispersed in gelatin network, leading to higher compressive strength. The prepared GCH 30 scaffold exhibited conducive and bioactive environment for MSC's attachment, spreading, proliferation, and differentiation into bone cells. In vivo evaluation of bioactivity of the scaffold using rabbit model is the next step to prove its high efficacy as a bone scaffold.

CHAPTER # 5

Development of Gelatin-Chitosan-58s Bioactive glass 3D Porous scaffold

The people who influence you are the people who believe in you.
Henry Drummond

Abstract

The aim of the present study was to prepare and characterize bioactive-gelatin-chitosan based composite scaffold and evaluate its bone regeneration ability at orthopaedic defect site. Bioactive 58s glass nanoparticles having composition SiO_2:CaO:P_2O_5 equals to 58:33:9 in mol.% was synthesized using the sol-gel method in the size between 80 to 100 nm. Porous scaffolds with varying bioglass composition from 10-30 wt% in chitosan, gelatin matrix were processed using the method of freeze-drying of slurry containing 40 wt% solids loading. Polymer matrix was crosslinked with glutaraldehyde to improve scaffold's mechanical strength with microstructure having interconnected porosity. The prepared scaffolds exhibited high (>80%) porosity with a mean pore size varying between 100-300 micron. With increase in bioactive glass amount up to 30 wt%, the compressive strength of the scaffold increased and showed a maximum of 2.2 ± 0.1 MPa for GCB30. Swelling and degradation studies showed that the scaffold possessed excellent hydrophilicity and controlled biodegradability. GCB30 scaffold was shown to be non-cytotoxic and supported mesenchymal stem cell attachment, proliferation and differentiation as indicated by MTT assay and RUNX-2 expression by the cultured MSC's. Higher cellular activity was observed in GCB 30 scaffold as compared to GCB 0 scaffold suggesting the fact that 58S bioactive glass nanoparticles addition into the prepared scaffold promoted better cell adhesion, proliferation and differentiation. Strongly positive osteocalcin signalling within 14 days of cell culture supported the fact that the prepared scaffolds stimulated new bone tissue regeneration. Thus, the study showed that the developed composite scaffolds are potential candidates for regenerating damaged bone tissue and could be useful in orthopaedic applications.

5.1 Introduction

Designing new biomaterials that can mimic the micro/nano-structure and chemical composition of the native extracellular matrix (ECM) is one of the most attractive and important research areas in the field of tissue engineering. ECM governs cell attachment, growth, migration and differentiation, as well as the formation of new tissues[229]. Scaffolds that mimics ECM of bone should ideally be processed from biomaterials with adequate properties such as biocompatibility, osteoconduction, bioactivity, osteoinduction, and biodegradatio [230]. Three dimensional (3D) porous structure of scaffolds provides necessary support for cells to proliferate and differentiate, and its architecture ultimately governs the shape of a new bone[231, 232]. Moreover, scaffolds for bone regeneration should mimic

bone morphology, structure, and function. Bone is composed of calcium phosphate (69–80 wt %, mainly hydroxyapatite), collagen (17–20 wt %), and other components (water, proteins, etc.).[232] For this reason, composites based on apatite crystals and natural biopolymers have received increasing attention in bone tissue engineering applications [233, 234].

Biocomposites based on biodegradable polymers and bioactive ceramics have been developed for applications in bone repair and reconstruction. Several polymers such as polylactic acid (PLA), polyglycolic acid (PGA), polylactic-coglycolic acid (PLGA), gelatin, alginate and chitosan (CH) are widely used for this purpose because of their proven biocompatibility and complete bioresorbability [180, 235-239].

Chitosan (CS) is a natural biopolymer extracted from crustacean. CS is a polysaccharide-type biological polymer possessing reactive amine and hydroxyl groups that promote osteoblast growth and in vivo bone formation [240-243]. Chitosan plays an important role in the attachment, differentiation and morphogenesis of osteoblasts, the bone forming cells, because of its structural similarities with glycosaminoglycans, a major component of bone and cartilage.[244-246]. Despite its tremendous promise in bone tissue engineering application, the poor mechanical properties of chitosan limits its clinical application in weight bearing bones, which has been addressed by the addition of bioceramics in chitosan scaffolds [247].

Gelatin, a non expensive and commercially available biomaterial that has gained interest in biomedical engineering, mainly because of its biocompatibility and biodegradability. Since it contains Arg–Gly–Asp (RGD)-like sequences that promote cell adhesion and migration, it has been blended with chitosan to improve biological activities of composite scaffold [248, 249]. Gelatin–chitosan scaffold has been tested for the regeneration of various tissues including skin [250], cartilage [251], and bone [252].

Bioactive glasses are a group of bioactive ceramic materials with good bioresorbility. When immersed in physiological solution, these bioactive materials can form hydroxyl carbonate apatite (HCA) layer that is chemically and compositionally similar to the mineral phase of human bone. The formation of apatite layer triggers chemical bonding between implant biomaterials and bone tissues [53, 253-255]. Shalumon et al.[256] investigated the effect of nanoscale bioactive glass and hydroxyapatite incorporation in PCL/chitosan nanofiber for bone and periodontal tissue engineering. Piergiorgio et al, Gentile et al.[257] in their study found that SiO_2-P_2O_5-CaO-MgO-Na_2O-K_2O containing bioglass in 70 wt% amount in chitosan –gelatin composite exhibit excellent bioactivity. Bioactivity and mechanical properties of composite scaffold comprising chitosan (CS) and 55S bioactive glass ceramic nanoparticles was reported by Mathew Peter et al.[258]. In another study, Mathew Peter et al

[219] investigated the effect of 55S bioglass nanoparticle addition on physio-chemical properties of chitosan-gelatin scaffold. The effect of 45S5 BG in Chi-Gel based scaffold on mesenchymal stem cell activity was reported elsewhere [259]. Previous reports demonstrated that 58S BG containing 58 mol% SiO_2– 33 mol% CaO–9 mol% P_2O_5 is suitable for bone repair due to its excellent biocompatibility, bioactivity and biodegradability[260, 261]. Despite none of the studies was focused on investigating the effect of addition of 58S bioglass nanoparticles into chitosan- gelatin based scaffold on mechanical properties and mesenchymal stem cell activity onto the scaffold.

Here we report the effect of compositional variation amongst chitosan, gelatin and synthesized 58S bioglass nanoparticles on physicochemical properties, microstructure, mechanical properties and bioactivity of the prepared scaffold. Optimization of the composition of the prepared scaffold was performed evaluating the pore size and its distribution, biodegradation kinetics and mechanical properties. In detail scaffold-MSCs *in-vitro* interaction was investigated on scaffolds using SEM, MTT assay and immunocytochemistry.

5.2 Materials and Methods

5.2.1 Materials

Chitosan (medium molecular weight , degree of deacetylation=85%) and gelatin (Type B extracted from bovine skin) were purchased from Sigma Aldrich (USA). Tetra Ethyl Ortho Silicate (TEOS: $C_8H_{20}O_4Si$), Triethyl Phosphate (TEP:$C_6H_{15}O_4P$) and calcium nitrate tetra hydrate ($Ca(NO_3)_2$,$4H_2O$) were purchased from Merck (India). Glacial acetic acid (96%) and ammonia solution (NH_4OH) were procured from LOBA chemical (India). Glutaraldehyde (GA)($C_5H_8O_2$) and 0.1M nitric acid (HNO_3) were purchased from Merck Inc (India).

5.2.2 Sol-Gel preparation of 58S bioactive glass

Figure 5.1 shows a schematic diagram of 58S bioactive glass nanopowder synthesis using sol-gel method through one step acid catalyzing process.The composition of the synthesized bioactive glass was 58% SiO_2 , 33% CaO and 9% P_2O_5 in molar percentages and composition was chosen based on the ternary phase diagram of CaO–SiO_2–P_2O_5 [262, 263]. In brief, 14.8 g of tetraethoxysilane (TEOS) was added to 30 ml of 0.1 M nitric acid, and the mixture was allowed to react for 30 min for maximum completion of acid hydrolysis of TEOS. Distilled water was added to the solution and allowed to mix until the solution became clear. The H_2O: (TEOS) molar ratio was 12:1. After 30 minutes, 0.85 gm of Triethyl Phosphate (TEP) was added to the stirred solution followed by the addition of 7.75 gm of

calcium nitrate after another 20 minutes. The solution was then stirred for an hour. The mixture was cast in a cylindrical teflon container and kept sealed for a week at room temperature to allow hydrolysis and a polycondensation reaction occurs in course of gelation of the sol. The gel was dried at 120◦C for two days in an oven. The dried powder was heated for 24 h at 600◦C for nitrate elimination and stabilization of gel. Subsequently, the powders were ball milled by planetary milling (Fritsch Company, Germany) at 400 rpm for six hr.

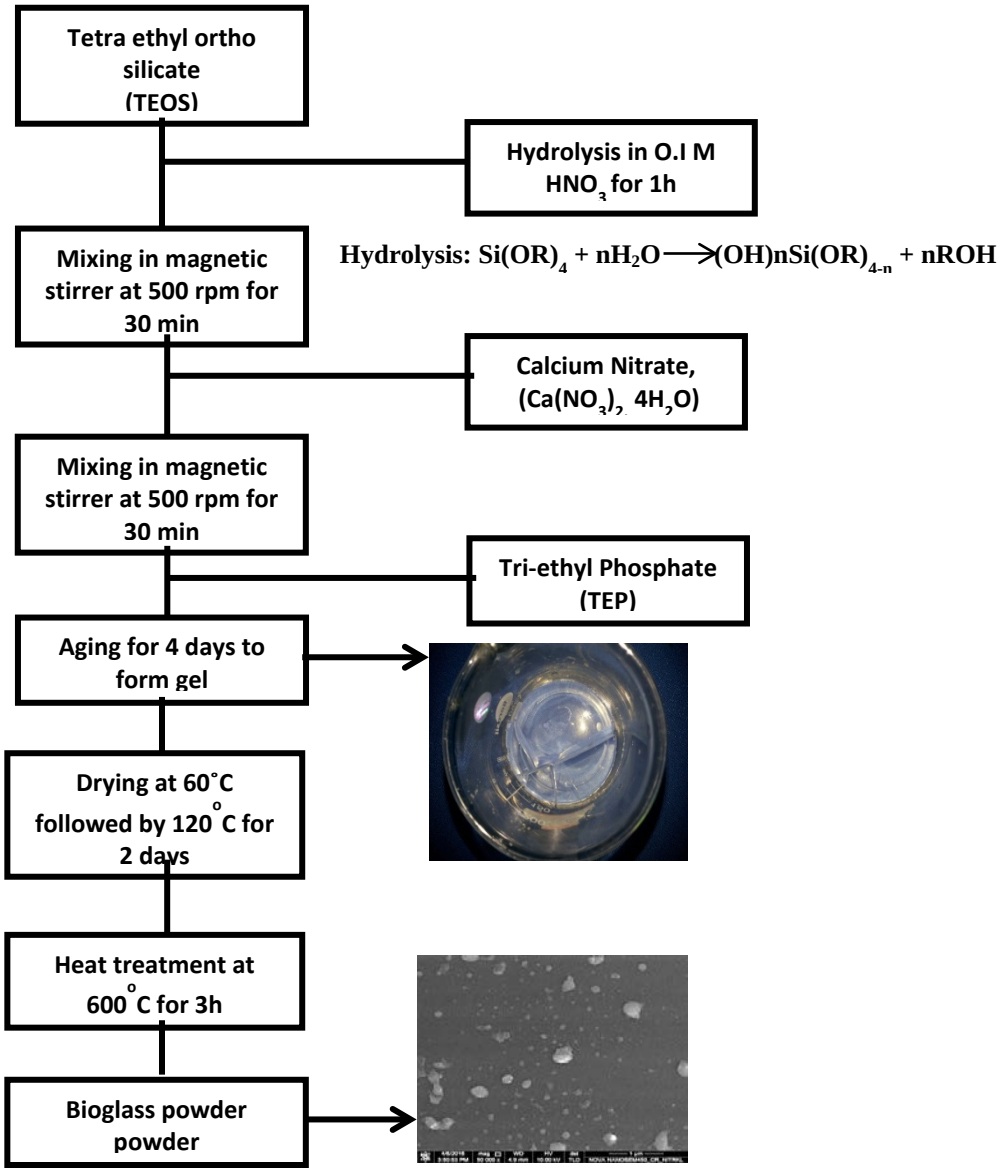

Figure5.1. A schematic diagram of bioactive glass powder production *via* acidic catalysed sol-gel process.

5.2.3 Preparation of porous Gelatin-Chitosan/Bioglass(GCB) composite scaffold

The GCB scaffolds were prepared with varying amount of synthesized 58S-BG nanopowder keeping the amount of gelatin constant at 30 wt% as listed in Table 5.1. Our previous work

indicated that increase in nanoceramic phase content beyond 30 wt% in gelatin-chitosan matrix resulted in <50 μm pore size in the prepared scaffold, rendered it not ideal for cell ingrowth and hence exhibiting osteoinduction. Similarly, scaffold's average pore size decreased below 40 μm on increasing gelatin content higher than 30 wt% with nanoceramic phase content varying between 10-30 wt% in the scaffold. As we found that 30 wt% gelatin content scaffold exhibited the highest compressive strength, our objective in this study was to evaluate the physicochemical and mechanical properties of the prepared scaffold on varying bioglass content from 10 wt%-30 wt% keeping gelatin content fixed at 30 wt%.

Figure 5.2 illustrates the preparation processes of GCB scaffolds. First, chitosan (Chi) solution was prepared by dissolving required amount of medium molecular weight chitosan in a solution containing 4 ml of acetic acid and 96 ml of deionized water with stirring for 5 h to get a perfectly transparent solution. A glutaraldehyde solution was prepared by dissolving 0.5 mL (50%) glutaraldehyde in 100 mL deionized water. Then, required amount of gelatin was dissolved in deionized water with continuous stirring at 40^{o}C for four hour. This solution was then added to the two wt% chitosan solution. Different weight percentages (10%, 20%, 30%) of 58S-BG was then added into the gelatin-chitosan solution and stirred for 4 hours. The resulting slurry (gelatin-chitosan-bioglass) was put in PTFE cylindrical mould and then rapidly prefreezed at -20˚C to solidify the water and kept overnight. Next, the frozen samples were lyophilized using a freeze-dryer (Labconco, US) at -52˚C for 24 hrs. Finally, samples were soaked in 1 wt% GA solution for 24 h and then carefully washed with de-ionized water to remove the remaining amount of GA. The crosslinked scaffold was further treated with sodium borohydride aqueous solution to block residual aldehyde groups, and then washed with ethanol-NaOH followed by deionized water. The washed porous scaffold was again freeze-dried to obtain the hybrid network of gelatin -chitosan- bioactiveglass. The schematic flow diagram is presented in Figure.5.3.

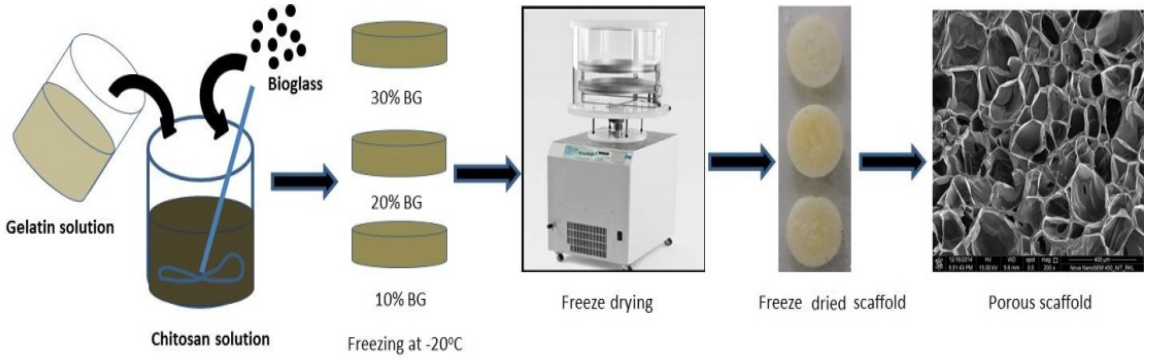

Figure.5.2. Fabrication procedure for the GCB scaffolds.

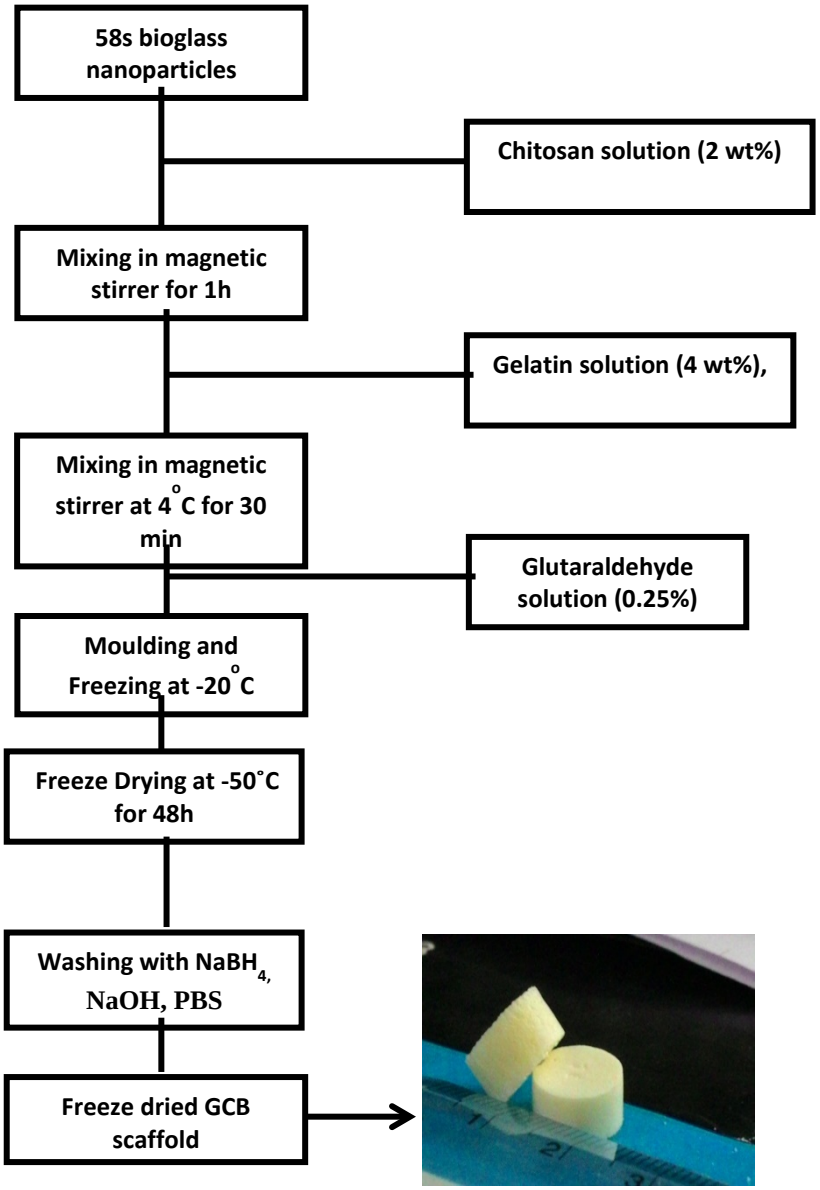

Figure.5.3. Schematic flow diagram of fabrication of GCB scaffolds.

Table.5.1. Composition of GCB scaffolds.

Specimen name	Gel concentration (w/w)%	Chitosan Concentration (w/w %)	CS-Gel/BG Ratio (w/w)%	Solid Loading (%)
GCB-0	30	70	100/0	40
GCB-10	30	60	90/10	40
GCB-20	30	50	80/20	40
GCB-30	30	40	70/30	40

5.2.4 Characterization

5.2.4.1 X-Ray Diffraction (XRD) analysis

The phases of composite scaffolds were characterized by X-ray diffraction (XRD) using fully automated X- ray diffractometer (Panalytical, USA) fitted with Ni filter. The detailed procedure was mentioned in Chapter4 in section 4.4.1.

5.2.4.2 Particle size analysis using dynamic light scattering (DLS)

Particle size of synthesized bioglass nano powder was measured using (DLS) technique by Malvern zetasizer (ZEN3690, USA). The detailed procedure was mentioned in Chapter4 in section 4.4.4.

5.2.4.3 Fourier Transform Infrared Spectroscopy (FTIR) analysis

The characteristic peaks of the composite scaffold were analysed using Fourier transform infrared (FTIR) (Perkin Elmer, USA) spectroscopy. The detailed procedure was mentioned in Chapter4 in section 4.4.2.

5.2.4.4 Transmission Electron Microscopy (TEM) of 58s bioactiveglass nanoparticles

The particle size, morphology and crystallinity of as synthesized 58s bioactive glass powder was studied by TEM (FEI, Nederland), SAED (Selected Area Electron Diffraction) pattern. The detailed procedure was mentioned in chapter 4 in section 4.4.4.

5.2.4.5 Scanning Electron Microscope (SEM) analysis

The composition of prepared bioactive glass powder was studied using energy dispersion X-ray (EDX) analysis. The morphology and microstructure of the scaffolds have been observed using field emission scanning electron microscopy (FESEM) (Novanano 450, FEI,

Netherland) operated at 78 μA, 15KV. The detailed procedure was mentioned in Chapter4 in section 4.4.6.

5.2.4.6 Mechanical behaviour (Compression test)

The mechanical properties of the composite scaffolds were determined using a Universal Testing Machine (Tinius Olsen, UK) with a crosshead velocity of 1 mm min^{-1} and a 1000N load cell. The detailed procedure was mentioned in Chapter4 in section 4.4.9.

5.2.4.7 Porosity of scaffold

The porosity of composite scaffold (diamter 5 mm, height 12 mm) was measured using Archimedes principle with xylene as liquid medium . The detailed procedure was mentioned in Chapter4 in section 4.4.7.

5.2.4.8 Swelling behaviour of GCB scaffold

The swelling properties of the chitosan–gelatin- bioactive glass scaffolds were investigated using PBS solution for 24 days. The detailed procedure was mentioned in Chapter4 in section 4.4.10.

5.2.4.9 Mineralization behaviour of GCB scaffold

The ability to form apatite when immersed into simulated body fluid (SBF) is an index of biocompatibility exhibited by the GCB scaffold. The detailed procedure was mentioned in Chapter4 in section 4.4.11.

5.2.4.10 In vitro biodegradability of GCB scaffold

The scaffolds were immersed into the phosphate buffer solution. and degradation assessment by monitoring the weight loss. The detailed procedure was mentioned in Chapter4 in section 4.4.12.

5.2.4.11 Cell Culture Study

5.2.4.11.1 Attachment and morphology of cell on GCB composite scaffolds

Human Umbelical Chord Mesehenchymal stem cells (MSCs) were grown in a Dulbecco's modified Eagle's medium (DMEM; Sigma-Aldrich, UK) supplemented with 10% fetal bovine serum (FBS; Sigma-Aldrich, UK) and 100 U/mL penicillin–streptomycin. The detailed procedure was mentioned in Chapter4 in section 4.4.13.3.

5.2.4.11.2 Analysis of viability differentiation of MSc cultured onto the scaffolds

Cell viability of MSCs cultured onto the scaffolds were determined after performing [3-(4,5-dimethylthiazol-2-yl)-2,5-diphenyltetrazolium bromide] (MTT) assay. The detailed procedure was mentioned in Chapter4 in section 4.4.13.4.

5.2.4.11.3 Inmunofluorescent imaging of cell markers: osteocalcin and RUN-X2

The expression of RunX2 and Osteocalcin, an osteogenic marker was examined using immunocytochemistry. The detailed procedure was mentioned in Chapter4 in section 4.4.13.5.

5.3 Statistical *Analysis*

All data are expressed as mean ± standard deviation. The data were compared using Student's t-test and differences were considered significant when *$p < 0.05$. A p-value more than 0.05 ($p > 0.05$) was taken as indicating no significant difference.

5.4 Results and Discussion

5.4.1 XRD and FTIR analysis

Figure.5.4 (a) shows the FT-IR spectrum of synthesized bioactive glass powder. The characteristic bands for different functional groups present in the powder are shown in Table.5.2. The band at 1638 cm^{-1} corresponds to carbonate (CO_3^-) coming from atmospheric CO_2 and attached to Ca^{2+}. The band at 1022 cm^{-1} arises from v^3 PO_4, whereas the band at 653 cm^{-1} suggests the presence of v^4 PO_4. The band at 836 cm^{-1} was assigned to the stretching vibration of Si-O- groups in bioglass. The abs option bands observed at 1076 cm^{-1} and 540 cm^{-1}were assigned to stretching vibration of Si-O-Si respectively and bending of Si-O-Si [264]. Typical absorption band at 1786 cm^{-1}, 1431 cm^{-1} are attributed to the deformation mode of adsorbed molecular water in the pores. Phase analysis of the composite nanopowder was performed using XRD. Figure.5.4 (b) clearly indicates the amorphous nature of the synthesized bioactive glass powder [257].

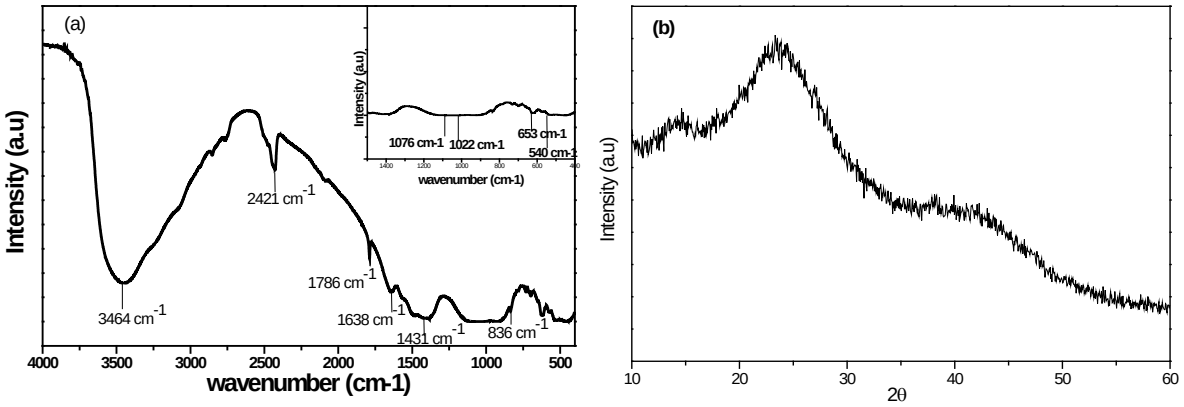

Figure.5.4. FTIR and XRD pattern of 58SBioglass powder prepared via sol-gel process.

Table.5.2. Peaks of infrared spectra assigned to synthesized bioactiveglass powder.

Bond	Infrared Frequency (cm^{-1})
Si-O-Si bending	540,1076 cm^{-1}
P-O bending vibration	1022,653 cm^{-1}
-OH	3456 cm^{-1}
CO_3-	1638 cm^{-1}
Adsorbed molecular water	1786,1431 cm^{-1}

5.4.2 Particle size, morphology and composition of nano-bioactiveglass powder

Figure.5.5 represents DLS particle size mesurement data of synthesized 58s bioactiveglass nanopowder. An average particle size of 85± 9.5 nm was obtained from the DLS mesurement which is little bit higher as compared to the particle size shown in the FESEM image in Figure 5.6(a). Particle size mesurement by DLS technique gives the hydrodynamic diameter of the particle and also bioglass particles were to some extent in agglomerated state in the suspension that suggest higher average particle size value in the DLS mesurement. From FESEM micrograph in Figure.5.6 (a) it is evident that the bioglass particles were spherical in morpology and agglomerated in course of drying. EDS analysis in Figure.5.6 (b) suggests that the synthesized powder with a molar composition of Si:Ca:P=56:30:9 closely resembled the theoritical composition as shown in Table.5.3.It can be seen from TEM analysis in Figure.5.6 (c,d) that bioactive glass powred exhibited an amorphous phase with a particle size less than 100 nm.

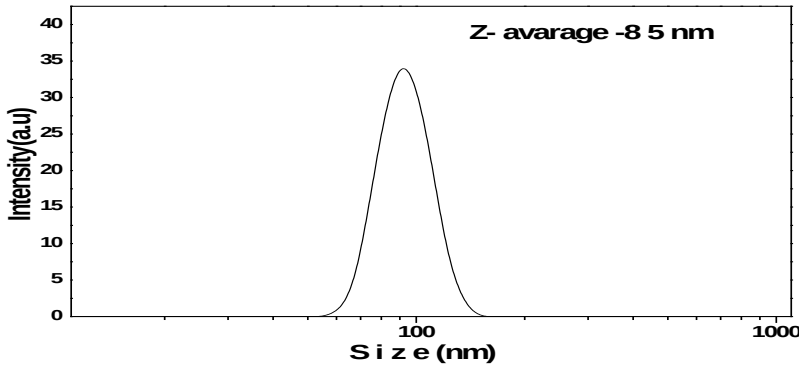

Figure.5.5. The particle size distribution of NBG measured by DLS.

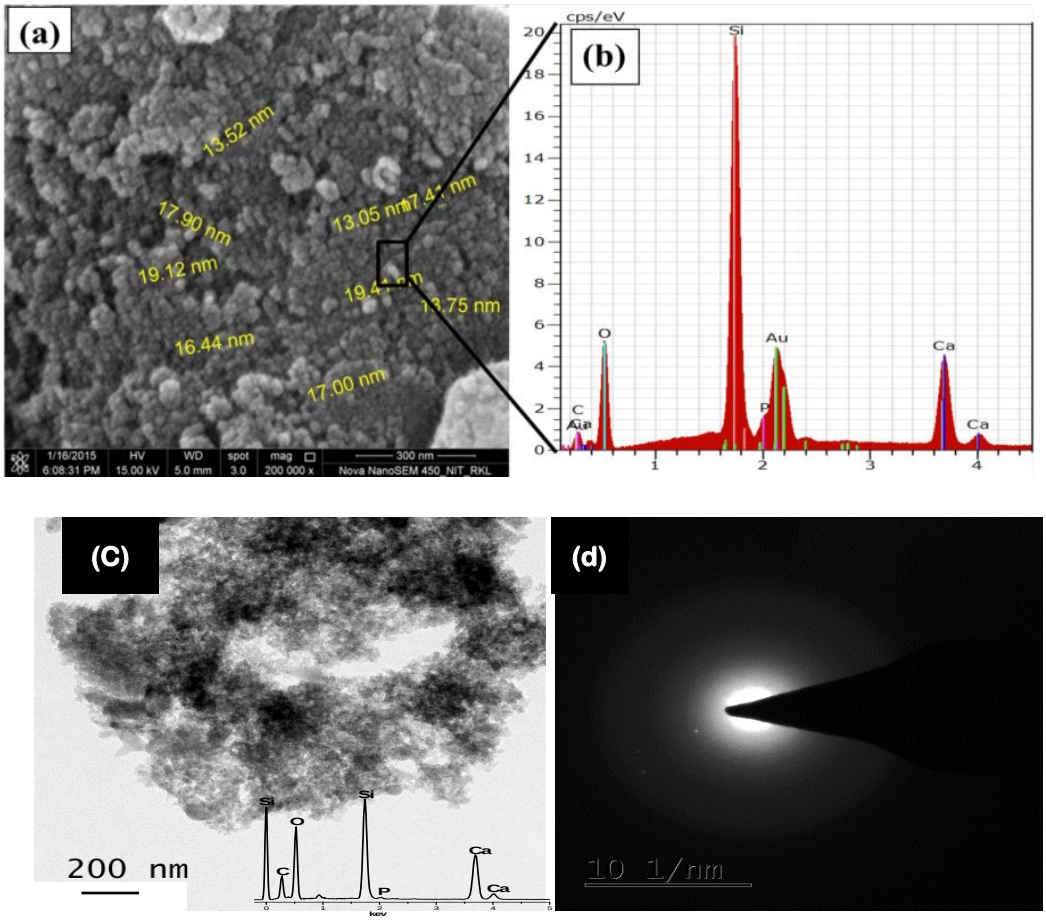

Figure.5.6.(a) FESSEM micrograph of synthesized bioglass nanopowders (b) Elemental composition analysis of the synthesized bioglass nanoparticles.(c) TEM image of 58 bioactive glass nanoparticle.(d) SAED pattern of bioactive glass particle.

Table.5.3. EDS analysis of 58s Bioglass powder.

Elements	Bioactive glass Atomic percent
Si	56.14
Ca	30.88
P	9.02
O	3.96

5.4.3 XRD analysis of composite scaffold

Phase analysis of the composite scaffolds was performed using XRD. The characteristic diffraction peaks for both chitosan and gelatin were suppressed by the huge amorphous peak of bioglass observed in the range between 2θ equals to 20^{o}-40^{o}. The broad amorphous peaks of bioglass confirmed that the prepared scaffolds were predominantly amorphous as shown in Figure.5.7.

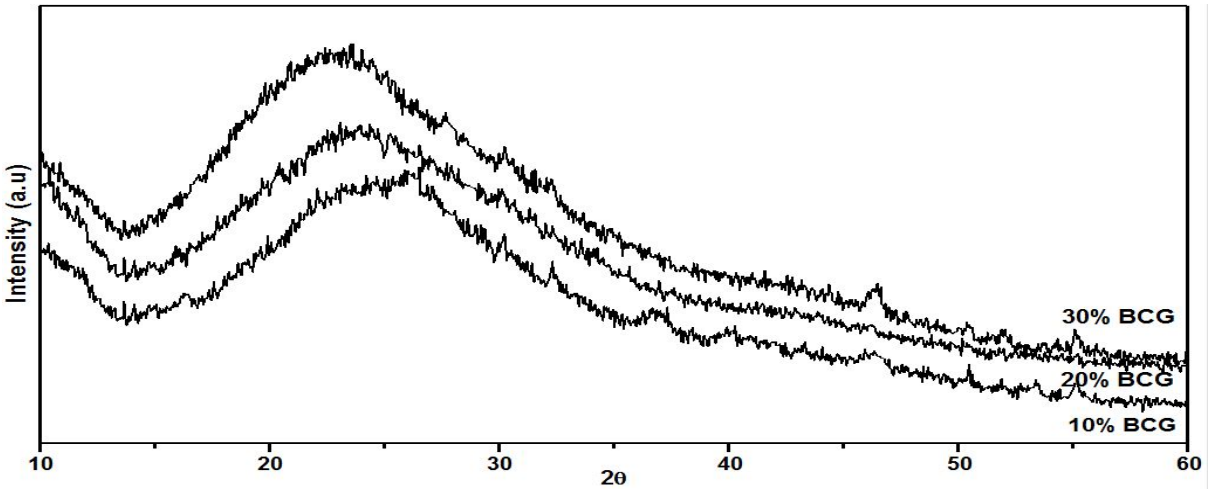

Figure.5.7. XRD analysis of GCB composite scaffold with varying amount of bioglass powder.

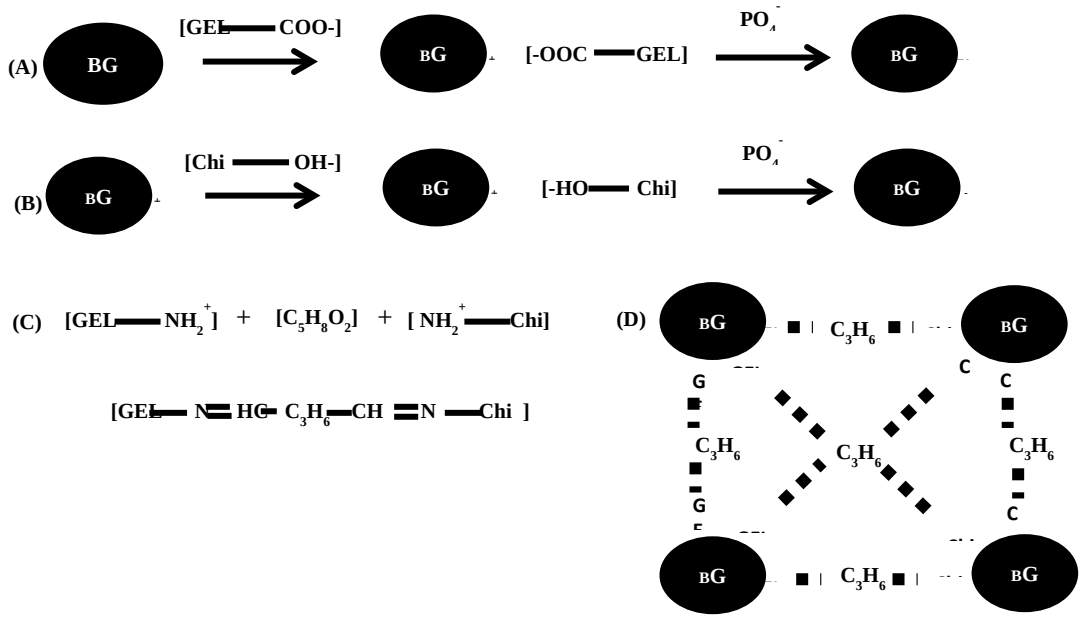

Figure.5.8. Possible chemical interaction between Bioactiveglass and Gelatin-Chitosan (a) Gelatin-Bioglass, (b) Chitosan-Bioglass, (c) Gelatin-Chi crosslinking, (d) Gelatin-Chi-BG complex.

5.4.4 Chemical structure study of composite scaffold

Chemical structure of composite scaffolds was investigated by FTIR, in order to examine the chemical interactions between the gelatin, chitosan and bioglass phases, as shown in Figure.5.9. Apart from corresponding peaks of PO_4^{3-} at 1026 and 651 cm^{-1}, Si-O-Si in bioactive glass at 1076 cm^{-1}, bands for amide I at 1662 cm^{-1}, amide III at 1232 cm^{-1} and carboxylate at 1446 cm^{-1} in gelatin, a distinct band at 1552 cm^{-1} was detected. This absorption band signifies the formation of –C=N- bond due to inter-gelatin and chitosan - gelatin cross linking to develop 3D interconnected network in the scaffold [265]. appearance of band at 1661 cm^{-1} indicates amide I of gelatin which suggested the predominantly alpha-helical protein configuration of gelatin in prepared GCB30 scaffolds [157], and this was further confirmed by the appearance of amide II mode at 1552 cm^{-1}. The band at 1330 cm^{-1} is attributed to the chemical bond formation between carboxylate group in gelatin and Ca^{+2} ion in bioactive glass to bind the particulate reinforced composite scaffold together [266, 267]. These interactions between the gelatin, chitosan and silica phases would enhance the stability of the composite gelatin–chitosan-bioactive glass hybrid scaffolds in a water-based environment as shown in Figure 5.8.

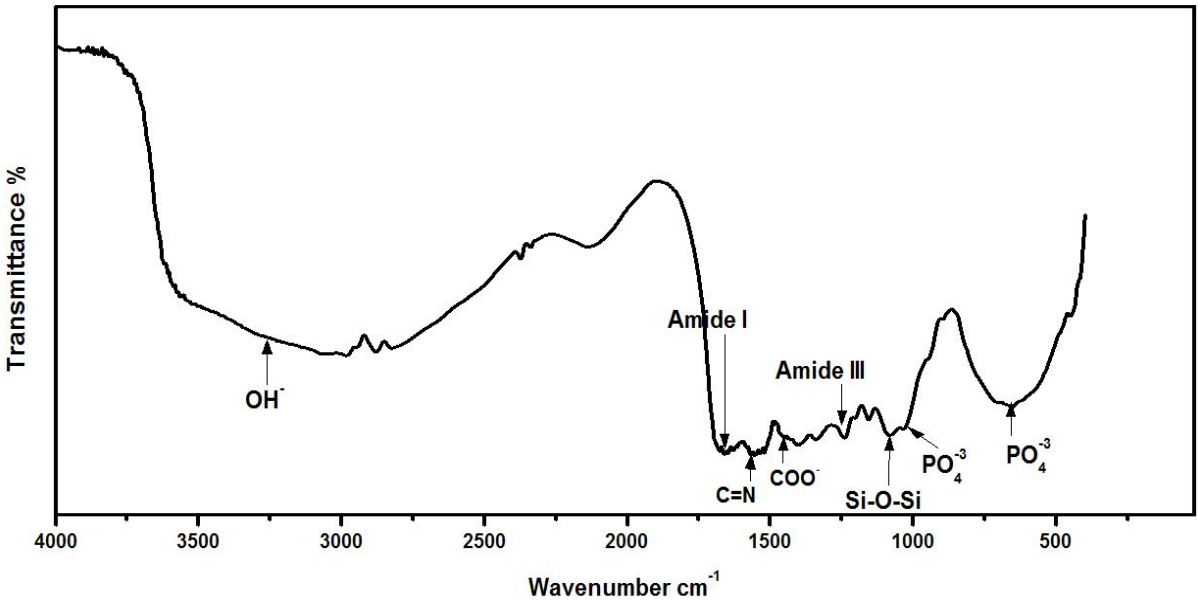

Figure.5.9. FTIR spectra of Gelatin/Chitosan/Bioglass (GCB 30) composite scaffold.

5.4.5 FESEM microstructure of fabricated GCB scaffold

The physical characteristic of a scaffold can be described by its average pore size, pore interconnectivity and pore shape. Pores are necessary for the bone tissue formation because they allow migration and proliferation of osteoblast and mesenchymal stem cells, as well as the proper vascularizton of the implant [268]. The morphology of BCG scaffolds before and after bioactiveglass incorporation is shown in Figure.5.10. FESEM micrograph of composite scaffolds (Figure 5.10) showed that scaffolds were macro porous in nature. The porosity was found to vary from 81 to 89% depending on the percent addition of bioactive glass powder. The average pore sizes of GCB scaffolds with 10wt% bioactive glass were varied between 200–250 μm. As the bioactive glass content increased to 30wt%, the average pore sizes of the scaffold was reduced to 115 μm and pore shape became irregular. With the augmentation of bioglass content in GCB slurry, the interactions between bioactiveglass particles and gelatin increased with consequent increase in solution's viscosity. Thus as we go from 10 – 30 wt% bioactiveglass content in scaffold, a higher and higher force was necessary for GCB slurry to be expelled by water molecules, so the ice crystals growth was hindered during freezing of slurry resulting in reduced size of inter trapped ice blocks and scaffolds with smaller pores were formed during subsequent sublimation[269]. A top view (Fig.5.10 (a-d)) and side view(Figure 5.10 (a_1-d_1)) representation of the scaffold are shown in Figure.5.10 that were used to calculate the average pore size. In particular, with an increase in bioactive glass content, increasing amount of bioactive glass particles were deposited onto the chitosan-

gelatin based pore walls (Figure 5.10a_{II}-d_{II}) as confirmed subsequently by FESEM examination. All results demonstrate that the prepared scaffolds exhibited a porous distribution with pore size varying between 94-250 micron with rough pore wall, crucial for protein and cell adhesion.

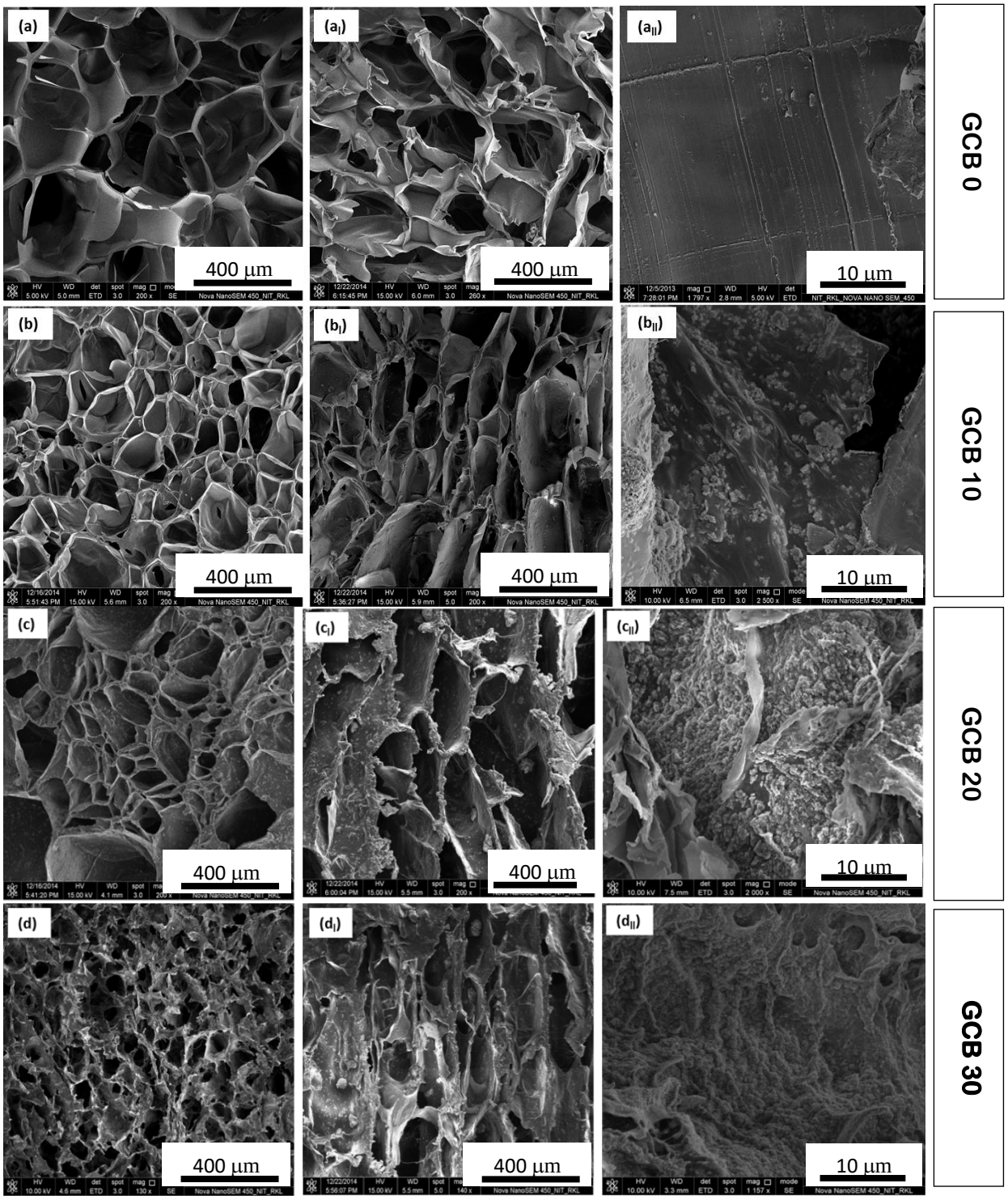

Figure.5.10. FESEM microstructure of GCB composite scaffolds. crossection (a-d), longitudinal (a_I-d_I), pore wall distribution (a_{II}-d_{II}).

5.4.6 Analysis of Pore size and its distribution in the scaffold

Table.5.4 indicates the total porosity and mean pore diameter values of different scaffolds with varying composition. The mean porosity value varied between 81%-89% suggesting that compositional variation did not affect the total porosity in a significant manner (all p values > 0.05). Pore size distribution data in Figure.5.11 also shows the unimodal pore size distribution for all the prepared scaffolds. The most frequent pore diameter in the scaffold was decreased from 250 μm to nearly 100 μm as we increase bioactive glass content from 10%-30% in GCB slurry. All the scaffolds showed the ideal pore size distribution for exhibiting osteoinductivity and osteoblast or stem cell ingrowth into the scaffold as the pore size distribution in the scaffold falls within 100-400 μm.

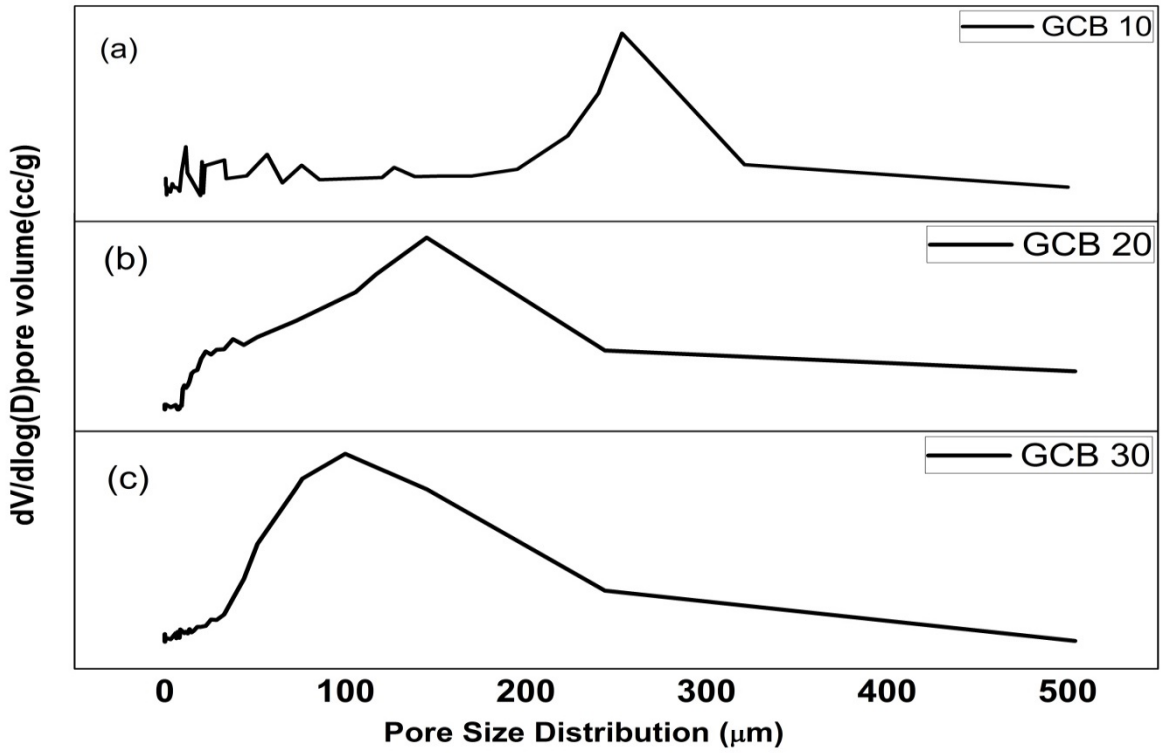

Figure.5.11. Pore size distribution data of Gelatin-chitosan-bioglass scaffold(a)GCB 10,(b) GCB 20, (c)GCB30

Table.5.4. Pore diameter and porosity of prepared GCB scaffold.

Sample name	Average Pore Diameter(□m)	Porosity
BCG 0	400 ± 13.6	89.3 ± 7.8
BCG 10	250 ± 26.3	82.4 ± 5.0
BCG 20	160±17.8	80.8 ± 3.3
BCG 30	100 ±25.9	81.3 ± 6.1

5.4.7 Compressive mechanical Properties of GCB scaffold

Figure.5.12 describes the stress-strain behaviour of GCB composite scaffolds under compression. The stress- strain curve can be decomposed in two stages. The first is the elastic region before yield point and second are the post yield stage i.e. deformation region and then densifying region where the pore wall collapses. In this case, compressive strength of the scaffold is denoted by the point that denotes the end of first linear region. With increase in bioactive glass concentration from 10%-30% wt% compressive strength continued to enhance significantly as in Table 5.5. The compressive strength of pure gelatin-chitosan scaffold are only 0.8 ± 0.16 MPa. After incorporating 30 wt% bioactive glass particles in gelatin-chitosan matrix, the compressive strength increased to 2.2 ± 0.02MPa. The composite scaffold was elastic up to yield point but after yield point some micro crack occurred. The interactions between bioactive glass particles and polymer network bridged the cracks in the scaffold that resulted in postponed final fracture. It is noteworthy that the slope of the deformation region in 30 wt% bioactive glass loaded scaffold was the maximum due to enhanced resistance from the ceramic particle to crack propagation.

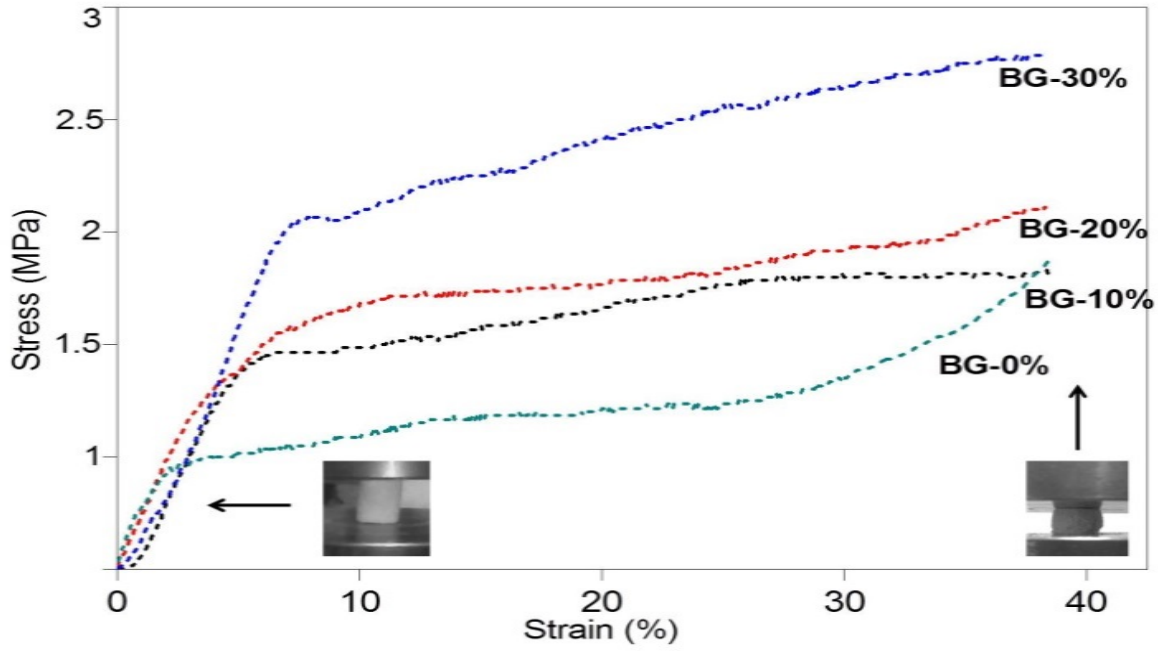

Figure.5.12. Stress-strain behaviour of GCB scaffolds prepared at different bioactive glass concentrations.

Table.5.5. Summary of mechanical properties of GCB scaffolds prepared from solutions of different bioactiveglass concentrations (wt%).

Bioactiveglass scaffolds specimens	Porosity (%)	Mechanical Properties Compressive Strength* (MPa)
BG 0%	89.3 ± 7.8	0.8 ± 0.16
BG 10%	82.4 ± 5.0	1.2 ± 0.01
BG 20%	80.8 ± 3.3	1.6 ± 0.01
BG 30%	81.3 ± 6.1	2.2 ± 0.02

***P*<0.05, by student's t-test, n=3, all values in each mechanical property category were found to be significantly different from each other.**

5.4.8 Mineralization ability of Gelatin Chitosan-bioactive glass composite scaffold

Mineralization ability of scaffold in SBF has been regarded as one of the key evidences of bioactivity for bone scaffold. It has been reported scaffold which support osteoblast cell growth, proliferation and differentiation in vitro and in vivo exhibits good mineralization behaviour in physiological environment. Highly dense bone-like carbonated apatite layer formation on SBF treated GCB30 scaffold (Figure.5.13) indicates that the prepared scaffolds are not only biocompatible, but also bioactive.

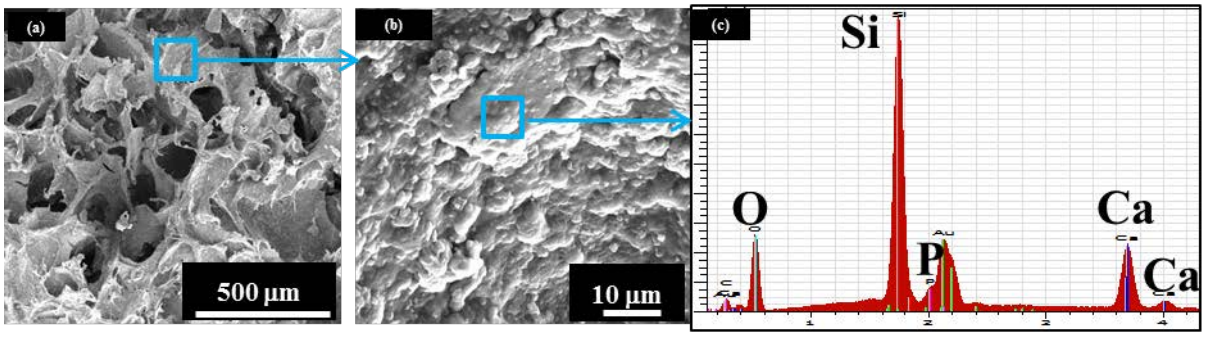

Figure.5.13. SEM micrographs of carbonated apatite layer formed on the surface of GCB30 composite scaffold immersed in SBF for 7 days.

5.4.9 Biodegradation study

Scaffold materials are expected to be biodegradable and bioresorbable with a proper rate to match the speed of new bone tissues formation. The controlled, and steady degradation behaviour of bone scaffold in physiological environments plays an important role in the regeneration of new bone tissues. The *in vitro* degradation of GCB scaffold in phosphate buffer solution (PBS) at 37°C is an important study to assess its resorbability under

physiologically relevant conditions. For long term mechanical stability and reliability, scaffold material should exhibit slow and controlled degradation behaviour. Figure.5.14 demonstrates the effect of bioactive glass contents on the degradation rate of the scaffold. With an increase in the bioactive glass content, the degradation rate in PBS solution at 37^{o}C decreased significantly. The bioactive glass particulate interacted through ionic and hydrogen bonding with the water molecules and weakened the interaction between the gelatin macromolecule and water. Bioactive glass also acted as a physical crosslinking sites to enhance the stability of the chitosan-gelatin network. Thus, the degradation rate and as a result strength retention in the physiological environment may be controlled by adjusting the bioactive glass contents in the scaffold.

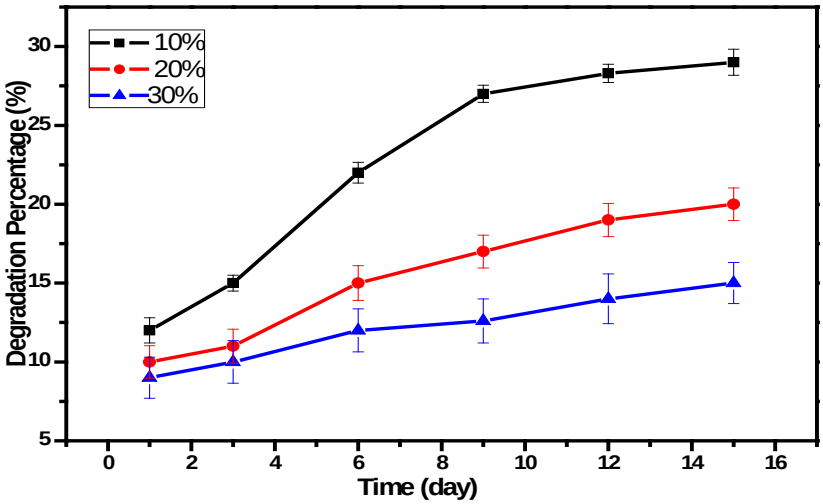

Figure.5.14. In vitro degradation of the GCB scaffold with different bioactive glass contents in PBS.

5.4.10 Swelling studies

The ability of the scaffold to swell plays an important role during the in vitro cell culture studies. Swelling of scaffold allows absorption of body fluid and transfer of cell nutrients and metabolites inside the scaffold. Swelling also increases the pore size and total porosity, thus maximizing the internal surface area of the scaffolds for cell infusion and attachment. However, swelling under physiological condition must be controlled otherwise it may cause weakening and rapid degradation of the bone scaffold.

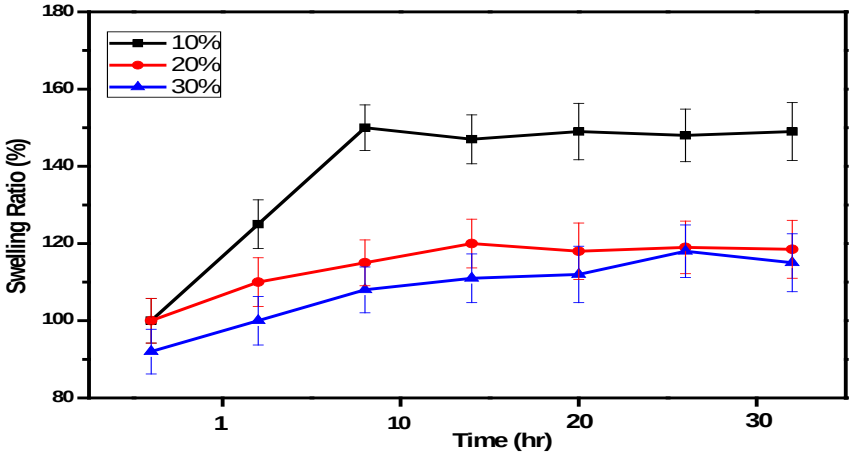

Figure.5.15. Swelling behaviour of GCB composite scaffolds with different bioactive glass contents in PBS.

Figure.5.15 shows that swelling in the GCB scaffold increased initially and gradually attained saturation after 10 hours of soaking in PBS at 37 ^{o}C. The degree of swelling was found to decrease with increasing bioactiveglass amount in the scaffold that may be attributed to the lower hydrophilicity of the inorganic phase as compared to the polymeric matrix having caroboxylate, amine and amide end groups: Thus the increase in predominantly covalent bonded bioglass content in the scaffold resulted in a decreased water sorption. Also, the enhanced polymer-bioactive glass interaction with increasing concentration of bioactive glass resulted in higher elasticity and slower relaxation of polymer chains and also accounted for decrease in swelling ratio.

5.4.11 Cell attachment study on GCB 30 scaffolds

Figure.5.16 shows cell density and morphology after culturing MSCs on GCB 30 for different days of culture time. Cell density, as well as number of lamellipodia and filopodia extensions from the cytoskeleton of MSCs, was increased with progress in cell culture time on composite scaffold. The cell presented a round shape initially [Figure5.16 (a)] and became elongated with increasing time of culture. After 14 days, MSCs cells adopted a polygonal morphology and spread well on the scaffolds [Figure5.16 (c)]. These results clearly indicate that MSCs were attached, proliferated and spread well with increasing cell culture time.

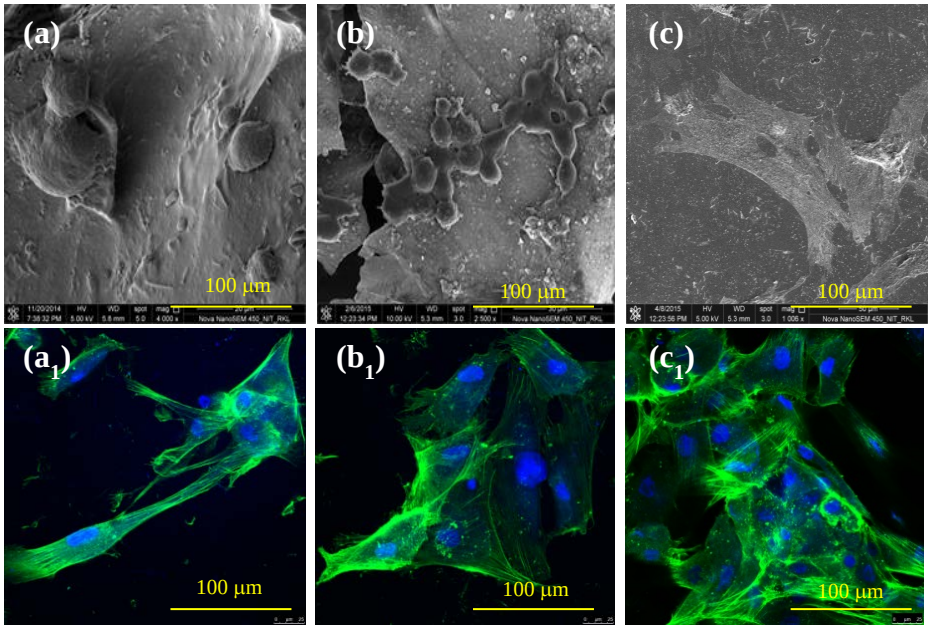

Figure.5.16. FESEM image of MSCs on gelatin-chitosan-bioactive glass (GCB 30) for (a) 1d (b) 3d (c) 14d of cell culture.

Figure.5.16 (a_1-c_1) shows confocal micrographs of MSC's on the GCB 30 scaffolds after 1, 3 and 14 days of culture. Confocal images revealed that a higher number of cells were attached to the scaffold on increasing days of cell culture time. Figures 5.16 (b_1,c_1) show a uniform interconnecting cytoskeleton of MSC's on the GCB 30 scaffolds after culturing cells for 3 and 14 days. The increasing numbers of lamellipodia and filopodia extensions from the cytoskeleton of MSC's were evident with progress in cell culture time as in Figure.5.16 (a_1-c_1). Extensive networks of polymerized β-tubulin and F-actin filaments as well as multiple cell–cell contacts indicate a higher degree of active cell spreading, movement, and signalling events with progress in cell culture. All the results revealed higher proliferation of MSCs on GCB 30 scaffolds after 14 days of cell culture.

5.4.12 Cell proliferation/MTT assay study

After culturing it on the GCB scaffold, MSCs viability study for 3-7 day was performed using MTT assay with cell culture media as negative control and MSCs cultured on tissue culture plate as a positive control. Keeping up with the same trend as exhibited by the positive control, the scaffold material showed higher and higher number of the viable cell with progress in cell culture time as in Figure.5.17. The cell density on five days' cell cultured GCB 30 sample was significantly higher (p value = 0.018) from that on three days sample. Again seven days' cell cultured GCB 30 sample showed significantly higher ($p < 0.001$)

viable cell density as compared to that on day 5 sample. For all incubation periods, GCB 30 presented significantly higher ($p = 0.026$) cell viability than that on GCB 0 scaffold which suggests that addition of 58S bioactive glass nanoparticles in the scaffold promoted better cell adhesion and proliferation. 58S nanoparticles helped in apatite mineralization onto the scaffold in the presence of cell culture media and acted as sites for cell adhesion through integrin mediated interactions from the MSCs. This showed that the selected scaffold was conducive to cell attachment and proliferation.

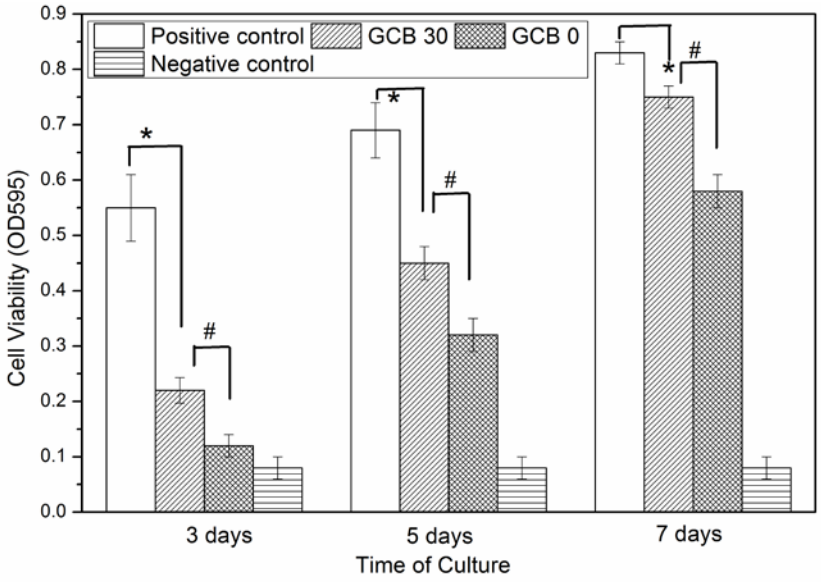

Figure.5.17. MTT assay for cell proliferation study in positive control, negative control, GCB0 and GCB 30 scaffold using human Mesenchymal stem cell on days 3, 5, and 7. * indicates significant difference at $p \leq 0.05$. # indicates significant difference at $p \leq 0.05$.

5.4.13 Study of MSC's differentiation into osteoblast

In order to assess the effect of material composition on cell differentiation, expression of osteoblastic transcription factor RUN-X2 and bone non-collagenous protein osteocalcin (OC) were studied using immunefluorescent markers. As can be seen in Figure.5.18(a-a_1) no RUNX2 marker was visible from 1-day cell cultured sample indicating nascent and premature stage of osteoprecursor cells. There was several fold decrease in the level of expression of most of the osteogenic genes on GCB 0 scaffold (Figure.5.18 (b-c)) as compared to the GCB 30 (Figure 5.18 (b_1-c_1)) at different stages of differentiation, which supports the fact that bioglass addition actually increased the bioactivity of the overall scaffold. RUNX2 expression appeared strongly positive in the GCB30 scaffold cultured for 7 days, supporting the differentiation of MSCs into osteoblast. RUNX2 is a marker for osteoblast differentiation, and an increase in the specific activity of RUNX2 with progress in

cell culture time in a population of mesenchymal stem cell indicates a corresponding shift to a more differentiated state (Figure5.18b_1-c_1).

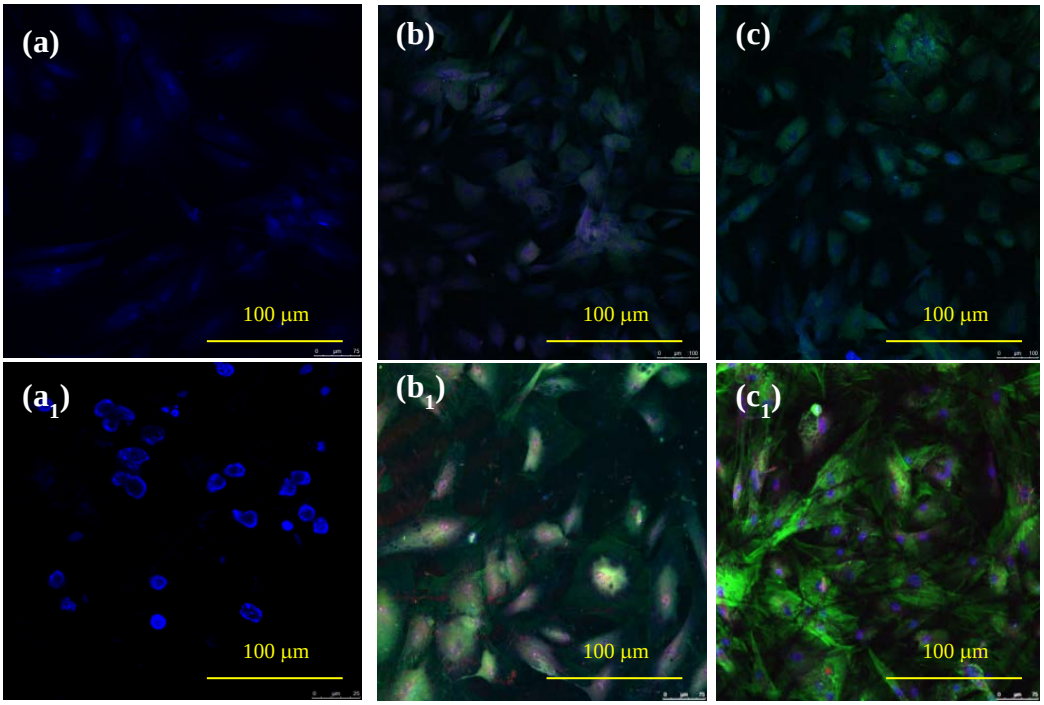

Figure.5.18. Confocal image of RUNX2 and osteocalcin after culturing MSCs on GCB 30 scaffolds on (a) 1 day, (b) 7 day (c) 14 day. In fluroscenes images, osteocalcin is stained green, RUNX2 stained red and nuclei stained blue.

Osteocalcin is a primary non-collagenous protein produced by osteoblasts, which signals termination of osteogenic differentiation and is commonly used to measure bone cell lineage and new bone formation [269]. Greater osteocalcin (green) deposits were seen in scaffolds of 14 days cell culture indicating a higher amount of new bone formation with progress in cell culture time (Figure.5.18(c)). Thus, our result suggests that MSCs in GCB30 scaffold were well committed to osteogenic lineage.

5.5 Conclusions

In summary, we have successfully fabricated GCB nanocomposite scaffolds by using freeze drying method. The scaffolds were highly porous with total porosity of about 80% and average pore size in the scaffold fell to nearly 95 µm from 250 µm with increase in bioactive glass content from 10 wt% to 30 wt% in the gelatin–chitosan matrix. The bioactive glass particles (BG) were well distributed in gelatin-chitosan matrix, significantly improving the compressive strength of the scaffolds. Thus, GCB 30 scaffold showed a compressive strength value comparative to that of natural cancellous bone. It was found that the swelling behaviour

of the scaffolds was reduced with the increase in 58S-BG nanopowder content in the scaffold. Biodegradation test in PBS showed that the increase in 58S-BG content resisted the biodegradability of the scaffold. Preliminary results on cell culture using MSCs suggested that cells could adhere, spread, proliferate and differentiate very well onto GCB 30 scaffolds. MSCs were also found to transform into the new bone cell within 14 days of cell culture on the GCB 30 scaffold making it promising artificial bone grafts.

CHAPTER # 6

Development, characterization and in vivo study of Gelatin-Chitosan-β-TCP scaffold for orthopaedic application

Facts are many, but the truth is one.
Rabindranath Tagore

Abstract

Bio-engineered bone scaffolds prepared imitating the extracellular matrix (ECM) of the native bone is an attractive area of research mainly because it can meet the essential demands and current challenges in bone replacement therapies. The primary aim of this study was to fabricate the gelatin/chitosan/β-tricalcium phosphate (GCT) composite scaffold to improve its compressive mechanical behaviour and *in-vivo* biocompatibility with predictable degradation rate. The β-TCP powder was synthesized in size range between 70-100 nm using aqueous precipitation route at a fixed Ca/P molar ratio of 1.5:1 at pH 10 and after subsequent heat treatment of the as precipitated powder at 800^{o} C for 4 hours. The composite scaffolds were fabricated using the solid-liquid phase separation of the slurry containing gelatin, chitosan, β-tricalcium phosphate in varying proportion and subsequent lyophilisation of the phase separated mixture. The phases, functional groups, and chemical bonds present in the GCT scaffolds were evaluated using X-ray diffraction and Fourier transform infrared (FTIR) spectroscopy respectively. The prepared scaffold exhibited high porosity of 86% with pore sizes ranging between 100-300 μm as determined using Hg-porosimetry. SEM result revealed that incorporation of β-TCP upto 30 wt% resulted in well-shaped and uniformly distributed interconnected pores of average pore size 100 μm in the scaffold. Compressive strength of the scaffolds was increased from 0.8 MPa to 2.45 MPa on increase in β-TCP content from 10 wt%-30 wt% in the scaffold. Human Umbilical Cord derived Mesenchymal stem cells were used to assess the biocompatibility of GCT30 scaffold after culturing them for 3, 7 and 14 days onto the scaffold. Higher degree of lamellopodia and phillopodia extensions and better spreading behaviour of MSC's were observed in FESEM micrograph of MSC cultured GCT 30 scaffold. MTT assay and immunocytochemistry studies with cultured MSC's revealed that GCT 30 scaffolds were more conducive to MSC's proliferation and differentiation into osteoblast lineage. *In vivo* implantation of GCT 30 scaffold subcuteneously into mice did not indicate any significant inflammatory reaction, and ongoing vascularization and scaffold degradation could be observed after four weeks of implantation into mice subcuteneously.

6.1 Introduction

Autograft and allograft bone substitute have been clinically performed worldwide for the treatment of large size uneven bone defects. However, autograft face problems due to limitation of donor supply and chances of infection during healing process [270]. On the other hand, allografts are associated with reduced bioactivity and potential for disease

transmission. To address these problems, bone tissue engineering is emerging as a novel solution that can regenerate the bone tissue on interaction with 3D scaffold that mimics closely to bone extra cellular matrix [271]. Bioceramic have attracted a great deal of attention as a way to mimic the structure of natural extracellular matrix by means of providing temporary support for self or implanted cells. The ECM of bone tissue typically form a nanoscale organized composite between the inorganic and organic ingredients. While calcium phosphate nanocrystals are the major constituents of the composite inorganic material, the organic part is composed of collagen protein network [32, 272, 273]. Mechanically, the organic network provides resilience, while the inorganic crystal hardened the matrix, contributing to a strong and tough ECM. Much research effort has been directed at combination of biopolymer and bioceramics based composite scaffold with improved mechanical and bone regeneration property [184, 274].

Chitosan as a biopolymer receives much attention due to its biocompatibility and biodegradability and its structural similarity with glycosaminoglycan's. Moreover, chitosan can interact with growth factors, receptors, and adhesion proteins. [275, 276]. Ding et al in 2006 investigated chitosan/ calcium phosphate composites for studying the effect of chitosan on the crystal phase of CaP [277]. Zhang et al. in 2009 investigated the two bone matrices (Col-CS-HA and Col-HA) and found that chitosan helped in osteoblast adhesion and proliferation in vivo by altering the surface chemistry, which in turn would accelerate the process of bone regeneration [278]. The unique features of chitosan have also been appreciated in tissue engineering [150, 279]. Gelatin is a potential candidate material for bone tissue engineering because of its biological origin, biodegradability, hydrogel properties and commercial availability at a relatively low cost [16]. Gelatin protein, derived from partial hydrolysis of collagen, has been extensively used in the orthopaedic field. It contains free carboxyl groups on its backbone and has the potential to blend with chitosan to form a network by hydrogen bonding [205, 280].

Calcium phosphate ceramics has been extensively studied as scaffold material for bone tissue engineering during last 30 years, because of possessing excellent biocompatibility and bioactivity. Beta-tricalcium phosphate (β-TCP), compared with hydroxyapatite, is more osteoconductive having excellent biodegradation properties and characterized by rapid absorption and replacement by new bone matrix [281, 282]. Because of its bioresorbability , it can induce an interface mechanism that leads to a release of calcium and phosphate ions. Ca is known to influence osteoblastic cells in vitro. Moreover, extracellular Ca plays an

important role in bone remodelling by directly activating intracellular mechanisms after controlling Ca-sensing receptors in osteoblastic cells. For example, Ca increases the expression of Insulin like growth factors IGF-I or IGFII, which regulate human osteoblast proliferation. These findings have been recently reviewed in the literature [283]. Inorganic Phosphate (P) was recently shown to stimulate expression of matrix Gla protein (MGP), a key regulator for bone formation, in osteoblastic cells when added (10 mmol) to cell culture medium [284].

Gelatin/chitosan/β-TCP (GCT) formulations must be bioactive, bioresorbable and possess favourable mechanical properties to be useful for tissue regeneration and clinical applications. Limited studies have investigated the efficacy of GCT scaffolds in the bone regeneration. MM Islam et al investigated the effect of γ-radiation on GCT composite scaffold. Khan et al successfully developed a bioactive, biocompatible scaffold using gelatin, chitosan, PEO and TCP. There have been many studies confirming the proliferative and osteoconductive properties of β-TCP particles but few with regard to effect of its particle size, and concentration over microstructure and mechanical properties of biopolymer based scaffold that is reported elsewhere [285, 286]. The goal of this work is to study the effect of compositional variation on mechanical and biological properties of fabricated composite scaffold to consolidate our understanding on the impact of nanoparticle incorporation into composite scaffold for bone tissue regeneration.

To the best of our knowledge, no study has been previously reported on the use of nanosized β-TCP particle for reinforcing gelatin-chitosan scaffolds. However, the commercialize micro β-TCP with a average particle size <85 nm) to reinforce freeze-dried or gelatin-collagen scaffolds has been reported [287]. Our objective here is to develop novel gelatin chitosan-based composite scaffolds with nano β-TCP as the reinforcement. In the present study, extensive research has been carried out to optimize the processing parameters that can retain interconnected 3D porous structure in bone scaffold. Porous gelatin/chitosan/β-TCP scaffold was prepared via thermally induced phase separation and lyophilisation and post crosslinking with glutaraldehyde a common synthetic crosslinking reagent, for intermolecular crosslinking between protein molecules [288]. Here we report the effect of compositional variation amongst chitosan, gelatin and synthesized β-TCP nanoparticles on physicochemical, microstructural, mechanical properties and bioactivity of the prepared scaffold. The *in vivo* study was designed to evaluate the preliminary biocompatibility of GCT composite scaffold after implanting this scaffold subcutaneously on mouse. The investigation represents a

successful contribution toward the development of superior porous structures for bone tissue engineering.

6.2 Materials and Methods

6.2.1 Materials

Chitosan [85%percentage deacetylated, medium molecular weight] and gelatin (pH- 4.4-5.4, Bloom Number 240) were purchased from Sigma Aldrich (USA). and calcium nitrate tetra hydrate [$Ca(NO3)2,4H2O$] and Di-ammonium hydrogen phosphate [$(NH_4)_2HPO_4$] were procured from Merk (India). Glacial acetic acid and ammonia solution ($NH4OH$) were obtained from LOBA chemical (India). Glutaraldehyde (GA) and all other chemicals were of analytical grade and were used as received from the manufacturer.

6.2.2 β–TCP powder synthesis

Calcium nitrate was dissolved in deionized water to form calcium nitrate solution. Ammonium di-hydrogen phosphate ($(NH_4)_2HPO_4$) solution was added drop wise to the calcium nitrate solution to maintain Ca/P molar ratio of 1.5 in the reaction mixture. The pH of the reaction mixture was maintained at 9 by the addition of ammonium hydroxide (NH_4OH). The reaction solution was aged for 24 h, filtered, washed thoroughly for 5 times, and dried overnight at 60˚C. Finally, the dried powder was calcined at 900 ˚C for 3 hr to obtain β-TCP nano powder.

6.2.3 Fabrication of Gelatin /Chitosan /TCP hybrid scaffolds

The process of scaffold fabrication is shown in Figure.6.1. Chitosan solution was prepared by dissolving 2 gm chitosan in 1% acetic acid solution and stirring continuously for 6 hr. Aqueous slurry of gelatin solution was prepared at 40˚C and mix with chitosan solution. The β-TCP nanoparticles were added into the gelatin-chitosan solution to maintain a specific composition of gelatin-chitosan-β-TCP as shown in Table.6.1. The mixed slurry was dispersed ultrasonically for 30 min and dispensed into glass vials with 2 ml of slurry per vial. The glass vials were rapidly transferred into a freezer at -50˚C and frozen overnight. The samples were lyophilized in a freeze-dryer (Freeze Dryer (LABCONCO, KOREA) LTFD 5505) under vacuum lower than 50 Pa for 3 days.

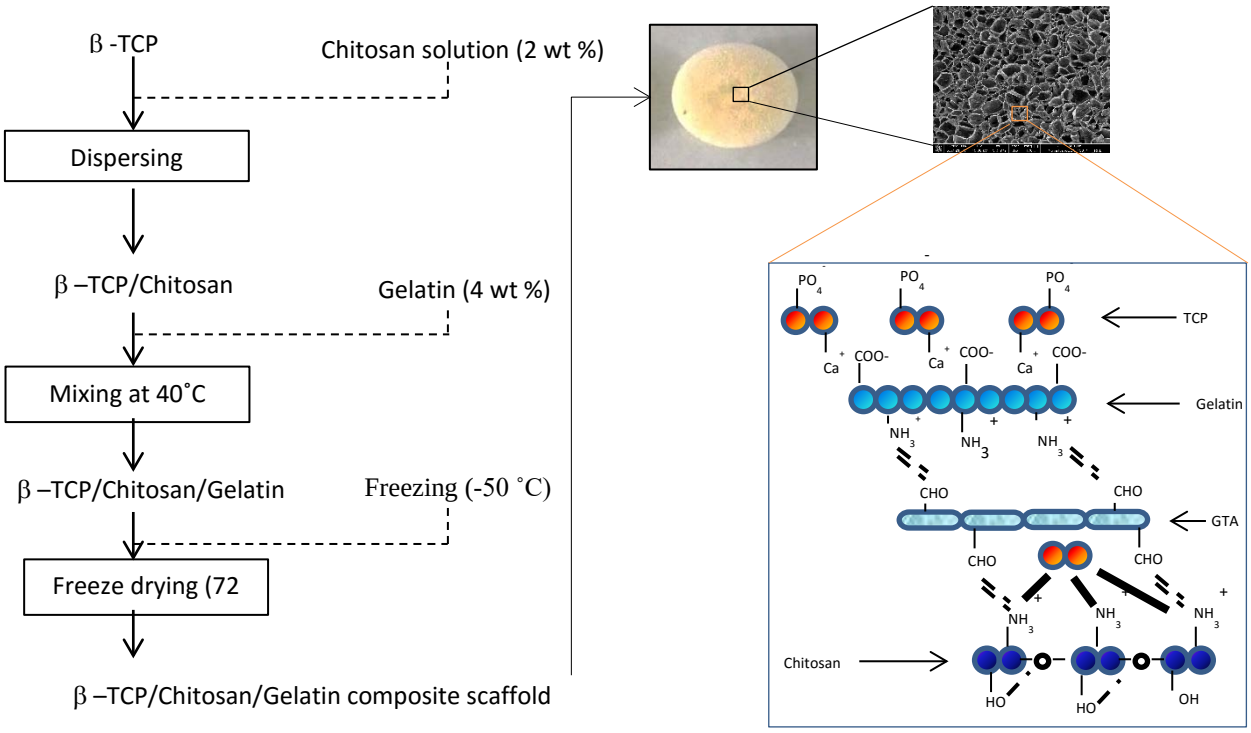

Figure.6.1. Schematic representation of fabrication of GCT scaffold.

Table.6.1. Composition of the scaffold prepared via Freeze drying.

Sample abbreviation	Gelatin/Chitosan	β-TCP	Freeze drying temp(˚C)	Crosslinking agent(%)
GCT 0	30/70	0	-50	0.25
GCT 10	30/60	10	-50	0.25
GCT 20	30/50	20	-50	0.25
GCT 30	30/40	30	-50	0.25
GCT 40	30/30	40	-50	0.25

6.2.4 Characterization

6.2.4.1 Studies on microstructure and chemical composition

X-ray diffraction analysis of β-TCP powder and GCT scaffold were performed with a Panalytical (USA) model operated at 40Kv and 40 mA using Cu Kα radiation. The detailed procedure was mentioned in Chapter4 in section 4.4.1.

Microstructure of the fabricated gel/chitosan/β-TCP scaffolds was observed by a Field emission scanning electron microscope (FEI Nova Nano, Nederland) operated at an

accelerating voltage of 15 kV. The detailed procedure was mentioned in Chapter4 in section 4.4.6.

6.2.4.2 Porosity measurement of the scaffold

The porosity value of the prepared composite scaffolds was measured by using Archimedes principle, using xylene as liquid media. The detailed procedure was mentioned in Chapter4 in section 4.4.7. The characteristic pore size distribution was evaluated using mercury (Hg) porosimetry. The detailed procedure was mentioned in Chapter4 in section 4.4.8.

6.2.4.3 Mechanical Properties of Gelatin /Chitosan /TCP Hybrid Scaffolds

Compressive strength of the GCT composite scaffolds (sample with 22 mm in hight and 5mm in diameter) was measured using a Universal Testing Machine (Tinius Olsen, UK) equipped with a load cell of 1 KN at a constant rate of 1 mm min-1 [28]. The detailed procedure was mentioned in Chapter4 in section 4.4.9.

6.2.4.4 Mineralization behaviour of GCT scaffold

The ability to form apatite when immersed into simulated body fluid (SBF) is an index of biocompatibility exhibited by the GCT scaffold. The detailed procedure was mentioned in Chapter4 in section 4.4.11.

6.2.4.5 Degradation of scaffolds

The degradation of the scaffolds was studied by placing them in phosphate buffer saline (PBS) at 37˚C for up to 28 days. The detailed procedure was mentioned in Chapter4 in section 4.4.12.

6.2.4.6 *In vitro* cell culture

6.2.4.6.1 Attachment and morphology of cell on GCB composite scaffolds

Human Umbelical Chord Mesehenchymal stem cells (MSCs) were grown in a Dulbecco's modified Eagle's medium (DMEM; Sigma-Aldrich, UK) supplemented with 10% fetal bovine serum (FBS; Sigma-Aldrich, UK) and 100 U/mL penicillin–streptomycin. The detailed procedure was mentioned in Chapter4 in section 4.4.13.3.

6.2.4.6.2 Proliferation Assays

Cell viability of MSCs cultured onto the GCT scaffolds were determined after performing [3-(4,5-dimethylthiazol-2-yl)-2,5-diphenyltetrazolium bromide] (MTT) assay. The detailed procedure was mentioned in Chapter4 in section 4.4.13.4.

6.2.4.6.3 Inmunofluorescent imaging of cell markers: osteocalcin and RUN-X2

The expression of RunX2 and Osteocalcin, an osteogenic marker on GCT scaffold was examined using immunocytochemistry. The detailed procedure was mentioned in Chapter4 in section 4.4.13.5.

6.2.4.7 *In vivo* experiment

6.2.4.7.1 Animal used in the experiment

In this study we aimed to assess preliminary biocompatibility *in vivo* using a skin defect model in the back skin of Albino white mouse (2-2.5kg) over a 8 week period. The study was in compliance with the standards of the Institutional Animal Ethics Committee of the West Bengal University of Animal and Fishery Sciences, India. Each implant scaffold had the dimensions of 1cm diameter and 3mm in hight , prepared of 30 wt.% TCP in cross-linked gelatin-chitosan matrix(GCT30). Scaffolds contained pores in the range of 100–200 μm. Before implantation, the cylindrical GCT composite scaffolds were cut into 6-mm-length sections and sterilized by exposure to 15 KGy of γ radiation and kept in a vaccum desiccator until use.

6.2.4.7.2 Surgical procedure and implant retrieval

The animal experiments were performed following an ethical committee approved protocol in West Bengal University of Animal and Fishery Sciences (WBUAFS), West Bengal, India. Mouse were anesthetized with isoflurane (20mg/kg body weight) in O_2, their backs shaved with an electric hair trimmer, injected with 100 μL bupivicaine (0.25% in sterile saline), and cleaned with an antiseptic lotion. Implant scaffolds were washed in sterile saline then inserted into 1 cm longitudinal incisions and then the wound was closed with 3–4 skin clips. After surgery, animals were postoperatively cared for in an oxygen-rich chamber until fully conscious then returned to their single-housing cages. At the end of each experiment (2,4,8 weeks), mouse were anesthetized with isofluorane in O_2 and euthanized with increasing CO_2. Each scaffold was removed, trimmed of connective tissue, washed in PBS, and fixed for 1 hour in 10% formalin.

6.2.4.7.3 Histological assessment

Hematoxylin and eosin stain (H&E stain or HE stain) is one of the principal stains in histology. It is the most widely used stain in medical diagnosis and is often the gold standard. The staining method involves application of hemalum, a complex formed from aluminium

ions and hematein (an oxidation product of haematoxylin). Hemalum colours nuclei of cells (and a few other objects, such as keratohyalin granules and calcified material) blue. The nuclear staining is followed by counterstaining with an aqueous or alcoholic solution of eosin Y, which colours eosinophilic structures in various shades of red, pink and orange. For histological analysis, scaffold specimens from the bottom of the original skin defect were collected, washed thoroughly with normal saline and were immediately fixed in 10% formalin for 7 days, followed by fixation with 4% paraformaldehyde. Finally, the samples were embedded in paraffin wax. 4 mm sections were prepared and stained with haematoxylin and eosin to assess the cellular response of the host skin to the implants.

6.3 Statistical Analysis

Quantitative data were presented as mean ± standard deviation (SD). The two-tailed Student's T-test (T-test) was employed to obtain p values, which determined the level of significance of the data. Difference between groups were statistically significant if $p < 0.05$ and highly significant if $p < 0.01$.

6.4. Results and Discussion

6.4.1 Particle size and phase analysis of β–TCP powder

The XRD patterns of β-TCP powders matched the JCPDS card no. 09-0169, with two intense diffraction peaks detected between $2\Theta = 25^{o}$-35^{o}, corresponding to the (214) and (0210) crystal planes, respectively [289]. Only characteristic peaks of pure β-TCP powder were indexed in Figure.6.2, suggesting that the synthesized powder was pure β-TCP with hardly presence of any other secondary phase. SEM examination clearly revealed the morphology of β-TCP powder (Figure.6.3 (a)), having spherical shape with an average particle size varying between 70-100 nm, which is corroborated well with the particle size data obtained from DLS measurement (Figure 6.3 (c)). The Ca/P ratio of as synthesized β-TCP powder was 1.5, as determined using EDX analysis (Figure.6.3 (b)).

Figure.6.3 (d) shows the crystal structure of synthesized β-TCP nanoparticle. Particle size measurement using FESEM and DLS was little bit higher compared to TEM measurement, which was the result of agglomeration of nano-particle Figure 6.3 (e) shows the HRTEM image of crystal planes of (0210) of crystallized β-TCP nanopowders.

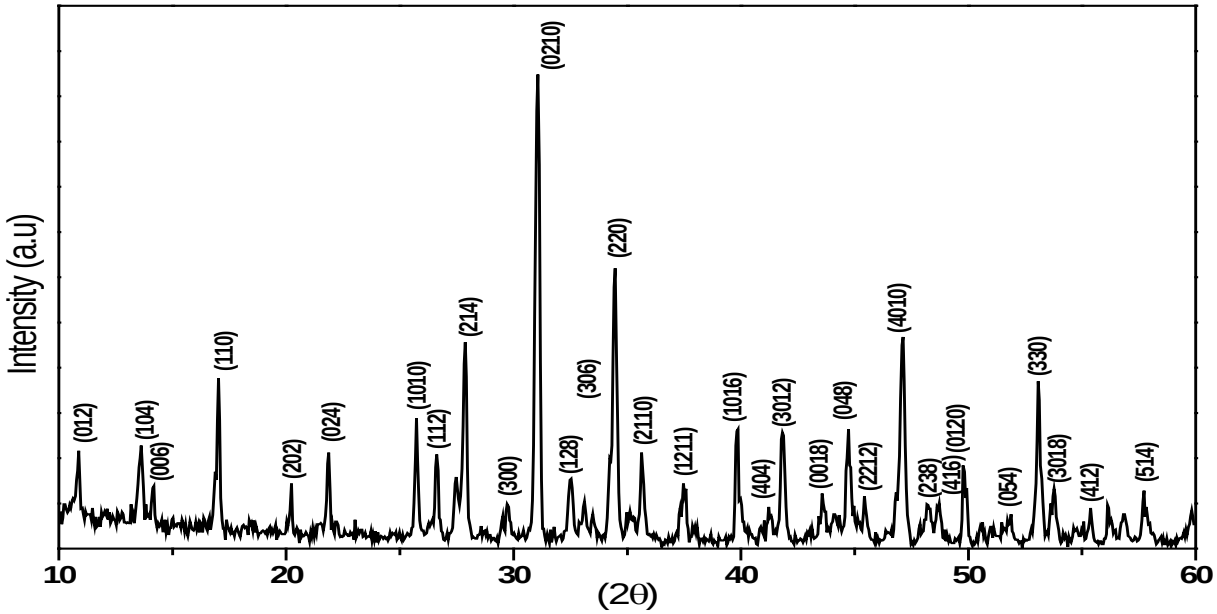

Figure.6.2. XRD plot of synthesized β-TCP powder (JCPDS file # 09-0169).

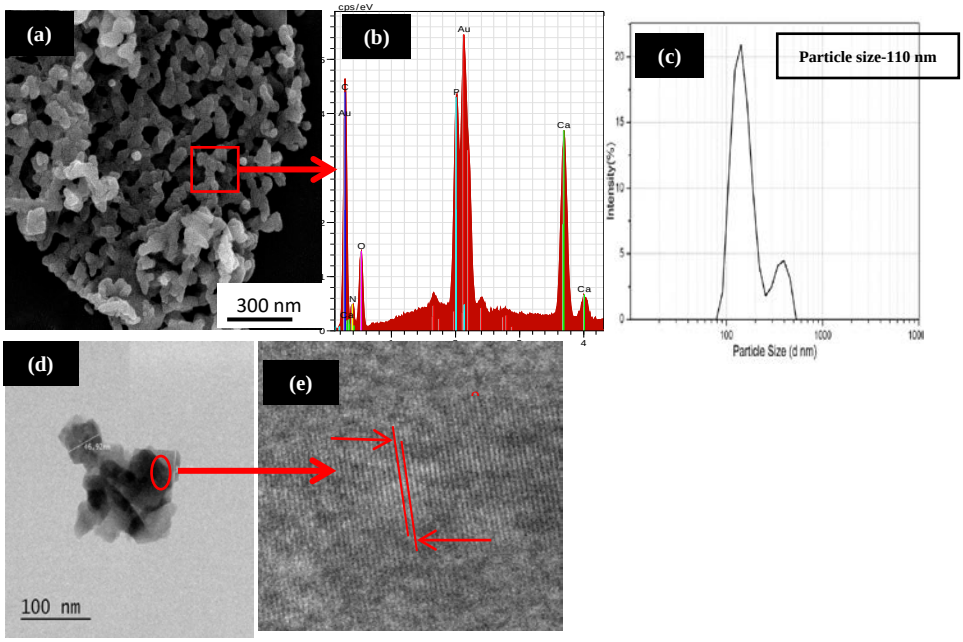

Figure.6.3. β-TCP nanoparticles prepared using co-precipitation method (a) FESEM image. (b) EDX analysis (c) DLS measurement (d) Bright field TEM image (e) HRTEM analysis.

6.4.2 XRD analysis of GCT composite scaffold

Figure.6.4 shows the XRD diffraction patterns of pure Chitosan, Gelatin, β-TCP, and GCT nanocomposites scaffold. Chitosan was identified with a characteristic peak at 2θ= 19.5. Gelatin showed a large amorphous hump between 2θ= 20-25 [290]. In nano-composites, the chitosan and gelatin peaks were subdued as compared to much highly crystalline β-TCP peaks. The slightly less crystalline nature of GCT 30 composite scaffold as compared to β -

TCP nanoparticle was due to the presence of amorphous gelatin-chitosan phase in the scaffold as in Figure. 4 (d).

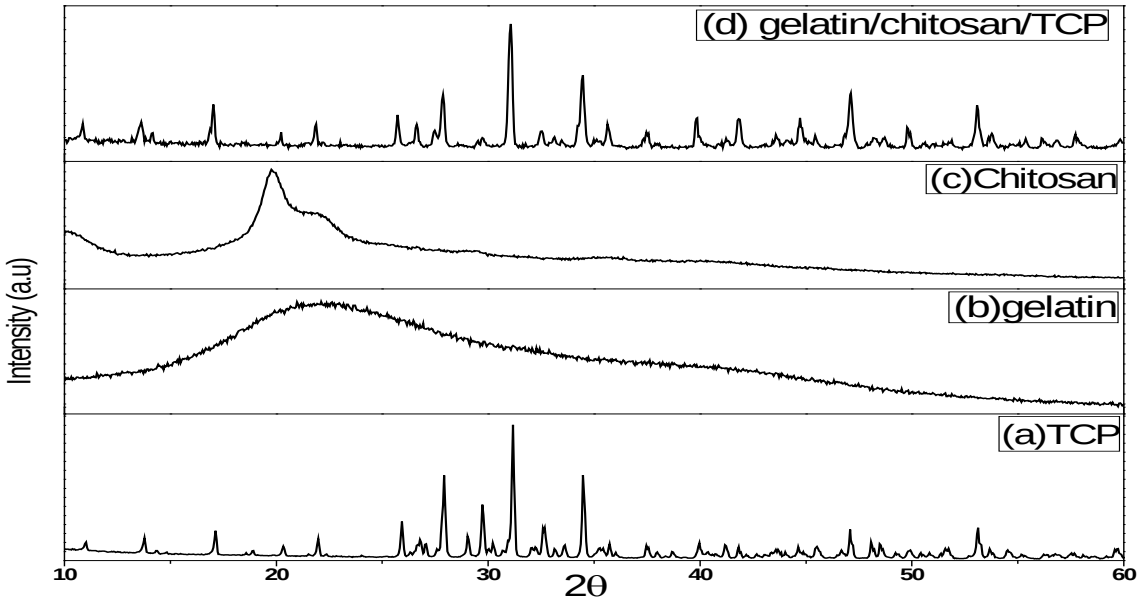

Figure.6.4. XRD pattern of GCT scaffold (a) β-TCP, (b) gelatin, (c) Chitosan, (d) gelatin/chitosan/β-TCP.

6.4.3 FTIR study of composite scaffold

The chemical structure of β-TCP, chitosan, Gel-CS, and Gel-CS-β-TCP composite scaffold was investigated using FTIR spectroscopy, as shown in Figure.6.5. Apart from peaks at 1045, 972, and 606 cm^{-1}corresponding to phosphate group , the absorption band observed at 553 and 1119 cm^{-1} were due to characteristic peaks of PO_4^- in β-TCP [291]. The characteristic peaks of chitosan observed at 1647 and 1597 cm^{-1}, assigned to amide I(C=O) and -NH_2 deformation, respectively [35]. Amino band at 1541 cm^{-1} and carbonyl peak at 1647 cm^{-1} correspond to the characteristic peaks of ampholytic gelatin [36]. The appearance of 1552 and 1655 cm^{-1} in scaffold attributed to the characteristics of imine C=N group, indicate the crosslinking reactions between amino groups of chitosan and gelatin with aldehyde groups of glutaraldehyde. The spectrum of chitosan– gelatin hybrid polymer network (CS–Gel HPN) in the composite scaffold was confirmed by the existence of the peak at 1552 and 1655 cm^{-1}. These peaks were also significant even when β-TCP fraction reached up to 30 wt%. The band at 1330 cm^{-1} confirmed the chemical interaction between Ca^+ ion in β-TCP and COO^- group in gelatin. This reaction can be observed in Figure.6.1. Further, the gelatin-chitosan network not only serves as a matrix, but also anchoring site for β-TCP particles which in turn enhances the stability of the composite scaffold in the water based environment [292].

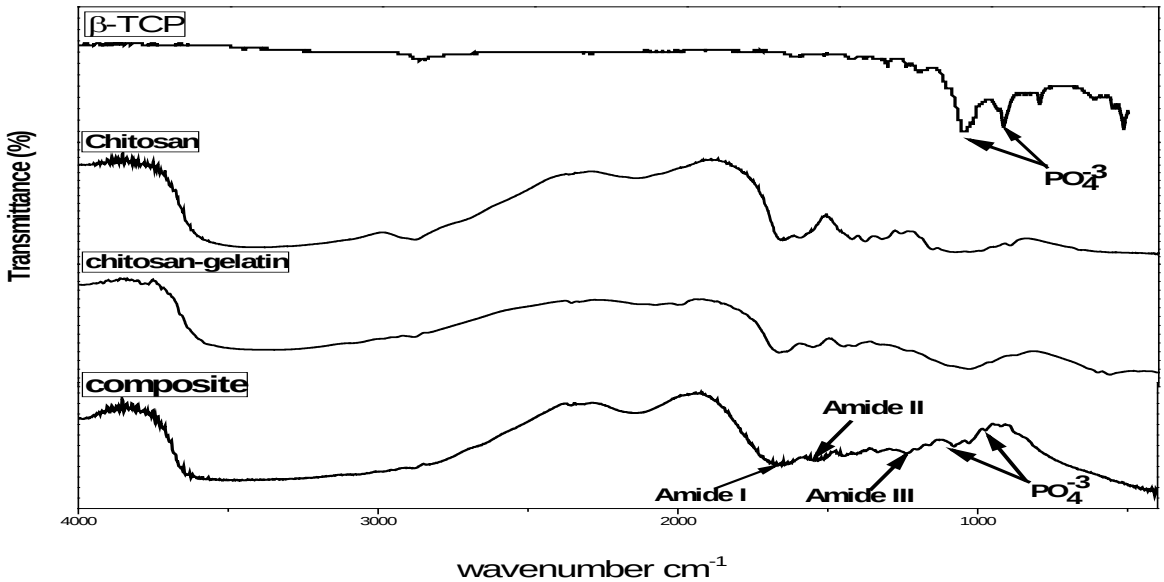

Figure.6.5. FTIR spectra of β-TCP, Chitosan, Gelatin-chitosan and (GCT 10) composite scaffold.

6.4.4 SEM observation of composite scaffold morphology

For successful diffusion of nutrients and oxygen a scaffold must have interconnected micro amd macroporosity [293]. Furthermore, recent studies show that multi-scale porosities in scaffold can perform better than only macro porosity [293]. Figure.6.6 shows a representative cross-sectional structure of Gel-CS-TCP composite scaffolds with varying concentrations of the composite slurry. We have demonstrated that composition of the scaffold had a significant effect ($P < 0.05$) on its mean pore size in the microstructure, and smaller pore structures resulted with an increase in β-TCP content (Table.6.2). The freeze dried porous scaffolds incorporating β-TCP up to 30 wt% showed to be well-shaped with a relatively uniform distribution of macropores, which was severely hampered with the incorporation of β-TCP above 30 wt%. The viscosity of composite slurry significantly affects the pore structure during the freeze drying process [294]. As we go upto 30 wt% of β-TCP content in the composite slurry, a higher force was necessary for migration of water molecules. This high viscosity resulting in reduced size of inters trapped ice blocks and smaller pores were formed during freeze drying in the composite scaffold. The mean pore size decreased from > 200 μm in Figure.6.6 (b) to 120μm Figure.6.6 (e). This content of β-TCP scaffold was considered to be the optimum for the fabrication of GCT nano-composite scaffolds. All scaffolds contained a high amount of total porosity of greater than 82%, which is known to be beneficial for cell infiltration and survival [295]. Keeping this in view, the average pore size of the GCT30 scaffold in the range of 120 μm was considered to be beneficial for bone tissue

engineering. Furthermore, it was reported that calcium from TCP has the ability to induce MSC's differentiation toward osteogenesis [296].

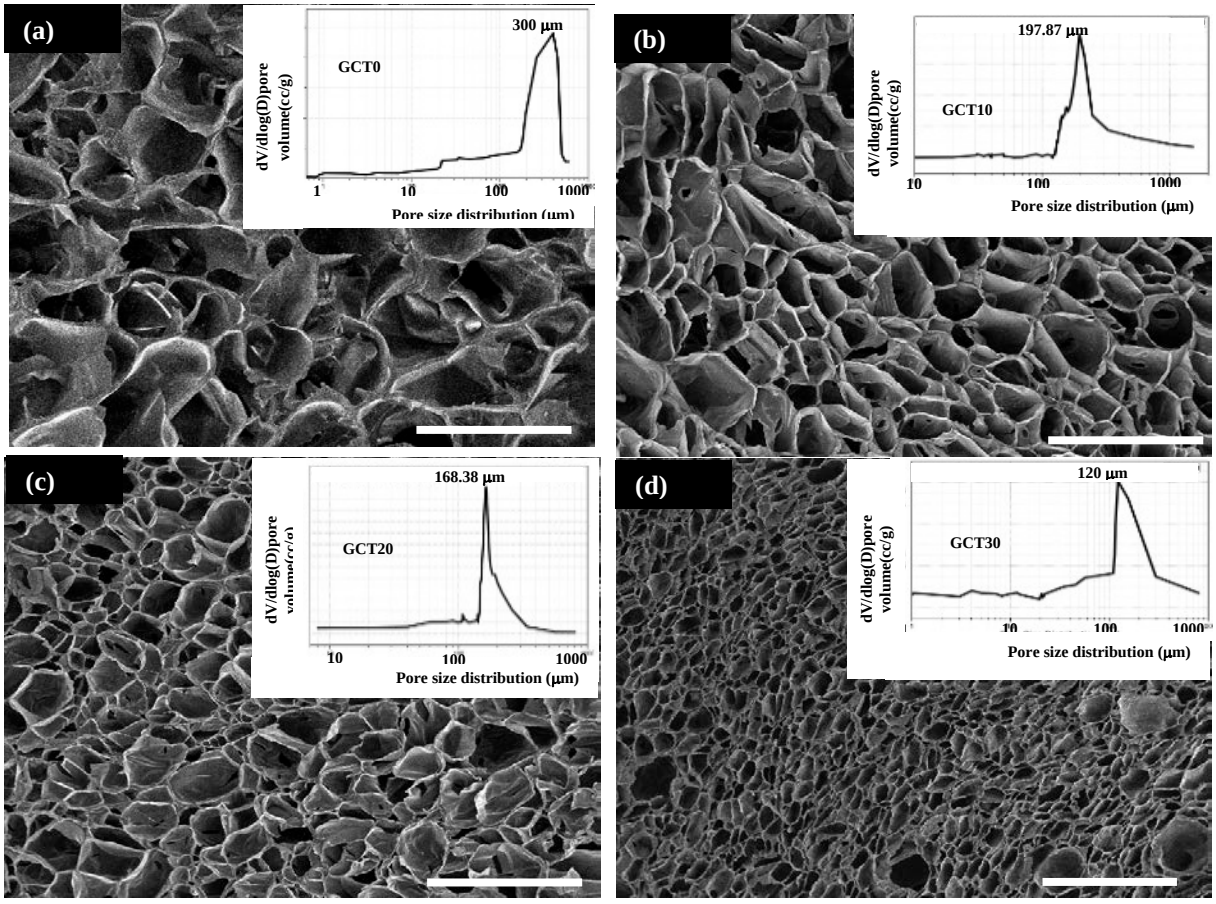

Figure.6.6. FESEM image of GCT composite scaffolds with different fraction of β-TCP (a) 0 wet% (b) 10 wt% (c) 20 wt% (d) 30% . scale bar designated as 500 µm.

Table.6.2. Pore diameter and porosity of GCT composite scaffold.

Sample abbreviation	β-TCP (%)	Avg Pore Diameter	Porosity(%)
GCT 0	0	300 ± 10.2	88 ± 5.6
GCT 10	10	197.87 ± 12.4	85 ± 7.3
GCT 20	20	168.38 ± 11.2	83 ± 8.4
GCT 30	30	120 ± 18.6	80 ± 7.3

6.4.5 Mechanical properties of scaffolds

The mechanical properties obtained from compression tests of both gelatin-chitosan and gelatin-chitosan-TCP composite scaffold are shown in Figure.6.7. The result shows that a maximum average compressive strength of 2.45 MPa registered by GCT 30 scaffold as compared to a paltry of 1 MPa of average compressive strength in non-βTCP based polymer

scaffold (Figure.6.7). However, any attempt to increase the β-TCP nano-particle content to higher values than 30 wt% cause a decrease in strength. In fact, compressive strength of spongy bone fall in the range between 1-7 MPa [297]. All of the scaffolds showed average porosity between 80 to 88% .GCT0 showed the highest average porosity of 88% and the lowest average porosity of 80% was exhibited by GCT 30. There is an inverse relationship between the nano powder content and percentage of porosity in scaffold. As it is summarized in Table.6.3, GCT 30 scaffold having a lower porosity and pore size exhibited the highest compressive strength. β- TCP reinforcement makes a significant improvement in compressive mechanical properties of the scaffolds. From the results it is clear that the mechanical property improved significantly with β-TCP nanoparticles loading upto 30 wt% in the scaffold. Addition of β-TCP particles in the composite slurry by more than 30 wt% caused enormous nanoparticle agglomeration and caused inhomogeneity in the scaffold matrix. Though, agglomerated particles broke down under application of compressive load to scaffold, broken agglomerates acted as stress-concentrating points leading to formation of macro cracks, reflected in an enormous decrease in the mechanical properties of the nano-composite scaffold (Figure.6.6 (f)). In terms of compressive strength, GCT 30 scaffold appeared to be the best among the prepared scaffolds for meeting the criteria of adequate compressive strength for bone tissue regeneration.

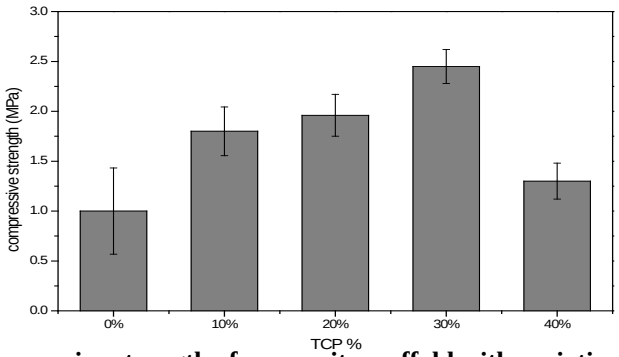

Figure.6.7. Compressive strength of composite scaffold with variation in TCP content.

Table.6.3. Summary of porosity and mechanical property of GCT scaffold.

Sample	Compressive strength (MPa)	Porosity (%)
GCT0	1±4.3	88 ± 5.6
GCT10	1.8±2.25	85 ± 7.3
GCT20	1.96±2.1	82 ± 8.4
GCT30	2.45±1.95	83 ± 7.3
GCT40	1.3±2.35	82 ± 9.2

6.4.6. Mineralization ability of GCT 30 composite scaffold

Mineralization ability of scaffold in SBF has been regarded as one of the key evidences of bioactivity for bone scaffold. It has been reported scaffold which support osteoblast cell growth, proliferation and differentiation in vitro and in vivo exhibits good mineralization behaviour in physiological environment. Highly dense bone-like carbonated apatite layer formation on SBF treated GCT30 scaffold (Figure.6.8) indicates that the prepared scaffolds are not only biocompatible, but also bioactive.

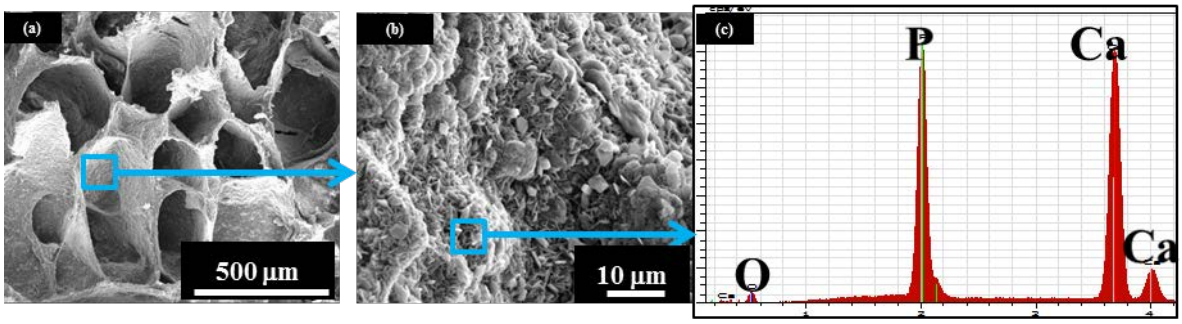

Figure.6.8. SEM micrographs of carbonated apatite layer formed on the surface of GCT30composite scaffold immersed in SBF for 7 days.

6.4.7 Biodegradation behaviour

As the tissue engineering aims at the regeneration of new tissues, the scaffolds has to be degraded with the formation of new bone tissues. The degradation behaviour of biomaterials in physiological environments plays an important role in the engineering process of a new tissue. In our work, the *in vitro* biodegradation performance of GCT scaffolds in PBS containing lysozyme was investigated. The degradation procedure involves hydrolyzation of gelatin and enzymatic degradation of chitosan. The lysozyme present in internal body fluids can hydrolyse the *β*-1, 4 *N*-acetyl-glucosamine groups of chitosan macromolecule[298]. The large quantity of hydrophilic amino and carboxyl groups exist in gelatin, makes it degrade quickly.

The scaffold degradation provided a progressive weight loss with a degradation rate almost constant over time, up to day 24. Figure.6.9 shows the effect of β-TCP addition on GCT scaffold after in-vitro degradation in PBS at 37^{o}C for 4 weeks. The degradation percentage dramatically decreased with addition β-TCP upto 30 wt%. It is reasonable to think that the strong interaction between gelatin macromolecular chains and β-TCP consumed some hydrophilic groups and decreased the solvent uptake, which protects the macromolecules from hydrolyzing. Moreover, the presence of β-TCP also serves as physical crosslinking

sites, which enhanced the stability of the network. All of the above results reveal that the degradation rate may be controlled by adjusting the β-TCP contents in the scaffold.

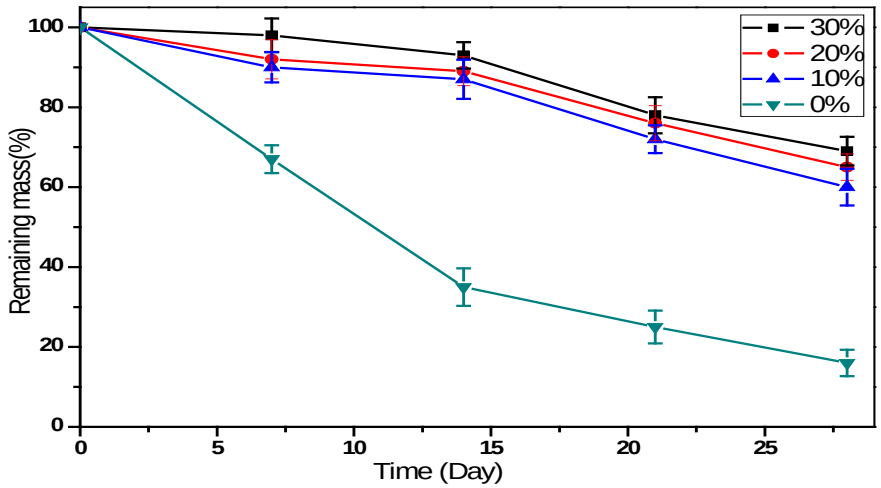

Figure.6.9. Gelatin-Chitosan–β-TCP scaffold degradation with varying percentage of β-TCP (0%,10%,20%,30%). The experiments were carried out for 30 days. Data were expressed as mean of three experiments ± SD (∗P < 0.05).

6.4.8 Cell morphology on GCT scaffold

It is well known that surface characteristic of materials play a crucial part for bone regeneration by supporting adhesion, proliferation and differentiation of bone cells [51]. We hypothesized that β-TCP particle with Gelatin-Chitosan scaffold would encourage the osteogenic capacity of MSC pre-osteoblast cells [299]. Such verification was performed based on GCT scaffolds prepared under Freeze drying process with 30% TCP loading, in comparison with the neat Gelatin-chitosan scaffold. Figure.6.10(a) shows pre-osteoblast morphology and bone cell– material interactions for cell adhesion, growth, and differentiation on a neat GC scaffold after 14 days and GCT 30 scaffold (Figure.6.10 (b) to (d)) after 3, 7, and 14 days of culture respectively. Cell attachment through small micro extensions onto the GC surface was evident after 14 days of the MSC culture (Figure.6.10 (a)). After day 7, cell density was higher on the surface of GCT 30 scaffold (Figure.6.10 (c)) as compared to that on day 3 [Figure 6.10 (b)]. After day 14, the cells displayed elongated morphology with numerous lamellipodia and filopodia extensions to attach and migrate onto the GCT 30 surface as shown in [Figure.6.10 (d)]. The cells in β-TCP embedded matrix appeared to cover and spread on the GCT 30 surface better than those in GC surface [Figure.6.10 (a, d)]. Some researchers stated the significant role of Ca^{2+} in the extracellular signalling by membrane mediated ionic transfer [300]. These facts implied that composite scaffolds would regulate osteoblastic differentiation in part triggered by bioresorbable β-TCP that releases Ca^{2+} in cell

culture medium. All the results suggest that MSC cells were able to grow and proliferate well on GCT 30 scaffold as compared to GC scaffold, which is a good sign for exhibiting enhanced bioactivity.

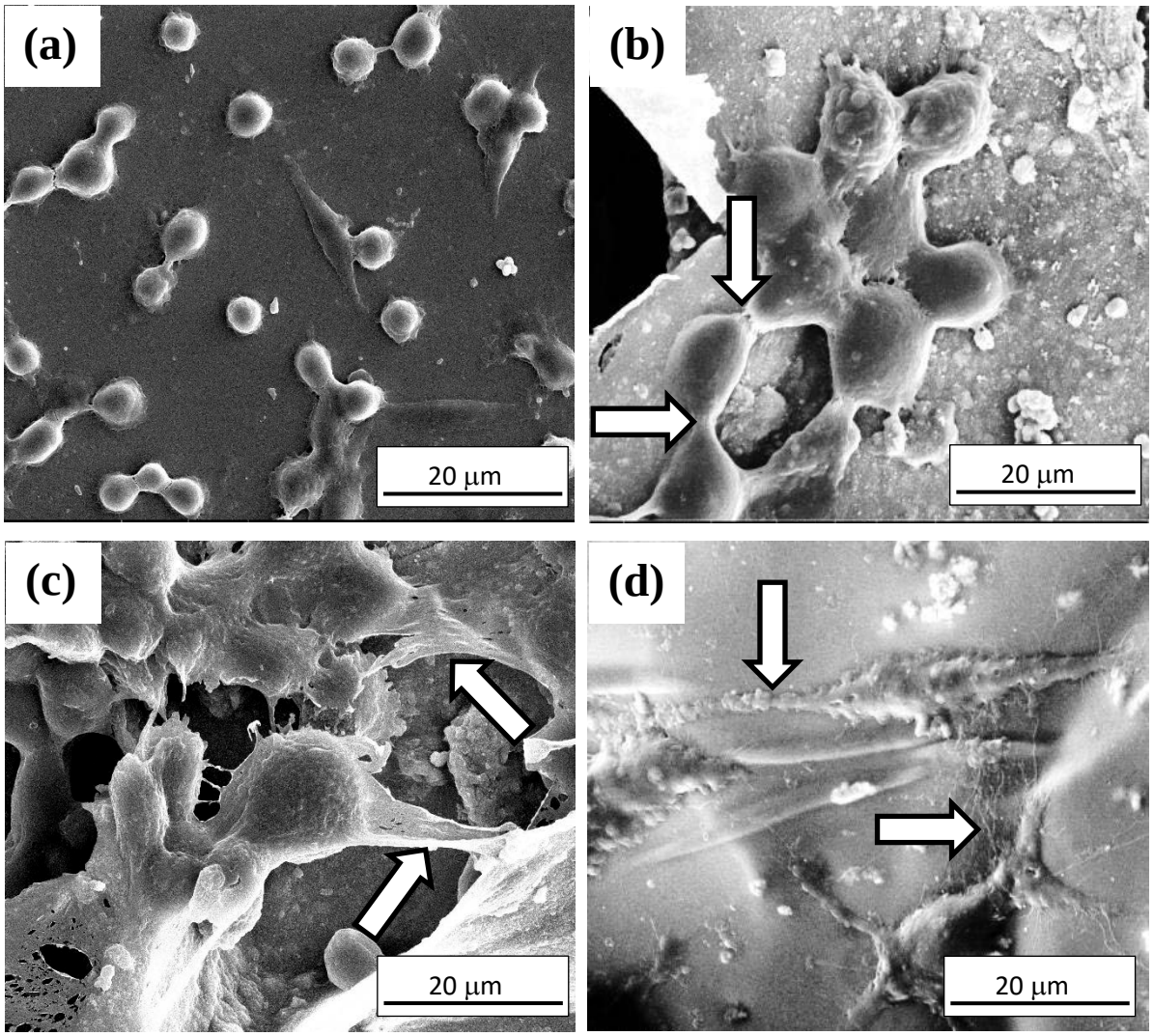

Figure.6.10. FESEM images showing MSCs attached on (a) GC control for 14 days and on GCT 30 scaffold for (b) 3 day, (c) 7 days, and (d) 14 days of cell culture.

6.4.9 Cell Proliferation/MTT assay

MSC's proliferation on GCT 0 and GCT 30 scaffolds up to 14 days of culture was studied through MTT assay treating cultured MSC's on sole tissue culture plate as a positive control. Compared with MSCs cultured onto GCT0, viable cell density on GCT30 was higher at all periods of cell culture, as shown in Figure.6.11. The cell density on GCT30 scaffold was significantly higher on day 1 (# $p < 0.05$) and on day 7 (# $p < 0.05$) than GCT0. Furthermore, a significant level of increase in proliferation (# $p < 0.05$) was seen in GCT 30 on day 14,

showing that the β-TCP with Gelatin-chitosan assisted in increased proliferation of the cultured MSCs.

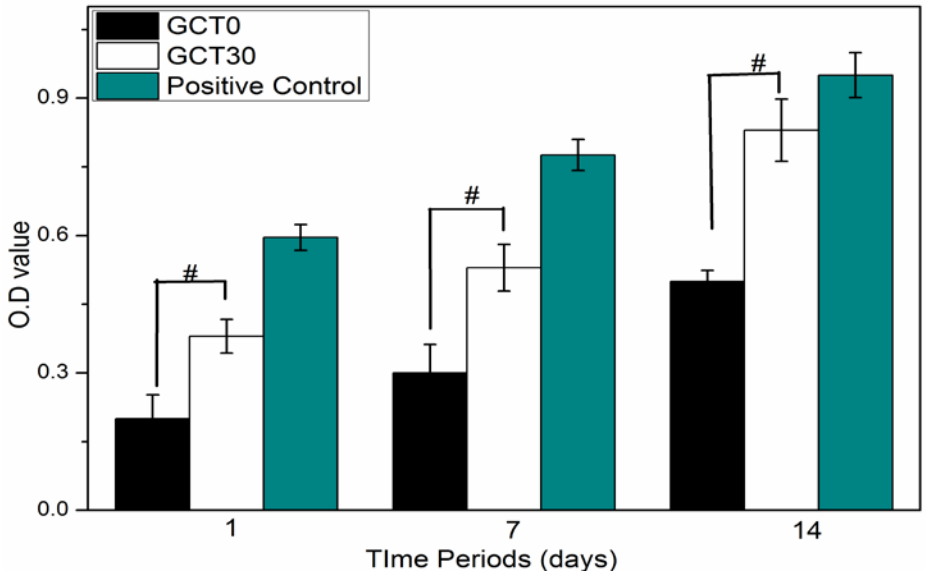

Figure.6.11. MTT assay for cell proliferation study in positive control, GCT0 and GCT 30 scaffold using human Mesenchymal stem cell on days 1, 7, and 14. * indicates significant difference at $p \leq 0.05$. # indicates significant difference at $p \leq 0.05$.

6.4.10 Study of MSC's differentiation into osteoblast onto GCT30 scaffold

The differentiation of MSCs toward the osteogenic lineage was ultimately demonstrated by the expression of genes that are usually associated with the mineralization during osteogenesis, such as transcription factor Runx2, and the matrix protein osteocalcin (OCN). Figure 6.12 shows the confocal microscopic images of expression of osteocalcin from MSCs cultured on GCT0 and GCT 30 scaffolds after 7 and 14 days of cell culture. Osetocalcin expression became gradually higher on both GCT0 and GCT 30 scaffolds with progress in cell culture periods from 7 to 14 days as suggesting the fact that both the scaffolds supported differentiation of MSCs into osteoblast and mineralization of extracellular matrix for osteogenesis. OCN expression was found to be higher on GCT 30 as compared to GCT 0 [Figure 6.12 (a), (c)]. With increase in cell culture period upto 14 days. Osteocalcin expression became even higher on GCT 30 as compared to GCT0 as shown in Figure 6.12 [(b), (d)]. Our results showed that differentiated MSCs produced higher OCN expression on GCT 30 than cells on GCT 0. The explanation for these phenomena lay in increasing ability of protein adsorption and continuous release of Ca^{2+} into medium from GCT30 composite scaffold as compared to GCT0. The protein affinity and bioresorbability of β-TCP nanoparticles present in GCT 30 helped in better mineralization of bone extracellular matrix

and hence triggered differentiation of MSCs into osteoblast to higher degree. Our result suggests that MSC's cultured onto GCT30 scaffold were well committed to osteogenic lineage.

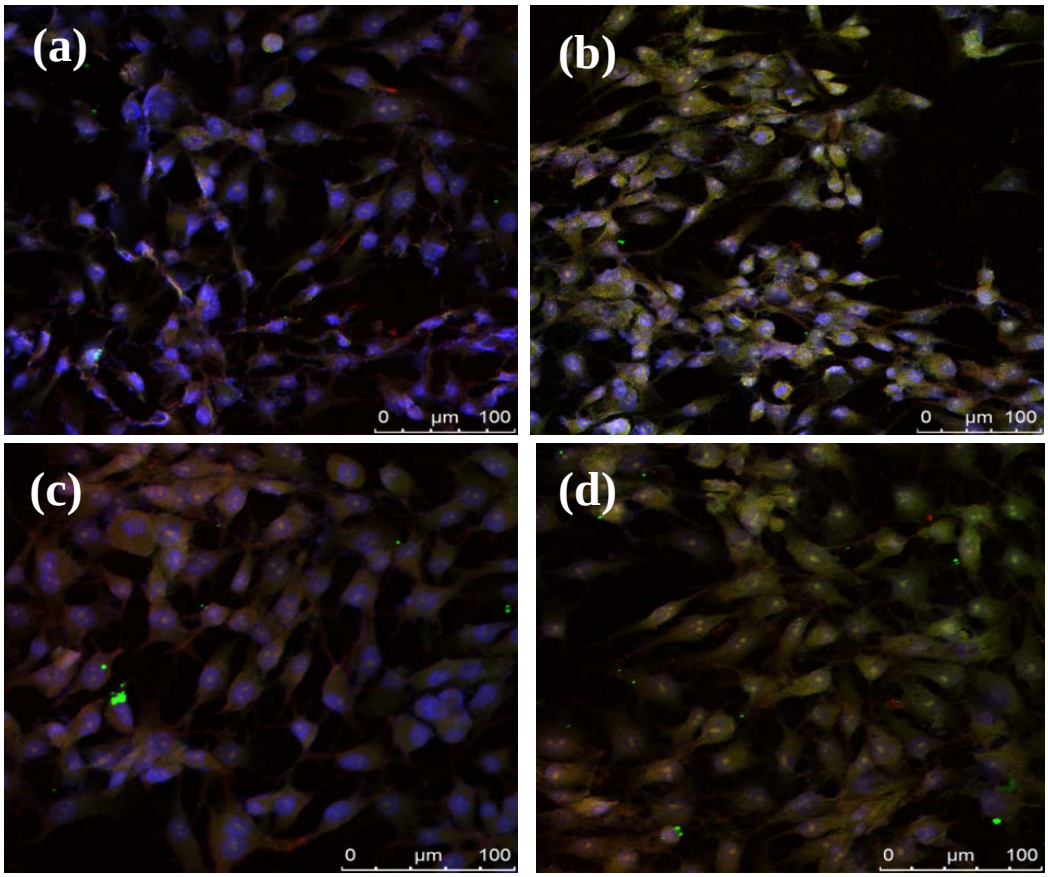

Figure.6.12. Representative immunofluorescent images for osteocalcin expression of MSCs in the GCT0 scaffolds after (a) 7 days (b) 14 days of cell culture and cells in the GCT-30 scaffolds after (c) 7 days (d) 14 days of cell culture. Cell nucleus stained with DAPI (blue), and Osteocalcin (Green) .

6.4.11 *In vivo* animal experiment

Histologically, after 2 weeks of implantation into mouse skin, the open pore morphology of the GCT 30 scaffold was maintained, but the scaffold integrity was worse [Figure.6.13 (a)]. The infiltrating cells began to change into lymphocytes and plasma cells, which was the indication of first phase of wound healing (Figure.6.13 (a1)). This is also reported as the initiation of minimal chronic inflammation [53].

At 4^{th} week [Figure.6.13 (b)] cellular infiltration had clearly decreased with formation of ECM throughout the composite scaffold. Blood capillaries began to appear in between almost disintegrated scaffold structure and scaffold interspaces were fully filled with ECM of fibroblast [Figure.6.13 (b1)].

As can be seen in Figure.6.13 (c), at 8th week after implantation, cellular infiltration had gradually decreased as the vascular structure was prominent inside composite scaffold [Figure.6.13 (c1)]. The scaffold structure was completely disintegrated and scaffold remnants were scattered in the surroundings. In addition, fibroblast can be seen in the interspace region throughout the composite scaffold. These findings indicate that GCT30 composite scaffolds showed excellent biocompatibility, tissue repair ability, and controlled biodegradability, which is a good sign of exhibiting its efficacy in bone tissue regeneration.

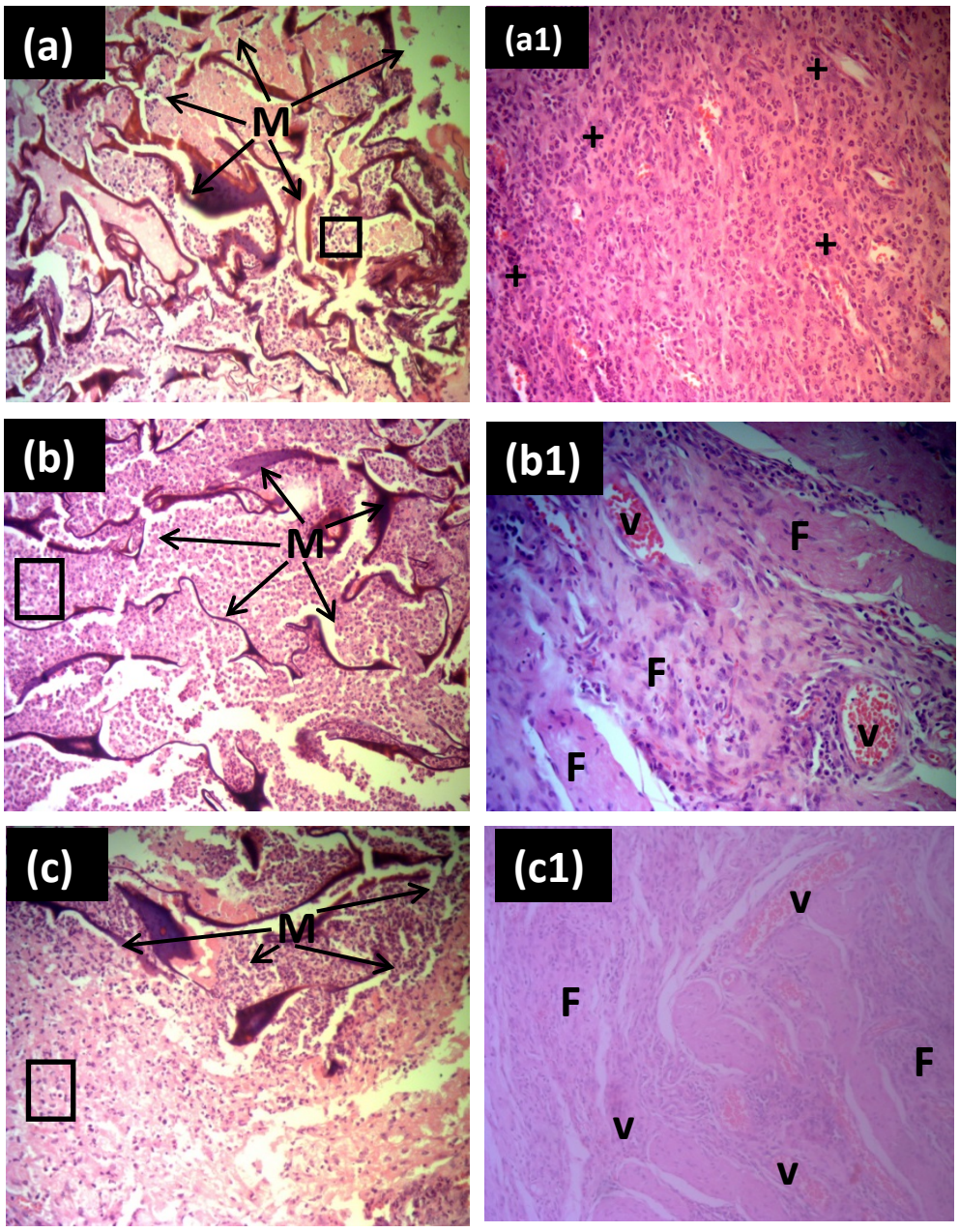

Figure.6.13. Histological images (× 10) of material degradation (a) 2 week (b) 4 week (c) 8 week after implantation. Magnification of image(×100) shown tissue response (a1) 2 week (b1) 4 week (c1) 8 week after implantation. M-material, v- blood vessel, F- fibroblast cells, +- Inflamatory cells.

6.5 Conclusions

In this study, Gelatin/Chitosan/β-TCP nano-composite scaffolds were successfully fabricated using the thermally induced phase separation method. Both pore size and mechanical properties of the nano-composite scaffold could be tailored by changing the β-TCP content in the scaffold. Increasing β-TCP content into the chitosan/Gelatin(CG) matrix significantly improved mechanical properties and upto 30 wt% addition of β-TCP resulted in a higher compressive strength in scaffolds. The GCT30 scaffolds showed 1.5 times higher compressive yield strength than those exhibited by GC scaffolds and eventually match with the lower range mechanical properties of cancellous bone. Furthermore, GCT30 scaffolds exhibited good biocompatibility and promoted better cell proliferation and MSC's differentiation into osteoblast than only neat Gelatin-chitosan scaffold up to 14 days of cell culture. Also, GCT30 composite scaffold was found to promote new blood vessels formation and skin tissue regeneration *in-vivo*. From the experiment it was found that GCT30 scaffold was highly biocompatible and non-toxic that rendered hardly any justification to carry out same test with other compositions of the prepared scaffolds. The scarcity of animals to perform in vivo test and limited resources of scaffold material also compelled us to restrict the number of such tests.

CHAPTER # 7

Comparative analysis of GCH 30, GCB 30 & GCT 30 composite scaffold

If you don't ask, you don't get.
Stevie Wonder

Abstract

The aim of this work is to compare the effect of hydroxyapatite-chitosan (HAp), β-TCP and 58sbioactiveglass nanoparticles in a gelatin-chitosan based composite scaffold aimed to regenerate bone at defect site. Gelatin-chitosan based scaffolds made of gelatin-chitosan(GC) and GC composites containing 30 wt% HAp, β-TCP and 58s bioactiveglass nanoparticles were fabricated using freeze drying technique. The porosity, protein absorption capacity, biodegradation and compressive strength of the all the prepared scaffolds were evaluated. The average pore pore size of all the prepared composite scaffolds was in the range between 90-125 μm. Most frequent pore size in GCT 30 scaffold was the highest of 120 μm whereas that for GCH 30 was the lowest of 96 μm as suggested by Hg porosimetry analysis. GCH30 scaffolds showed the highest average compressive strength of 3.45 MPa with high degree interconnected porosity appropriate for cellular colonization. Biodegradation ability of all the composite scaffold did not vary too much, but certainly lower than neat gelatin-chitosan(GC) scaffold. BSA protein adsorption was found to be the maximum of 24 mg/cc onto GCB 30 scaffold whereas a lowest of 13 mg/cc adsorption was shown by neat gelatin-chitosan scaffold. To study the effect of different bioceramics phases on MSCs differentiation, scaffolds were cell cultured for up to 14 days in osteogenic medium. GCB 30 scaffold showed higher capacity to proliferate MSCs cultured onto it as compared to other composite scaffolds. Degree of differentiation of MSCs into osteoblast was higher in GCB 30 scaffolds than in the GCH 30 and GCT 30 composite scaffold as evident from higher amount of RUNX2 and Osteocalcin expression in the former upto 14 days of cell culture. Inclusion of 58s bioactive glass particles showed positive effects on cell differentiation. In coherence with the in vitro appearance, histomorphometric analysis and flurochrome study in a rabbit tibia model showed a significantly greater amount of new bone formation in GCB30 compared to other composite scaffolds. The results demonstrated that the prepared GCB30 scaffold could be a better candidate as bone substitute material for its higher bioactivity in bone tissue regeneration.

7.1 Introduction

Bone is a tissue with a high regeneration capacity. In most cases fractures and small defects heal alone without any surgical intervention. But in the case of osteopenia or osteoporosis replacement and regeneration of large defect bone is a major challenge in orthopaedic surgery. The preferred clinical option like autograft (patient own tissue) and allografts (tissue

from another patient) suffer from many drawbacks including limited supply and risk of disease transmission [270]. For these reasons bone substitutes have been developed out of synthetic biomaterials. The final objective is the design of a product that induces differentiation and the integration of the construct into the surrounding bone with sufficient mechanical strength which can be used as bone graft materials. The successful engineering of damaged tissue depends on the control of interactions between cells and scaffold, and therefore it is critical to develop an ideal scaffold to direct desirable cell response. Bone tissue engineering has focused mainly on bioceramics and polymers to reach these aims. Bone substitutes based on bioceramics use a wide range of inorganic materials with composition similar to bone [274].

Hydroxyapatite, a bioceramics from synthetic or natural origin, has been reported to induce osteoblast differentiation [69]. The synthetic hydroxyapatite has a stoichiometric composition ($Ca_{10}(PO_4)_6(OH)_2$) and high crystallinity, in contrast to the biological apatites, having very low crystal size with variable composition and generally calcium-deficient in nature [301]. As a result, *in vivo* resorption rate for synthetic HAp is longer than many other calcium phosphates [302].

Tricalcium phosphate implants have been used for two decades as synthetic bone void fillers in orthopaedic and dental applications [303]. The small particle size and interconnected microporosity are believed to improve osteoconductive properties and promote timely resorption combined with the process of remodelling [304]. The 58Sbioactiveglass (58% SiO2, 33%CaO, and 9% P_2O_5) is a bioactive glass based on the three dimensional silica network. Through degradation reactions on the surface of bioactive glass, ions are released to the medium. These ions have been seen to mediate positive effects on osteoblast proliferation and collagen secretion [305]. The biopolymers used in bone tissue engineering can be either of natural origin (such as proteins as collagen, or polysaccharides as hyaluronic acid, chitosan and others) or synthetic origin (biodegradable polyesters, polyfumarates or poly-a-hydroxyesters and others). The principal deficiency of synthetic polymers for tissue engineering is their low intrinsic bioactivity[306]. On the other hand, the principal advantage of natural polymers is their good biological properties, close to those of natural tissues. Using composite scaffolds is a great approach for designing bone substitutes because composites combine the advantages of two biomaterials classes [307]. As a matter of fact, bone is a composite, and its outstanding biological and mechanical properties are due to its composite

nature formed by an organic protein phase (collagen and other bone proteins) in which nanometric particles of mineral phase (apatite) are embedded [308].

In this work, we use chitosan because of its natural nature (obtained by alkaline deacetylation of chitin), non-toxicity, biocompatibility, and biodegradability. Due to its desired properties, chitosan-based materials are widely considered to fabricate scaffolds for tissue engineering and regenerative medicine[309]. Many composites of HAp and Bioactive glass mixed with either natural or synthetic polymers have been studied [186]. Osteoconductivity of HAp is implicated in its direct interaction with natural bone tissues. In the comparative study between porous HAp, β-TCP ceramics, former showed greater potential for promoting the differentiation of osteoblasts than β-TCP [310]. Other studies show that for scaffold having 5% bioactive glass reinforced PCL enhances the cell adhesion compared to pure PCL scaffold [311].

To the authors' knowledge no study has yet been carried out to investigate mechanical mechanical and biological performance of GC scaffold containing either HAp or β-TCP or BG as reinforced nano particulate in macroporous structure of scaffolds. The objective of this study was to develop three series of GC composite scaffolds with 30% (w/w) hydroxyapatite/58s Bioglass/β-TCP using a mixed technique of thermal induced phase Separation (TIPS) followed by freeze drying. Physicochemical, mechanical, in vitro and in vivo bioactivities of compositionally different three composite scaffolds were compared in a sequential manner to understand their efficacies in bone tissue engineering.

7.2 Methods

7.2.1 Physicochemical Characterization

7.2.1.1 Studies on microstructure and chemical composition

X-ray diffraction analysis of GCH30, GCB30 and GCT30 scaffold were performed with a Panalytical (USA) model operated at 40Kv and 40 mA using Cu Kα radiation. The detailed procedure was mentioned in Chapter4 in section 4.4.1.

Microstructure of the fabricated GCH30, GCB30 and GCT30scaffolds was observed by a Field emission scanning electron microscope (FEI Nova Nano, Nederland) operated at an accelerating voltage of 15 kV. The detailed procedure was mentioned in Chapter4 in section 4.4.6.

7.2.1.2 Porosity measurement of the scaffold

The porosity value of the prepared GCH 30, GCB 30 and GCT 30 composite scaffolds was measured by using Archimedes principle, using xylene as liquid media. The detailed procedure was mentioned in Chapter4 in section 4.4.7.

7.2.1.3 Mechanical Properties of Gelatin /Chitosan /TCP hybrid Scaffolds

Compressive strength of the GCH30, GCB30 and GCT30 composite scaffolds (sample with 22 mm in hight and 5mm in diameter) was measured using a Universal Testing Machine (Tinius Olsen, UK) equipped with a load cell of 1 KN at a constant rate of 1 mm min-1 [28]. The detailed procedure was mentioned in Chapter4 in section 4.4.9.

7.2.1.4 Degradation of scaffolds

The degradation of the GCH30, GCB30 and GCT30 scaffolds was studied by placing them in phosphate buffer saline (PBS) at 37˚C for up to 28 days. The detailed procedure was mentioned in Chapter4 in section 4.4.12.

7.2.1.5. *In vitro* cell culture

7.2.1.5.1 Attachment and morphology of cell on GCB composite scaffolds

Human Umbelical Chord Mesehenchymal stem cells (MSCs) were grown in a Dulbecco's modified Eagle's medium (DMEM; Sigma-Aldrich, UK) supplemented with 10% fetal bovine serum (FBS; Sigma-Aldrich, UK) and 100 U/mL penicillin–streptomycin. The detailed procedure was mentioned in Chapter4 in section 4.4.13.3.

7.2.1.5.2 Proliferation Assays

Cell viability of MSCs cultured onto the GCH 30, GCB 30 and GCT 30 scaffolds were determined after performing [3-(4,5-dimethylthiazol-2-yl)-2,5-diphenyltetrazolium bromide] (MTT) assay. The detailed procedure was mentioned in Chapter4 in section 4.4.13.4.

7.2.1.5.3 Inmunofluorescent imaging of cell markers: osteocalcin and RUN-X2

The expression of RunX2 and Osteocalcin, an osteogenic marker on GCH30, GCB30 and GCT30 scaffold was examined using immunocytochemistry. The detailed procedure was mentioned in Chapter4 in section 4.4.13.5.

7.2.2 BSA protein adsorption on GCH 30, GCB 30 and GCT 30 composite scaffold

Bovine serum albumin (BSA) was selected for the protein adsorption study. Bicinchoninic acid (BCA) assay was used to determine the amount of adsorbed protein on the scaffold. The

three different small pieces of composite scaffolds of 12 mm in height and 5 mm in diameter was sliced down by steel blade and immersed in 10 ml BSA solution of 5 mg/ml initial concentration and kept in an incubator at 37 °C for different time duration from 6 h to 144 hour. The supernatant solutions were collected from individual solution through centrifuge at 100 rpm for 10min. The adsorbed BSA protein amount was quantified by taking 0.1 ml of supernatant from each specimen and mixed it with 2 ml of bicinchoninic acid solution (Thermo Pierce, Bicinchoninic acid protein assay kit). UV-vis spectrophotometer (Perkin Elmer, Lambada 35) at 562 nm was used to obtain absorbance peaks and to estimate BSA concentration with the help of a predetermined standard BSA concentration vs intensity calibration curve. The estimated concentrations of protein were the average of protein concentration from three wells. The adsorbed amount of protein on the 3-D porous scaffolds was determined by subtracting the amount of proteins left in the supernatant solution after adsorption from the amount of protein in starting BSA solution under the same condition.

7.2.3 Micro-architectural analysis of composite scaffold

X-ray microtomographic (μ-CT) systems have been widely used as a non-destructive technique to study or characterize microstructural morphology of various biomaterials [312, 313]. For tomography experiment the detector was placed at 450 mm away from the sample stage. The sample was rotated in steps of (0.2°) and was exposed to a beam energy (E = 28 keV) for a duration of 5 sec for all the samples. Dark field and flat field corrections were performed to limit CCD and beam related artifacts during reconstruction. The maximum size of the sample was 12mm. The 2-D images generated by X-ray were recorded from a slice to another slice with a rotation of 0.4° by rotating the sample through 180°. The scanned images were acquired at a pixel size of 11.4 μm. Total acquisition time was approximately 20 min and more than 900 2-D images were recorded for each sample. The images of 3-D microstructures were produced with suitable software [314]. Interconnectivity was calculated as follows:

$$\text{Interconnectivity} = 100(V - V_{\text{shrink-wrap}})(V - V_{\text{m}})^{-1}$$

where V is the total volume of the VOI, $V_{\text{shrink-wrap}}$ is the VOI volume after shrink-wrap processing, and V_{m} is the volume of the material.[319]

7.2.4 Expression of osteogenic specific genes

Semi-quantitative RT-PCR was performed to assess the expression of osteoblast related markers at mRNA level for cells cultured upto 14 days. Primer sequences used for the study are shown in Table 7.1. For RT-PCR analysis, the total cellular RNA from osteoblasts (differentiated from hMSCs) was extracted by TRIzol. Synthesis of cDNA was carried out using first strand cDNA synthesis kit following the manufacturer's protocol. The synthesized cDNA was used as a template for the semi-quantitative RT-PCR following the procedure followed elsewhere [315]. The GAPDH gene was used as a housekeeping gene for normalizing mRNA level of Col-1, RUNX2, OCN, OPN gene. The PCR reaction mixture consists of 1X PCR buffer, 50 mM mgCl2, 10 mM dNTPs, 0.2 μM of each primer, 1U Taq polymerase and autoclaved water. PCR chain reactions were performed at 94°C for 2 min, 35 cycles at 96°C for 30s, 55–63°C for 45s, and 72°C for 45s and 72°C for 10 min. Finally, the amplified DNA fragments (PCR products) were subjected to electrophoresis on 1.5% agarose gel and the band intensity was analysed using Image J software for evaluating the relative expression of selected genes (BioRad, USA).

Table.7.1. RT-PCR Primers used for expression of osteogenic specific genes.

Gene	Direction	Primer Sequence
Osteocalcin	Forward	5^1- CCC AGG CGC TAC CTGTAT CAA-3^1
	Reverse	5^1- GGT CAG CCA ACT CGTCAC AGTC-3^1
Osteopontin	Forward	5^1-CATCTCAGAAGCAGAATCTCC-3^1
	Reverse	5^1-CCATAAACCACACTATCACCTC-3^1
RUNX2	Forward	5^1-TGGTTACTGTCATGGCGGGTA-3^1
	Reverse	5^1-TCTCAGATCGTTGAACCTTGCTA-3^1
Col1	Forward	5^1- GGCAATAGCAGGTTCACGTACA -3^1
	Reverse	5^1- CGATAACAGTCTTGCCCCACTT-3^1

7.2.5 *In-vivo* animal study

7.2.5.1. Animal experimentation

Animal experimentation was carried out following the procedures confirming to the standards of the institutions Animal ethical committee of the West Bengal University of Animal and Fishery Sciences, India. Eighteen clinically healthy adult Newzeland white

rabbits (12-15 months) of either sex, weighing 2.5-3 kg, were used in this study. They were randomly distributed into three groups of six animal each: Control (Group I) i.e gelatin-chitosan(GC) scaffold, gelatin-chitosan-HAp (GCH 30) scaffold (Group II), gelatin-chitosan-TCP (GCT 30) scaffold (Group III) and gelatin-chitosan-bioactive glass (GCB 30) scaffold (Group IV).Prior to surgery, the rabbits were housed in individual cages in a humidity control room, given water ad libitum and were without restriction of movement. All surgeries were performed under standard anaesthesia. This 90 days study evaluated early stage *in vivo* osteogenesis and bone remodelling using a bone defect model in the proximal tibia of Newzeland white rabbit.

7.2.5.2 Surgical procedure

The animal experiments were performed following an ethical committee approved protocol in West Bengal University of Animal and Fishery Sciences (WBUAFS), West Bengal, India (E.C/180). Sixteen adult New Zealand White rabbits (1.5–2 kg) were randomized into four groups (n = 4), control group I (GC) and the test animals, group II (GCH 30), group III (GCT 30) and group IV (GCB 30) with bilateral implantation (Figure.7.1 (e)).

Surgeries were performed under aseptic conditions and sedation by intramuscular injection of xylazine hydrochloride (5mg/kg) and ketamine hydrochloride at 25mg/kg body weight. A motorize drill was used to create 2×2×5 mm^3 (Figure7.1 a-d) in the medial aspect of proximal Tibia (Figure.7.1.a) The implants were inserted in the defects and secured a position by suturing the muscle, subcutaneous tissue and skin in layers (Figure.7.1 c-d). Treated animals were daily administered with cefotaxime sodium (Mapra, India) at 20mg/kg body weight intramuscularly for 5 days at 12-hour interval and meloxicam at 0.2mL/kg body weight. Surgical wounds were inspected daily and appropriate wound care was taken. The operated animals were observed carefully upto 3 months postoperatively, to note any associated sign of local inflammatory reactions, fracture by visual or manual examinations.

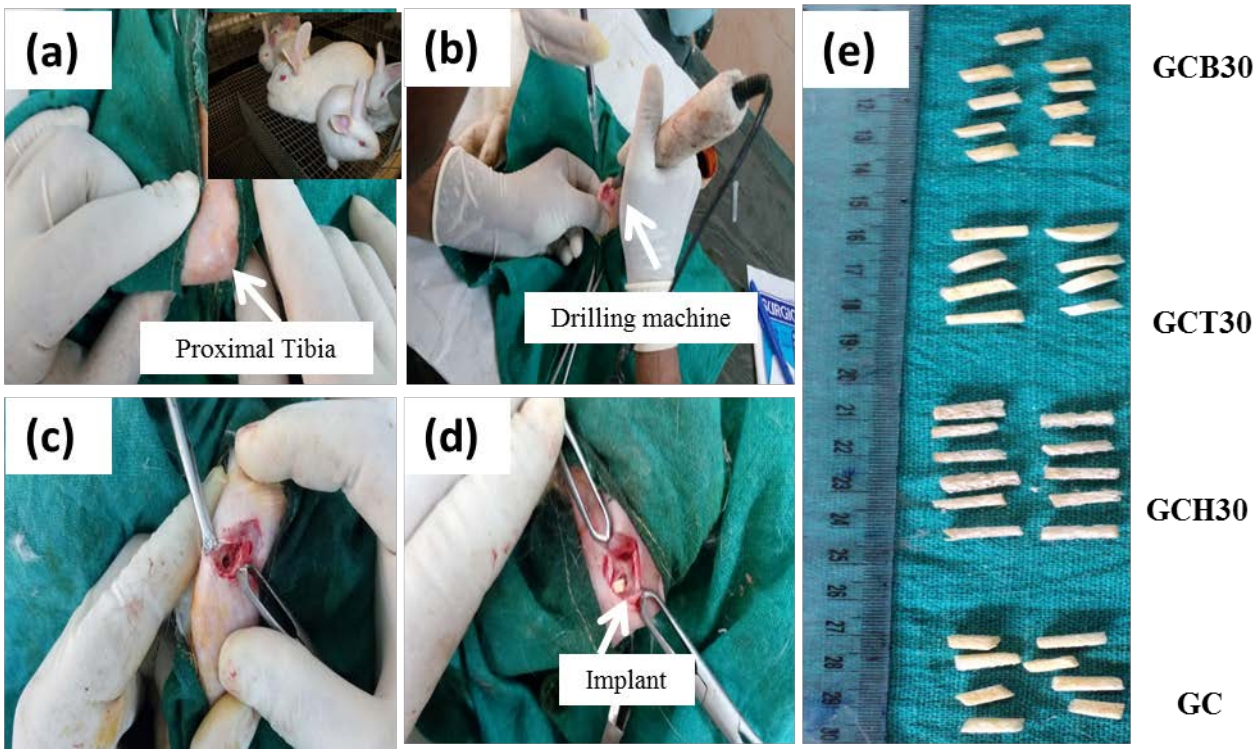

Figure.7.1. Surgical placement of porous scaffold into Rabbit tibia. Digital image of sample used in *in vivo* experiment.

7.2.5.3 Radiological study

Sequential radiographs of the femur bone were recorded at regular intervals (days 0,1,2,3 months postoperatively) in a medical diagnostic X ray machine (300 mA, M.E, X-Ray, India) to study the status of the implant and the degree of host bone –material interaction.

7.2.5.4 Histology analysis

The radiological results were further verified histological investigations of the operated sites in order to understand distribution and development of osseous tissue in-growth at the defect site. After sacrificing the animals at the end of 1,2 and 3 months post operatively, the bone specimen were collected , washed with normal saline, cut into thin sections containing the implant and preserved in 10% formalin. For histological analysis, decalcccified tissues(using Goodling and Stewart's fluid) were stained with hematoxylene and eosin to observe the matrix formation in optical microscope.

7.2.5.5 Fluorochrome labelling study

Fluorochrome labelling analysis of the implanted bony sections was carried out using an Orthoplan microscope (Excitation filter, BP-400range, Leitz,,USA)to understand the new bone formation as well as the mineralization process. For this study oxytetracycline

dehydrate (OTC) (Pfizer India, India),a bone forming marker, was administered to each animal (intramuscularly at25mg/kg body weight) 25days before the sacrifice of 2 month samples i.e., on days35,36 and after a gap of 6 days on day43,44(2-6-2)post-operatively for double toning of the new bone. Again on days 65 and 66 and then on 71, 72 days, OTC was administered to each animal for 3 months' sample. For the analysis, thin and un-decalcified sections were prepared from the implanted bone specimens which were observed under UV light. Data obtained was further taken in LeicaDM2000 Bright light phase contrast and fluorescence microscope including Leica Qwin software. In the said microscope, area of bone formation (golden yellow fluorescence) has been measured in mm^2 and subsequently converted to percentage of bone formation and finally statistical analysis was carried out.

7.2.5.6 ESEM analysis of implant material

The radiological results were further verified by microscopic evidences using Environmental scanning electron microscope (ESEM, Quanta FEG 250, Nederland) investigations of the operated sites in order to understand the distribution and development of the osseous tissue in-growth at the defect site. For ESEM analysis, the wet samples were directly put into the ESEM chamber before imaging.

7.3 Statistical Analysis

Quantitative data were presented as mean ± standard deviation (SD). The two-tailed Student's T-test (T-test) was employed to obtain p values, which determined the level of significance of the data. Difference between groups were statistically significant if $p < 0.05$ and highly significant if $p < 0.01$.

7.4 Results and Discussion

7.4.1 X-Ray diffraction analysis

Phase analysis of the prepared scaffolds was performed using XRD analysis as shown in Figure 7.2. Only characteristic peaks of GCT30 were indexed in Figure.7.2 (a), suggesting that the synthesized powder was β-TCP with hardly presence of any other secondary phase. The sharp peaks of (002) and (112) plane in GCH30 [Figure.7.2 (b)] confirmed that presence of phase pure hydroxyapatite in the fabricated GCH30 scaffold. The broad amorphous peaks of 58s bioactive glass confirmed that the synthesized scaffolds were predominantly amorphous [Figure.7.2(c)]. The characteristic diffraction peaks for both chitosan and gelatin

were suppressed by the huge amorphous peak of bioactive glass observed in the range between 2θ equal to 20°–40°. It is clearly evident from figure.7.2 that composite scaffolds contain sharp peak of HAp in GCH30, β-TCP phase in GCT30 and a big amorphous hump of bioactive glass in GCB30, demonstrating the presence of respective bioceramics component in the scaffold.

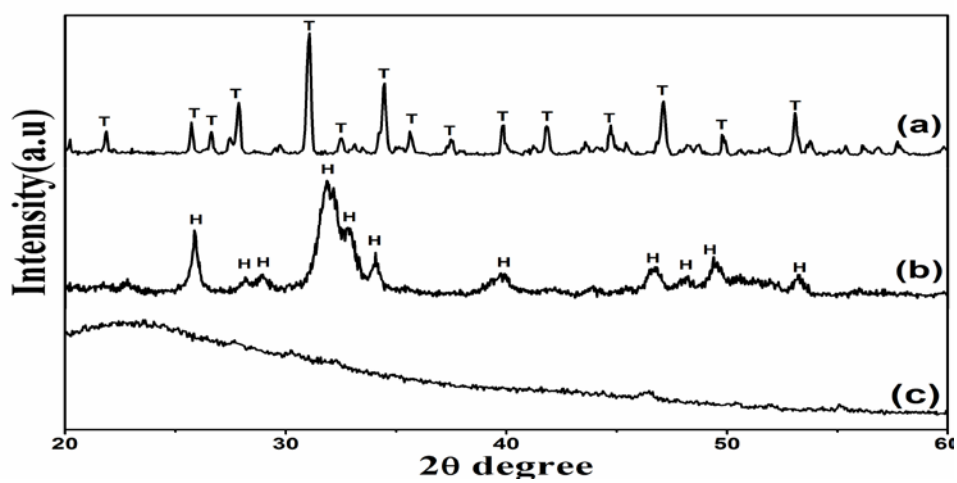

Figure.7.2. XRD pattern of composite scaffold (a) GCT30, (b) GCH30, (c) GCB30.prepared using freeze drying technique.

7.4.2 FTIR analysis

Figure7.3 shows the FTIR spectra of GCH 30, GCT 30, GCB 30 composite scaffolds to determine that the blended scaffolds were fabricated successfully. GCH 30 composite shows that the N-H bending vibration of chitosan band shifted from 1556 cm^{-1} to 1544 cm^{-1}, this bond shift was result from the interaction between HAp with Gelatin-Chitosan matrix respectively [316]. The spectra of GCB 30 composite scaffold showed 1300 cm^{-1} band due to the interaction between Ca^{+2} of bioactive glass and COO^{-} of gelatin molecule. The shift of N-H vibration band to 1555 cm^{-1} suggest the interaction between β-TCP with gelatin-chitosan matrix in GCT 30 scaffold[225]. The peak near 1552(inset graph) in all composite scaffold corresponds to the C=N bond of cross linked gelatin-chitosan in all composite scaffold on reacting with glutaraldehyde solution.

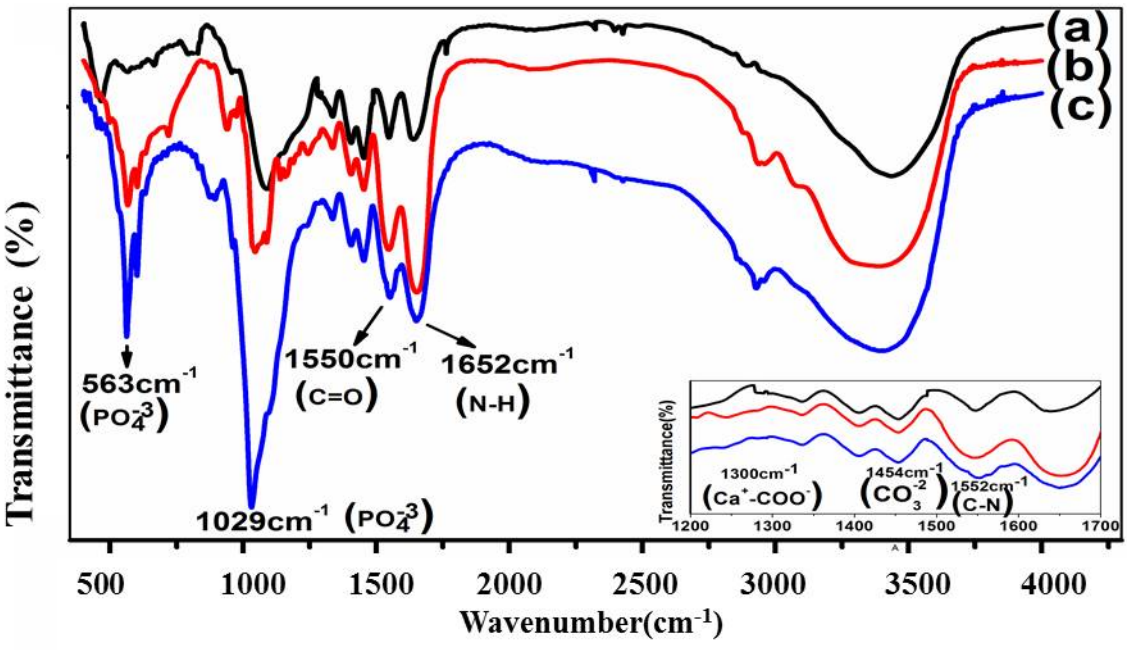

Figure.7.3. FTIR-ATR analysis of (a) GCH30 scaffold (b) GCT30 scaffold, (c) GCB30 scaffold, analysed in the 500 cm−1 ~4000 cm−1 regions.

Table7 2. Characteristic band of fabricated composite scaffold [317].

Wavenumber (cm^{-1})	Assignment	Material
~1652	Amide I(C=O stretch)	Characteristic bond of Chitosan and Gelatin
~1550	Amide II (N-H bend and C-H stretch)	Characteristic bond of Chitosan and Gelatin
~975-480	v2 stretching vibration	Characteristic vibration modes of PO_4^{-3} in GCH and GCT.
~1090, 1035, 607, 550	v3 and v4 vibration modes	Characteristic vibration modes of PO_4^{-3} in GCH and GCT
~448, 1410, 1640	to carbonate ions (CO_3^{2-})	Carbonate ion of ceramic phase
~1300	Ca^{+}-Coo^{-}	Interaction between organic and inorganic phase
1552	-C-N-	crosslinking of chitosan and gelatin via glutaraldehyde
~463	Si-O-Si bending	Characteristic of silicate network in Bioglass
~1029	Si-O-Si stretching (asymmetric)	Stretching vibration bond in Bioglass

7.4.3 SEM analysis of GCH 30, GCB 30 and GCT 30 composite scaffold

Scanning electron microscope was used to observe porous microstructure of the glutaraldehyde cross-linked composite scaffolds. As shown in Figure.7.4 (a,b,c) the pores in the composite scaffolds were interconnected in the size range between 90-120 μm, which is ideal for exhibiting osteoinduction. From SEM images (Figure 7.4 (a-d), it is clear that

bioceramic reinforced scaffolds possessed lower pore sizes as compared to neat gelatin-chitosan based (GC) scaffold. GCH 30 exhibited the lowest average pore size of 94±5.2 μm, whereas the average pore size of GCT 30 was the highest of 120±6.4 μm amongst the composite scaffolds as evident from Table7.3. EDX analysis in Figure.7.4a_1-c_1 confirmed the presence of Calcium (Ca), Phosphorous (P) in GCH30, GCT30 and Silicon(Si), Calcium (Ca), Phosphorous (P) in GCB30 scaffold prepared using freeze drying technique. GCT 30 exhibited the highest value of most frequent pore diameter of 118 μm whereas that for GCH 30 is the lowest of 96 μm as evident from Hg porosimetry data in Figure 7.4 (a_2, c_2). The most frequent pore size of GCB 30 scaffold was close to an intermediate value of 100 μm (Figure 7.4 b_2).Figure 7.4 (d).

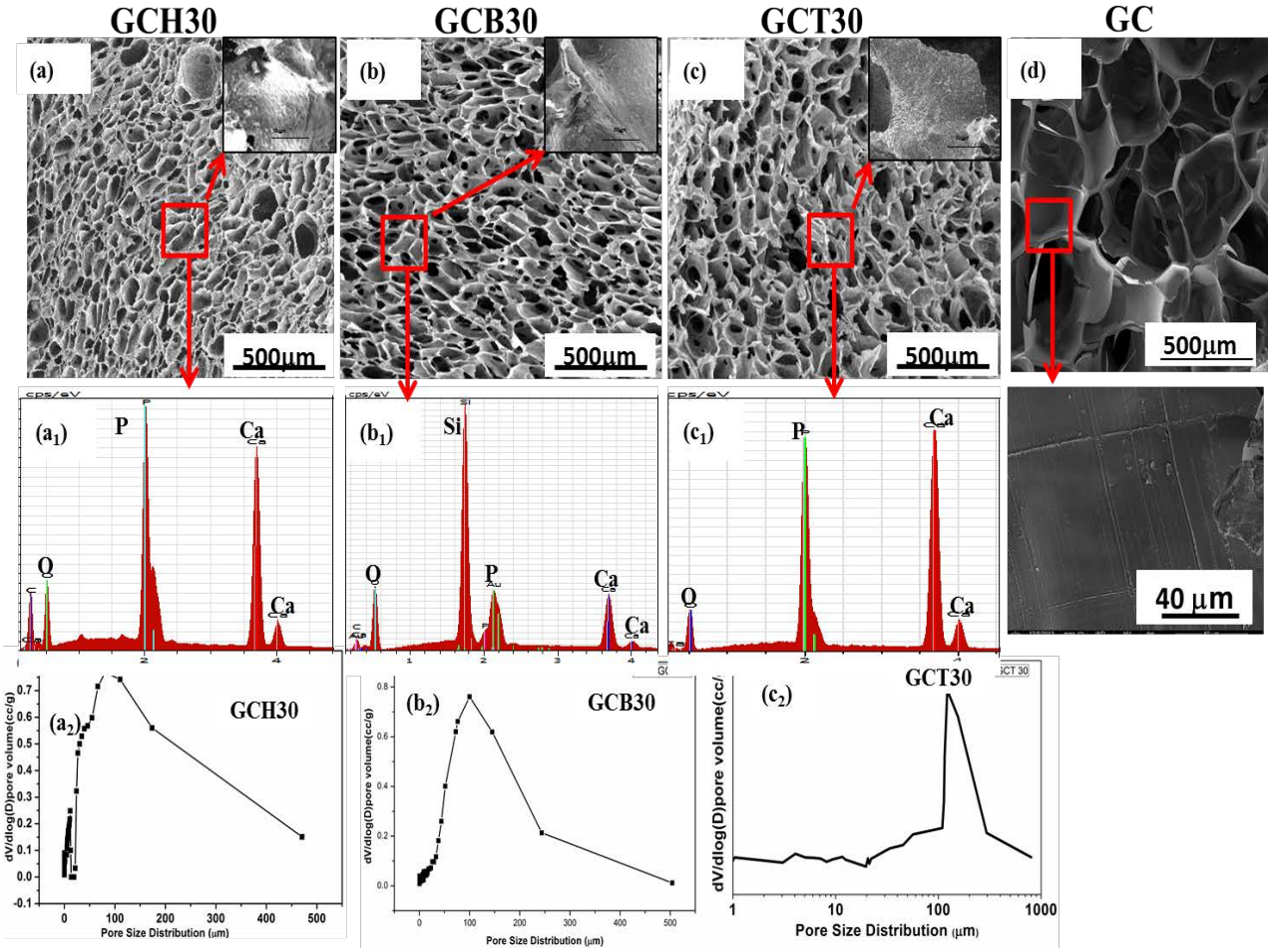

Figure.7.4. SEM micrographs of cross-section of scaffolds (a) GCH30 (b) GCB30 (c) GCT30 (d) GC. EDX analysis and pore size distribution of (a_1,a_2) GCH30, (b_1,b_2) GCB30, (c_1,c_2) GCT30 scaffold.

7.4.4 Mechanical characterization of the scaffold: compression resistance

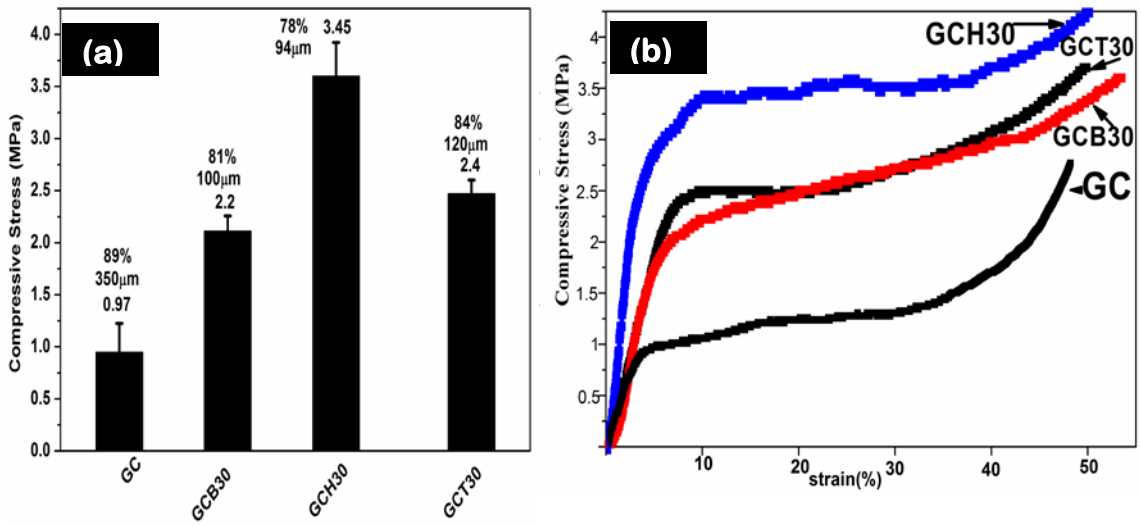

Figure.7.5.(a) Average compressive strength of the prepared scaffolds (b). Typical stress strain plot of GCH 30, GCT 30, GCB 30 and GC scaffold.

Average compressive strengths of GCB 30, GCH 30 and GCT 30 scaffolds are shown in Figure.7.5a. The compressive strengths of three types of scaffolds were in the range between 1–4 MPa [Figure.7.5(a)]. It is clear that bioceramics reinforced scaffolds have a significantly higher compressive strength (~4 MPa) than pure gelatin-chitosan scaffolds (~0.97 MPa) while the scaffolds porosity varied very little between 78–83% as shown in Table.7.3. GCH 30 scaffold showed the highest compressive strength due to effective anchoring of nanoparticulate with gelatin-chitosan matrix. Higher surface area and higher number of unsaturated ionic bonding sites of HAp- chitosan nanopowders were mainly responsible for better bonding interaction with gelatin matrix in GCH 30 scaffolds and accounted for it's lower average pore diameter and highest compressive strength among all the prepared scaffolds. Stress-strain behaviours of all the prepared scaffolds are represented in Figure 7.5 (b). All the scaffolds showed similar stress–strain behaviour: the stress increased linearly upto elastic deformation zone, then reduced in slope in plastic deformation zone, followed by an abrupt stress increase at high strain in densification zone [318]. Owing to the high flexibility of gelatin, no final fracture was observed. Average maximum compressive strength of 3.45 MPa was exhibited by GCH 30, whereas the other composite scaffolds showed a lower compressive strength of 2.47 MPa by GCT 30 and 2.24 MPa by GCB 30.

Table.7.3. Porosity,pore size and compressive strength of composite scaffold.

Sample ID	Porosity (%)	Compressive Strength(MPa)	Pore Size (μm) (SEM)
GCB30	81.08±6	2.24±0.01	100±8.6
GCH30	78.12±3.2	3.45±0.04	94±6.9
GCT30	83.11±8	2.47±0.02	120±6.4

7.4.5 Micro CT scanning of GCH 30, GCB 30 and GCT 30 composite scaffold

Micro-CT scanning on the prepared scaffold was conducted to quantify the pore size, porosity and interconnected porosity. Figure 7.6 depicts 2D cross-sectional and 3D reconstructional images of the scaffolds. All GCH 30, GCT 30 and GCB 30 scaffolds presented roughly homogenous porous structures, with high degree of interconnected and open porosity (Table 7.4). The measured interconnected porosities of GCH 30, GC T30 and GCB 30 were 63 ± 1.37%, 67 ± 2.65, 72 ± 3.24% respectively, indicating that the interconnected porosities of the prepared composite scaffolds could be well controlled and GCB 30 showed the highest interconnected porosity in the prepared scaffolds.. This study confirms that scaffolds were prepared with sufficient degree of interconnected porosity which is important for *in vivo* osteogenesis. The average pore size values obtained from micro CT and as well as from SEM investigation of microstructures of prepared scaffolds were found in good proximity.

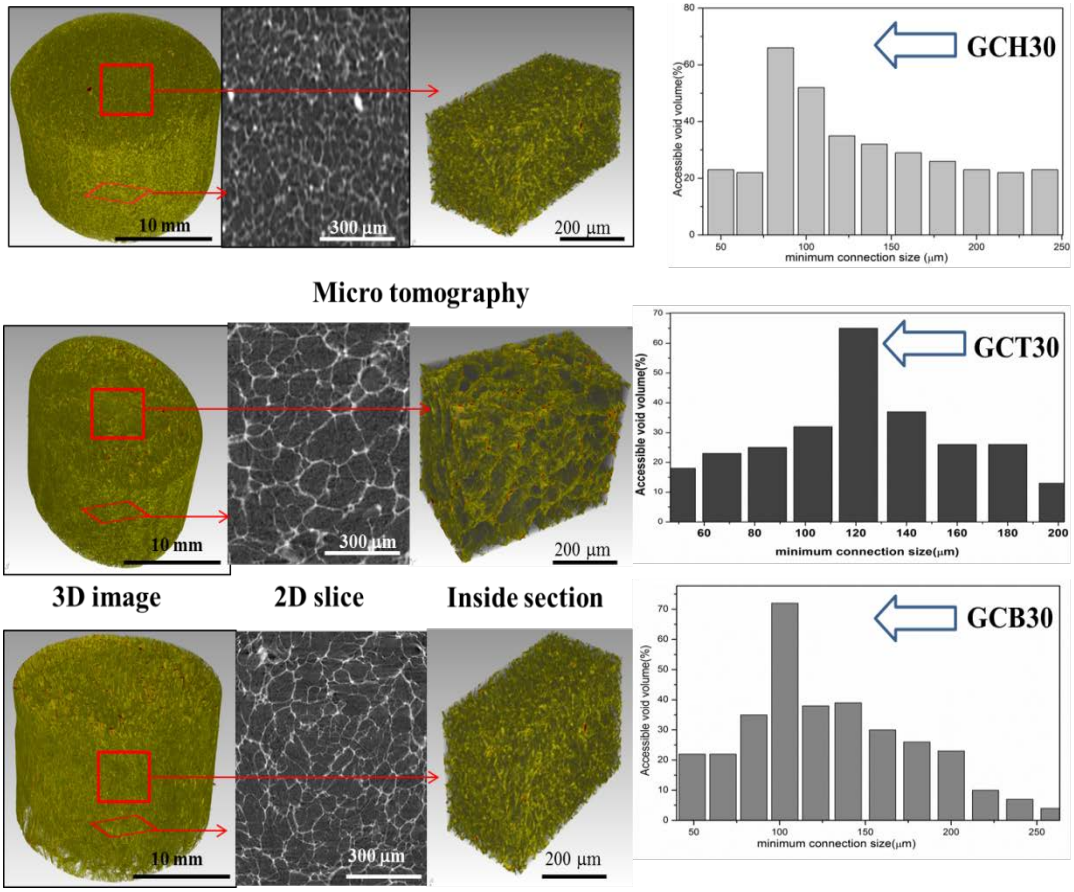

Figure.7.6. 2D and 3D images of GCH 30, GCB30 and GCT30 scaffolds acquired from micro-CT scanning.

Table.7.4. Measurement of porosities in the prepared scaffolds by Micro-CT scan.

	Unit	GCH 30	GCB 30	GCT 30
Pore size	Micrometre (µm)	96 ± 2.41	102 ± 3.01	118 ± 2.84
Total porosity	Percent (%)	79 ± 3.41	81 ± 4.01	83 ± 3.29
Open Porosity	Percent (%)	79 ± 3.41	81 ± 4.01	83 ± 3.29
Interconnected Porosity	Percent (%)	63 ± 1.37	72 ± 3.24	67 ± 2.65
All data shown as average ± standard deviation				

7.4.6 BSA protein adsorption study by composite scaffold

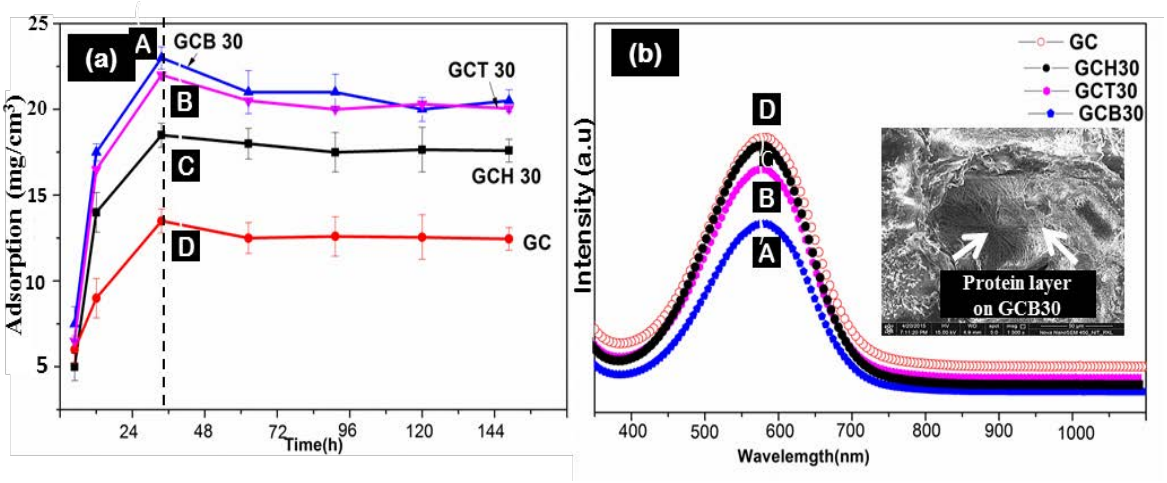

Figure.7.7. (a) BSA protein uptake by different composite scaffold (b) UV visible spectrum of BSA in supernatant solution after its adsorption onto different composite scaffold after 36h of study.

BSA adsorption on three composite scaffolds was evaluated for different time intervals from 10 to 144 hours as shown in Figure 7.7(a). BSA concentration in supernatant at solution was measured in the wavelength region of ~560-570 nm using UV-visible spectrophotometer after adsorption of protein onto scaffolds from a standard BSA solution. In all the scaffolds the amount of protein adsorption was the highest up to 36 hours and then became more or less saturated. After 36 hours of incubation in BSA solution, protein adsorption was found to be maximum of 24 mg/cm^3 in GCB 30 scaffold and minimum of 13 mg/cm^3 in GC scaffold. Report says that, incorporation of HAp into PLLA scaffold improved protein adsorption capacity of the composite scaffold by forming a microenvironment on the scaffold surface favourable for protein adsorption [320]. In composite scaffold higher protein adsorption was evident because of higher surface area due to the presence of hydrophilic bioceramic nanoparticulate that interacted with the hydrophilic parts of the protein to bind more amount of protein on the surface as compared to the neat gelatin-chitosan (GC) scaffolds. Figure 7.7(b) shows lower amount of BSA concentration in supernatant solution from GCB 30 scaffold as compared to neat gelatin-chitosan(GC) scaffolds because of higher amount of protein adsorption onto GCB 30 surface from standard BSA solution after 36 hours of incubation. It appeared that GCB 30 scaffold had the maximum protein adsorption capacity among all the scaffold tested here after 36 hour of incubation in protein solution. The ability of surface protein adsorption is considered as an important factor contributing to the biocompatibility of materials, as it could influence cell adhesion, proliferation, differentiation [321].

7.4.7 Degradation Study of GCH30, GCB30 and GCT30 composite scaffold

Degradability of the prepared scaffold was measured after immersing them in PBS solution having pH 7.4 for 25 days. Figure.7.8 represents the percent weight loss of GC and composite scaffolds after immersing them for upto 25 days in SBF. All the composite scaffolds showed lower rate of degradation as compared to neat GC scaffold upto 25 days of immersion in PBS. The nanoparticulate ceramic phase addition into GC matrix resisted the rate of degradation due to stronger bonds between Ca^{2+} and COO^{-} or PO_4^{3-} and NH_3^{+} present in bioceramic and gelatin- chitosan matrix.

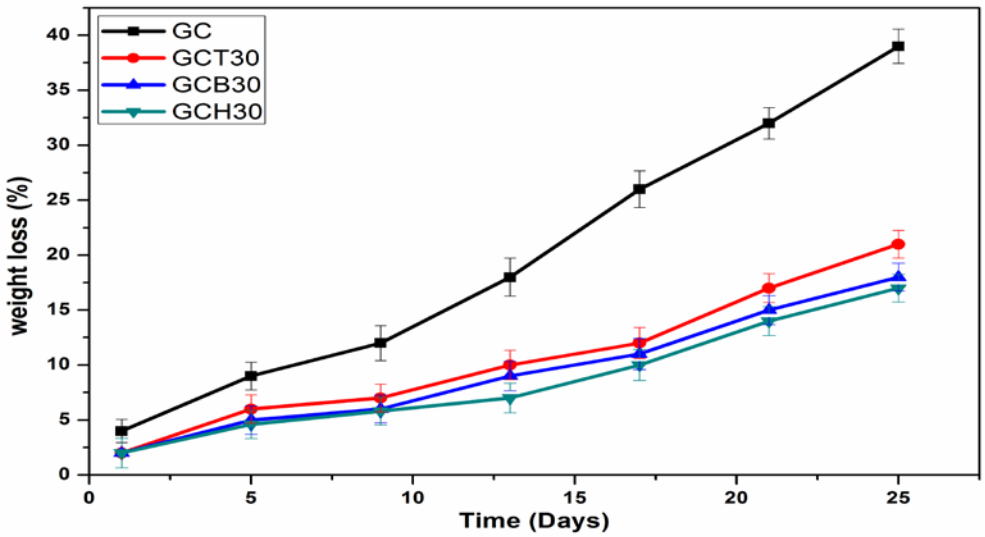

Figure.7.8 Degradation kinetics of GC, GCT30, GCB30 and GCH30 scaffolds. Data represent mean value of three independent experiments.

The average weight loss of GCH 30 and GCB 30 scaffold was found to be 16% and 17% respectively after 25 days of immersion in PBS, whereas GCT 30 scaffold exhibited higher weight loss of 20% for same period of immersion in PBS. All the composite scaffolds showed a similar trend in degradation rate in PBS upto 25 days, which supports the fact that there exists no significant difference ($p>0.05$) in degradation capability among the prepared scaffolds. That means the nature of existed bioceramics phase did not exert any significant influence on the degradation capability of the prepared composite scaffolds.

7.4.8 Cell attachment on GCH30, GCB30 and GCT30 composite scaffold

Cell attachment and migration within the scaffold are essential for exhibiting osteoconduction and osteoinduction. MSCs were seeded and cultured onto GC, GCH 30, GCT 30 and GCB 30 scaffolds for 7 and 14 days taking GC scaffold as control. As observed from SEM images in Figure 7.9 (a), though MSCs were sparsly distributed on the surface of composite scaffolds

after 7 days of culture, densities of attached MSCs were higher on composite scaffolds as compared to neat GC scaffold.

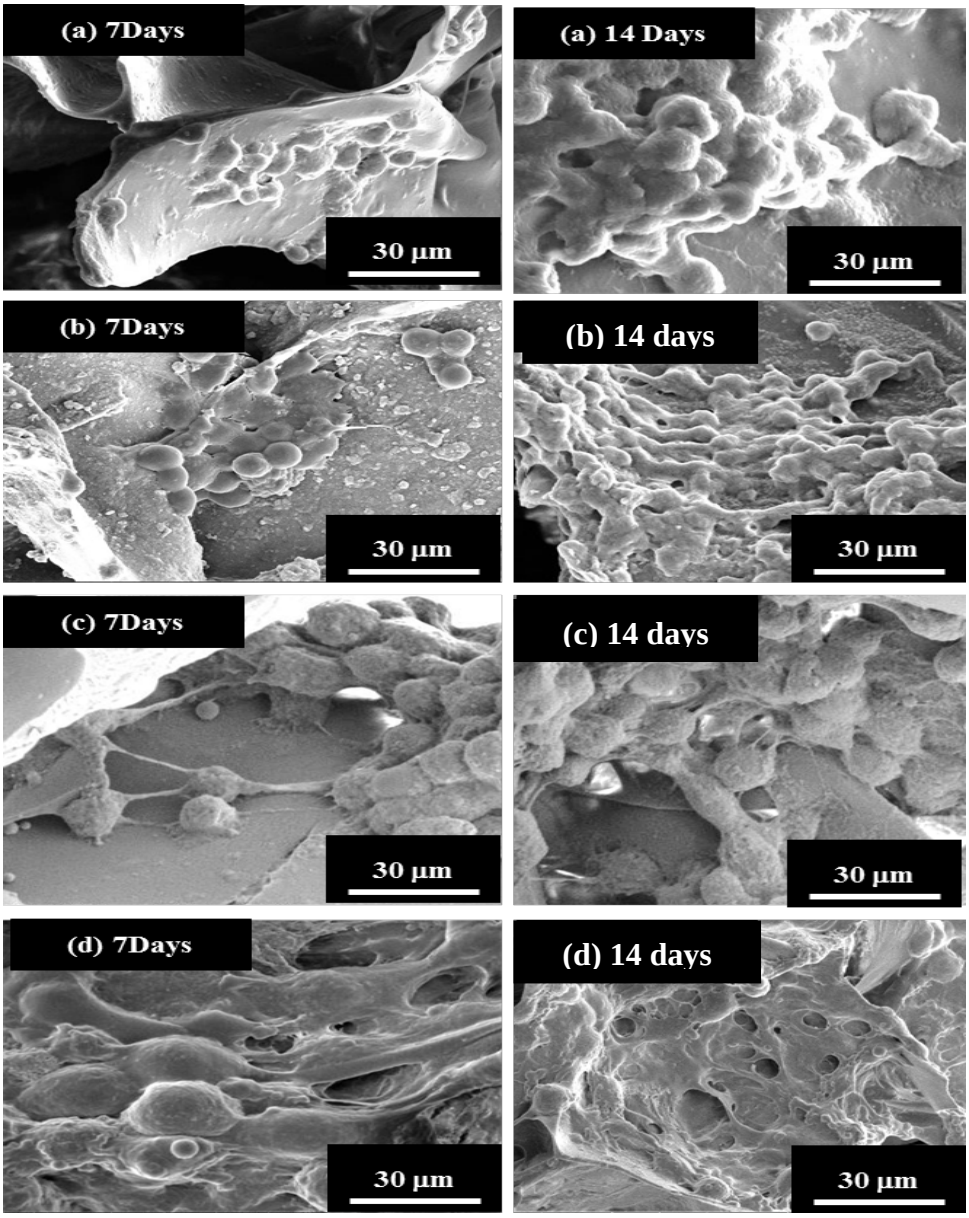

Figure.7.9. Scanning electron microscope (SEM) images of human mesenchymal stem cells (hMSCs) grown on (a)GC, (b)GCH30, (c)GCT30 and (d)GCB30 scaffolds after 7 days and 14 days.

The cells maintained round shapes on the surface of GCH30 and GCT30 scaffold, whereas the morphology of cells was little bit flattened on GCB30 scaffold after 7 days of culture. In contrast to 7 days' culture scaffold, 14 days cultured sample showed higher cell density and flattened morphology. As compared to other scaffolds, the MSCs cultured on GCB30 attached fully to cover the whole surface with numerous lamellipodia and filopodia

extensions exhibiting better attachment and excellent spreading behaviour. The cells cultured onto GCH 30 and GCT 30 scaffold after 14 days were rather round shape and clingged together as compared to the GCB 30. MSCs showed better attachment, spreading and growth onto composite scaffolds as compared to neat gelatin-chitosan scaffold.

7.4.9 Cell proliferation on GCH 30, GCB 30 and GCT 30 composite scaffold

Proliferation ability of MSCs cultured in osteogenic medium and onto composite scaffolds was studied using MTT assay after 1, 3, 5 and 7 days. With progress in cell culture time the cell density in all the scaffold increased as shown in Figure.7.10.

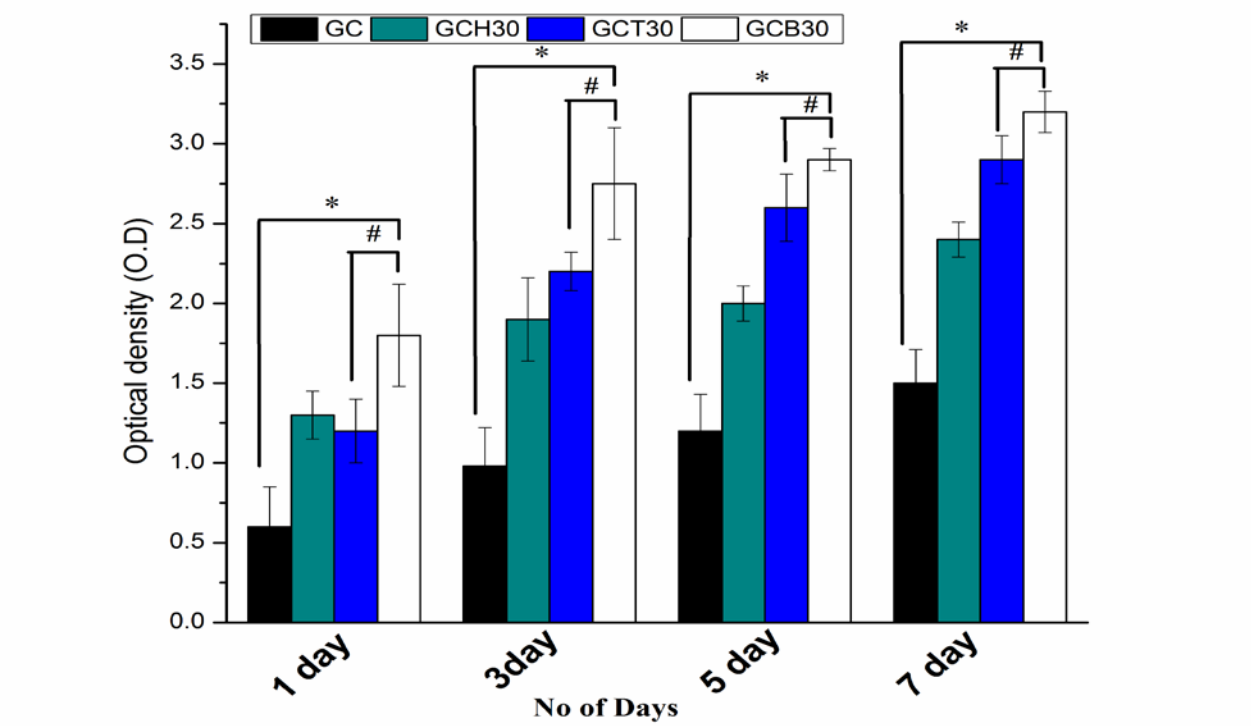

Figure.7.10. MTT assay for proliferation of MSCs cultured in osteogenic medium at various periods of cell culture at 1,3,5 and 7 days, onto GC, GCH30,GCT30 and GCB30 scaffold. Error bars represent means ±SD for n = 3. *p<0.05, #p < 0.01 (compared to MSCs cultured in osteogenic medium).

The cell densities in composite scaffolds were significantly higher (*p <0.05) as compared to control during all periods of cell culture. Moreover, GCB 30 scaffold exhibited better proliferation ability of MSCs compared to GCT 30 scaffold as suggested by p values (# <0.01) for all the periods of cell culture. This reflects the fact that MSCs proliferation tendency was enhanced after addition of bioactive glass nanoparticles into gelatin-chitosan matrix of GCB 30.

7.4.10 Differentiation of MSCs in contact with Scaffolds

Treating GAPDH as a control, the expression levels of RUNX2, COL-1, OCN and OPN were detected with the help of rt-PCR at two different time points of cell culture onto each type of composite scaffold. The band intensities obtained after gel electrophoresis of respective proteins are shown in Figure.7.11. It is evident from Figure.7.11 that RUNX2 expressions were more prominent at 7 days of cell culture compared to later time point of 14 days, which is consistent with MSC's differentiation into preosteoblast and then bone lineage at later time points.

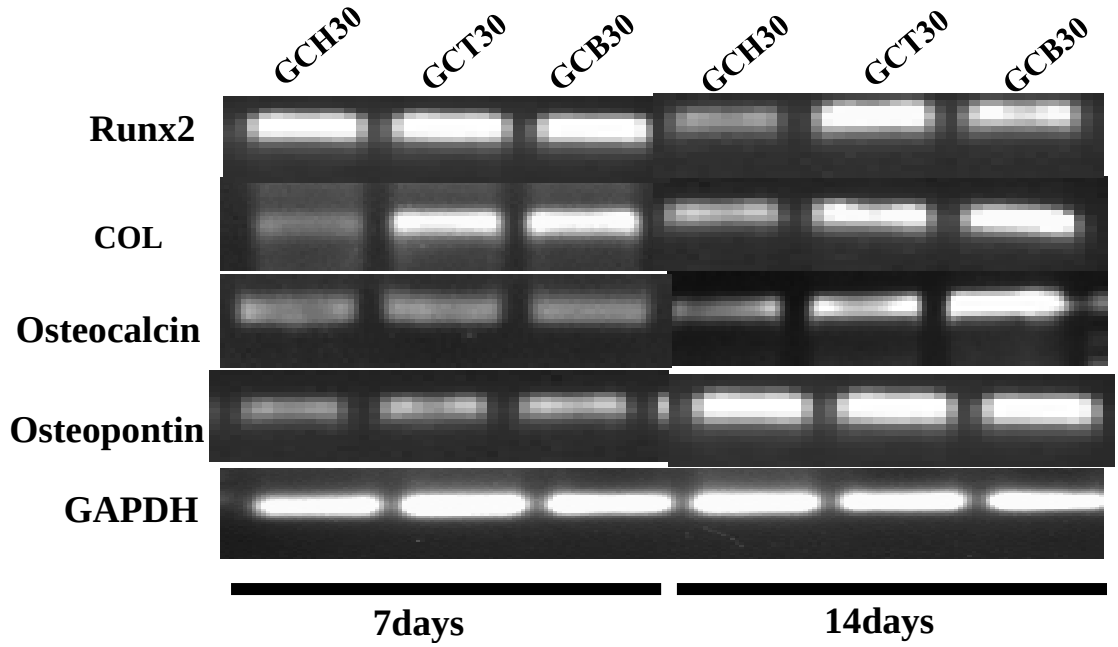

Figure.7.11. Images of amplified cDNA products using GAPDH as control for hMSCs cultured on GC, GCH30, GCT30 and GCB30 composite scaffolds in osteogenic media for 7 days and 14 days.

On the other hand, expression levels of COL-1, OPN and OCN were higher on later time point (14 days) of cell culture compared to earlier time point (7 days). Higher expression of COL-1, OCN and OPN at later time point of cell culture is consistent with the higher degree of bone matrix mineralization and mature osteoblast formation in each group of scaffold.

7.4.11 Osteogenic Gene expression study

Figure.7.12 shows osteogenic gene expression profile of MSCs cultured onto GCH 30, GCT 30 and GCB 30 scaffold. Semi quantitative result showed that relative expression of RUNX2 in GCB 30 scaffold was higher (# $p < 0.05$) on 7 days than that is on 14 days as in Figure 7.12 (a). At the same time GCB 30 showed higher (** $p<0.01$) expression of RUN X-2 as compared to GCT 30 on earlier time point of 7 days reflecting its better capacity to differentiate MSCs into preosteoblast.

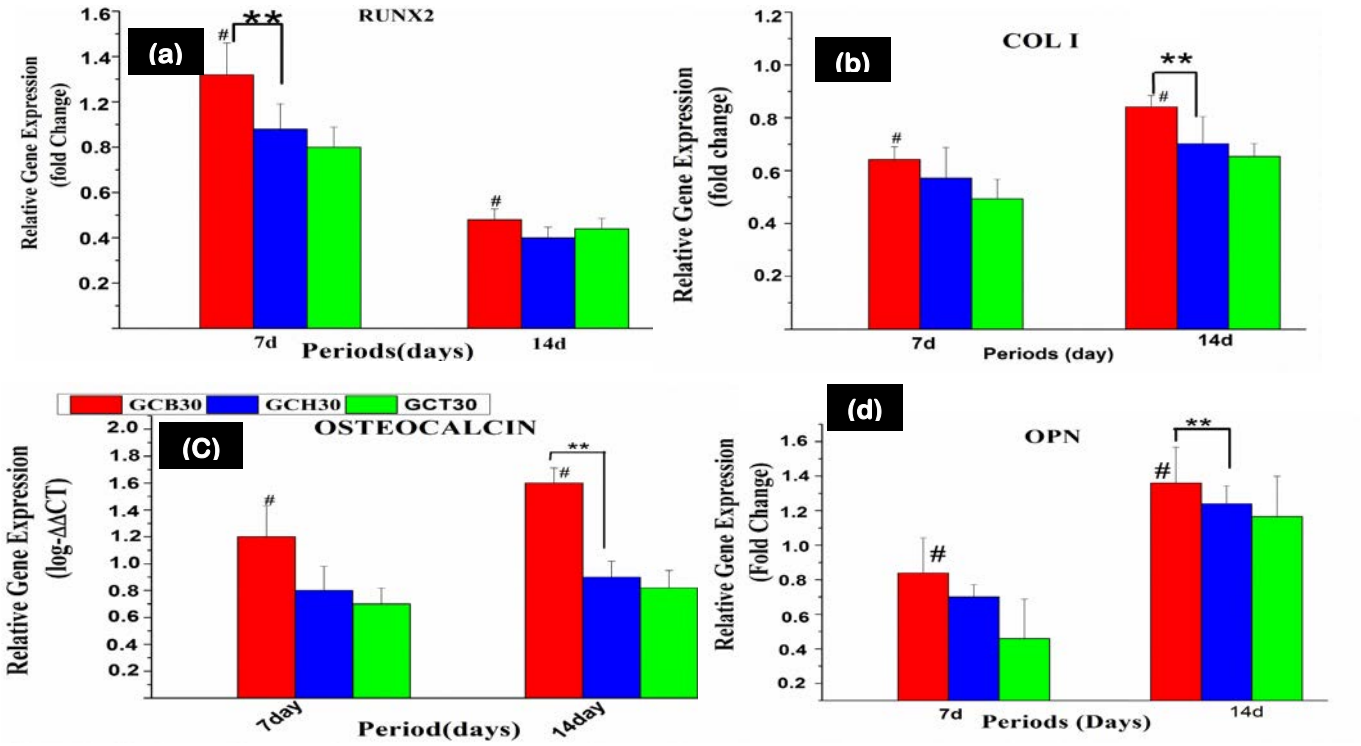

Figure.7.12. Quantitative analysis of osteogenic markers upto 14 days on composite scaffold of (a) RUNX2, (b) COL I (c) Osteocalcin (d) OPN expression of MSCs cultured on scaffolds by Q-PCR. *Represents statistically significant difference (P < 0.05).

Expression of COL-1, OCN, OPN found to be higher on all the scaffolds particularly on GCB 30 (# all p values < 0.05) at later time point of 14 days as compared to 7 days which is corroborated well with MSCs commitment to matured osteoblast, bone lineage and bone matrix mineralization. Moreover, gene expressions of COL-1, OPN, OCN appeared to be significantly higher (** p values< 0.01) on GCB 30 as compared to GCT 30 and GCH 30 after 14 days of culture of MSCs [Figure 7.12 (b), (c), (d)]. The reason behind the increasing osteoblastic gene expressions may be attributed to the synergic effect between Ca^{2+} and Si^{4+} ion released from GCB30 scaffold in cell culture media that helps in enhanced differentiation of MSCs seeded onto GCB30 scaffold as compared to other composite scaffold. This clearly reflects higher efficiency of GCB 30 scaffold to regenerate bone tissue *in vitro* as compared to other composite scaffolds.

7.4.12 Confocal microscopic analysis of GCH 30, GCB30 and GCT30 composite scaffold

The confocal images for expression of osteogenic marker RUNX2 and Osteocalcin by MSCs cultured onto GC, GCH30, GCT30 and GCB30 scaffold for 14 days are shown in Figure.7.13. The cultured MSCs differentiated into osteogenic lineage to elicit dual expression of RUNX2 and osteocalcin after 14 days of culture onto prepared scaffolds as shown in Figure.7.13.

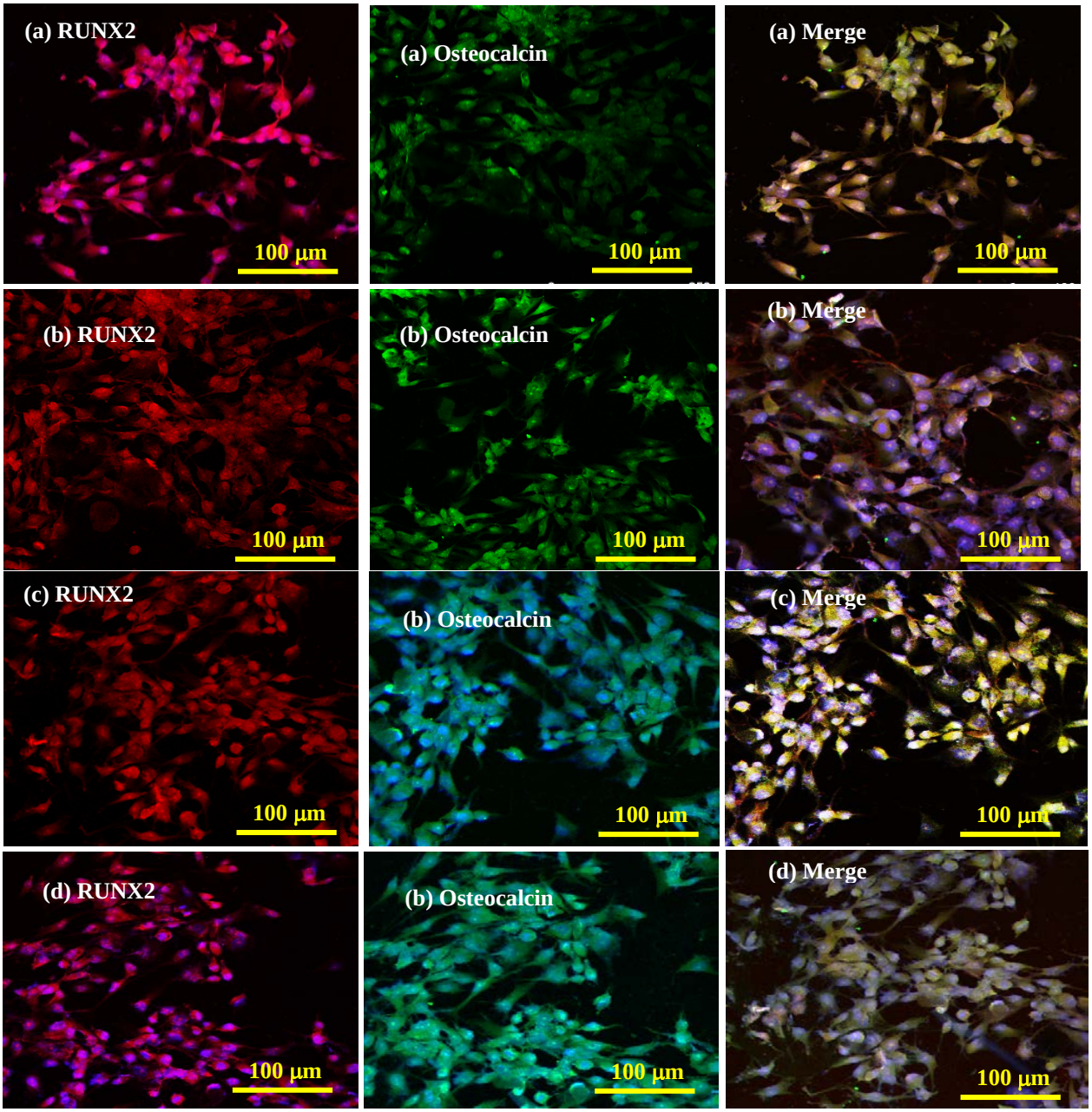

Figure.7.13. Dual immunocytochemical analysis for the expression of RUNX2 and osteocalcin, differentiation marker of MScs into osteoblast, on (*a*) control GC, (b) GCH30, (c) GCT30 and (d) GCB30 at 100× magnification after 14 days of cell culture. Nucleus (blue) stained with DAPI.

RUNX2 is an enzyme expressed by MSCs during osteogenesis and well defined marker of osteoblastic lineage [30]. Osteocalcin is an enzyme expressed during matrix mineralization. Previous studies reported that extracellular Ca^{2+} and inorganic phosphorous released by CaP biomaterials, favour MSCs differentiation into osteoblast and matrix mineralization through activating calcium sensing receptor in osteoblast cells [16-48]. All the composite scaffolds contained Ca^{2+} and PO_4^{3-} which were released during cell culture period to promote better differentiation of MSCs into osteoblast and bone matrix mineralization as indicated by higher degree of RUNX2 and osteocalcin expression in the composite scaffold as compared

to neat GC scaffold. Furthermore, GCB30 appeared to have higher ability to promote MSCs differentiation into osteoblast and matrix mineralization as compared to other composite scaffold as evident from higher degree of RUNX2 and osteocalcin expression on GCB30 [Figure 7.13(d)] among the all prepared scaffolds studied here. Apart from calcium and phosphate, Si^{4+} released from bioactive glass in GCB30 scaffold helped in better stimulation of MSCs into osteoblast and higher degree of bone matrix mineralization.

7.4.13 *In vivo* study

7.4.13.1 Radiological analysis

In GC scaffold, radiological plate showed partial radio dense implant placed in created defect of distal end of femur bone at 0 day. After 1 month, the material was observed within the defect with slightly reduced radio density. There was minute amount of gap between material and host bone in the created defect. At 2 and 3 months, implant was still visible with reduced radio density and negligible gap between bone and implant indicating initiation of bone formation.as shown in Figure.7.14 (a).

In GCH 30 scaffold on “0” day, the radio dense implant was visible in the distal part of femur. On 1 month, the material was observed in defect but with reduced radio density indicating initiation of new bone formation. The radiograph taken on 2 months showed further reduced radio density of implant material in substantial quantity in defect indicating in-growth of new bony tissue at the defect site. At 3 months, the implant’s radio density was comparable with the host bone indicating satisfactory healing under progress as evident from Figure.7.14 (b).

Implanted GCT 30 scaffold on “0” day showed a radio dense part as placed in the created defect of distal metaphysis of femur. At 1 month, the bony defect was observed filled with the implant material though the radio density of implant decreased subsequently than what it was on “0” day. The radiograph taken on 2 month showed reduced size and shape of implant material in defect site indicating better in-growth of new bony tissue. At 3 months, an impression of implant was visible with further reduced shape, size and radio density indicating better healing in progress, as indicated by Figure.7.14 (c).

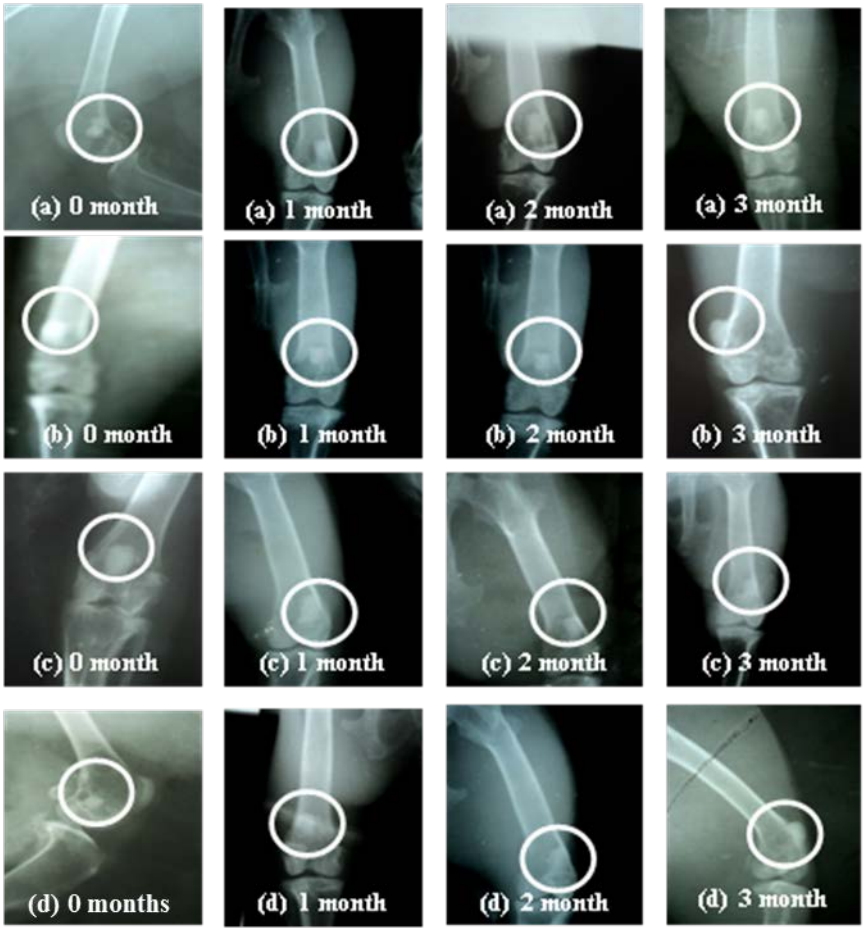

Figure.7.14. Radiograph observations at defect site, taken after 0,1,2 and 3 months post operatively (a)GC, (b)GCH 30, (c)GCB 30 and (d)GCT 30 implant.

The "0" day radiograph of bony defect of epiphyseal area implanted with GCB 30 scaffold showed round shape area packed with radio dense implant material. At 1-month radiograph showed narrowing of bony defect as well as substantially reduced radio density of implant. Subsequent radiograph was taken on 2 months showed negligible impression of implant and bony defect. The radio density in targeted area was almost comparable to the adjacent of the healthy bone indicating good stage of remodelling. At 3 months, implant was not visible indicating degradation of material *vis-a-vis* in-growth of satisfactory amount of new osseous tissue in the defect site as shown in Figure 7.14 (d).

7.4.13.2 Histological assessment

Figure.7.15 demonstrated the histological evaluation of implanted bony specimens after 1 month postoperatively, to figure out the cellular response at the host-implant interface. After 1 month, osteogenesis was not visible at GC sample and angiogenesis was lesser in amount in GC sample as compared to composite scaffold as shown in Figure.7.15 (a-d). The section of

GCH 30 sample in Figure 7.15 (b) showed well-formed bony matrix surrounded by few osteocytes, osteoblast and fibrin network with little bit of angiogenesis observed at the centre of specimen after 1 month of implantation. The angiogenesis at the certain points was well marked specially at the trabecular margin of GCT 30 sample (Figure 7.15 (c)) after 1 month.

GCB 30 sample in Figure 7.15 (d) was composed of osteoblast, osteocytes, few RBC and slight masses of fibrin and angiogenesis was visible at certain points after 1 month of implantation.

After 2 months' (Figure.7.15 a-d), mild angiogenesis was observed in GC sample. The bony trabeculae and periosteum were lined by dense fibrous tissue and mononuclear cells in GCH30 sample. GCT30 sample depicted a well formed bony structure containing numerous Haversian canals, medullary cavities and number of angiogenic points. On the other hand, GCB30 sample showed a well organised pattern of bony structure consisting of numerous bony medulla, Haversian system and bony lacunae. Moreover, the trabaculae around bony structure consisted of collagenous matrix of osseous tissue and fibrocytes.

As shown in Figure.7.15(a-d), 3 months GC sample showed a trabecular structure with proportionate amount of osteoblast, osteocyte and marginal fibrous tissue and medulla consisted of large amount of RBC, osteoblast, and fibrinous deposits. Angiogenesis was well marked almost throughout the section in GCH3 0 sample, although some medullary cavities were relatively avascular. Sufficient proliferation of osteoblast was seen in GCT 30 and GCB 30. However, in GCB 30, the peri-osseous tissues were highly vascular and composed of large masses of RBC, mononuclear cells, osteocytes and fibrinous network. The presence of osteoblastic and osteoclastic activity indicated remodelling of bone at the implanted site of GCB 30. In comparison to other samples, GCB 30 exhibited visibly higher angio proliferation with numerous Haversian system and lacunae and canalicuilar space after 3 months of in vivo study in rabbit tibia.

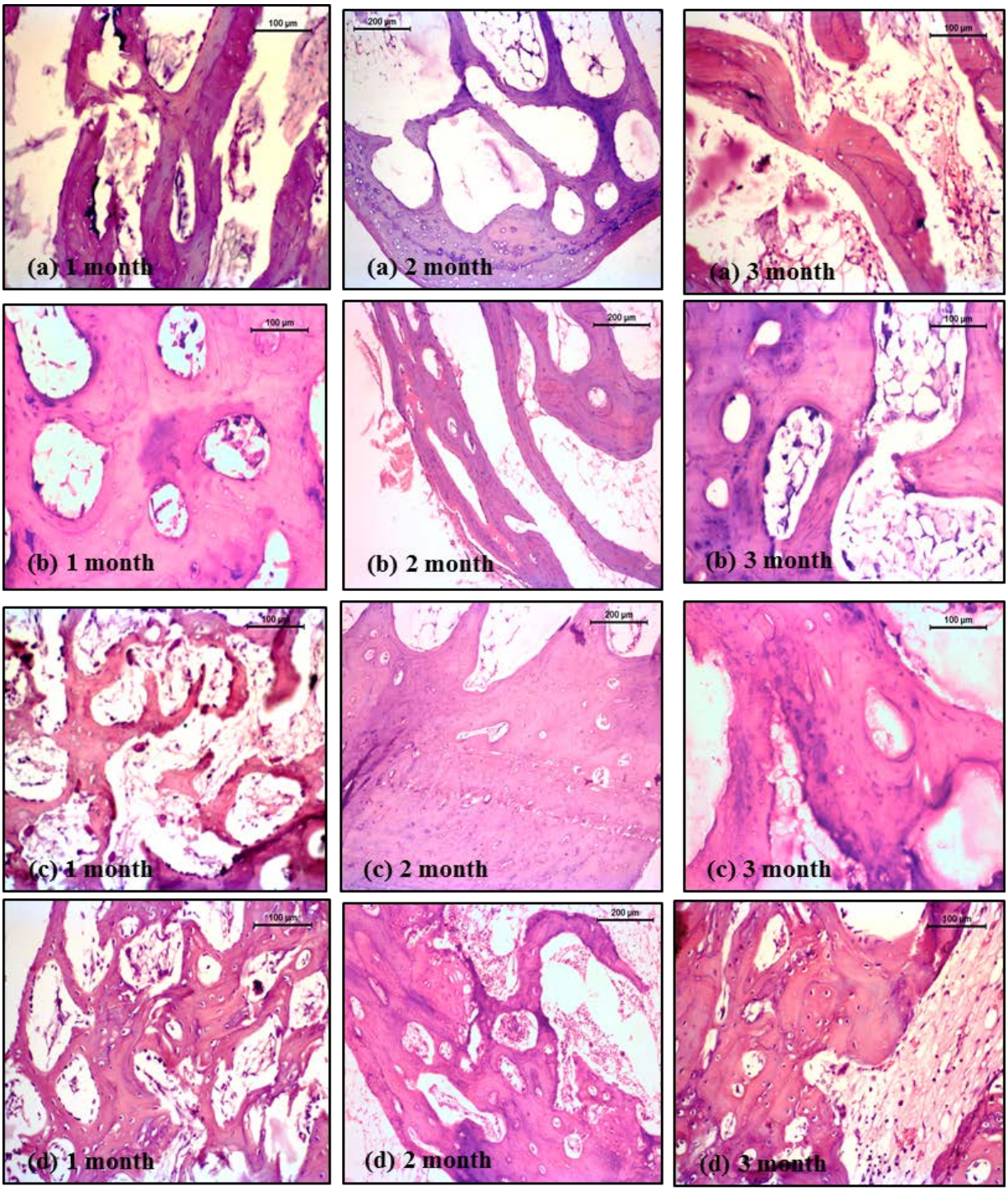

Figure.7.15. Histological sections taken after 1,2 and 3 months post-operatively implanted with (a) Control(GC), (b) GCH 30, (c) GCT 30 and (d) GCB 30 scaffolds.

7.4.13.3 Flurochrome labelling study

Under UV radiations, the oxytetracycline (OTC) labelled new bone gives characteristic bright golden yellow fluorescence while the old bone areas give deep sea green fluorescence. Figure.7.16 (a, b, c, d) exhibited the OTC labelled implanted specimens, collected after sacrificing the animals at 1,2 and 3 months. At 1 month, GCB 30 scaffold showed more.

Intense golden yellow fluorescence, compared to other three samples. As evident from Figure.7.16 (a-d) the amount of new bone formation was also higher for 2 months as compared to 1 month in all the samples. In control and GCH30 sample, the golden yellow fluorescence was observed in the centre but few patches of new bone formations could be seen in different regions of the section, both on endosteal and periosteal side after 2 months. GCT 30 and GCB 30 samples showed greater area of golden yellow fluorescence indicating more new bone formation after 2 months of implantation.

At three months, the golden yellow fluorescence in control sample was visible on few concentrated patches as in Figure.7.16 (a) that reflected the mild activity for new bone formation at the implant site. In GCH30 sample, fluorescence micrograph imparted a golden yellow fluorescence in wider zone, suggesting new bone formation was more as compared to control (GC) sample (Figure.7.16 (b)). In contrast, the implanted site of GCT 30, showed even wider regions of golden yellow fluorescence indicating rapid new bone regeneration in a particular region as shown in Figure.7.16(c). In GCB 30 sample [Figure.7.16 (d)], intensity of new bone formation was the highest as compared to other three samples although fluorescence was little patchy in nature, but throughout the section demonstrating their higher effectiveness in bone regeneration. Based on the calculation, percentage of bone formation through fluorochrome labelling images at three-time points of 1,2 and 3 months was performed and is given in Table 7.4 and compared in Figure.7.17. It is evident from Table 7.4 and Figure 7.17 that percent new bone formations at the GCB 30 implanted site was higher (*p value <0.05, ** p value < 0.05) as compared to the sites of other implanted scaffolds which is well corroborated with the in vitro bioactivity of GCB 30 scaffold in terms of MSCs attachment, proliferation and differentiation.

Table.7.5. Percentage bone formation onto composite scaffold after 1,2 and 3 months of implantation.

	1 month(%)	2 month(%)	3 month(%)
GC	16.215 ± 2.43	20.389 ± 2.72	29.643 ± 1.58
GCH 30	19.095 ± 2.61	21.351 ± 1.06	37.542 ± 3.62
GCT 30	20.895 ± 3.42	39.031 ± 3.42	62.177 ± 2.92
GCB 30	33.209 ± 2.43	43.333 ± 2.61	70.450 ± 2.63

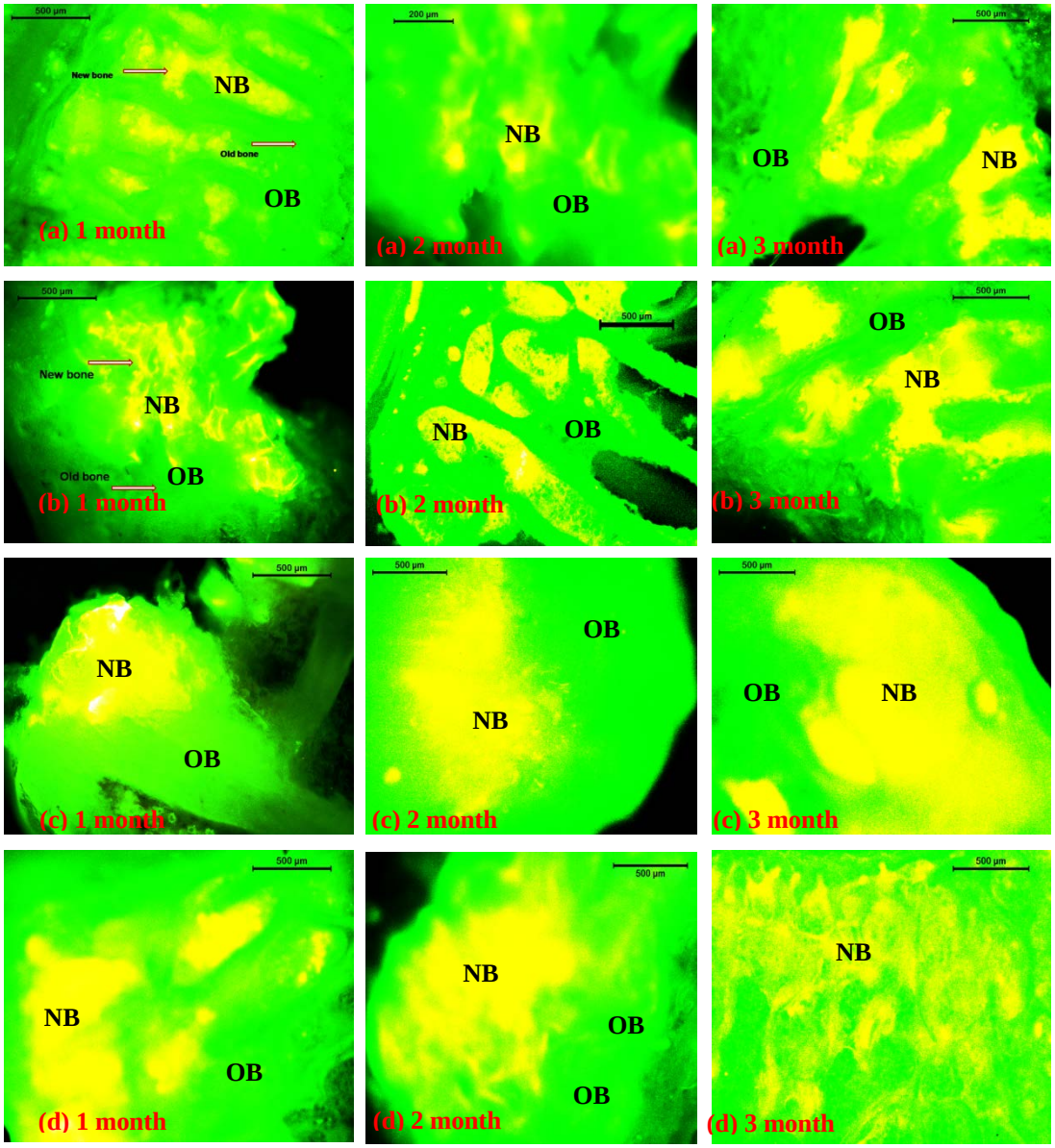

Figure.7.16. Flurochrome labelling images taken after 1,2 and 3 months post-operatively implanted in (a) GC (b) GCH 30 (c) GCT 30 (d) GCB 30 showing the golden yellow new bone and the deep sea green old bone zone.

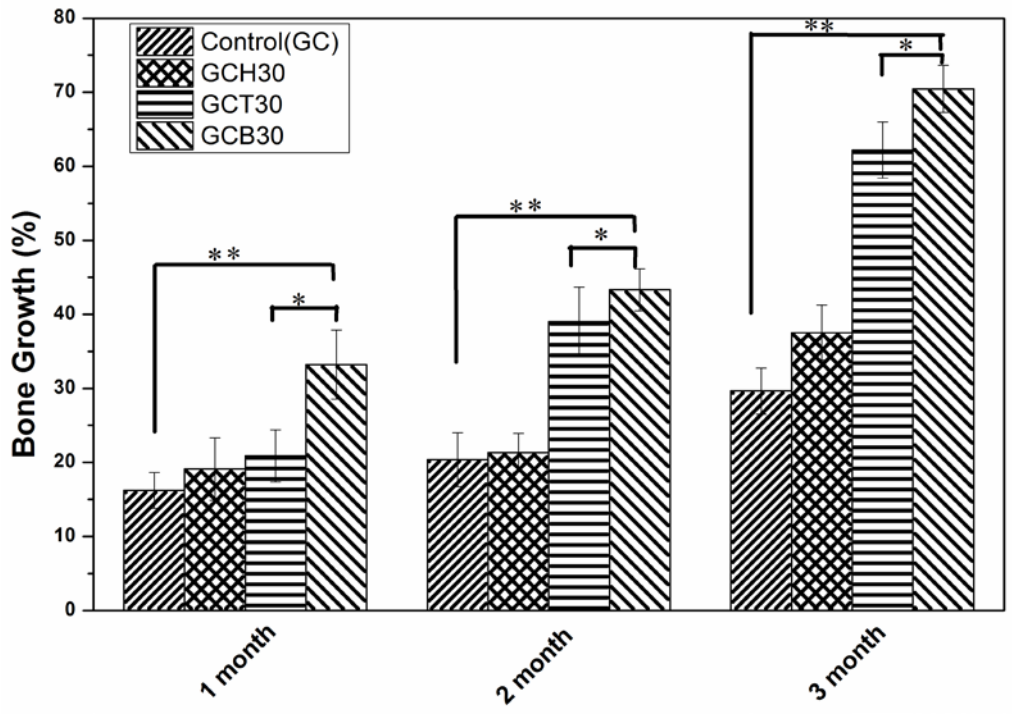

Figure.7.17. Bone ingrowth in GC, GCH 30, GCT 30 and GCB 30 composite scaffolds after 1,2 and 3 months of implantation

7.4.13.4 ESEM investigation on the implanted site of scaffolds

Figure.7.18 (a-d) exhibited ESEM micrographs of the host implant interface postoperative at 1 month and 3 months, respectively, for investigation of osseous ingrowth processes inside the scaffolds and across the interfacial regions. Figure 7.18 shows that osseous tissue growth was much higher in 3 months' samples as compared to 1-month sample irrespective of the nature of scaffold indicating good osteogenesis in all scaffolds tested here. While comparing the ESEM images of respective scaffold- bone tissue interfaces, substantial interfacial gap with little tissue growth was observed at the host–graft interface of GC implanted site in Figure.7.18 (a). In case of composite scaffolds such as GCH 30, GCT 30, GCB 30 [Figure.7.18 (b-d)], there was considerable reduction in the interfacial gap with substantial osseous ingrowth indicating superior bone mineralization and ECM formation. New bone regions were clearly observed at the interfacial zone of the implanted sites of GCH3 0, GCT 30, GCB 30 both after 1 month and 3 months postoperatively. Interfacial zone was almost collapsed in GCT 30 and GCB 30 scaffolds after 3 months of implantation indicating better osteointegration between bone and scaffolds. In figure.7.18 (d), the GCB 30 implanted site both after 1 month and 3 months postoperatively, showed densification of extra cellular bone matrix leading to strengthening of the scaffold –bone tissue interface.

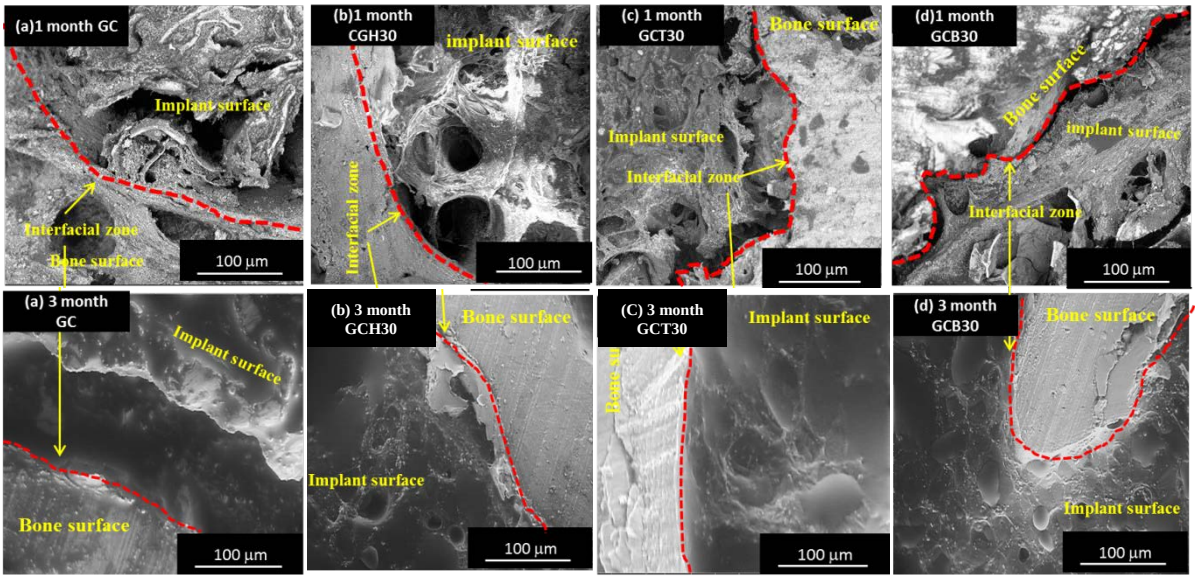

Figure.7.18. ESEM image of host implant interface in (a) GC, (b) GCH 30, (c) GCT 30 and (d) GCB 30 scaffolds post operatively after 1 month (above) and 3 months (below).

7.5 Conclusions

Gelatin and chitosan based composite scaffolds reinforced with 30 wt% HAp, β-TCP and 58s bioactive glass nanoparticles were prepared using freeze drying technique. The prepared composite scaffolds possessed high porosity varying between 75 to 83% where GCT 30 exhibited the highest average pore size of 120 µm. The protein adsorption capacity onto GCB 30 was found to be the highest. Cultured MSCs proliferated to a better extent onto GCB 30 scaffold as compared to other scaffolds. Expression of osteogenic genes was significantly enhanced on the composite scaffold as compared to neat GC scaffold. On the other hand, MSCs differentiation into osteoblast was much faster and more pronounced on GCB 30 scaffolds than on other composite scaffolds. In *in vivo* study, GCB 30 showed significantly improved bone-forming efficiency as compared to GC scaffold as well as other composite scaffolds. Bioactive 58s glass reinforced gelatin -chitosan scaffold offers a new dimension in 3D porous bioactive scaffolds with synergistically improved physicochemical and biological properties for improved bone tissue engineering.

CHAPTER # 8

Effect of Cryogenic Treatment on the Strength Retention and Biological property in GCB 30 scaffold under physiological condition

There's a way to do it better - find it.
Thomas A. Edison

Abstract

The highly porous GCB 30 scaffold was prepared through freeze drying technique. Mechanical property such as compressive strength was improved after curing it in liquid nitrogen. The compressive strength of GCB 30 scaffold was increased up to 5.5 MPa on 5 h of cryogenic treatment but decreased beyond that because of abrupt excessive internal stress and micro-cracking. From CD and FTIR analysis of amide bond in gelatin present in GCB30 scaffold, it is evident that there was no significant change in the relative content of secondary structures after cryogenic treatment, which supports insignificant denaturisation of protein structures after 5 hours of treatment in liquid nitrogen. MTT assay confirmed excellent cell attachment and growth on 5 hours cryo treated GCB 30 scaffold as compared to untreated scaffold.

8.1 Introduction

One of the main limitations of gelatin based scaffold is its strength retardation in contact with physiological fluid, primarily because of considerable solubility of gelatin in water based solution. This imparts a serious concern for gelatin based scaffold in its handling in moderately load bearing site. Though being a dehydrated derivative of collagen, gelatin shows excellent bioactivity, its poor mechanical strength under physiological condition seriously limits its application in orthopaedic sites.

Earlier there was report on enhanced crystallinity of epoxy based resin on cryogenic treatment . On this ground we may hypothized that cryo treatment of gelatin based scaffold might have an effect on increasing its crystallinity. This increase in crystallinity should have an effect in lowering the rate of dissolution of gelatin based scaffold under physiological environment, and to enhance its strength retention capability on exposure to physiological fluid. In the present work, we have performed cryogenic treatment on GCB30 after immersing it for 1h,2h,5h and 8h in liquid nitrogen chamber (Table.8.1), and studied a comparative compressive strength analysis of cryo treated and untreated GCB30 scaffold with a subsequent investigation on its degradation in PBS solution of pH 7.4 at room temperature. We have also tried to analyse the changes in conformation of gelatin secondary structure in cryo treated and untreated scaffold using FTIR and Circular dichromism study.

Table.8.1. Sample identification of GCB 30 scaffold for different treatment time with liquid nitrogen.

Sample id	Liquid N_2 treatment time (hours)
$GCB_0$30	0 hour
$GCB_2$30	2 hour
$GCB_5$30	5 hour
$GCB_8$30	8 hour

8.2 Materials and Methods

Cryogenic treatment of scaffold

The freeze dried GCB 30 scaffold sample of 12 mm in height and 5 mm in diameter was treated in liquid nitrogen at 77 K for different time duration of 2, 5, and 8 hours inside a cryo chamber. Original GCB 30 scaffold as well as liquid nitrogen treated scaffolds was further characterized using XRD, FT-IR and compressive strength analysis.

8.2.1 XRD analysis of GCB_0 30 and GCB_5 30 scaffold

X-ray diffraction analysis of GCB_0 30 and GCB_5 30 scaffold were performed with a Panalytical (USA) model operated at 40Kv and 40 mA using Cu Kα radiation. The detailed procedure was mentioned in Chapter4 in section 4.4.1.

8.2.2 FTIR analysis of GCB_0 30 and GCB_5 30 scaffold

The characteristic peaks of pure GCB_0 30 and GCB_5 30 were analysed using Fourier transform infrared (FTIR) (PerkinElmer, USA) spectroscopy. The detailed procedure was mentioned in Chapter4 in section 4.4.2.

8.2.3 Mechanical Strength analysis

Compressive strength analysis of the scaffold was performed using an universal mechanical testing machine (Instron, Tinius Olsen,UK). Cylindrical specimens with dimensions of 12 mm in height and 5 mm in diameter were used for the tests at both “Cryo treated” and “Untreated” states. Compressive strength analysis of both treated and untreated samples was performed in a dry state at 25°C. For testing mechanical behaviour of GCB_5 30 scaffold in physiological environment, the specimens were submerged in PBS for 2 days and were tested under compression *in situ* in PBS using Universal Testing Machine (UTM) at the rate of 1 mm min^{-1} at 37^oC.

8.2.4 CD analysis

Circular Dichroism (CD) spectroscopy is the most widespread technique used for estimating the secondary structures of proteins and polypeptides in solution [322]. This technique can be used to distinguish between unordered (random coil) and ordered (alpha-helix or beta-sheet) secondary structures in a protein [2,3].CD detects wavelength-dependent differences in the absorption of right and left circularly polarized light by optically active molecules such as peptides and proteins. The CD spectrum of unordered peptides is usually characterized by a positive band at 220 nm, whereas alpha-helical structures usually present a negative band at 208 nm; beta-sheet structures typically shows a negative band at 217 nm.

CD spectra were recorded using a spectrophotometer (JASCO,Model J-1500, USA) equipped with a Peltier temperature controller. Spectra were obtained from 190 to 250nm at a scanning speed of 10nm/min at 25 °C. CD data are reported as mean residue ellipticity ([Θ], degree·cm^2·$dmol^{-1}$)

8.2.5 Biodegradation study

The degradation of the GCB_0 30 and GCB_5 30 scaffolds was studied by placing them in phosphate buffer saline (PBS) at 37˚C for up to 28 days. The detailed procedure was mentioned in Chapter4 in section 4.4.12.

8.2.6 MTT analysis

Cell viability of MSCs cultured onto the GCB_0 30 and GCB_5 30 scaffolds were determined after performing [3-(4,5-dimethylthiazol-2-yl)-2,5-diphenyltetrazolium bromide] (MTT) assay. The detailed procedure was mentioned in Chapter4 in section 4.4.13.4.

8.3 Statistical Analysis

Quantitative data were presented as mean ± standard deviation (SD). The two-dimensional student t-test (T-test) was employed to obtain p values, which determined the level of significance of the data. Differences between groups were statistically significant if $p \leq 0.05$ and highly significant if $p \leq 0.01$.

8.4.Results and Discussion

8.4.1 XRD analysis of cryo-treated GCB scaffold

X-ray analysis of the GCB_0 30 and GCB_5 30 are shown in Figure. 8.1. Increase in peak intensity and decrease in the hump area from 15-35^o in $GCB_0$30 to 19-32^o in GCB_5 30 is

associated with increase in crystallinity of polymeric matrix after treatment in liquid nitrogen upto 5h.

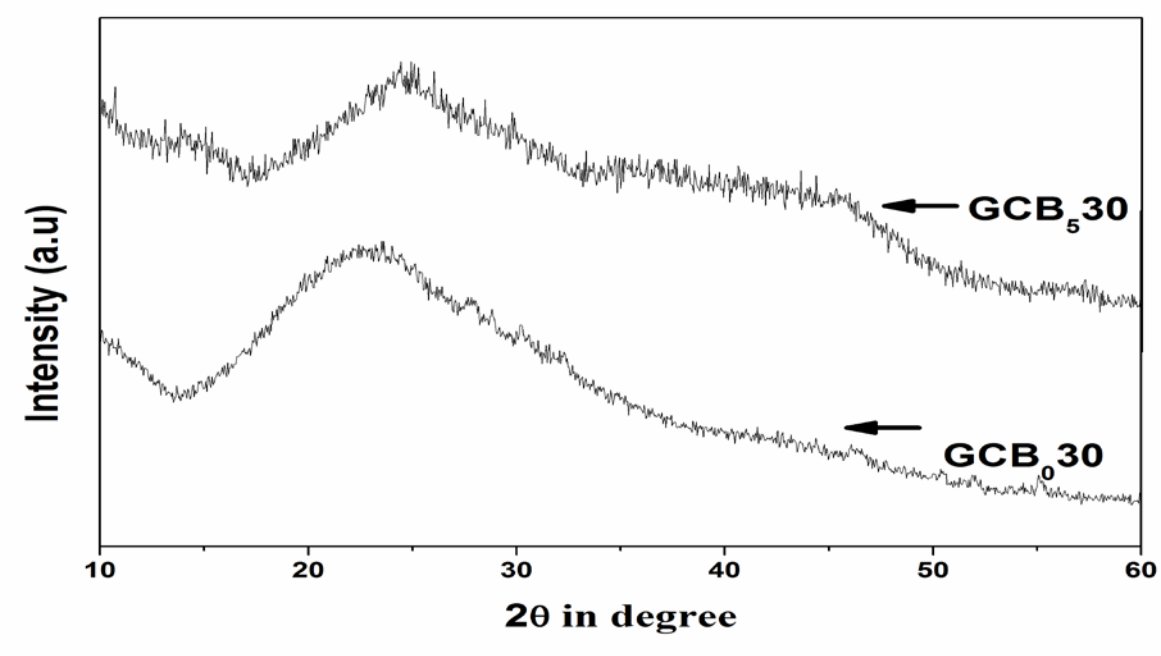

Figure.8.1. XRD analysis of untreated GCB30 and 5 hour cryo treated GCB30 scaffold.

8.4.2 FTIR analysis of cryo-treated scaffold

Figure 8.2(a) demonstrates FTIR spectra of freeze dried untreated and 5-hour liquid nitrogen treated scaffold. The absorption band at 3219cm^{-1} is associated with the characteristic stretching vibration of OH^-. The absorption bands at 1076 cm^{-1} and 661cm^{-1} describe the Si-O-Si and P-O stretching vibration of bioactive glass in GCB_0 30 scaffold [265]. The bands at 2876 cm^{-1} and 1552 cm^{-1} show the C-H stretching of gelatin and N-H stretching vibration of amide in $GCB_0$30 scaffold. However, shifting of amide bond to higher wave number from 1648 cm^{-1} in untreated scaffold to 1667 cm^{-1} in 5 hour cryo treated scaffold as well as similar shift in amine bond from 1552 cm^{-1} in untreated scaffold to 1568 cm^{-1} in $GCB_5$30 scaffold signifies strengthening of corresponding bonds in polymer matrix after cryogenic treatment. Absorption at higher wavenumber with high intensity occurs in FTIR spectra due to shorter and stronger bonds between consecutive atoms. This is because, cryogenic environment freezes the thermal oscillation of atoms, leading to shortening in C-O,C-C, C-N bonds and strengthens the hydrocarbon matrix.

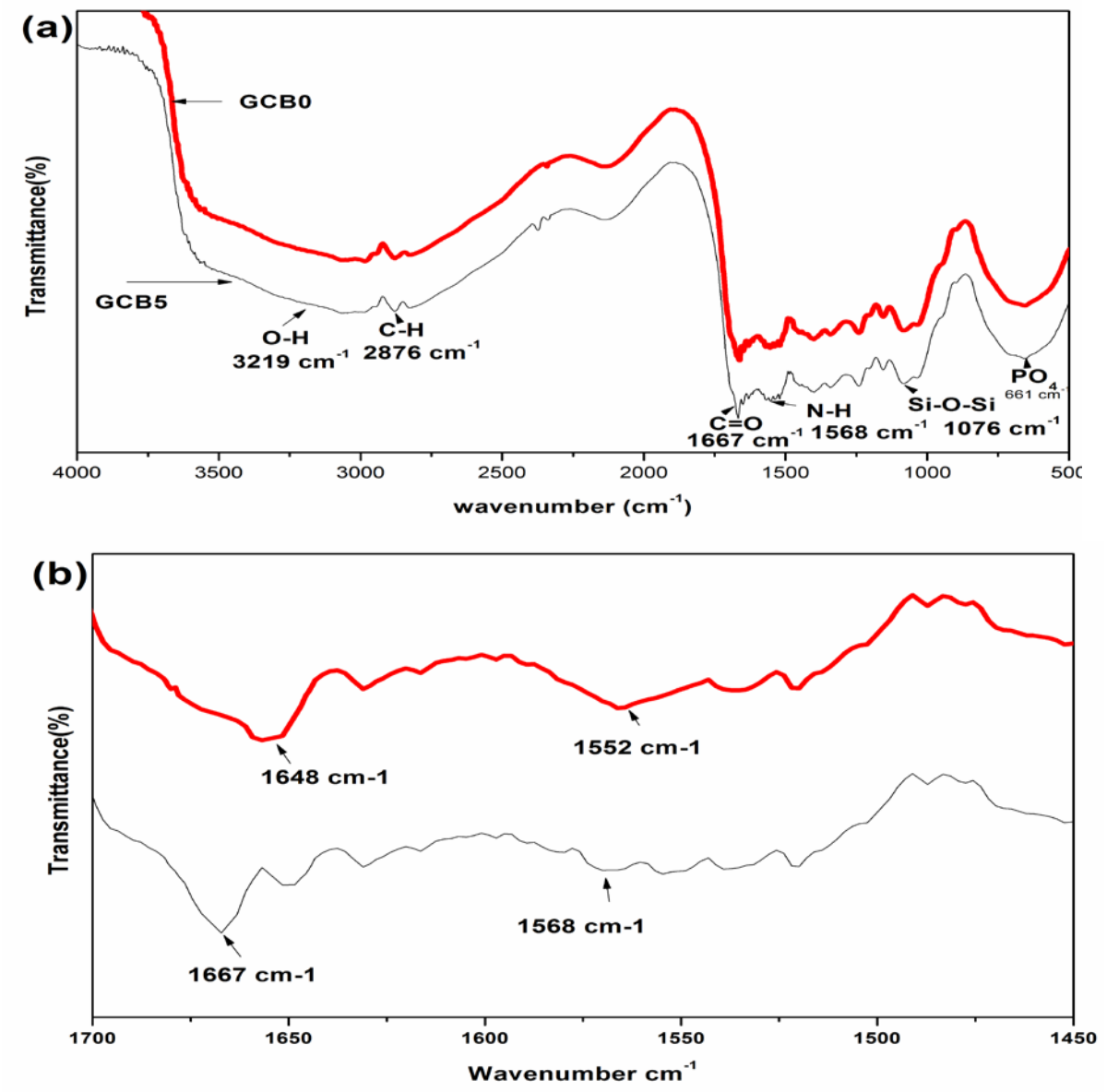

Figure.8.2. FTIR plot of (a) Freeze dried $GCB_0$30 scaffold and liquid nitrogen treated GCB_5 30 scaffold (b) shift of amide peak in $GCB_5$30 scaffold in the wave number region of 1500-1700 cm^{-1}.

8.4.3. Compressive behaviour of cryo-treated GCB scaffold

Figure 8.3 represents the characteristic stress-strain curve of original and 2, 5, 8 hours cryo-treated $GCB_5$30 scaffold under compression. The untreated GCB_0 30 scaffold exhibited a linear elastic region upto a peak stress of 2.2MPa after which a plateau region started where pore walls touched each other causing collapse of the hydrocarbon matrix. The compressive yield stress was higher (4.5 MPa) after 2h liquid nitrogen treatment, and was even higher (5.5 MPa) after 5h treatment at 77 K. Comparative data analysis shows that 5 hours cryo treated GCB_5 30 scaffold had the highest compressive strength of 5.5 MPa beyond that a gradual reduction of compressive strength was observed. The continuous increase and then decrease in compressive strength after 5 hours of liquid nitrogen treatment was due to a combination

of shortening in hydrocarbon bond length and internal stress associated with thermal conductivity mismatch at such low temperature. Micro cracking occurred in the polymer matrix due to generation of internal stress and mismatch between thermal expansion co-efficients of bioactive glass and biopolymers at 77K. This factor dominated over the strength enhancement due to shortening in hydrocarbon bond length from decrease in thermal oscillation in atoms of polymer matrix after 5 h treatment at cryogenic temperature.

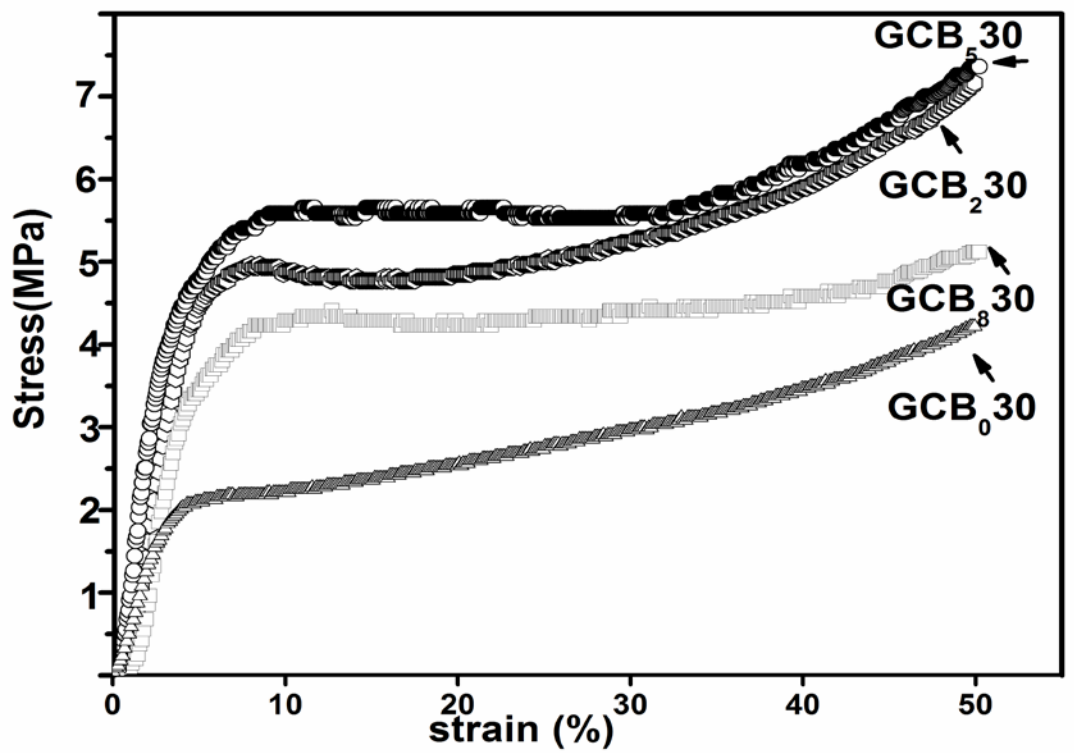

Figure 8.3. Stress -strain curve of untreated and liquid nitrogen treated scaffold for 2,5,8 hours.

8.4.4 *In vitro* biodegradability

Figure.8.4 demonstrates the bio-degradation study of $GCB_5$30 and $GCB_0$30 scaffold in PBS buffer solution at 37^{o}C and pH 7.4 up to 14 days of immersion. Weight loss percentage for untreated scaffold was significantly higher as compared to 5 hours treated scaffold at all period of immersion in PBS. The rate of degradations of GCB30 scaffolds though slower upto 5 days, enhanced after that period of immersion in PBS. The lower rate of degradation in 5 hours treated scaffold may be explained on the basis of its higher bond strength and higher capability to resist water penetration after 5 hours of treatment in liquid nitrogen.

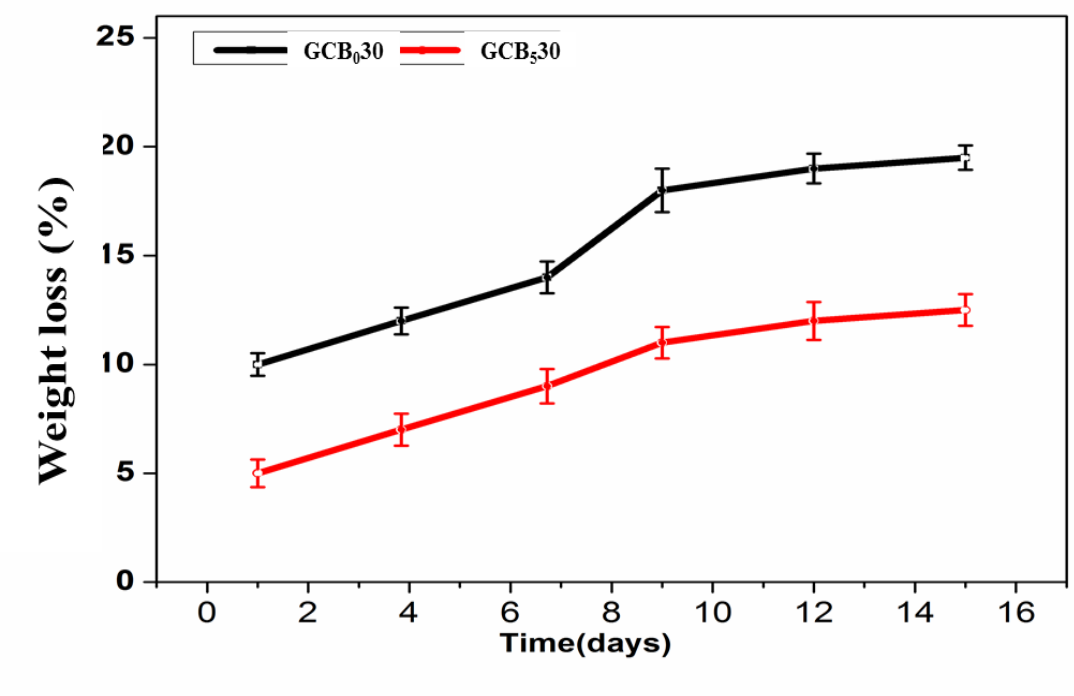

Figure.8.4. Biodegradation study of cryo-treated $GCB_5$30 and untreated $GCB_0$30 scaffold with variation in incubation time in PBS.

8.4.5 Compressive behaviour after in vitro ageing of GCB_5 30 scaffold in PBS

Since gelatin polymer is bioresorbable, degradation of the polymer occurs over time. This results in polymer matrix losing strength and stability in the implant. It is well known that, in some cases migration of water through the interface can cause spontaneous degradation [323].

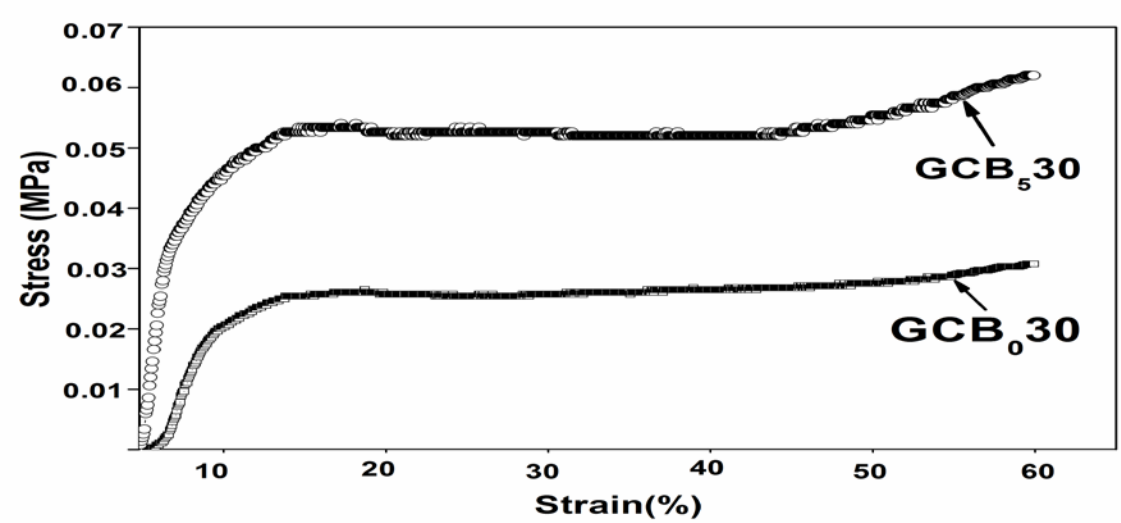

Figure.8.5. Stress-strain curves of the GCB_0 30 and GCB_5 30 after 2 days of incubation in PBS solution.

Figure.8.5 demonstrates the stress-strain curve of GCB_0 30 and GCB_5 30 scaffold immersed in PBS solution up to 2d. The result showed that for both the scaffolds the mechanical

strength decreased noticeably after 2d of ageing. However compressive strength of $GCB_{30}5$ scaffold was significantly higher than $GCB_0 30$ after ageing for 2ds in PBS. After 5 h of exposure to cryogenic environment bond strength between inorganic and organic phases was enhanced that was reflected in marked differences in the stress vs. strain curves for cryo treated and untreated scaffold. The higher compressive strength of GCB30 scaffold after 2 days of ageing in PBS might be because of its lower rate of degradation and hence lesser strength retardation in PBS solution as compared to untreated scaffold.

8.4.6. Circular Dichroism of cryo-treated gelatin protein

Figure.8.6 describes the CD spectrum of untreated and liquid nitrogen treated gelatin based scaffold for the conformational analysis of gelatin proteins, which indicates relative proportion of various secondary structures present in gelatin. Table.8.2 shows the percentage of various secondary unit (α-helix, β-turn, β-sheet and random coil) of treated and untreated sample. It indicates that there were very negligible changes in relative proportions of α-helix, β-turn, β-sheet and random coil content in secondary structure of gelatin after cryo treatment for 5 hours at 77K. It has been reported that upon complete denaturation of gelatin, the positive peak at 222 nm disappears completely while the negative band shifts to nearly 230 nm . However, our results showed that the increase in treatment time of gelatin did not cause the positive band at 222 nm to disappear, and there was negligible change in the negative elipticity in CD spectrum of gelatin in $GCB_5 30$ scaffold.

This shows that liquid nitrogen treatment brought about a very little change in conformations of secondary structure and did not change the triple helical conformation of gelatin. Maintaining the triple helical conformation of gelatin or collagen-based biomaterials during preparation is important in eliciting the desired biomedical functions of both.

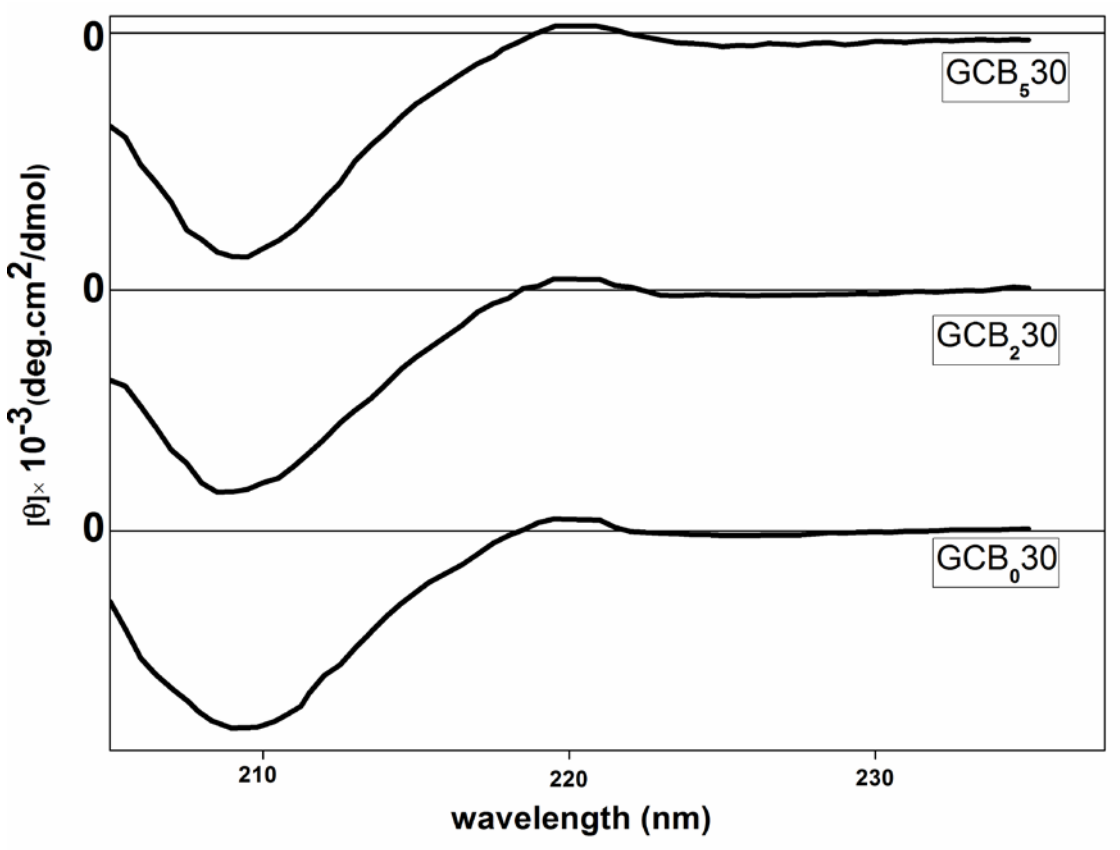

Figure.8.6. CD spectrum of GCB0 and liquid nitrogen treated (GCB_2 30,GCB_5 30) gelatin sample.

Table.8.2: Relative content of secondary structures in gelatin in $GCB_5$30, $GCB_2$30, $GCB_0$30 from CD analysis.

Secondary structure	$GCB_0$30	$GCB_2$30	$GCB_5$30
α-helix	1.9	1.2	1.6
β-sheet	23.5	20.6	19.1
β-turn	19.4	19.3	20.4
Random coil	55.2	58.9	58.9

8.4.7 Secondary structure analysis of Gelatin protein

The secondary structure of gelatin in GCB_0 30 treated with liquid nitrogen upto 5h was analysed using FTIR spectroscopy as shown in Figure 8.7. The relative content as shown in Table.8.3 after deconvoluting FTIR peak at 1600 cm^{-1} to 1700 cm^{-1} of untreated and cryo treated in liquid nitrogen for 5 hours. There was very little difference between the values

obtained from CD spectroscopy and FTIR peak deconvolution. Both from CD and FTIR data it is clear that there was minor change in secondary structure in gelatin after 5 hours of liquid nitrogen treatment of GCB30 at77 K.

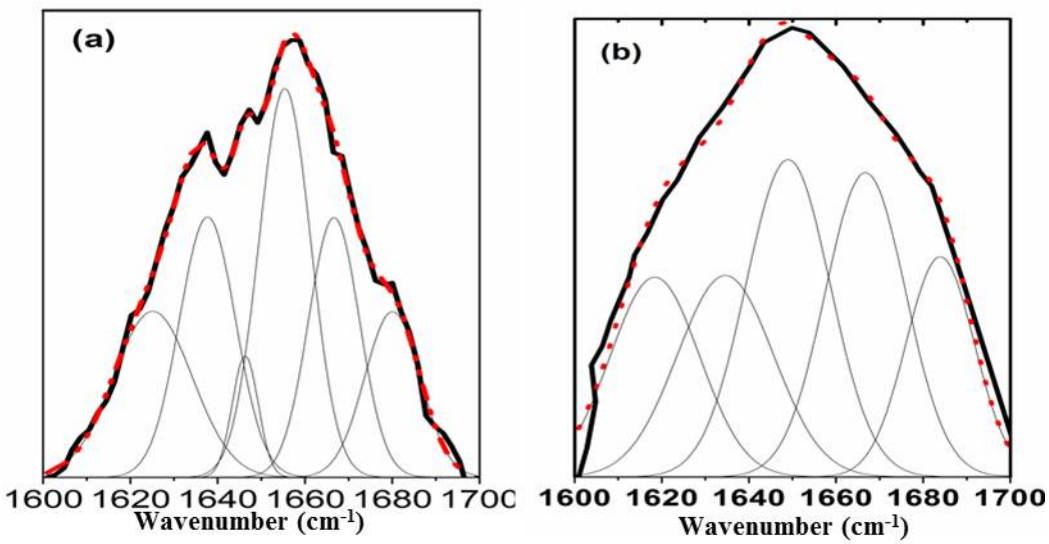

Figure.8.7. Infrared spectra of gelatin in the amide I region and their gaussian curve-fitting (a) untreated gelatin in GCB_0 30 and (b) treated gelatin in GCB_5 30 sample for 5h.

Table.8.3. Relative content of secondary structures in gelatin in $GCB_5$30 and $GCB_0$30 from FTIR analysis

Secondary structure	$GCB_0$30	$GCB_5$30
α-helix	1.8	1.7
β-sheet	25.7	23.2
β-turn	21.4	20.4
Random coil	51.1	54.7

8.4.8. MTT assay of cryo-treated GCB_5 30 scaffold

Metabolic activity of MSCs cultured onto 5 hours cryo treated and untreated $GCB_5$30 scaffold was analysed using MTT assay after 3, 5, and 7 days of cell culture using tissue culture plate with TritonX100 in cell culture media as negative control. The rate of proliferation of MSCs in both cryo treated and untreated scaffold was higher as compared to negative control. From the MTT assay it is evident that there was no significant difference ($p > 0.05$) in number of viable MSCs or MSCs density on 5 hour cryo treated and untreated GCB30 scaffold upto 7 days of culture. This signifies that proliferation ability of MSCs cultured onto GCB30 scaffold did not vary significantly after cryogenic treatment of the

scaffold upto 5 hours as shown in Figure.8.8.

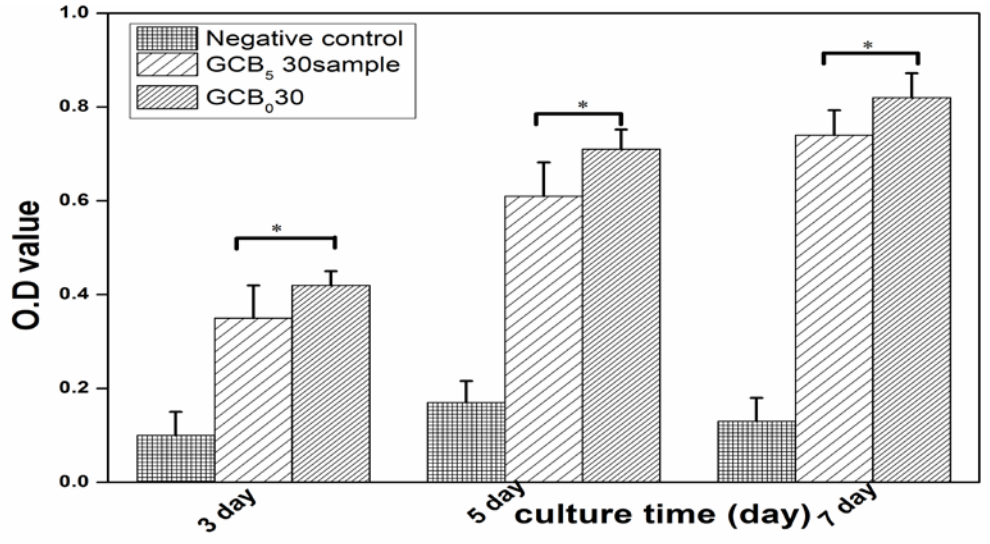

Figure.8.8. MTT assay for cell proliferation study in $GCB_0$30, $GCB_5$30 and negative control scaffold using human Mesenchymal stem cell on days 3, 7, and 14. * indicates significant difference at $p \leq 0.05$.

8.5 Conclusions

Gelatin polymer is very prone to degrade in physiological media for its strong hydrophilic nature, which is a concern for its application as bone graft. In this study, a simple method was used to enhance the mechanical property of GCB scaffold without compromising on its bioactivity and to improve its strength retention capacity in contact with physiological environment. Five hours cryo treated GCB_5 30 scaffolds developed the highest compressive strength of 5.5 MPa in comparison to its counterpart untreated GCB_0 30 scaffold. This increase in compressive strength was associated with slower degradation of GCB_5 30 scaffold in physiological medium. FTIR and CD analysis of the proteina structure present in cryo treated scaffold proved that there was hardly any change in conformations of secondary structures after 5 hours of cryo treatment. MTT assay of the cultured MSCs onto cryo treated scaffold showed that there was no significant difference in viable cell density as compared to that on untreated scaffold after 7 days of cell culture.

CHAPTER # 9

Conclusions

You just can't beat the person who never gives up.

Babe Ruth

Highly porous composite scaffolds from gelatin, chitosan biopolymer and nanoparticulates of bioactive ceramic such as hydroxyapatite, β-tricalcium phosphate, 58s bioactive glass was successfully prepared using the method lyophilisation and characterized both *in vitro* and *in vivo* for a possible biomedical application in reconstructing musculoskeletal disorder in human system. First, GCH scaffolds with varying compositions were prepared and optimization of phase composition in scaffold was performed after measuring their physicochemical and mechanical properties. HAp- chitosan nanoparticles in different weight ratios were synthesized in situ and used for the fabrication of GCH scaffolds. GCH scaffolds having gelatin content fixed at 30 wt% and HAp content ≤ 28 wt% were found to possess desirable pore size distribution for scaffolds to exhibit osteoinduction. With increase in HAp-chi nanoparticulate contents in the prepared GCH scaffolds, average pore size in the scaffold found to decrease. GCH 30 scaffold with a phase composition of (gel:chi:HAp) 30: 42: 28 showed an optimum pore size distribution between 75-110 μm with high degree of interconnected porosity and maximum mechanical strength of 3.46 MPa. HAp phase content in the scaffold greater than 30 wt% led to a decrease in compressive strength due to agglomeration of ceramic particulate as well as non-homogeneous phase distribution in the scaffold. On the other hand, gelatin content greater than 30 wt% in the scaffold showed a decrease in average pore diameter below 75 μm which is not optimum for bone cell ingrowth and exhibition of osteoinduction by the scaffold. GCH scaffolds showed an increase in compressive strength compared to neat GC scaffold because of reinforcement from nanoparticulate HAp with varying composition from 10-30wt%. β-TCP and 58S bioactive glass based scaffold was thus studied using a phase composition of gelatin fixed at 30 wt% and varying the bioactive ceramic phase content from 10-30 wt.%. With increase in bioceramic phase content from 10-30 wt%, compressive strengths of all the prepared scaffolds increased. In general, with increasing bioactive ceramic phase content from 10-30 wt%, bioactivity of the scaffold increased which was evident from MTT assay, confocal microscopic images for RUNX2 osteocalcin expressions from cultured MSCs onto the scaffolds.

Thus, physicochemical, mechanical and biological properties of the scaffolds were studied and compared after preparing scaffolds from 30 wt% of nano bioceramic content. GCH 30 showed the maximum compressive strength of 3.46 MPa while a lowest average compressive strength of 2.2MPa was recorded for GCB 30 scaffolds. Most frequent pore size of GCT 30 was the highest of 120 μm whereas that for GCH 30 was the lowest of 94 μm

among 30 wt% bioceramic based scaffolds. GCB 30 scaffold showed the highest protein adsorption capacity of 24mg/cm^3 and a lowest of 19mg/cm^3 exhibited by GCH 30 primarily because of higher proportion of exposed hydrophilic sites in GCB 30 scaffold compared to GCT 30 and GCH 30. The rate of biodegradation did not vary in a significant manner with change in bioceramic phase content at 30 wt%, but certainly all GCB 30, GCT 30, GCH 30 scaffolds showed a lower rate of biodegradation as compared to neat GC scaffold. Higher extent of expression of osteoblast differentiation marker genes such as osteocalcin, RUNX2 were identified after 1,7, and 14 days of MSC's culture onto GCB 30, GCT 30 and GCH 30 scaffolds as compared to neat GC scaffold. All the composite scaffolds exhibited higher capacity in differentiating MSCs into osteoblast as compared to neat gelatin-chitosan scaffold. Moreover, MSCs cultured onto GCB 30 produced higher level of osteocalcin expression than that onto GCT30 and GCH 30 upto 14 days demonstrating higher efficiency of GCB 30 in differentiating MSCs into osteoblast. The result from rtPCR analysis of the cell cultured scaffold clearly demonstrated that the expression level of both OPN and OCN in hMSC's cultured on GCB 30 scaffolds were higher than that on GCT 30 and GCH 30 scaffold after 14 days of culture. As a whole, GCB 30 appeared to be a better scaffold to differentiate MSCs into osteoblast within shorter time period.

Histology study on GCB 30, GCH 30, GC T30 scaffold implanted in rabbit tibia for 1 month demonstrated a well organised bony plate characterised by formation of a clusters of bony osteoblast, osteoclast, and numerous osteocytes. Angiogenesis was visible at certain points at the centre of the bony plate in implanted sites of all the scaffolds. All the GCH 30, GCT 30 and GC B30 scaffolds, as well as neat GC scaffold showed considerable ability of new bone formation after 3 months of implantation in rabbit tibia. Based on the histological, radiological and flurochrome labelling results, 58s bioactive glass reinforced GCB30 scaffold showed higher efficiency in enhanced early-stage bone formation at the defect site of rabbit tibia as compared to other scaffolds.

Cryo treatment on GCB 30 scaffold using liquid nitrogen was carried out to increase its compressive strength and improve its strength retention capability in physiological environment. Five hours of liquid nitrogen treatment to GCB 30 proved to be effective in increasing the compressive strength of GCB30 up to 5.6 MPa with improved strength retention capability in PBS solution up to 2 days. MTT assay of cryo treated GCB 30 scaffold exhibited no significant difference in cell proliferation up to 14 days of cell culture.

References

1. Hench, L.L., *Bioceramics: from concept to clinic.* Journal of the American Ceramic Society, 1991. **74**(7): p. 1487-1510.
2. Kruger, J.M., et al., *Cost-effectiveness of the arthritis self-help course.* Archives of Internal Medicine, 1998. **158**(11): p. 1245-1249.
3. Arya, V., et al., *Vitamin D status and its relationship with bone mineral density in healthy Asian Indians.* Osteoporosis international, 2004. **15**(1): p. 56-61.
4. Mithal, A., et al., *The Asia-pacific regional audit-epidemiology, costs, and burden of osteoporosis in India 2013: a report of international osteoporosis foundation.* Indian journal of endocrinology and metabolism, 2014. **18**(4): p. 449.
5. Nymark, T., et al., *Short time-frame from first to second hip fracture in the Funen County Hip Fracture Study.* Osteoporosis international, 2006. **17**(9): p. 1353-1357.
6. Sundelacruz, S. and D.L. Kaplan. *Stem cell-and scaffold-based tissue engineering approaches to osteochondral regenerative medicine*. in *Seminars in cell & developmental biology*. 2009. Elsevier.
7. Cancedda, R., P. Giannoni, and M. Mastrogiacomo, *A tissue engineering approach to bone repair in large animal models and in clinical practice.* Biomaterials, 2007. **28**(29): p. 4240-4250.
8. Griffith, L.G. and G. Naughton, *Tissue engineering--current challenges and expanding opportunities.* Science, 2002. **295**(5557): p. 1009-1014.
9. Cancedda, R., et al., *Tissue engineering and cell therapy of cartilage and bone.* Matrix Biology, 2003. **22**(1): p. 81-91.
10. Discher, D.E., P. Janmey, and Y.-l. Wang, *Tissue cells feel and respond to the stiffness of their substrate.* Science, 2005. **310**(5751): p. 1139-1143.
11. Bruder, S.P. and B.S. Fox, *Tissue Engineering of Bone: Cell Based Strategies.* Clinical orthopaedics and related research, 1999. **367**: p. S68-S83.
12. Schantz, J.-T., et al., *Repair of calvarial defects with customised tissue-engineered bone grafts II. Evaluation of cellular efficiency and efficacy in vivo.* Tissue engineering, 2003. **9**(4, Supplement 1): p. 127-139.
13. De Boer, R., et al., *Rat sciatic nerve repair with a poly-lactic-co-glycolic acid scaffold and nerve growth factor releasing microspheres.* Microsurgery, 2011. **31**(4): p. 293-302.
14. Whitaker, M., et al., *Growth factor release from tissue engineering scaffolds.* Journal of Pharmacy and Pharmacology, 2001. **53**(11): p. 1427-1437.
15. Dankers, P.Y., et al., *A modular and supramolecular approach to bioactive scaffolds for tissue engineering.* Nature materials, 2005. **4**(7): p. 568-574.
16. Weng, J., M. Wang, and J. Chen, *Plasma-sprayed calcium phosphate particles with high bioactivity and their use in bioactive scaffolds.* Biomaterials, 2002. **23**(13): p. 2623-2629.
17. Stock, U.A. and J.P. Vacanti, *Tissue engineering: current state and prospects.* Annual review of medicine, 2001. **52**(1): p. 443-451.
18. Shi, S. and S. Gronthos, *Perivascular niche of postnatal mesenchymal stem cells in human bone marrow and dental pulp.* Journal of bone and mineral research, 2003. **18**(4): p. 696-704.
19. Nguyen, L.H., et al., *Vascularized bone tissue engineering: approaches for potential improvement.* Tissue Engineering Part B: Reviews, 2012. **18**(5): p. 363-382.
20. Engh, G.A., P.J. Herzwurm, and N.L. Parks, *Treatment of major defects of bone with bulk allografts and stemmed components during total knee arthroplasty.* J Bone Joint Surg Am, 1997. **79**(7): p. 1030-9.
21. Younger, E.M. and M.W. Chapman, *Morbidity at bone graft donor sites.* Journal of orthopaedic trauma, 1989. **3**(3): p. 192-195.
22. Buckwalter, J. and H. Mankin, *Instructional Course Lectures, The American Academy of Orthopaedic Surgeons-Articular Cartilage. Part I: Tissue Design and Chondrocyte-Matrix Interactions*†.* J Bone Joint Surg Am, 1997. **79**(4): p. 600-11.
23. Clarke, B., *Normal bone anatomy and physiology.* Clinical journal of the American Society of Nephrology, 2008. **3**(Supplement 3): p. S131-S139.
24. CARTER, D.R. and D.M. Spengler, *Mechanical properties and composition of cortical bone.* Clinical orthopaedics and related research, 1978. **135**: p. 192-217.
25. Taicher, G.Z., et al., *Quantitative magnetic resonance (QMR) method for bone and whole-body-composition analysis.* Analytical and bioanalytical chemistry, 2003. **377**(6): p. 990-1002.
26. Buckwalter, J., et al., *Bone biology.* J Bone Joint Surg Am, 1995. **77**(8): p. 1256-1275.
27. Rho, J.-Y., L. Kuhn-Spearing, and P. Zioupos, *Mechanical properties and the hierarchical structure of bone.* Medical engineering & physics, 1998. **20**(2): p. 92-102.

28. Eriksen, E.F., et al., *Evidence of estrogen receptors in normal human osteoblast-like cells.* Science, 1988. **241**(4861): p. 84-86.
29. Baiotto, S. and M. Zidi, *Theoretical and numerical study of a bone remodeling model: the effect of osteocyte cells distribution.* Biomechanics and modeling in mechanobiology, 2004. **3**(1): p. 6-16.
30. Detsch, R., H. Mayr, and G. Ziegler, *Formation of osteoclast-like cells on HA and TCP ceramics.* Acta biomaterialia, 2008. **4**(1): p. 139-148.
31. Friedenstein, A., I. Piatetzky-Shapiro, and K. Petrakova, *Osteogenesis in transplants of bone marrow cells.* Development, 1966. **16**(3): p. 381-390.
32. Fratzl, P., et al., *Structure and mechanical quality of the collagen–mineral nano-composite in bone.* Journal of materials chemistry, 2004. **14**(14): p. 2115-2123.
33. Bonfield, W. and P. Datta, *Young's modulus of compact bone.* Journal of biomechanics, 1974. **7**(2): p. 147-149.
34. Ashman, R.B. and J.Y. Rho, *Elastic modulus of trabecular bone material.* Journal of biomechanics, 1988. **21**(3): p. 177-181.
35. Anderson, C.H., et al., *The mechanism of bone induction and bone healing by human osteosarcoma cell extracts.* Clinical orthopaedics and related research, 1995. **313**: p. 129-134.
36. Remedios, A., *Bone and bone healing.* Veterinary clinics of North America: small animal practice, 1999. **29**(5): p. 1029-1044.
37. Callejo, J., et al., *Long-term ovarian function evaluation after autografting by implantation with fresh and frozen-thawed human ovarian tissue.* The Journal of Clinical Endocrinology & Metabolism, 2001. **86**(9): p. 4489-4494.
38. Messerli, D., et al., *Multipiece allograft implant*. 2009, Google Patents.
39. Finkemeier, C.G., *Bone-grafting and bone-graft substitutes.* J Bone Joint Surg Am, 2002. **84**(3): p. 454-464.
40. Lam, J.S., O. Shvarts, and A.J. Pantuck, *Changing concepts in the surgical management of renal cell carcinoma.* European urology, 2004. **45**(6): p. 692-705.
41. Kelly, C.M., et al., *The use of a surgical grade calcium sulfate as a bone graft substitute: results of a multicenter trial.* Clinical orthopaedics and related research, 2001. **382**: p. 42-50.
42. Niinomi, M., *Recent metallic materials for biomedical applications.* Metallurgical and materials transactions A, 2002. **33**(3): p. 477-486.
43. LeGeros, R.Z., *Calcium phosphate-based osteoinductive materials.* Chemical reviews, 2008. **108**(11): p. 4742-4753.
44. Venugopal, J., et al., *Mineralization of osteoblasts with electrospun collagen/hydroxyapatite nanofibers.* Journal of Materials Science: Materials in Medicine, 2008. **19**(5): p. 2039-2046.
45. Cao, W. and L.L. Hench, *Bioactive materials.* Ceramics international, 1996. **22**(6): p. 493-507.
46. Törmälä, P., T. Pohjonen, and P. Rokkanen, *Bioabsorbable polymers: materials technology and surgical applications.* Proceedings of the Institution of Mechanical Engineers, Part H: Journal of Engineering in Medicine, 1998. **212**(2): p. 101-111.
47. Bergsma, J., et al., *Late degradation tissue response to poly (L-lactide) bone plates and screws.* Biomaterials, 1995. **16**(1): p. 25-31.
48. Schaldach, I.M., *Materials in Pacemaker Technology*, in *Electrotherapy of the Heart*. 1992, Springer. p. 169-190.
49. NakaNo, T., *Mechanical properties of metallic biomaterials.* Metals for Biomedical Devices, 2010: p. 71.
50. Huiskes, R., H. Weinans, and B. Van Rietbergen, *The relationship between stress shielding and bone resorption around total hip stems and the effects of flexible materials.* Clinical orthopaedics and related research, 1992. **274**: p. 124-134.
51. Wu, S., et al., *A biomimetic hierarchical scaffold: natural growth of nanotitanates on three-dimensional microporous Ti-based metals.* Nano letters, 2008. **8**(11): p. 3803-3808.
52. Katti, K.S., *Biomaterials in total joint replacement.* Colloids and Surfaces B: Biointerfaces, 2004. **39**(3): p. 133-142.
53. Best, S., et al., *Bioceramics: past, present and for the future.* Journal of the European Ceramic Society, 2008. **28**(7): p. 1319-1327.
54. Jarcho, M., *Calcium phosphate ceramics as hard tissue prosthetics.* Clinical orthopaedics and related research, 1981. **157**: p. 259-278.
55. Selvig, K.A., *The crystal structure of hydroxyapatite in dental enamel as seen with the electron microscope.* Journal of ultrastructure research, 1972. **41**(3): p. 369-375.
56. Kay, M.I., R. Young, and A. Posner, *Crystal structure of hydroxyapatite.* Nature, 1964. **204**: p. 1050.

57. Kamitakahara, M., C. Ohtsuki, and T. Miyazaki, *Review paper: behavior of ceramic biomaterials derived from tricalcium phosphate in physiological condition.* Journal of biomaterials applications, 2008. **23**(3): p. 197-212.
58. Descamps, M., J. Hornez, and A. Leriche, *Effects of powder stoichiometry on the sintering of β-tricalcium phosphate.* Journal of the European Ceramic Society, 2007. **27**(6): p. 2401-2406.
59. Martinez, I., P. Velasquez, and P. De Aza, *Synthesis and stability of α-tricalcium phosphate doped with dicalcium silicate in the system Ca 3 (PO 4) 2–Ca 2 SiO 4.* Materials Characterization, 2010. **61**(7): p. 761-767.
60. Dickens, G.R., M.M. Castillo, and J.C. Walker, *A blast of gas in the latest Paleocene: Simulating first-order effects of massive dissociation of oceanic methane hydrate.* Geology, 1997. **25**(3): p. 259-262.
61. Dickens, B., L. Schroeder, and W. Brown, *Crystallographic studies of the role of Mg as a stabilizing impurity in β-Ca3 (PO4) 2. The crystal structure of pure β-Ca3 (PO4) 2.* Journal of Solid State Chemistry, 1974. **10**(3): p. 232-248.
62. Kannan, S., et al., *Synthesis and structural characterization of strontium-and magnesium-co-substituted β-tricalcium phosphate.* Acta Biomaterialia, 2010. **6**(2): p. 571-576.
63. De Aza, A., et al., *Crack growth resistance of alumina, zirconia and zirconia toughened alumina ceramics for joint prostheses.* Biomaterials, 2002. **23**(3): p. 937-945.
64. Mah, T., T. Parthasarathy, and L. Matson. *Processing and mechanical properties of Al2O3/Y3Al5O12 (YAG) eutectic composite.* in *14th Annual Conference on Composites and Advanced Ceramic Materials, Part 2 of 2: Ceramic Engineering and Science Proceedings, Volume 11, Issue 9/10*. 1990. Wiley Online Library.
65. SWAIN, M. and L. HE, *Mechanical properties of bioceramics.* Bioceramics and their Clinical Applications, 2008: p. 78.
66. Karageorgiou, V. and D. Kaplan, *Porosity of 3D biomaterial scaffolds and osteogenesis.* Biomaterials, 2005. **26**(27): p. 5474-5491.
67. Ducheyne, P. and Q. Qiu, *Bioactive ceramics: the effect of surface reactivity on bone formation and bone cell function.* Biomaterials, 1999. **20**(23): p. 2287-2303.
68. Kokubo, T., et al., *Solutions able to reproduce in vivo surface-structure changes in bioactive glass-ceramic A-W3.* Journal of biomedical materials research, 1990. **24**(6): p. 721-734.
69. Burg, K.J., S. Porter, and J.F. Kellam, *Biomaterial developments for bone tissue engineering.* Biomaterials, 2000. **21**(23): p. 2347-2359.
70. Rasal, R.M., A.V. Janorkar, and D.E. Hirt, *Poly (lactic acid) modifications.* Progress in polymer science, 2010. **35**(3): p. 338-356.
71. Hubbell, J.A., *Biomaterials in tissue engineering.* Bio/technology (Nature Publishing Company), 1995. **13**(6): p. 565-576.
72. Weadock, K., R.M. Olson, and F.H. Silver, *Evaluation of collagen crosslinking techniques.* Biomaterials, medical devices, and artificial organs, 1983. **11**(4): p. 293-318.
73. García-Valdez, O., et al., *Grafting of Chitosan with Styrene and Maleic Anhydride via Nitroxide-Mediated Radical Polymerization in Supercritical Carbon Dioxide.* Macromolecular Chemistry and Physics, 2013. **214**(12): p. 1396-1404.
74. Sashiwa, H. and S.-i. Aiba, *Chemically modified chitin and chitosan as biomaterials.* Progress in Polymer Science, 2004. **29**(9): p. 887-908.
75. Pal, K., A. Banthia, and D. Majumdar, *Polyvinyl alcohol—gelatin patches of salicylic acid: preparation, characterization and drug release studies.* Journal of biomaterials applications, 2006. **21**(1): p. 75-91.
76. Ashby, M.F. and R.M. Medalist, *The mechanical properties of cellular solids.* Metallurgical Transactions A, 1983. **14**(9): p. 1755-1769.
77. Mark, J.E., *Physical properties of polymers handbook.* Vol. 1076. 2007: Springer.
78. Buchman, A., et al., *Medical implants made of wear-resistant, high-performance polyimides, process of making same and medical use of same*. 2004, Google Patents.
79. Schmid, J., et al., *Membrane permeability is unnecessary for guided generation of new bone. An experimental study in the rabbit.* Clinical Oral Implants Research, 1994. **5**(3): p. 125-130.
80. Middleton, J.C. and A.J. Tipton, *Synthetic biodegradable polymers as orthopedic devices.* Biomaterials, 2000. **21**(23): p. 2335-2346.
81. Baksh, D., L. Song, and R. Tuan, *Adult mesenchymal stem cells: characterization, differentiation, and application in cell and gene therapy.* Journal of cellular and molecular medicine, 2004. **8**(3): p. 301-316.
82. Kern, S., et al., *Comparative analysis of mesenchymal stem cells from bone marrow, umbilical cord blood, or adipose tissue.* Stem cells, 2006. **24**(5): p. 1294-1301.

83. Dani, C., et al., *Differentiation of embryonic stem cells into adipocytes in vitro.* Journal of cell science, 1997. **110**(11): p. 1279-1285.
84. Alison, M.R., et al., *Cell differentiation: hepatocytes from non-hepatic adult stem cells.* Nature, 2000. **406**: p. 257.
85. Pittenger, M.F., et al., *Multilineage potential of adult human mesenchymal stem cells.* science, 1999. **284**(5411): p. 143-147.
86. Meregalli, M., A. Farini, and Y. Torrente, *Mesenchymal stem cells as muscle reservoir.* Journal of Stem Cell Research & Therapy, 2012. **2011**.
87. Hollister, S.J., *Porous scaffold design for tissue engineering.* Nature materials, 2005. **4**(7): p. 518-524.
88. Hing, K.A., *Bioceramic bone graft substitutes: influence of porosity and chemistry.* International journal of applied ceramic technology, 2005. **2**(3): p. 184-199.
89. Harley, B.A. and L.J. Gibson, *In vivo and in vitro applications of collagen-GAG scaffolds.* Chemical Engineering Journal, 2008. **137**(1): p. 102-121.
90. Yeong, W.-Y., et al., *Rapid prototyping in tissue engineering: challenges and potential.* Trends in biotechnology, 2004. **22**(12): p. 643-652.
91. Liao, C.J., et al., *Fabrication of porous biodegradable polymer scaffolds using a solvent merging/particulate leaching method.* Journal of biomedical materials research, 2002. **59**(4): p. 676-681.
92. Harris, L.D., B.-S. Kim, and D.J. Mooney, *Open pore biodegradable matrices formed with gas foaming.* Journal of biomedical materials research, 1998. **42**(3): p. 396-402.
93. Mooney, S., *Bioinformatics approaches and resources for single nucleotide polymorphism functional analysis.* Briefings in bioinformatics, 2005. **6**(1): p. 44-56.
94. Wang, W., *Lyophilization and development of solid protein pharmaceuticals.* International journal of pharmaceutics, 2000. **203**(1): p. 1-60.
95. Lloyd, D.R., K.E. Kinzer, and H. Tseng, *Microporous membrane formation via thermally induced phase separation. I. Solid-liquid phase separation.* Journal of Membrane Science, 1990. **52**(3): p. 239-261.
96. Hua, F.J., T.G. Park, and D.S. Lee, *A facile preparation of highly interconnected macroporous poly (D, L-lactic acid-co-glycolic acid)(PLGA) scaffolds by liquid–liquid phase separation of a PLGA–dioxane–water ternary system.* Polymer, 2003. **44**(6): p. 1911-1920.
97. Zeugolis, D.I., et al., *Electro-spinning of pure collagen nano-fibres–just an expensive way to make gelatin?* Biomaterials, 2008. **29**(15): p. 2293-2305.
98. Billiet, T., et al., *A review of trends and limitations in hydrogel-rapid prototyping for tissue engineering.* Biomaterials, 2012. **33**(26): p. 6020-6041.
99. Leong, K., C. Cheah, and C. Chua, *Solid freeform fabrication of three-dimensional scaffolds for engineering replacement tissues and organs.* Biomaterials, 2003. **24**(13): p. 2363-2378.
100. Lee, S.-J., et al., *Development of a scaffold fabrication system using an axiomatic approach.* Journal of Micromechanics and Microengineering, 2006. **17**(1): p. 147.
101. Nam, Y.S. and T.G. Park, *Biodegradable polymeric microcellular foams by modified thermally induced phase separation method.* Biomaterials, 1999. **20**(19): p. 1783-1790.
102. Sin, D., et al., *Polyurethane (PU) scaffolds prepared by solvent casting/particulate leaching (SCPL) combined with centrifugation.* Materials Science and Engineering: C, 2010. **30**(1): p. 78-85.
103. Hutmacher, D.W., M. Sittinger, and M.V. Risbud, *Scaffold-based tissue engineering: rationale for computer-aided design and solid free-form fabrication systems.* TRENDS in Biotechnology, 2004. **22**(7): p. 354-362.
104. Jiang, T., W.I. Abdel-Fattah, and C.T. Laurencin, *In vitro evaluation of chitosan/poly (lactic acid-glycolic acid) sintered microsphere scaffolds for bone tissue engineering.* Biomaterials, 2006. **27**(28): p. 4894-4903.
105. Dupont, K.M., et al., *Synthetic scaffold coating with adeno-associated virus encoding BMP2 to promote endogenous bone repair.* Cell and tissue research, 2012. **347**(3): p. 575-588.
106. Venugopal, J., et al., *Interaction of cells and nanofiber scaffolds in tissue engineering.* Journal of Biomedical Materials Research Part B: Applied Biomaterials, 2008. **84**(1): p. 34-48.
107. Bundela, H. and A. Bajpai, *Designing of hydroxyapatite-gelatin based porous matrix as bone substitute: Correlation with biocompatibility aspects.* Express Polym Lett, 2008. **2**: p. 201-213.
108. Murphy, C.M., M.G. Haugh, and F.J. O'Brien, *The effect of mean pore size on cell attachment, proliferation and migration in collagen–glycosaminoglycan scaffolds for bone tissue engineering.* Biomaterials, 2010. **31**(3): p. 461-466.
109. Loh, Q.L. and C. Choong, *Three-dimensional scaffolds for tissue engineering applications: role of porosity and pore size.* Tissue Engineering Part B: Reviews, 2013. **19**(6): p. 485-502.

110. Kuboki, Y., Q. Jin, and H. Takita, *Geometry of carriers controlling phenotypic expression in BMP-induced osteogenesis and chondrogenesis.* J Bone Joint Surg Am, 2001. **83**(1 suppl 2): p. S105-S115.
111. Di Martino, A., M. Sittinger, and M.V. Risbud, *Chitosan: a versatile biopolymer for orthopaedic tissue-engineering.* Biomaterials, 2005. **26**(30): p. 5983-5990.
112. Borden, M., et al., *Tissue engineered microsphere-based matrices for bone repair:: design and evaluation.* Biomaterials, 2002. **23**(2): p. 551-559.
113. Yucel, D., G.T. Kose, and V. Hasirci, *Polyester based nerve guidance conduit design.* Biomaterials, 2010. **31**(7): p. 1596-1603.
114. Gibson, L.J., *The mechanical behaviour of cancellous bone.* Journal of biomechanics, 1985. **18**(5): p. 317-328.
115. Bledzki, A. and J. Gassan, *Composites reinforced with cellulose based fibres.* Progress in polymer science, 1999. **24**(2): p. 221-274.
116. Sanchez, C., et al., *Applications of hybrid organic–inorganic nanocomposites.* Journal of Materials Chemistry, 2005. **15**(35-36): p. 3559-3592.
117. Green, A.A., et al., *A transformation for ordering multispectral data in terms of image quality with implications for noise removal.* IEEE Transactions on geoscience and remote sensing, 1988. **26**(1): p. 65-74.
118. Yoneyama, M., et al., *The RNA helicase RIG-I has an essential function in double-stranded RNA-induced innate antiviral responses.* Nature immunology, 2004. **5**(7): p. 730-737.
119. Zhang, J., P. Yedlapalli, and J.W. Lee, *Thermodynamic analysis of hydrate-based pre-combustion capture of CO2.* Chemical Engineering Science, 2009. **64**(22): p. 4732-4736.
120. Wang, Y., et al., *The Holocene Asian monsoon: links to solar changes and North Atlantic climate.* Science, 2005. **308**(5723): p. 854-857.
121. Chesnutt, B.M., et al., *Design and characterization of a novel chitosan/nanocrystalline calcium phosphate composite scaffold for bone regeneration.* Journal of biomedical materials research Part A, 2009. **88**(2): p. 491-502.
122. Chen, D.-M. and H. Zhao, *Strong lensing probability for testing TeVeS theory.* The Astrophysical Journal Letters, 2006. **650**(1): p. L9.
123. Athanasiou, K.A., G.G. Niederauer, and C.M. Agrawal, *Sterilization, toxicity, biocompatibility and clinical applications of polylactic acid/polyglycolic acid copolymers.* Biomaterials, 1996. **17**(2): p. 93-102.
124. Pitt, C.G., et al., *Aliphatic polyesters. I. The degradation of poly (ϵ-caprolactone) in vivo.* Journal of Applied Polymer Science, 1981. **26**(11): p. 3779-3787.
125. Ma, P.X., *Scaffolds for tissue fabrication.* Materials today, 2004. **7**(5): p. 30-40.
126. Miao, X., et al., *Porous calcium phosphate ceramics modified with PLGA–bioactive glass.* Materials Science and Engineering: C, 2007. **27**(2): p. 274-279.
127. Balandin, A.A., et al., *Superior thermal conductivity of single-layer graphene.* Nano letters, 2008. **8**(3): p. 902-907.
128. Agarwal, S., J.H. Wendorff, and A. Greiner, *Use of electrospinning technique for biomedical applications.* Polymer, 2008. **49**(26): p. 5603-5621.
129. Xu, H., et al., *Chronic inflammation in fat plays a crucial role in the development of obesity-related insulin resistance.* The Journal of clinical investigation, 2003. **112**(12): p. 1821-1830.
130. Chen, Q. and A. Boccaccini, *Poly (D, L-lactic acid) coated 45S5 Bioglass®-based scaffolds: Processing and characterization.* Journal of Biomedical Materials Research Part A, 2006. **77**(3): p. 445-457.
131. Misra, S.K., et al., *Polyhydroxyalkanoate (PHA)/inorganic phase composites for tissue engineering applications.* Biomacromolecules, 2006. **7**(8): p. 2249-2258.
132. Sánchez-Salcedo, S., A. Nieto, and M. Vallet-Regí, *Hydroxyapatite/β-tricalcium phosphate/agarose macroporous scaffolds for bone tissue engineering.* Chemical engineering journal, 2008. **137**(1): p. 62-71.
133. Puértolas, J., et al., *Compression behaviour of biphasic calcium phosphate and biphasic calcium phosphate–agarose scaffolds for bone regeneration.* Acta biomaterialia, 2011. **7**(2): p. 841-847.
134. Zhao, F., et al., *Preparation and histological evaluation of biomimetic three-dimensional hydroxyapatite/chitosan-gelatin network composite scaffolds.* Biomaterials, 2002. **23**(15): p. 3227-3234.
135. Itatani, K., et al., *Preparation of various calcium-phosphate powders by ultrasonic spray freeze-drying technique.* Materials research bulletin, 2000. **35**(4): p. 575-585.

136. Samavedi, S., A.R. Whittington, and A.S. Goldstein, *Calcium phosphate ceramics in bone tissue engineering: a review of properties and their influence on cell behavior.* Acta biomaterialia, 2013. **9**(9): p. 8037-8045.
137. Min, B.-M., et al., *Electrospinning of silk fibroin nanofibers and its effect on the adhesion and spreading of normal human keratinocytes and fibroblasts in vitro.* Biomaterials, 2004. **25**(7): p. 1289-1297.
138. Miroiu, F., et al., *Composite biocompatible hydroxyapatite–silk fibroin coatings for medical implants obtained by Matrix Assisted Pulsed Laser Evaporation.* Materials Science and Engineering: B, 2010. **169**(1): p. 151-158.
139. Bhumiratana, S., et al., *Nucleation and growth of mineralized bone matrix on silk-hydroxyapatite composite scaffolds.* Biomaterials, 2011. **32**(11): p. 2812-2820.
140. Spotnitz, W.D., *Fibrin sealant: past, present, and future: a brief review.* World journal of surgery, 2010. **34**(4): p. 632-634.
141. Le Guéhennec, L., P. Layrolle, and G. Daculsi, *A review of bioceramics and fibrin sealant.* Eur Cell Mater, 2004. **8**(13): p. 1e11.
142. Walker-Bone, K., et al., *Regular review: medical management of osteoarthritis.* British Medical Journal, 2000. **321**(7266): p. 936.
143. Liu, H., et al., *A study on a chitosan-gelatin-hyaluronic acid scaffold as artificial skin in vitro and its tissue engineering applications.* Journal of Biomaterials Science, Polymer Edition, 2004. **15**(1): p. 25-40.
144. Yodsuwan, N., et al. *Effect of carbon and nitrogen sources on bacterial cellulose production for bionanocomposite materials*. in *1st Fah Luang University international conference, Thailand*. 2012.
145. Lee, J.-Y., et al., *Transforming growth factor (TGF)-β1 releasing tricalcium phosphate/chitosan microgranules as bone substitutes.* Pharmaceutical research, 2004. **21**(10): p. 1790-1796.
146. Samira, J., et al., *Cytocompatibility, gene-expression profiling, apoptotic, mechanical and 29Si, 31P solid-state nuclear magnetic resonance studies following treatment with a bioglass-chitosan composite.* Biotechnology letters, 2014. **36**(12): p. 2571-2579.
147. Huang, D., et al., *Optical coherence tomography.* Science (New York, NY), 1991. **254**(5035): p. 1178.
148. Mohammadi, Y., et al., *Nanofibrous poly (epsilon-caprolactone)/poly (vinyl (alcohol)/chitosan hybrid scaffolds for bone tissue engineering using mesenchymal stem cells.* International journal of artificial organs, 2007. **30**(3): p. 204.
149. Liu, X., et al., *Characterization of structure and diffusion behaviour of Ca-alginate beads prepared with external or internal calcium sources.* Journal of microencapsulation, 2002. **19**(6): p. 775-782.
150. Kim, I.-Y., et al., *Chitosan and its derivatives for tissue engineering applications.* Biotechnology advances, 2008. **26**(1): p. 1-21.
151. Saravanan, S., et al., *Preparation, characterization and antimicrobial activity of a bio-composite scaffold containing chitosan/nano-hydroxyapatite/nano-silver for bone tissue engineering.* International journal of biological macromolecules, 2011. **49**(2): p. 188-193.
152. Chronopoulou, L., et al., *Chitosan-coated PLGA nanoparticles: a sustained drug release strategy for cell cultures.* Colloids and surfaces B: biointerfaces, 2013. **103**: p. 310-317.
153. Mohammadi, Y., et al., *Osteogenic Differentiation of Mesenchymal Stem Cells on Novel Three-Dimensional Poly (L-Lactic Acid)/Chitosan/Gelatin/Beta-Tricalcium Phosphate Hybrid Scaffolds.* Iranian Polymer Journal, 2007. **16**(1): p. 57.
154. Wang, Z. and T.-W. Qin, *Review: Vitreous Cryopreservation of Tissue-engineered Compositions for Tissue Repair.* Journal of Medical and Biological Engineering, 2013. **33**(2): p. 125-132.
155. Yeo, J.H., et al., *The effects of Pva/chitosan/fibroin (PCF)-blended spongy sheets on wound healing in rats.* Biological and Pharmaceutical Bulletin, 2000. **23**(10): p. 1220-1223.
156. Wang, M., *Bioactive calcium phosphates and nanocomposite scaffolds for bone tissue engineering.* Ceramic Transactions, 2010. **218**: p. 175-183.
157. Chang, M.C. and J. Tanaka, *FT-IR study for hydroxyapatite/collagen nanocomposite cross-linked by glutaraldehyde.* Biomaterials, 2002. **23**(24): p. 4811-4818.
158. Li, X., et al., *Collagen-based implants reinforced by chitin fibres in a goat shank bone defect model.* Biomaterials, 2006. **27**(9): p. 1917-1923.
159. Spilker, M., et al., *The effects of collagen-based implants on early healing of the adult rat spinal cord.* Tissue Engineering, 1997. **3**(3): p. 309-317.
160. Weadock, K.S., et al., *Physical crosslinking of collagen fibers: comparison of ultraviolet irradiation and dehydrothermal treatment.* Journal of biomedical materials research, 1995. **29**(11): p. 1373-1379.

161. Lahav, J., M.A. Schwartz, and R.O. Hynes, *Analysis of platelet adhesion with a radioactive chemical crosslinking reagent: interaction of thrombospondin with fibronectin and collagen.* Cell, 1982. **31**(1): p. 253-262.
162. Reiser, K., R. McCormick, and R. Rucker, *Enzymatic and nonenzymatic cross-linking of collagen and elastin.* The FASEB Journal, 1992. **6**(7): p. 2439-2449.
163. Chang, C.H., et al., *Cartilage tissue engineering on the surface of a novel gelatin–calcium-phosphate biphasic scaffold in a double-chamber bioreactor.* Journal of Biomedical Materials Research Part B: Applied Biomaterials, 2004. **71**(2): p. 313-321.
164. Schonauer, C., et al., *The use of local agents: bone wax, gelatin, collagen, oxidized cellulose.* European Spine Journal, 2004. **13**(1): p. S89-S96.
165. Li, M., et al., *Electrospun protein fibers as matrices for tissue engineering.* Biomaterials, 2005. **26**(30): p. 5999-6008.
166. Sawyer, A., et al., *The stimulation of healing within a rat calvarial defect by mPCL–TCP/collagen scaffolds loaded with rhBMP-2.* Biomaterials, 2009. **30**(13): p. 2479-2488.
167. Habraken, W., J. Wolke, and J. Jansen, *Ceramic composites as matrices and scaffolds for drug delivery in tissue engineering.* Advanced drug delivery reviews, 2007. **59**(4): p. 234-248.
168. Ko, C.-C., et al., *Mechanical properties and cytocompatibility of biomimetic hydroxyapatite-gelatin nanocomposites.* Journal of materials research, 2006. **21**(12): p. 3090-3098.
169. Vacanti, J.P. and R. Langer, *Tissue engineering: the design and fabrication of living replacement devices for surgical reconstruction and transplantation.* The Lancet, 1999. **354**: p. S32-S34.
170. Mohamed, K.R., H.H. Beherei, and Z.M. El-Rashidy, *In vitro study of nano-hydroxyapatite/chitosan–gelatin composites for bio-applications.* Journal of advanced research, 2014. **5**(2): p. 201-208.
171. Li, J., et al., *Surface characterization and biocompatibility of micro-and nano-hydroxyapatite/chitosan-gelatin network films.* Materials Science and Engineering: C, 2009. **29**(4): p. 1207-1215.
172. Choi, Y.S., et al., *Study on gelatin-containing artificial skin: I. Preparation and characteristics of novel gelatin-alginate sponge.* Biomaterials, 1999. **20**(5): p. 409-417.
173. Li, J., et al., *Effect of nano-and micro-hydroxyapatite/chitosan-gelatin network film on human gastric cancer cells.* Materials Letters, 2008. **62**(17): p. 3220-3223.
174. Sharma, S., et al., *Bone healing performance of electrophoretically deposited apatite–wollastonite/chitosan coating on titanium implants in rabbit tibiae.* Journal of tissue engineering and regenerative medicine, 2009. **3**(7): p. 501-511.
175. Dorozhkin, S.V., *Calcium orthophosphate-containing biocomposites and hybrid biomaterials for biomedical applications.* Journal of functional biomaterials, 2015. **6**(3): p. 708-832.
176. Lien, S.-M., W.-T. Li, and T.-J. Huang, *Genipin-crosslinked gelatin scaffolds for articular cartilage tissue engineering with a novel crosslinking method.* Materials Science and Engineering: C, 2008. **28**(1): p. 36-43.
177. Araki, K. and J.W. Halloran, *Porous ceramic bodies with interconnected pore channels by a novel freeze casting technique.* Journal of the American Ceramic Society, 2005. **88**(5): p. 1108-1114.
178. Liotta, L., et al., *Metastatic potential correlates with enzymatic degradation of basement membrane collagen.* Nature, 1980. **284**(5751): p. 67-68.
179. Pals, D. and J. Hermans, *Sodium salts of pectin and of carboxy methyl cellulose in aqueous sodium chloride. I. Viscosities.* Recueil des Travaux Chimiques des Pays-Bas, 1952. **71**(5): p. 433-457.
180. Shikinami, Y. and M. Okuno, *Bioresorbable devices made of forged composites of hydroxyapatite (HA) particles and poly-L-lactide (PLLA): Part I. Basic characteristics.* Biomaterials, 1999. **20**(9): p. 859-877.
181. Kumar, M.N.R., *A review of chitin and chitosan applications.* Reactive and functional polymers, 2000. **46**(1): p. 1-27.
182. Willats, W.G., et al., *Pectin: cell biology and prospects for functional analysis*, in *Plant Cell Walls*. 2001, Springer. p. 9-27.
183. Uragami, T., et al., *Structure of chemically modified chitosan membranes and their characteristics of permeation and separation of aqueous ethanol solutions.* Journal of membrane science, 1994. **88**(2): p. 243-251.
184. Rezwan, K., et al., *Biodegradable and bioactive porous polymer/inorganic composite scaffolds for bone tissue engineering.* Biomaterials, 2006. **27**(18): p. 3413-3431.
185. Ghasemi-Mobarakeh, L., et al., *Electrospun poly (ε-caprolactone)/gelatin nanofibrous scaffolds for nerve tissue engineering.* Biomaterials, 2008. **29**(34): p. 4532-4539.
186. Boccaccini, A.R. and V. Maquet, *Bioresorbable and bioactive polymer/Bioglass® composites with tailored pore structure for tissue engineering applications.* Composites Science and Technology, 2003. **63**(16): p. 2417-2429.

187. Scott, P., et al., *An outbreak of multidrug-resistant Acinetobacter baumannii-calcoaceticus complex infection in the US military health care system associated with military operations in Iraq.* Clinical Infectious Diseases, 2007. **44**(12): p. 1577-1584.
188. Woolf, A.D. and B. Pfleger, *Burden of major musculoskeletal conditions.* Bulletin of the World Health Organization, 2003. **81**(9): p. 646-656.
189. Laurencin, C.T., et al., *Tissue engineering: orthopedic applications.* Annual review of biomedical engineering, 1999. **1**(1): p. 19-46.
190. Guertler, L.G., *Virus safety of human blood, plasma, and derived products.* Thrombosis Research, 2002. **107**: p. S39-S45.
191. Uchida, A., et al., *The use of calcium hydroxyapatite ceramic in bone tumour surgery.* Bone & Joint Journal, 1990. **72**(2): p. 298-302.
192. Cooke, F.W., *Ceramics in orthopedic surgery.* Clinical orthopaedics and related research, 1992. **276**: p. 135-146.
193. Tai, K., F.-J. Ulm, and C. Ortiz, *Nanogranular origins of the strength of bone.* Nano letters, 2006. **6**(11): p. 2520-2525.
194. Vallet-Regí, M. and J.M. González-Calbet, *Calcium phosphates as substitution of bone tissues.* Progress in Solid State Chemistry, 2004. **32**(1): p. 1-31.
195. Pilliar, R., et al., *Porous calcium polyphosphate scaffolds for bone substitute applications—in vitro characterization.* Biomaterials, 2001. **22**(9): p. 963-972.
196. Daftari, T.K., et al., *Nicotine on the Revascularization of Bone Graft: An Experimental Study in Rabbits.* Spine, 1994. **19**(8): p. 904-911.
197. Meyer, J. and E. Eanes, *A thermodynamic analysis of the amorphous to crystalline calcium phosphate transformation.* Calcified tissue research, 1978. **25**(1): p. 59-68.
198. Maji, K. and S. Dasgupta, *Hydroxyapatite-chitosan and gelatin based scaffold for bone tissue engineering.* Transactions of the Indian Ceramic Society, 2014. **73**(2): p. 110-114.
199. Lynn, A., et al., *Composition-controlled nanocomposites of apatite and collagen incorporating silicon as an osseopromotive agent.* Journal of Biomedical Materials Research Part A, 2005. **74**(3): p. 447-453.
200. Kikuchi, M., et al., *Glutaraldehyde cross-linked hydroxyapatite/collagen self-organized nanocomposites.* Biomaterials, 2004. **25**(1): p. 63-69.
201. Azami, M., F. Moztarzadeh, and M. Tahriri, *Preparation, characterization and mechanical properties of controlled porous gelatin/hydroxyapatite nanocomposite through layer solvent casting combined with freeze-drying and lamination techniques.* Journal of Porous Materials, 2010. **17**(3): p. 313-320.
202. Liao, S., F. Cui, and Y. Zhu, *Osteoblasts adherence and migration through three-dimensional porous mineralized collagen based composite: nHAC/PLA.* Journal of Bioactive and Compatible polymers, 2004. **19**(2): p. 117-130.
203. Bigi, A., et al., *Bonelike apatite growth on hydroxyapatite–gelatin sponges from simulated body fluid.* Journal of biomedical materials research, 2002. **59**(4): p. 709-715.
204. Zhang, S., et al., *Synthesis and biocompatibility of porous nano-hydroxyapatite/collagen/alginate composite.* Journal of Materials Science: Materials in Medicine, 2003. **14**(7): p. 641-645.
205. Kim, H.-W., H.-E. Kim, and V. Salih, *Stimulation of osteoblast responses to biomimetic nanocomposites of gelatin–hydroxyapatite for tissue engineering scaffolds.* Biomaterials, 2005. **26**(25): p. 5221-5230.
206. Yasuda, H.Y., et al., *Effect of. BETA.-TCP Size on Bone-Like Layer Growth and Adhesion of Osteoblast-Like Cells in Hydroxyapatite/. BETA.-TCP Composites.* Materials transactions, 2006. **47**(9): p. 2368-2372.
207. Thein-Han, W. and R. Misra, *Biomimetic chitosan–nanohydroxyapatite composite scaffolds for bone tissue engineering.* Acta Biomaterialia, 2009. **5**(4): p. 1182-1197.
208. Park, S.-N., et al., *Characterization of porous collagen/hyaluronic acid scaffold modified by 1-ethyl-3-(3-dimethylaminopropyl) carbodiimide cross-linking.* Biomaterials, 2002. **23**(4): p. 1205-1212.
209. Uchida, M., et al., *Bonelike apatite formation induced on zirconia gel in a simulated body fluid and its modified solutions.* Journal of the American Ceramic Society, 2001. **84**(9): p. 2041-2044.
210. Bissoyi, A. and K. Pramanik, *Role of the apoptosis pathway in cryopreservation-induced cell death in mesenchymal stem cells derived from umbilical cord blood.* Biopreservation and biobanking, 2014. **12**(4): p. 246-254.
211. Grayson, W.L., et al., *Effects of initial seeding density and fluid perfusion rate on formation of tissue-engineered bone.* Tissue Engineering Part A, 2008. **14**(11): p. 1809-1820.
212. Soleimani, M. and S. Nadri, *A protocol for isolation and culture of mesenchymal stem cells from mouse bone marrow.* Nature protocols, 2009. **4**(1): p. 102-106.

213. Shi, J., et al., *Incorporating protein gradient into electrospun nanofibers as scaffolds for tissue engineering.* ACS applied materials & interfaces, 2010. **2**(4): p. 1025-1030.
214. White, J., W. Amos, and M. Fordham, *An evaluation of confocal versus conventional imaging of biological structures by fluorescence light microscopy.* The Journal of cell biology, 1987. **105**(1): p. 41-48.
215. Oliveira, J.M., et al., *Novel hydroxyapatite/chitosan bilayered scaffold for osteochondral tissue-engineering applications: Scaffold design and its performance when seeded with goat bone marrow stromal cells.* Biomaterials, 2006. **27**(36): p. 6123-6137.
216. Yamaguchi, I., et al., *Preparation and microstructure analysis of chitosan/hydroxyapatite nanocomposites.* Journal of biomedical materials research, 2001. **55**(1): p. 20-27.
217. Inoue, K., et al. *Control of crystal orientation of hydroxyapatite by using a high magnetic field*. in *Key Engineering Materials*. 2003. Trans Tech Publ.
218. Cheng, M., et al., *Study on physical properties and nerve cell affinity of composite films from chitosan and gelatin solutions.* Biomaterials, 2003. **24**(17): p. 2871-2880.
219. Peter, M., et al., *Novel biodegradable chitosan–gelatin/nano-bioactive glass ceramic composite scaffolds for alveolar bone tissue engineering.* Chemical Engineering Journal, 2010. **158**(2): p. 353-361.
220. Deville, S., E. Saiz, and A.P. Tomsia, *Freeze casting of hydroxyapatite scaffolds for bone tissue engineering.* Biomaterials, 2006. **27**(32): p. 5480-5489.
221. Carter, D.R. and W.C. Hayes, *The compressive behavior of bone as a two-phase porous structure.* The Journal of Bone & Joint Surgery, 1977. **59**(7): p. 954-962.
222. Tuzlakoglu, K. and R. Reis, *Formation of bone-like apatite layer on chitosan fiber mesh scaffolds by a biomimetic spraying process.* Journal of Materials Science: Materials in Medicine, 2007. **18**(7): p. 1279-1286.
223. Barrere, F., et al., *Osteointegration of biomimetic apatite coating applied onto dense and porous metal implants in femurs of goats.* Journal of Biomedical Materials Research Part B: Applied Biomaterials, 2003. **67**(1): p. 655-665.
224. Zheng, J.P., et al., *Preparation of biomimetic three-dimensional gelatin/montmorillonite–chitosan scaffold for tissue engineering.* Reactive and Functional Polymers, 2007. **67**(9): p. 780-788.
225. Kundu, B., et al., *Development of porous HAp and β-TCP scaffolds by starch consolidation with foaming method and drug-chitosan bilayered scaffold based drug delivery system.* Journal of Materials Science: Materials in Medicine, 2010. **21**(11): p. 2955-2969.
226. Lee, J.H., et al., *Control of Osteogenic Differentiation and Mineralization of Human Mesenchymal Stem Cells on Composite Nanofibers Containing Poly [lactic-co-(glycolic acid)] and Hydroxyapatite.* Macromolecular bioscience, 2010. **10**(2): p. 173-182.
227. Viereck, V., et al., *Differential regulation of Cbfa1/Runx2 and osteocalcin gene expression by vitamin-D3, dexamethasone, and local growth factors in primary human osteoblasts.* Journal of cellular biochemistry, 2002. **86**(2): p. 348-356.
228. Anselme, K., *Osteoblast adhesion on biomaterials.* Biomaterials, 2000. **21**(7): p. 667-681.
229. Stevens, M.M. and J.H. George, *Exploring and engineering the cell surface interface.* Science, 2005. **310**(5751): p. 1135-1138.
230. Gronthos, S., et al., *Integrin-mediated interactions between human bone marrow stromal precursor cells and the extracellular matrix.* Bone, 2001. **28**(2): p. 174-181.
231. Di Chen, J., et al., *Self-organization of hydroxyapatite nanorods through oriented attachment.* Biomaterials, 2007. **28**(14): p. 2275-2280.
232. Wang, Y., et al., *Development and Characterization of Novel Biomimetic Composite Scaffolds Based on Bioglass-Collagen-Hyaluronic Acid-Phosphatidylserine for Tissue Engineering Applications.* Macromolecular materials and engineering, 2006. **291**(3): p. 254-262.
233. Rodrigues, C., et al., *Characterization of a bovine collagen–hydroxyapatite composite scaffold for bone tissue engineering.* Biomaterials, 2003. **24**(27): p. 4987-4997.
234. Mann, S., *Molecular tectonics in biomineralization and biomimetic materials chemistry.* Nature, 1993. **365**(6446): p. 499-505.
235. Rich, J., et al., *In vitro evaluation of poly (ε-caprolactone-co-DL-lactide)/bioactive glass composites.* Biomaterials, 2002. **23**(10): p. 2143-2150.
236. Walsh, D., T. Furuzono, and J. Tanaka, *Preparation of porous composite implant materials by in situ polymerization of porous apatite containing ε-caprolactone or methyl methacrylate.* Biomaterials, 2001. **22**(11): p. 1205-1212.
237. Qiu, Q.Q., P. Ducheyne, and P.S. Ayyaswamy, *New bioactive, degradable composite microspheres as tissue engineering substrates.* Journal of biomedical materials research, 2000. **52**(1): p. 66-76.

238. Devin, J.E., M.A. Attawia, and C.T. Laurencin, *Three-dimensional degradable porous polymer-ceramic matrices for use in bone repair.* Journal of Biomaterials Science, Polymer Edition, 1996. **7**(8): p. 661-669.
239. Deng, X., J. Hao, and C. Wang, *Preparation and mechanical properties of nanocomposites of poly (D, L-lactide) with Ca-deficient hydroxyapatite nanocrystals.* Biomaterials, 2001. **22**(21): p. 2867-2873.
240. Levengood, S.K.L. and M. Zhang, *Chitosan-based scaffolds for bone tissue engineering.* Journal of Materials Chemistry B, 2014. **2**(21): p. 3161-3184.
241. Croisier, F. and C. Jérôme, *Chitosan-based biomaterials for tissue engineering.* European Polymer Journal, 2013. **49**(4): p. 780-792.
242. Nandi, S.K., B. Kundu, and D. Basu, *Protein growth factors loaded highly porous chitosan scaffold: a comparison of bone healing properties.* Materials Science and Engineering: C, 2013. **33**(3): p. 1267-1275.
243. Ghosh, P., et al., *2, 5-Dimethoxy 2, 5-dihydrofuran crosslinked chitosan fibers enhance bone regeneration in rabbit femur defects.* RSC Advances, 2014. **4**(37): p. 19516-19524.
244. Shen, Y., et al., *Multifunctioning pH-responsive nanoparticles from hierarchical self-assembly of polymer brush for cancer drug delivery.* AIChE journal, 2008. **54**(11): p. 2979-2989.
245. Nagahama, H., et al., *Preparation and characterization of novel chitosan/gelatin membranes using chitosan hydrogel.* Carbohydrate polymers, 2009. **76**(2): p. 255-260.
246. VandeVord, P.J., et al., *Evaluation of the biocompatibility of a chitosan scaffold in mice.* Journal of biomedical materials research, 2002. **59**(3): p. 585-590.
247. Gravel, M., et al., *Responses of mesenchymal stem cell to chitosan–coralline composites microstructured using coralline as gas forming agent.* Biomaterials, 2006. **27**(9): p. 1899-1906.
248. Mao, J.S., et al., *Structure and properties of bilayer chitosan–gelatin scaffolds.* Biomaterials, 2003. **24**(6): p. 1067-1074.
249. Chen, T., et al., *Enzyme-catalyzed gel formation of gelatin and chitosan: potential for in situ applications.* Biomaterials, 2003. **24**(17): p. 2831-2841.
250. Mao, J., et al., *Study of novel chitosan-gelatin artificial skin in vitro.* Journal of Biomedical Materials Research Part A, 2003. **64**(2): p. 301-308.
251. Xia, W., et al., *Tissue engineering of cartilage with the use of chitosan-gelatin complex scaffolds.* Journal of Biomedical Materials Research Part B: Applied Biomaterials, 2004. **71**(2): p. 373-380.
252. Yin, Y., et al., *Preparation and characterization of macroporous chitosan–gelatin/β-tricalcium phosphate composite scaffolds for bone tissue engineering.* Journal of Biomedical Materials Research Part A, 2003. **67**(3): p. 844-855.
253. Hench, L.L., et al., *Bonding mechanisms at the interface of ceramic prosthetic materials.* Journal of Biomedical Materials Research, 1971. **5**(6): p. 117-141.
254. Oudadesse, H., et al., *Study of various mineral compositions and their bioactivity of bioactive glasses.* Biocera, 2009. **22**: p. 379-82.
255. Hench, L.L. and J.K. West, *Biological applications of bioactive glasses*. 1996: Harwood Academic Publishers.
256. Shalumon, K., et al., *Effect of incorporation of nanoscale bioactive glass and hydroxyapatite in PCL/chitosan nanofibers for bone and periodontal tissue engineering.* Journal of biomedical nanotechnology, 2013. **9**(3): p. 430-440.
257. Gentile, P., et al., *Bioactive glass/polymer composite scaffolds mimicking bone tissue.* Journal of Biomedical Materials Research Part A, 2012. **100**(10): p. 2654-2667.
258. Peter, M., et al., *Nanocomposite scaffolds of bioactive glass ceramic nanoparticles disseminated chitosan matrix for tissue engineering applications.* Carbohydrate Polymers, 2010. **79**(2): p. 284-289.
259. Xynos, I., et al., *Bioglass® 45S5 stimulates osteoblast turnover and enhances bone formation in vitro: implications and applications for bone tissue engineering.* Calcified Tissue International, 2000. **67**(4): p. 321-329.
260. Bielby, R.C., et al., *Enhanced derivation of osteogenic cells from murine embryonic stem cells after treatment with ionic dissolution products of 58S bioactive sol-gel glass.* Tissue engineering, 2005. **11**(3-4): p. 479-488.
261. Li, H., R. Du, and J. Chang, *Fabrication, characterization, and in vitro degradation of composite scaffolds based on PHBV and bioactive glass.* Journal of biomaterials applications, 2005. **20**(2): p. 137-155.
262. Garcia, C., S. Cere, and A. Duran, *Bioactive coatings prepared by sol–gel on stainless steel 316L.* Journal of non-crystalline solids, 2004. **348**: p. 218-224.
263. Hench, L.L. and J. Wilson, *An introduction to bioceramics*. Vol. 1. 1993: World Scientific.

264. Mi, F.-L., *Synthesis and characterization of a novel chitosan-gelatin bioconjugate with fluorescence emission.* Biomacromolecules, 2005. **6**(2): p. 975-987.
265. Niu, Q.-x., C.-y. Zhao, and Z.-a. Jing, *An evaluation of the colorimetric assays based on enzymatic reactions used in the measurement of human natural cytotoxicity.* Journal of immunological methods, 2001. **251**(1): p. 11-19.
266. Federman, S.R., et al., *Sol-Gel SiO2-CaO-P2O5 biofilm with surface engineered for medical application.* Materials Research, 2007. **10**(2): p. 177-181.
267. Ji Yin, Y., et al., *Preparation and characterization of hydroxyapatite/chitosan–gelatin network composite.* Journal of applied polymer science, 2000. **77**(13): p. 2929-2938.
268. Itoh, S., et al., *Development of a novel biomaterial, hydroxyapatite/collagen (HAp/Col) composite for medical use.* Bio-medical materials and engineering, 2005. **15**(1, 2): p. 29-41.
269. Kuboki, Y., et al., *BMP-induced osteogenesis on the surface of hydroxyapatite with geometrically feasible and nonfeasible structures: topology of osteogenesis.* Journal of biomedical materials research, 1998. **39**(2): p. 190-199.
270. Kenyon, K.R. and S. Tseng, *Limbal autograft transplantation for ocular surface disorders.* Ophthalmology, 1989. **96**(5): p. 709-22; discussion 722-3.
271. Pham, Q.P., et al., *The influence of an in vitro generated bone-like extracellular matrix on osteoblastic gene expression of marrow stromal cells.* Biomaterials, 2008. **29**(18): p. 2729-2739.
272. Viguet-Carrin, S., P. Garnero, and P. Delmas, *The role of collagen in bone strength.* Osteoporosis International, 2006. **17**(3): p. 319-336.
273. Gupta, H.S., et al., *Cooperative deformation of mineral and collagen in bone at the nanoscale.* Proceedings of the National Academy of Sciences, 2006. **103**(47): p. 17741-17746.
274. Yunos, D.M., O. Bretcanu, and A.R. Boccaccini, *Polymer-bioceramic composites for tissue engineering scaffolds.* Journal of Materials Science, 2008. **43**(13): p. 4433-4442.
275. Schultz, G.S. and A. Wysocki, *Interactions between extracellular matrix and growth factors in wound healing.* Wound repair and regeneration, 2009. **17**(2): p. 153-162.
276. Kleinman, H.K., D. Philp, and M.P. Hoffman, *Role of the extracellular matrix in morphogenesis.* Current opinion in biotechnology, 2003. **14**(5): p. 526-532.
277. Ding, S.-J., *Preparation and properties of chitosan/calcium phosphate composites for bone repair.* Dental materials journal, 2006. **25**(4): p. 706-712.
278. Zhang, Q.-Q., et al., *Porous hydroxyapatite reinforced with collagen protein.* Artificial Cells, Blood Substitutes, and Biotechnology, 1996. **24**(6): p. 693-702.
279. Madihally, S.V. and H.W. Matthew, *Porous chitosan scaffolds for tissue engineering.* Biomaterials, 1999. **20**(12): p. 1133-1142.
280. Lopez-Cebral, R., et al., *Chemically modified gelatin as biomaterial in the design of new nanomedicines.* Medicinal Chemistry, 2011. **7**(3): p. 145-154.
281. Suchanek, W. and M. Yoshimura, *Processing and properties of hydroxyapatite-based biomaterials for use as hard tissue replacement implants.* Journal of Materials Research, 1998. **13**(01): p. 94-117.
282. Best, S., et al., *The dependence of osteoblastic response on variations in the chemical composition and physical properties of hydroxyapatite.* Journal of Materials Science: Materials in Medicine, 1997. **8**(2): p. 97-103.
283. Hankinson, S.E., et al., *Circulating concentrations of insulin-like growth factor I and risk of breast cancer.* The Lancet, 1998. **351**(9113): p. 1393-1396.
284. Julien, M., et al., *Phosphate-Dependent Regulation of MGP in Osteoblasts: Role of ERK1/2 and Fra-1.* Journal of Bone and Mineral Research, 2009. **24**(11): p. 1856-1868.
285. Ji, B. and H. Gao, *Mechanical properties of nanostructure of biological materials.* Journal of the Mechanics and Physics of Solids, 2004. **52**(9): p. 1963-1990.
286. Norton, I. and W. Frith, *Microstructure design in mixed biopolymer composites.* Food Hydrocolloids, 2001. **15**(4): p. 543-553.
287. Liu, X. and P.X. Ma, *Phase separation, pore structure, and properties of nanofibrous gelatin scaffolds.* Biomaterials, 2009. **30**(25): p. 4094-4103.
288. Khan, M.N., J.M. Islam, and M.A. Khan, *Fabrication and characterization of gelatin-based biocompatible porous composite scaffold for bone tissue engineering.* Journal of Biomedical Materials Research Part A, 2012. **100**(11): p. 3020-3028.
289. Kwon, S.-H., et al., *Synthesis and dissolution behavior of β-TCP and HA/β-TCP composite powders.* Journal of the European Ceramic Society, 2003. **23**(7): p. 1039-1045.
290. Ki, C.S., et al., *Characterization of gelatin nanofiber prepared from gelatin–formic acid solution.* Polymer, 2005. **46**(14): p. 5094-5102.

291. Chen, J., et al., *A simple sol-gel technique for synthesis of nanostructured hydroxyapatite, tricalcium phosphate and biphasic powders.* Materials Letters, 2011. **65**(12): p. 1923-1926.
292. Serra, I., et al., *Production and characterization of chitosan/gelatin/β-TCP scaffolds for improved bone tissue regeneration.* Materials Science and Engineering: C, 2015. **55**: p. 592-604.
293. Bose, S., M. Roy, and A. Bandyopadhyay, *Recent advances in bone tissue engineering scaffolds.* Trends in biotechnology, 2012. **30**(10): p. 546-554.
294. Sofie, S.W., *Fabrication of Functionally Graded and Aligned Porosity in Thin Ceramic Substrates With the Novel Freeze–Tape-Casting Process.* Journal of the American Ceramic Society, 2007. **90**(7): p. 2024-2031.
295. Blakeney, B.A., et al., *Cell infiltration and growth in a low density, uncompressed three-dimensional electrospun nanofibrous scaffold.* Biomaterials, 2011. **32**(6): p. 1583-1590.
296. Marino, G., et al., *β-Tricalcium phosphate 3D scaffold promote alone osteogenic differentiation of human adipose stem cells: in vitro study.* Journal of Materials Science: Materials in Medicine, 2010. **21**(1): p. 353-363.
297. Goldstein, S., *The mechanical properties of trabecular bone: dependence on anatomic location and function.* Journal of biomechanics, 1987. **20**(11): p. 1055-1061.
298. Kim, S.-K. and N. Rajapakse, *Enzymatic production and biological activities of chitosan oligosaccharides (COS): A review.* Carbohydrate polymers, 2005. **62**(4): p. 357-368.
299. Kucharska, M., et al., *Fabrication of in-situ foamed chitosan/β-TCP scaffolds for bone tissue engineering application.* Materials Letters, 2012. **85**: p. 124-127.
300. Glogauer, M., et al., *Calcium ions and tyrosine phosphorylation interact coordinately with actin to regulate cytoprotective responses to stretching.* Journal of cell science, 1997. **110**(1): p. 11-21.
301. Wopenka, B. and J.D. Pasteris, *A mineralogical perspective on the apatite in bone.* Materials Science and Engineering: C, 2005. **25**(2): p. 131-143.
302. Kikuchi, M., et al., *Self-organization mechanism in a bone-like hydroxyapatite/collagen nanocomposite synthesized in vitro and its biological reaction in vivo.* Biomaterials, 2001. **22**(13): p. 1705-1711.
303. Giannoudis, P.V., H. Dinopoulos, and E. Tsiridis, *Bone substitutes: an update.* Injury, 2005. **36**(3): p. S20-S27.
304. Gunzburg, R. and M. Szpalski, *Use of a novel β-tricalcium phosphate-based bone void filler as a graft extender in spinal fusion surgeries.* Orthopedics, 2002. **25**(5): p. S591-S595.
305. Jell, G., et al., *Bioactive glass-induced osteoblast differentiation: A noninvasive spectroscopic study.* Journal of Biomedical Materials Research Part A, 2008. **86**(1): p. 31-40.
306. Tomalia, D.A., *Birth of a new macromolecular architecture: dendrimers as quantized building blocks for nanoscale synthetic polymer chemistry.* Progress in Polymer Science, 2005. **30**(3): p. 294-324.
307. Sherwood, J.K., et al., *A three-dimensional osteochondral composite scaffold for articular cartilage repair.* Biomaterials, 2002. **23**(24): p. 4739-4751.
308. Hildebrand, T. and P. RÜEGSEGGER, *Quantification of bone microarchitecture with the structure model index.* Computer Methods in Biomechanics and Bio Medical Engineering, 1997. **1**(1): p. 15-23.
309. Suh, J.-K.F. and H.W. Matthew, *Application of chitosan-based polysaccharide biomaterials in cartilage tissue engineering: a review.* Biomaterials, 2000. **21**(24): p. 2589-2598.
310. Banerjee, S.S., et al., *Understanding the influence of MgO and SrO binary doping on the mechanical and biological properties of β-TCP ceramics.* Acta Biomaterialia, 2010. **6**(10): p. 4167-4174.
311. Jo, J.H., et al., *In vitro/in vivo biocompatibility and mechanical properties of bioactive glass nanofiber and poly (ε-caprolactone) composite materials.* Journal of Biomedical Materials Research Part B: Applied Biomaterials, 2009. **91**(1): p. 213-220.
312. Stupp, S.I. and P.V. Braun, *Molecular manipulation of microstructures: biomaterials, ceramics, and semiconductors.* Science, 1997. **277**(5330): p. 1242-1248.
313. Jones, A.C., et al., *Assessment of bone ingrowth into porous biomaterials using MICRO-CT.* Biomaterials, 2007. **28**(15): p. 2491-2504.
314. Van Dalen, G., et al., *3-D imaging, analysis and modelling of porous cereal products using x-ray microtomography.* Image Analysis and Stereology, 2007. **26**: p. 169-178.
315. Marone, M., et al., *Semiquantitative RT-PCR analysis to assess the expression levels of multiple transcripts from the same sample.* Biol Proced Online, 2001. **3**(1): p. 19-25.
316. Zandi, M., et al., *Biocompatibility evaluation of nano-rod hydroxyapatite/gelatin coated with nano-HAp as a novel scaffold using mesenchymal stem cells.* Journal of biomedical materials research Part A, 2010. **92**(4): p. 1244-1255.
317. Rajkumar, M., et al., *Nanohydroxyapatite–chitosan–gelatin polyelectrolyte complex with enhanced mechanical and bioactivity.* Materials Science and Engineering: C, 2013. **33**(6): p. 3237-3244.

318. Harley, B.A., et al., *Mechanical characterization of collagen–glycosaminoglycan scaffolds.* Acta biomaterialia, 2007. **3**(4): p. 463-474.
319. De Nardo, L., et al., *Shape memory polymer cellular solid design for medical applications.* Smart Materials and Structures, 2011. **20**(3): p. 035004.
320. Zhao, F., et al., *Effects of hydroxyapatite in 3-D chitosan–gelatin polymer network on human mesenchymal stem cell construct development.* Biomaterials, 2006. **27**(9): p. 1859-1867.
321. Wilson, C.J., et al., *Mediation of biomaterial-cell interactions by adsorbed proteins: a review.* Tissue engineering, 2005. **11**(1-2): p. 1-18.
322. Martin, S.R. and P.M. Bayley, *Absorption and Circular Dichroism Spectroscopy*, in *Calcium-Binding Protein Protocols: Volume 2: Methods and Techniques*, H.J. Vogel, Editor. 2002, Springer New York: Totowa, NJ. p. 43-55.
323. Neuendorf, R.E., et al., *Adhesion between biodegradable polymers and hydroxyapatite: Relevance to synthetic bone-like materials and tissue engineering scaffolds.* Acta Biomaterialia, 2008. **4**(5): p. 1288-1296.

Dissemination

Journal Articles

1. Kanchan Maji,Sudip Dasgupta"Hydroxyapatite-chitosan and gelatin based scaffold for bone tissue engineering" ,Transaction of indian ceramic society,2014;73:110-114.

2. Kanchan Maji,Sudip dasgupta,Biswanath Kundu, Akalabya Bissoyi " Development of Gelatin-Chitosan-Hydroxyapatite Based Bioactive Bone Scaffold with Controlled Pore Size and Mechanical Strength-. Journal of Biomaterials Science, Polymer Edition, 2015;26(16):1190-1209.

3. **Kanchan Maji**, Sudip Dasgupta "Bioglass and biopolymer based composite scaffold for bone regeneration", Transaction of Indian ceramic society,2015: 74(4):1-7.

4. Kanchan Maji, Sudip Dasgupta, Krishna Pramanik, Akalabya Bishoyi**,**"Preparation and evaluation of novel chitosan-gelatin-nano-Bioglass 3D porous scaffold for Bone Tissue Engineering"-International Journal Of Biomaterials,2016,14.

Conference Presentations

1. K.Maji, Sudip Dasgupta," Fabrication and Characterization of Hydroxyapatite and biopolymer based composite for bone healing" 2ndInternational Conference on Tissue Engineering & Regenerative Medicine (ICTERM-2013) 15th–17thNovember, NIT Rourkela,INDIA,2013 .

2.K.Maji, S. Dasgupta, D.Pani , "Reinforcement of Calcium Phosphate Cement with E-Glass Fibre", 17th International Conference on Materials Engineering and Technology(ICMET 2015), Wembley, London, UK, 2015.

3. S.Dasgupta, **K.Maji,**" Comparative study on Mechanical Strength of Macroporous Hydroxyapatite-Biopolymer Based Composite Scaffold" International Conference on Advances in Engineering and Technology (ICAET'2014) March 29-30, Singapore, 2014.

4. K.Maji, Sudip Dasgupta, " Development of Tri-Calcium Phosphate-Chitosan and Gelatin Based Scaffold for Bone Tissue Engineering", International Conference on Biomaterials, Biodiagonistics, Tissue Engineering, Drug Delivery and Regenerative Medicine (BITERM-2016), April 15-17,IIT Delhi, 2016.